The role of human endothelium and microRNAs as active participants in the immune response and pathogenesis during malaria

Dissertation with the aim of achieving a doctoral degree at the Faculty of Mathematics, Informatics and Natural sciences

Department of Biology
University of Hamburg

Submitted by
Yifan Wu
Hamburg, 2023

Eidesstattliche Versicherung - Declaration on oath：

Hiermit erkläre ich an Eides statt, dass ich die vorliegende Dissertationsschrift selbst verfasst und keine anderen als die angegebenen Quellen und Hilfsmittel benutzt habe.

I hereby declare, on oath, that I have written the present dissertation by my own and have not used other than the acknowledged resources and aids.

Hamburg, 15.05.2023   **Signature**

Date of disputation: 28.08.2023

First evaluator: Prof. Dr. Iris Bruchhaus

Bernhard Nocht Institute for Tropical Medicine

Research Group: Host Parasite Interaction

Bernhard-Nocht-Straße 74, 20359 Hamburg, Germany

Second evaluator: Prof. Dr. Tim Gilberger

Bernhard Nocht Institute for Tropical Medicine

Department of Cellular Parasitology

Bernhard-Nocht-Straße 74, 20359 Hamburg, Germany

Contribution declaration:

This is a cumulative dissertation and a total of four publications are included.

In publication one: ***Plasmodium falciparum* infection reshapes the human microRNA profiles of red blood cells and their extracellular vesicles.**
I conducted project planning, prepared *P. falciparum* culture, isolated EVs from RBC and iRBC culture, prepared EV samples for transmission electron microscope and nanoparticle tracking dectection, miRNA isolation and the manuscript writing, review and editing.

In publication two: **Analysis of the interaction between *Plasmodium falciparum*-infected erythrocytes and human endothelial cells using a laminar flow system, bioinformatic tracking and transcriptome analysis.**
I conducted the establishment of laminar flow system and the manuscript writing, review and editing.

In publication three: **CD36-a host receptor necessary for malaria parasites to establish and maintain infection.**
I conducted the manuscript writing, review and editing.

In publication four: **Altered cytokine response of human brain endothelial cells after stimulation with malaria patient plasma.**
I conducted the manuscript writing, review and editing.

PhD candidate signature   **Supervisor signature**

Language Certificate

I am a native speaker, have read the present PhD thesis, titled "The role of human endothelium and microRNAs as active participants in the immune response and pathogenesis during malaria" and hereby confirm that it complies with the rules of the English language.

Hamburg, 15.05.2023   **Dr. Madeleine Hamley**

Acknowledgement:

I would like to express my sincere gratitude to the following people for their valuable assistance and support throughout the project.

First of all, I would like to thank Prof. Dr. Iris Bruchhaus for offering me the opportunity to pursue my Doctoral degree at BNITM and all the assistance during my scholarship application. You have always been supportive and helpful. I appreciate your supervision and patience throughout my doctoral project. You have shown tolerance when I made mistakes. I learned from you how to cope with mistakes. Mistakes can happen to everyone, the more important thing is how to better organize it and learn lesson from it. Thank you for all the encouragement.

Warm thanks to Dr. Nahla Galal Metwally. The four years of working with you was truly wonderful. You always go above and beyond to help solve problems in experiments. Whenever I got confused and disappointed by experiments, I can get support, motivation and direction from you. The discussion of scientific questions with you was definitely enjoyable. You are more than a supervisor for me, also a reliable friend. I am sincerely grateful for you.

I appreciate all the Bruchhaus group members I met: Maximilian, Philip, Torben, Susann, Constantin, Jerry, David, Tabea, Barbara, Jakob, Hanifeh, Johannes, Juliett, Agnes, Milad, Pilar, Ibrahim, Fatima, Florian, Maryy and Sara. I will keep all of you in mind.

What I harvested is more than knowledge, also a precious memory.

Thanks to Ralf Hennings for the accommodation. I wish you a good life and all the best.

In the end, I would like to say thanks to my fiancée, Wei Yuzhu.
在欧洲这四年里，最美好和最幸运的事就是遇见了小玉竹。我遇见了全世界对我最重要的人。每次踏上去格罗宁根的火车，都是我最期待的时刻。每次见到小玉竹，是我感觉最放松和开心的时候。感谢小玉竹的陪伴和支持。

Table of Contents

Abstract:

Plasmodium falciparum (*P. falciparum*) infection remains a life-threatening disease and causes the most lethal form of malaria. Different theories have been proposed to explain the pathogenesis and pathophysiological changes in malaria progression. Of which, extracellular vesicles (EVs) are considered as a key player in host-parasite interaction as they are associated with malaria severity. However, the mechanism behind this is still elusive. This study aimed to characterize the EVs derived from uninfected erythrocytes and *P. falciparum*-infected erythrocytes (IEs). At first, EVs were purified and the morphology of isolated EVs were further identified by transmission electron microscope and nanoparticle tracking system. Secondly, we investigated the miRNA profiles of uninfected erythrocytes and IEs as well as their secreted EVs by next generation sequencing (NGS). The expression level of a wide range of miRNAs were altered significantly in erythrocytes and their secreted EVs upon *P. falciparum* infection. Thirdly, the target genes of differentially expressed miRNAs were predicted by bioinformatics approaches, and functional enrichment analysis indicated that these miRNA candidates might play a role in immune regulation during *P. falciparum* infection.

Moreover, cytoadhesion, which refers to IEs adhere to tissue vasculature, is considered to be of great significance in malaria complications. Cytoadhesion is characterized by ligand-receptor interactions between IEs and human endothelium. IEs express various surface antigens and bind to the adhesion receptors on the endothelial surface. The primary parasite antigen responsible for cytoadhesion are *P. falciparum* erythrocyte membrane protein 1 (*Pf*EMP1) proteins, which are encoded by a group of the *var* multigene family. In this part, we aimed to decipher the *var* genes that mediate the cytoadhesion to human brain microvascular endothelial cells (HBMECs) and unravel the effect of cytoadhesion on HBMECs. Firstly, a laboratory-adapted *P. falciparum* strain (IT4) was enriched over HBMECs to select a *P. falciparum* population with high binding affinity to HBMECs. Secondly, the transcriptomic analysis revealed the significant upregulation of IT4_var19 and IT4_var13 in enriched IT4. Thirdly, binding assays of enriched IEs demonstrated their binding capacity to the endothelial cell receptors intercellular adhesion molecule 1 (ICAM-1) and endothelial protein C receptor (EPCR). Finally, enriched IT4 was co-incubated with HBMECs for 4 and 8 hours and the transcriptome of HBMECs was analyzed

by NGS to decipher the cytoadhesion-induced cellular response. The enriched IEs had a significant impact on HBMECs, leading to the dysregulation of numerous differentially expressed genes. Reactome pathway analysis revealed that the 101 differentially expressed genes (DEGs) from 4 hours of comparison were mainly clustered into cytokine signaling in immune system, including interferon induced signaling and signaling by interleukins.

In order to investigate the role of plasmodial factors in the pathogenesis of malaria, we stimulated immortalized brain endothelial cells (HBEC-5i) with plasma derived from malaria patients. Upon stimulation, HBEC-5i showed significantly elevated secretion level of IL-11, CXCL5, CXCL8, CXCL10, vascular endothelial growth factor (VEGF) and angiopoietin-like protein 4 (ANGPTL4) compared to the HBEC-5i stimulated with plasma from healthy donors. Transcriptome study of HBEC-5i further identified that 43 genes were upregulated in expression after co-incubation with plasma from malaria patients. Bioinformatic analyses suggested these DEGs are mainly involved in the biological processes such as cell migration, cell proliferation and tube development.

Besides, a laminar flow system was established to reflect the real sequelae *in vivo*. In this system, endothelial cells (ECs) were exposed to adequate shear stress during the cytoadhesion and stimulation with IEs. This system can reflect the human blood circulation by simulating vascular mechanobiology under physiological condition. Therefore, it provides a better way to investigate the interaction between IEs and ECs during *P. falciparum* infection.

Zusammenfassung

Die Infektion mit *Plasmodium falciparum* (P. *falciparum*) ist nach wie vor eine lebensbedrohliche Erkrankung und verursacht die tödlichste Form der Malaria. Zur Erklärung der Pathogenese und der pathophysiologischen Veränderungen während der Malaria wurden verschiedene Theorien vorgeschlagen. Eine davon betrifft extrazelluläre Vesikel (EVs). Diese werden als ein Schlüsselfaktor in der Interaktion zwischen Wirt und Parasit angesehen, da sie mit dem Schweregrad der Malaria in Verbindung gebracht werden. Der zugrunde liegende Mechanismus ist jedoch noch nicht geklärt. Das Ziel dieser Studie war, die EVs aus nicht infizierten und mit *P. falciparum* infizierten Erythrozyten (IE) zu charakterisieren. Der erste Schritt war die Aufreinigung der EVs und die Identifizierung der Morphologie der isolierten EVs mit Hilfe eines Transmissionselektronenmikroskops und eines Nanopartikel-Tracking-Systems. In einem zweiten Schritt wurden die miRNA-Profile der nicht infizierten Erythrozyten und der IEs sowie der von ihnen sezernierten EVs mittels Next Generation Sequencing (NGS) untersucht. Die Expression verschiedener miRNAs war in Erythrozyten und deren EV nach Infektion mit *P. falciparum* signifikant erhöht. Drittens wurden die Zielgene der differentiell exprimierten miRNAs mit bioinformatischen Ansätzen vorhergesagt, und eine funktionale Anreicherung zeigte, dass diese miRNA-Kandidaten eine Rolle in der Immunregulation während einer Infektion mit *P. falciparum* spielen.

Darüber hinaus wird der Zytoadhäsion, d. h. der Anheftung der Erreger an die Blutgefäße des Gewebes, eine große Bedeutung im Zusammenhang mit den Komplikationen der Malaria zugeschrieben. Die Zytoadhäsion zeichnet sich durch Liganden-Rezeptor-Interaktionen zwischen IE und dem menschlichen Endothel aus. IE exprimieren verschiedene Oberflächenantigene und binden an Adhäsionsrezeptoren, die sich auf der Oberfläche des Endothels befinden. Das primäre parasitäre Antigen, das die Zytoadhäsion vermittelt, wird durch das *P. falciparum* Erythrozytenmembranprotein 1 (PfEMP1) kodiert, das von einer Gruppe der var-Multigen-Familie kodiert wird. Das Ziel dieses Teilprojektes war die Entschlüsselung der var-Gene, die die Adhäsion an humane Hirnmikrogefäßendothelzellen (HBMEC) vermitteln. Um eine Population von *P. falciparum* mit hoher Bindungsaffinität zu HBMECs zu selektieren, wurde zunächst ein im Labor adaptierter *P. falciparum*-Stamm (IT4) auf HBMECs angereichert.

Mittels Transkriptomanalyse wurde eine signifikante Hochregulation von IT4_var19 und IT4_var13 nachgewiesen. Die Bindungsfähigkeit des angereicherten IT4 an die Endothelzellrezeptoren intercellular adhesion molecule 1 (ICAM-1) und endothelial protein C receptor (EPCR) wurde anschließend mit Hilfe von Bindungsassays nachgewiesen. Um die durch Zytoadhäsion ausgelöste zelluläre Reaktion zu entschlüsseln, wurde angereichertes IT4 mit HBMECs für 4 und 8 Stunden ko-inkubiert und das Transkriptom der HBMECs mittels NGS analysiert. Der Einfluss der IEs auf die HBMECs war signifikant. Die Analyse der Reactome-Signalwege zeigte, dass die 101 unterschiedlich exprimierten Gene (DEGs), die im 4-Stunden-Vergleich gefunden wurden, hauptsächlich im Bereich der Zytokin-Signalwege des Immunsystems zusammengefasst sind. Dazu zählten die Interferon-induzierten Signalwege und die Interleukin-Signalwege.

Wir haben immortalisierte Hirnendothelzellen (HBEC-5i) mit Plasma von Malariapatienten stimuliert, um die Rolle plasmodialer Faktoren in der Malariapathogenese zu untersuchen. Nach der Stimulation zeigten HBEC-5i eine signifikant erhöhte Sekretion von IL-11, CXCL5, CXCL8, CXCL10, Vascular Endothelial Growth Factor (VEGF) und Angiopoietin-like Protein 4 (ANGPTL4) im Vergleich zu HBEC-5i, die mit Plasma gesunder Spender stimuliert wurden. Die Transkriptomstudie an HBEC-5i zeigte außerdem, dass die Expression von 43 Genen nach Koinkubation mit Plasma von Malariapatienten erhöht war. Bioinformatische Analysen zeigten, dass diese DEGs hauptsächlich an biologischen Prozessen wie Zellmigration, Zellproliferation und Tubulusentwicklung beteiligt sind.

Darüber hinaus wurde ein Laminar-Flow-System etabliert, um die tatsächlichen Effekte in vivo widerzuspiegeln. In diesem System wurden Endothelzellen (ECs) während der Zytoadhäsion und der Stimulation mit IEs einer angemessenen Scherbelastung ausgesetzt. Dieses System kann den menschlichen Blutkreislauf widerspiegeln, indem es die vaskuläre Mechanobiologie unter physiologischen Bedingungen simuliert. Daher bietet es eine bessere Möglichkeit, die Interaktion zwischen IEs und ECs während einer Infektion mit *P. falciparum* zu untersuchen.

Abbreviations:

Ago2	Argonaute 2
APC	Activated Protein C
ATAD2	ATPase family AAA Domain-Containing Protein 2
ATF2	Activating Transcription Factor 2
ATS	Acidic intracellular Terminal Segment
Cav-1	Caveolin-1
CD	Cluster of Differentiation
CHO	Chinese Hamster Ovary
cICAM-1	circulating Intercellular Adhesion Molecule-1
CIDR	Cysteine-rich Interdomain Region
clag	Cytoadherence-Linked Asexual Protein
CM	Cerebral Malaria
CPM	Counts Per Million
CSA	Chondroitin Sulfate A
DAMP	Danger-Associated Molecular Patterns
DBL	Duffy-Binding-Like
DC	Domain Cassette
DEG	Differentially Expressed Gene
DGCR8	DiGeorge Syndrome Critical Region 8
dsRNA	double-stranded RNA
ECR	Endothelial Cell Receptor
ELISA	Enzyme-Linked Immunosorbent Assay
EPCR	Endothelial Protein C Receptor
etramp	Early Transcribed Membrane Protein
EV	Extracellular Vesicle
FTL	Ferritin Light Chain
g	gram
gC1qR	Complement C1q Receptor
Hb	Hemoglobin
HBEC-5i	Immortalized Human Brain Endothelial Cell

HBMEC	Human Brain Microvascular Endothelial Cell
HRP2	Histidine-Rich Protein 2
HSP90AA1	Heat Shock Protein 90 alpha Family Class A Member 1
HSV-1	Herpes Simplex Virus Type 1
ICAM-1	Intercellular Adhesion Molecule-1
IE	Infected Erythrocytes
IFIT	Interferon Induced Protein with Tetratricopeptide Repeats
IFN	Interferon
IL	Interleukin
ILV	Intraluminal Vesicles
iRBC	infected Red Blood Cell
IRF	Interferon Regulatory Transcription Factor
ISG	Interferon-Stimulated Gene
JHMV	JHM strain of mouse hepatitis Virus
LDL	Low-Density Lipoprotein
LFA-1	Lymphocyte Function-Associated antigen 1
MA-ARDS	Malaria-Associated Acute Respiratory Distress Syndrome
MAC-1	Macrophage Antigen 1
MDA5	Melanoma Differentiation-Associated Protein 5
MRE	miRNA Response Element
NCAM	Neuronal Cell Adhesion Molecule
NGS	Next Generation Sequencing
nMFI	normalized Median Fluorescence Intensity
NOS3	Nitric Oxide Synthase 3
OAS	2'-5'-Oligoadenylate Synthetase
P.	*Plasmodium*
P.f.	*Plasmodium falciparum*
P-adj	Adjusted *p*-value
PAMP	Pathogen-Associated Molecular Pattern
PAR-1	Proteinase-Activated Receptor 1
PBMC	Peripheral Blood Mononuclear Cell
pDC	plasmacytoid Dendritic Cell
PECAM-1	Platelet Endothelial Cell Adhesion Molecule-1

*Pf*EMP1	*Plasmodium falciparum* Erythrocyte Membrane Protein 1
phist	*Plasmodium* Helical Interspersed Subtelomeric
PKA-R	cAMP-Dependent Protein Kinase
PM	Placental Malaria
pre-miRNA	precursor microRNA
pri-miRNA	primary microRNA
PRR	Pattern Recognition Receptor
qPCR	quantitative Polymerase Chain Reaction
RBC	Red Blood Cell
rEPCR	recombinant Endothelial Protein C Receptor
RESA	Ring-infected Erythrocyte Surface Antigen
rif	Repetitive Interspersed Families of Polypeptides
RISC	RNA Induced Silencing Complex
RNaseL	Ribonuclease L
RPL41	Ribosomal Protein L41
RPS12	Ribosomal Protein S12
STAT1	Signal Transducer and Activator of Transcription 1
stevor	Subtelomeric Variant Open Reading Frame
STING	Stimulator of Interferon Genes
surfin	Surface-Associated Interspersed Protein
TARE	Telomere-Associated Repeat Element
TBK1	Tank Binding Kinase-1
TGF-β	Transforming Growth Factor-β
TNF-α	Tumor Necrosis Factor-α
UPS	Upstream Promoter Sequence
UTR	Untranslated Region
VCAM-1	Vascular Cell Adhesion Molecule-1

1. Introduction

1.1 Malaria disease:

Malaria remains one of the most severe infectious diseases all over the world. There were estimated 247 million malaria cases globally in 2021 including 619,000 death cases[1]. The causative agent of malaria is *Plasmodium spp.*. Among 200 species of *Plasmodium*, *P. falciparum*, *P. vivax*, *P. malariae*, *P. ovale* and *P. knowlesi* are capable of infecting human beings. The last few decades have seen advances in our knowledge of malaria disease and *Plasmodium* biology, the discovery of novel antimalarial drugs and more efficacious malaria vaccines. Although these progresses have dramatically limited the spreading of malaria, the elimination of malaria remains a distant goal yet to be achieved[2].

P. falciparum is the most lethal species of malaria parasite and is widely distributed in tropical and subtropical regions of the world, particularly in sub-Saharan Africa, Southeast Asia, and South America. In these regions, *P. falciparum* is responsible for a significant burden of illness and death, particularly in young children and pregnant women[3]. *P. falciparum* is a highly virulent parasite that causes severe illness and can quickly progress to life-threatening complications. Therefore, research on the prevention, treatment and control of *P. falciparum* has drawn the vast majority of research attention and funding. *P. falciparum*-infected red blood cells have the ability to adhere to the walls of small blood vessels, a process called cytoadherence. This can cause blockages in blood flow, leading to microvascular damage and organ dysfunction[4].

P. vivax is the most geographically widespread human malaria posing a significant public health threat, especially in the region of Americas and South-East Asia. Although it is less lethal than *P. falciparum*, this parasite is not benign and able to cause severe even fatal clinical outcomes[5, 6]. One of the unique features of *P. vivax* is its ability to form dormant liver stages, known as hypnozoites, which can remain in the host for months to years and reactivate, causing relapses of the disease[7]. Individuals infected with *P. vivax* usually exhibit low parasitemia due to the parasite's preferential invasion of reticulocytes. Hence thick blood smears are recommended for accurate diagnosis[8].

P. ovale was described by Dr. Stephens for the first time in 1922. This parasite exhibits high similarities to *P. vivax* in terms of morphology and biology[9]. Schüffner's dots can be demonstrated in the blood smear of both *vivax* malaria and *ovale* malaria patients. These tiny dark stipplings are actually caveola-vesicle complexes originating from parasites and can serve as a unique morphological feature[10].

P. malariae is known for its prolonged erythrocytic stage, lasting for 72 hours and fever occurs in *malariae* malaria patients in 72-hour intervals[11]. *P. knowlesi* has been recognised as the fifth human-infectious *Plasmodium* species. Owing to human activity in the habitat of long-tailed macaque, this emerging simian parasite *P. knowlesi* has been the most common cause of malaria in Southeast Asia and leads to fatal infections[12].

1.2   The life cycle of *Plasmodium*:

Malaria parasites are usually transmitted to vertebrates by female *Anopheles* mosquitoes. After female *Anopheles* mosquitoes bite the human body, sporozoites are injected into the dermis and penetrate the walls of blood vessels to enter the circulation[13]. Then sporozoites glide into the liver and pass through the hepatic sinusoidal barrier containing endothelial cells and Kupffer cells, ending with the hepatocyte invasion. Over the next 2 to 10 days, the sporozoites develop and replicate inside the liver cells, eventually dividing into approximately 40,000 merozoites, which are released into the bloodstream upon liver cells rupturing. Afterwards, free merozoites quickly enter the red blood cells via a series of processes within 2 min. Once the erythrocytic stage is established, merozoites continuously proliferate into rings, trophozoites and schizonts in the subsequent 36-72 hours, resulting in the destruction of red blood cells (RBCs) membrane and the release of 16-32 merozoites. Merozoites can invade new host cells and initiate the next round of asexual life cycle[14]. In some cases, a small percentage of merozoites differentiate into male or female gametocytes, which can be taken up by a mosquito vector during a blood meal. Male and female gametocytes fuse together and form an oocyst in the midgut of mosquito vectors. Oocysts differentiate into sporozoites and migrate from the abdomen of mosquitoes to the salivary glands[15, 16]. Consequently, mosquitoes containing sporozoites can bite a new host and spread the infection.

1.3   Clinical features of *falciparum* malaria:

The incubation period of malaria varies from 9 to 40 days, with the shortest incubation period being for *falciparum* malaria and the longest for *malariae* malaria. During this period, patients usually have no symptoms. In the next 2 to 3 days, patients experience symptoms similar to a mild viral infection, such as fatigue, headache, joint pain, and muscle pain. This is followed by fever which is the most crucial feature of malaria infection and spikes rapidly up to 40 ℃ in children[17]. The febrile response often occurs in periodic intervals and is accompanied by abdominal pain, nausea, vomiting, diarrhea, pallor and jaundice. This is due to the rupture of mature schizonts and immune response stimulated by parasite-derived antigens. These protean symptoms tend to recede gradually after appropriate and timely anti-malaria treatment[18].

1.3.1   Severe *falciparum* malaria:

The severity of malaria in patients is influenced by a series of factors, including *Plasmodium* species, age, genetic constitution, malaria-specific immunity, previous exposure to anti-malarial drugs and parasite density[19, 20]. Non-severe malaria refers to patients show malaria symptoms and a positive parasitological test either by microscopy or rapid diagnostic test but with no features of severe malaria. Severe malaria or complicated malaria is defined by one or more of the manifestations including impaired consciousness, prostration, shock, pulmonary edema, jaundice, acidosis, etc., occurring without an identified cause and in the presence of *P. falciparum* asexual parasitemia[21]. This is a medical emergency and lethal without intervention[22]. Most of the death cases occur in children and are presented by three syndromes separately or simultaneously: severe anemia, cerebral malaria (CM) and respiratory distress[23].

1.3.1.1 Anemia:

Although there is a wide variation in the definitions of anemia in cases of malaria, hemoglobin concentration is the most common indicator of anemia classification in high-transmission areas. Acute malaria patients can be defined as mild anemia if their hemoglobin (Hb) concentration is between 8 g/dL and 11 g/dL, moderate anemia if Hb is between 5 g/dL and 8 g/dL, and severe

anemia if Hb is less than 5 g/dL. The primary cause of anemia is high parasite density, which leads to the destruction of both parasitized and unparasitized RBCs. Concomitant contributors include inadequate healthcare system and infrastructure, the presence of multiple infectious diseases and nutritional deficiencies[24].

1.3.1.2 Cerebral malaria:

Cerebral malaria refers to patients presenting unrousable coma of unknown origin and *P. falciparum* parasitemia[21]. Malarial retinopathy is characterized by a range of abnormalities in the retina, including retinal whitening, vessel changes, retinal hemorrhages, and papilledema. Examination of the retina may serve as a clinical feature to differentiate malarial from non-malarial induced coma[25]. CM is uncommonly observed in adults, but more prevalent among children under the age of 5 residing in high-transmission regions[1]. Even with early and prompt treatments, the mortality rate of cerebral malaria is estimated to be between 15% and 25%. Additionally, around 25% of individuals who survive cerebral malaria may experience long-term sequelae such as cognitive and sensory impairment, epilepsy, and stroke[26].

Multiple factors are involved in the pathophysiology of CM. Of them, parasite sequestration is considered the main cause, which results in the swelling of brain capillaries and post-capillary venules, leading to impaired microcirculation and disruption of the blood-brain barrier (BBB). All of these events ultimately lead to cerebral hypoxia and impaired glucose metabolism, as evidenced by elevated lactate and alanine concentrations in CM patients[27]. Moreover, the roles of immune cell accumulation and coagulation dysfunction in the development of CM have also been increasingly recognized as systematic inflammatory responses and activation of coagulation observed in CM patients[28]. However, our understanding to the dynamic interactions of these three mechanisms are still for the most part incomplete[29].

1.3.1.3 Acute respiratory distress syndrome

Malaria-associated acute respiratory distress syndrome (MA-ARDS) is a severe complication of malaria infection that typically affects adults rather than children[30]. MA-ARDS is characterized by marked, diffuse inflammation in the lungs, which leads to damage of the

alveolar-capillary membrane, increased permeability of blood vessels, insufficient exchange of gases and the accumulation of fluid in the alveoli[31]. Apart from the classical vascular sequestration factor, the margination and infiltration of inflammatory cells, platelets, and red blood cells in blood vessels, interstitial tissue, and alveoli of the lungs are crucial determinants of the pathogenesis of MA-ARDS[32].

1.4 Multigene families of *P. falciparum*

P. falciparum has a 23-megabase genome which encodes about 5,300 genes and is spread across 14 chromosomes. Genes responsible for antigenic variation are predominantly clustered within the subtelomeric regions of chromosomes. Compared to the genomes of free-living organisms, the genome of *P. falciparum* contains a larger number of genes that are involved in immune evasion and host-parasite interaction[33]. One unique genome characterization that different with other *Plasmodium* spp. is the significant genetic diversity in the subtelomeric regions and conserved sequence in the central regions of chromosomes[33, 34]. Sequence variation can arise from different genetic mechanisms, such as the insertion, deletion, or transposition of gene variants, mutations, or segmental duplications during mitotic growth, as well as translocations between chromosomes[35-39]. The noncoding subtelomeric region in *P. falciparum* genome is composed of six distinct telomere-associated repeat elements (TARE), which is adjacent to telomere repeats[40]. TARE region is followed by a *var* gene member that encodes *Plasmodium falciparum* erythrocyte membrane protein 1 (*Pf*EMP1), which is a virulence factor that is involved in the adherence of infected red blood cells to the vascular endothelium[41]. Following the *var* gene member, there are *rif* and *stevor* genes that encode *P. falciparum*-encoded repetitive interspersed families of polypeptides (*rif*) and subtelomeric variant open reading frame (*stevor*), respectively. These genes belong to multigene families that are unique to *P. falciparum*[42-45]. Other multigene families that are found in the subtelomeric region of the *P. falciparum* genome include *etramp*, *surfin*, *phist*, *clag* and *fikk*, which encode early transcribed membrane protein, surface-associated interspersed protein, *Plasmodium* helical interspersed subtelomeric, cytoadherence-linked asexual protein, and FIKK kinase, respectively[46-50].

1.4.1   *Pf*EMP1:

*Pf*EMP1 is encoded by *var* genes and considered the most important surface antigen. There are approximately 60 *var* genes per *P. falciparum* genome[33]. Each *var* gene contains two exons. Exon I encodes the extracellular part of *Pf*EMP1, which encompasses cysteine-rich interdomain regions (CIDRs) and Duffy-binding-like (DBL) domains. While exon 1 exhibits intraclonal and interclonal sequence variation, exon 2 is relatively conserved and responsible for encoding the transmembrane domain and the acidic intracellular terminal segment (ATS)[51]. One key feature of *var* genes is they are expressed in a mutually exclusive manner, meaning that only one member of *var* genes is expressed in an individual parasite while the others are silenced or repressed[52].

DBL domains could be divided into four main types (α, β, γ, δ, ε, ζ, x) and CIDR domains into three main types (α, β, γ), each with additional subtypes[51]. Despite the massive sequence diversity, *Pf*EMP1 proteins can be categorized into group A, group B, group B/A, group C, group B/C and group E based on their chromosomal position, upstream promoter sequence (UPS), and the direction in which the *var* genes that encode them are transcribed[53]. *var* genes belonging to group A, group B, and group B/A are commonly located in the subtelomeric regions of chromosomes, whereas group C and group B/C *var* genes are typically found in internal regions of chromosomes 4, 7, 8, and 12. The transcription direction of group A *var* genes is towards the telomere, whereas that of group B and B/A *var* genes is towards the centromere[33, 51, 53, 54].

The N-terminus of the *Pf*EMP1 molecule typically contains a semi-conserved head structure composed of a DBLα domain and a CIDR domain in tandem. Head structure is followed by DBL-CIDR pair in most *Pf*EMP1 proteins belonging to group B, B/C and C. However, group A and B/A *Pf*EMP1 proteins are relatively large and constituted by further DBL-CIDR tandem and DBL domains[55]. Although there are multiple subtypes of DBL and CIDR domains, their pairing is not random. These specific combinations are identified as domain cassettes (DCs), such as DC8 (DBLα2-CIDRα1.1-DBLβ12-DBLγ4/6) and DC13 (DBLα1.7-CIDRα1.4)[51].

1.4.2   RIFIN:

RIFIN proteins are encoded by ~150 *rif* genes, which usually contain ~1,000 bp and two exons[33]. The functions of RIFINs for the most part remain unknown. One study has found that RIFIN displayed the ability to cause massive rosetting, which defined as the binding of uninfected red blood cells to an infected one (iRBC). This process is mediated by this specific RIFIN and blood group A antigen on RBCs[56]. Rosetting phenomenon is directly linked to malaria severity as *Plasmodium* isolates from severe malaria patients show a higher capacity of rosette formation than those from mild malaria patients[57, 58].

It is proposed that rosetting provides huge advantages for parasites survival. IRBCs are protected from the attacks from host immune cells by hiding among uninfected RBCs[59]. Moreover, surrounding RBCs serve as ideal invasion targets for freshly released merozoites once the central iRBCs rapture[60]. A systematic meta-analysis has concluded that blood group O population is not prone to severe malaria whereas blood antigen A, B and AB are the risk factors for severe malaria[61]. This conclusion may further stress the importance of RIFINs and rosetting during severe malaria progression.

1.4.3   STEVOR:

STEVOR proteins show similar features as B-RIFINs. Both are encoded by ~30 copies of each gene family and absence of insertion-deletion domain in their extracellular structure. In addition, some STEVORs and B-RIFINs are expressed on RBC surface during merozoite and gametocyte stages[62]. STEVORs also play a role in rosetting via binding to glycophorin C on uninfected RBC membrane[45]. Although the detailed function of most STEVORs still under investigation, one study has suggested STEVORs may alter the mechanical properties of erythrocyte membrane and are linked to the decreased deformability and increased rigidity of iRBCs[63].

1.5   Pathogenesis of *P. falciparum* infection:

The development manner of malaria infection is a rather complex story, including numerous factors, settings and mechanisms. The pathogenesis of *P. falciparum* infection is an intricate

network that build by massive players from *P. falciparum* and host cells. Cytoadhesion is considered the principal mechanism and the most studied to date. IRBCs sequester in the microvasculature of various organs, leading to vessel occlusion, reduced blood flow, and ultimately vital organ dysfunction[64]. Besides, *P. falciparum*-induced inflammation is also a critical contributor for malaria development. Inflammation can be triggered by various factors, including *P. falciparum*-derived antigens which are immunogenic as well as *P. falciparum*-secreted extracellular vesicles[65].

1.5.1   Cytoadhesion:

Cytoadhesion, which refers to iRBCs become sticky and adhere to tissue vasculature, is considered of great significance.[64] By anchoring to tissue endothelium, iRBCs are able to form blood clots and blook the bloodstream, ultimately lead to in inflammation, tissue hypoxia and necrosis and organ dysfunction. This phenomenon is observed particularly in vital organs such as brain, lung and kidney, indicating cytoadhesion as a key player in severe malaria pathogenesis[66, 67].

Cytoadhesion is considered as a strategy of growth protection of *Plasmodium* by avoiding splenic clearance. One of the principal functions of spleen in circulation system is filtering RBCs, so that RBCs with low deformability are unable to cross inter-endothelial slits and are destroyed by local macrophages[68]. However, by sticking to the endothelial wall, iRBCs escape from the inspection of splenic macrophages even though parasites remodel host cells and alter the mechanical features of the RBC membrane[4].

Cytoadhesion is characterized by ligand-receptor interactions between iRBCs and human endothelium. IRBCs express various surface antigens such as *Pf*EMP1, RIFIN and STEVOR and bind to the adhesion receptors on endothelial surface. *Pf*EMP1 is the most extensively studied antigen and the critical virulence factor of *P. falciparum*[69]. Till now, at least 24 endothelial cell receptors (ECRs) have been described as the binding receptors of iRBCs. These include cluster of differentiation 36 (CD36), intercellular adhesion molecule-1 (ICAM-1), endothelial protein C receptor (EPCR), chondroitin sulfate A (CSA), platelet endothelial cell

adhesion molecule-1 (PECAM-1), vascular cell adhesion molecule-1 (VCAM-1), neuronal cell adhesion molecule (NCAM), P-selectin, E-selectin, etc[70-74].

1.5.1.1 Cytoadhesion via CD36:

CD36, also known as platelet glycoprotein 4, is a protein that is primarily expressed on the surface of various cells, including red blood cells, platelets, and endothelial cells. CD36 plays multiple physiological functions, including lipid metabolism, inflammation, angiogenesis, and innate immunity[75]. CD36 serves as a scavenger receptor that binds to a wide range of ligands, including fatty acids, oxidized lipids, lipoproteins, and thrombospondin-1. It plays an important role via the recognition and clearance of apoptotic cells and the uptake of oxidized low-density lipoprotein (LDL) by macrophages[75, 76].

Mounting evidence indicates CD36 as the primary binding receptor in cytoadhesion as both the majority of clinical isolates from patients and laboratory-adapted strains bind to CD36[77]. CD36 exhibits the binding affinity to CIDRα2-6 domain in the head structure of *Pf*EMP1 and at least 75% of *Pf*EMP1 putatively contain this CD36-binding domain[78]. Although CD36-binding CIDRα2-6 domains exhibit massive sequence diversity, they still share a conserved hydrophobic pocket that can accommodate a phenylalanine residue located at the membrane-distal tip of CD36[79]. CD36 is widely expressed on a range of endothelial cells, but it also shows different expression tropism. The expression of CD36 is more abundant in non-vital tissues like skin, muscle and adipose tissue than the brain[77]. Moreover, there is no compelling evidence that indicates the association between binding to CD36 with complicated malaria[80].

Altogether, these findings suggest CD36-mediated cytoadhesion is universal to various *P. falciparum* isolates with the significance of promoting parasite survival and spread while causing limited damage to host.

1.5.1.2 Cytoadhesion via ICAM-1:

ICAM-1 is a cell surface glycoprotein that is constitutively expressed at low levels in various cells including immune cells, endothelial cells, and epithelial cells. However, its expression can be upregulated in response to various inflammatory stimuli such as cytokines including tumor

necrosis factor-α (TNF-α), interleukin-1 β (IL-1β) and interferon γ (IFNγ) [81]. ICAM-1 is well-known for serving as adhesion receptor and recruiting leukocytes from circulation to the inflammation sites, thereby aiding in the clearance of pathogens and damaged tissues[82]. The physiological ligands of ICAM-1 include cognate lymphocyte function-associated antigen 1 (LFA-1) and macrophage antigen 1 (Mac-1) present on the surface of various immune cells[83]. Intriguingly, numerous studies have demonstrated that ICAM-1 also displays with some types of *Pf*EMP1 on iRBCs via binding to certain domain structures. For group A *Pf*EMP1 proteins, DBLβ1 and DBLβ3 are the specific subclasses that have been shown to bind ICAM-1, while for group B, it is the DBLβ5 subclass that is capable of binding ICAM-1[72].

Post-mortem studies of fatal malaria cases have also shown that ICAM-1 is highly expressed in cerebrovascular tissue[80]. One study described clinical isolates from cerebral malaria patients can bind to HBMECs under flow condition and this binding phenotype can be inhibited by specific αICAM-1 antibody. In addition, the mRNA expression level of *var* genes encoding ICAM-1 binding domains of DBLβ1, DBLβ3, and DBLβ5 were significantly higher in CM isolates compared to uncomplicated malaria isolates[84]. Moreover, a recent study has revealed the precise structural characterizations for ICAM-1 binding to corresponding DBLβ domains employing crystallography approaches[85]. Collectively, ICAM-1 as a key adhesion receptor may play a vital role in cerebral malaria infection.

1.5.1.3 Cytoadhesion via EPCR:

EPCR is a transmembrane glycoprotein expressed on the surface of endothelial cells, which line the inner surface of blood vessels. EPCR serves as a receptor for activated protein C (APC), a key regulator of blood coagulation and inflammation[86]. When APC binds to EPCR on the surface of endothelial cells, it promotes the cleavage of proteinase-activated receptor 1 (PAR-1). The activation of PAR-1 inhibits the nuclear factor-κB pathway and induces anti-inflammatory and anti-apoptotic activity. Therefore, this delicate system of APC and EPCR is essential to maintain the balanced cytokine response, anti-apoptotic effect and endothelial barrier integrity[87].

However, iRBCs can compete for the binding site on EPCR with protein C. Accordingly, these iRBCs might interfere with normal ligands and disrupt their protective effects[88]. The first

consequence is the increased release of IL-1 and TNFα which act as pro-inflammatory cytokines, inducing EPCR shedding from the endothelial surface and upregulating ICAM-1 expression levels. ICAM-1 severs as a key adhesion receptor and further exacerbates the vascular sequestration. Furthermore, iRBC-EPCR interaction also interrupts PAR-1-mediated barrier protection, triggering enhanced endothelial permeability and impairment of tight junctions and barrier integrity[89].

This iRBC-EPCR interaction may particularly affect the microvascular endothelium of the brain. The CIDRα1 domain in the head structure of PfEMP1 is thought to be responsible for adhesion to EPCR as measured by biophysical approach and verified by binding assay using recombinant PfEMP1 containing CIDRα1 and Chinese hamster ovary cells (CHO) overexpressing EPCR[73]. CIDRα1 domain presents in PfEMP1 containing DC8 (DBLα2-CIDRα1.1-DBLβ12-DBLγ4/6) and DC13 (DBLα1.7-CIDRα1.4)[51]. In addition, a significantly upregulated transcription level of CIDRα1 domain subtypes, such as CIDRα1.1, CIDRα1.4, CIDRα1.5a, CIDRα1.6a and CIDRα1.7, were observed in P. falciparum isolates from cerebral malaria patients versus UM cases[84]. Besides, the EPCR-binding PfEMP1 is linked with brain swelling in pediatric cerebral malaria, which indicates poor outcomes and high malaria mortality[90].

1.5.1.4 Cytoadhesion via CSA:

CSA is a low-sulfated glycosaminoglycan and expressed in the syncytiotrophoblast layer of the placenta, which is the outermost layer of cells that come in contact with maternal blood[91]. A specific group E PfEMP1, also known as VAR2CSA, can adhere to the syncytiotrophoblastic lining of the fetal villus via binding to CSA and cause placental malaria (PM)[92]. PM is a leading cause of maternal and fetal morbidity and mortality in areas of high malaria transmission[93]. The infection results in the accumulation of iRBCs in the placenta, causing placental inflammation and impaired function, leading to adverse outcomes such as low birth weight, preterm delivery, and fetal death[94]. VAR2CSA binding phenotype is unique as VAR2CSA is the only parasite-derived antigen that binds to placental CSA[92]. Additionally, although var gene family is known for its extensive genetic diversity, var2csa is highly

conserved across all strains of *P. falciparum*[95]. VAR2CSA is a relatively large-weight protein of 350 kDa and the DBL2x domain is considered the CSA-binding region[96].

1.5.2   Other parasite-derived factors:

Although VSA-mediated cytoadhesion is considered the most principal pathogenesis during malaria infection, the contribution of other *P. falciparum*-derived players has also been recognized in the pathophysiological trajectories of disease. These foreign antigens may serve as pathogen-associated molecular patterns (PAMPs) and danger-associated molecular patterns (DAMPs) and recognized by endothelial cells and innate immune cells that equipped with pattern recognition receptors (PRR), triggering corresponding immune reactions and disease progression[97].

P. falciparum histidine-rich protein 2 (HRP2) is produced and exported by the parasite into the RBC cytosol and released into the bloodstream as host cell rupture. HRP2 can bind to an unknown receptor on human brain endothelial cells and activate inflammasome, leading to the recruitment of caspase-1 and maturation of IL-1β[98]. IL-1β and IL-1R-mediated signal aggregates with the downstream signaling from inflammasome activation, resulting in the activation of NFkB and eventually causing the redistribution of tight junction proteins and impaired BBB integrity[98].

P. falciparum can uptake host hemoglobin into food vacuole and convert it into an insoluble and detoxified crystalline form called hemozoin. Once liberated during schizogony, free hemozoins are rapidly engulfed by immune cells and induce the production of IL-1β in NLRP3 inflammasome-dependent manner in macrophages and dendritic cells[99]. In addition, a study has revealed that plasmodial genomic DNA that coated on hemozoins may activate the core stimulator of interferon genes (STING)-Tank binding kinase-1 (TBK1)-interferon regulatory transcription factors (IRF) signaling pathway[100].

Altogether, these lines of studies imply that parasite-derived factors implicate as triggers of innate immune response by the recognition of corresponding sensors and facilitate vascular inflammation.

1.5.3   Extracellular vesicle as a new player:

The last 20 years have witnessed a rapidly growth in researches of extracellular vesicles (EVs) in malaria biology and disease development. Mounting studies have highlighted the importance of EVs in malaria susceptibility, pathogenesis and cell-cell communication.

EVs can be classified into exosomes and microvesicles in terms of their size and different origins. Exosomes are typically smaller in size, ranging from about 30-150 nanometers (nm) in diameter, and display a cup-shaped appearance with a lipid bilayer membrane viewed under an electron microscope[101]. Exosomes are derived from the endosomal pathway, where they are formed as intraluminal vesicles (ILVs) within endosomes and are subsequently released as exosomes once the endosomes fuse with the plasma membrane[102]. Microvesicles, on the other hand, are generally larger in size, ranging from about 100-1000 nm, and may have a more irregular shape compared to exosomes. Microvesicles are formed by outward budding and fission of the plasma membrane, resulting in the shedding of vesicles directly from the cell surface[103]. EVs are known to contain a diverse array of molecular cargo, including proteins, lipids, DNAs, and RNAs. EVs can fuse with the plasma membrane of target cells or be internalized by endocytosis, allowing the transfer of incorporated contents into the cytoplasm of the recipient cells[104].

1.5.3.1 EVs in malaria:

The diverse functions and cellular potency of EVs have garnered significant attention in the field of malaria research. A study was initiated to investigate the relationship between circulating erythrocyte-derived EVs and malaria infection. They detected significantly higher RBC-derived EV concentration in patients infected with *P. falciparum, P. vivax* or *P. malariae* in comparison of healthy controls on admission. Moreover, RBC-derived EV concentrations are linked to disease severity as severe *falciparum* malaria patients showed a significantly higher RBC-derived EV concentrations than in patients with mild *falciparum* malaria. The authors also used ring-infected erythrocyte surface antigen (RESA), a unique *Plasmodium* protein on the membrane of iRBCs, to distinguish whether the circulating RBC-derived EVs are from uninfected RBCs or iRBCs. The results proved RESA-positive EVs account for a high proportion of the total EVs, denoting the vital role of iRBCs in EVs production[105].

Afterwards, researchers focused on the distinct roles of RBC-derived EVs, particularly in intercellular communication and immunomodulatory functions. In 2013, Regev-Rudzki et al generated two genetically modified parasite strains and each strain was transfected with plasmid separately expressing drug resistance genes for the resistance to WR99210 or blasticidin. Interestingly, they observed when the two parasite strains were cocultured and treated with both WR and blasticidin simultaneously, some parasites can survive from the drug selection pressure in spite of the fact that each strain was capable of resisting only one drug. This observed drug resistance-sharing phenotype can be achieved without direct cell-cell contact, implying there are undefined communicators responsible for plasmid transfer[106]. Actin and microtubules are crucial molecules for vesicle secretion[107]. Potent inhibitors of actin and microtubules significantly decreased the number of survived parasites from drug selection in a dose-dependent manner, further indicating EV are the key messenger mediating communication between cells. In addition, EVs may also influence the differentiation of blood-stage parasite since the author observed increased number of gametocytes in the survival of drug-selected parasites[106].

Following studies further investigated the exact components of RBC-derived EVs and their roles in mediating parasite-host interaction. In one study, parasite-derived EVs were purified from culture supernatants of 3D7 and CS2 strains and protein profiles were identified using a mass spectrometry-based approach. Both host RBC-derived proteins and parasite-derived materials were detected, containing proteins related to RBC lipid rafts such as stomatin and band 3, as well as parasite membrane-associated antigens such as SBP1 and RESA. Further Gene Oncology enrichment analysis of parasite-derived proteins revealed that these proteins were involved in Maurer's clefts activity, parasitophorous vacuole membrane and merozoite invasion behavior. Next, the phenotypic effect of EVs on different subsets of immune cells were illustrated. CD14^{+} monocytes were the main recipient cells of EVs and coculture of EVs and differentiated macrophages revealed upregulated expression of proinflammatory cytokines such as IL-6, IL-12 and IL-1β and the anti-inflammatory cytokine IL-10 at both mRNA and protein expression levels[108]. The miRNA contents were also analyzed by the same research group. A subset of miRNAs was identified in EVs and miR-451a is the most dominate. Human protein Argonaute 2 (Ago2) also exists in EVs and is able to form a functional stable silencing complex with miRNAs[109]. Besides, parasite genomic DNAs also appeared in EVs. Double-

strand DNAs can be sensed by cytosolic STING protein and activate the STING-TBK1-IRF3 axis in monocytes[110]. NK cells can uptake EVs purified from iRBCs and the RNA cargo can activate Melanoma Differentiation-Associated Protein 5 (MDA5), an intracellular PRR sensing pathogen-derived RNA, and downstream effector molecules[111].

1.5.3.2 MiRNA as key player in EVs:

As the multiple functions of EVs have been illustrated, accumulating studies further explored the roles of exact cargoes, particularly miRNAs, which utilize EVs as vehicles for propagation. MiRNAs are a class of small non-coding RNAs of 18-23 nucleotides in length and involved in a series of biological process via regulating gene expression in different ways[112].

The majority of miRNA sequence locations are on the non-coding region of genome and its biogenesis can be grouped into the dominant canonical pathway and non-canonical pathway[113]. The first step of canonical pathway is the synthesis of the initial primary miRNAs (pri-miRNAs) from their genes. Pri-miRNAs have a duplex and characteristic hairpin structure. Then a protein called DiGeorge Syndrome Critical Region 8 (DGCR8) and Drosha, a ribonuclease enzyme, Drosha, can form a microprocessor complex and cleave pri-miRNAs into precursor miRNAs (pre-miRNAs)[114]. Pre-miRNAs are transported into cytoplasm by exportin 5 and RanGTP complex and cropped by the RNase endonuclease Dicer[115]. The terminal loop structure is removed by this process, generating a mature miRNA duplex which contains a guide strand and a passenger strand[116]. Afterwards, duplex structure is unwound and the guide strand can be loaded into Ago proteins and form a functional RNA induced silencing complex (RISC) whereas the passenger strand is degraded[117].

Due to the complementarity between the mature miRNA and the target mRNA, the guide strand of miRNA can specifically bind to the 3' untranslated region (3' UTR), 5' UTR, the coding sequence as well as the gene promotor regions[118]. The complementary sequences on target mRNA are deemed miRNA response elements (MREs). A highly matched complementarity between the mature miRNA and MREs in target mRNA activates AGO2 endonuclease function and catalyze the cleavage of the target mRNAs at specific sites[119]. This cleavage results in the degradation of the target mRNA, preventing its translation into protein and effectively silencing the gene[120]. In addition, a partial complementarity may induce translational

repression. In this case, RISC complex can inhibit translation by preventing the ribosome from initiating translation or by stalling the ribosome during translation[117]. Notably, one single miRNA can have multiple mRNAs as targets therefore regulate a huge number of genes and several miRNAs can function in parallel on the same mRNA candidate[117].

1.5.3.3 MiRNA and malaria:

Since the observed impact of EVs on malaria biology and host immunoregulation, the profiles and key functions of miRNAs have also been investigated. In one study, EVs were isolated from patients infected with *falciparum* malaria or *vivax* malaria and 5 potentially involved miRNAs were detected by quantitative polymerase chain reaction (qPCR). The expression levels of EV-derived has-miR-150-5p and has-miR-15-5p were significantly increased in *P. vivax*-infected patients compared to healthy individuals and has-let-7a-5p was highly expressed in both *vivax* malaria patients and *falciparum* malaria patients. Bioinformatic prediction revealed that the target genes of these miRNAs are involved in adherens junction and transforming growth factor-β (TGF-β) pathways[121]. Adherens junction is crucial to maintain the integrity of BBB and TGF-β has been proved as a regulator of immunological balance in malaria infection, suggesting miRNAs might be the potential contributors in malaria pathogenesis[122].

Moreover, miRNAs also have impact on parasite biology. Human Ago2 protein and an array of miRNA has been detected in the cytoplasm of both iRBCs and uninfected RBCs. *P. falciparum* is able to import Ago2 and miRNAs into the nucleus[123]. Since *P. falciparum* lacks the essential functional proteins such as Dicer and Drosha for miRNA maturation, it is believed that *P. falciparum* cannot express miRNAs by itself[124]. Researcher speculated *P. falciparum* might utilize human Ago and miRNAs to regulate gene expression. In one study, researchers firstly used *in silico* hybridization method and found the putative target gene of miR-150-3p and miR-197-5p, the gene encoding apicortin, which constitutes the apical complex structure. Transfection of miR-150-3p and miR-197-5p downregulated apicortin at both mRNA and protein expression level. In addition, hindered *P. falciparum* growth rate and impaired invasion to host erythrocytes were observed when parasite exposed to synthesized miR-150-3p and miR-197-5p mimics[125].

1.6 Aim of the study:

In this study, we seek to investigate the interplay between the host and *P. falciparum* from two different aspects: cytoadhesion and inflammation. In chapter I, we set out to characterize EVs secreted from *P. falciparum*-infected erythrocytes. Firstly, EVs derived from uninfected erythrocytes and *P. falciparum*-infected erythrocytes were purified. Secondly, the morphology of isolated EVs were further identified by transmission electron microscope and nanoparticle tracking system. Thirdly, the miRNA profiles of EVs derived from uninfected erythrocytes and *P. falciparum*-infected erythrocytes were analyzed by next generation sequencing (NGS).

In chapter II, we focused on the effect of *P. falciparum* cytoadhesion signal on human brain microvascular cells (HBMECs). Firstly, a laboratory-adapted *P. falciparum* strain (IT4) was enriched over HBMECs to select out a *P. falciparum* population exhibiting high binding affinity to HBMECs. Secondly, the transcriptome of enriched IT4 was analyzed by NGS to elucidate the *var* genes that mediate cytoadhesion. Thirdly, enriched IT4 was co-incubated with HBMECs for 4 and 8 hours. In the end, the transcriptome of HBMECs was analyzed by NGS to decipher cytoadhesion-induced cellular response.

2. Chapter I:

2.1 *Plasmodium falciparum* infection reshapes the human microRNA profiles of red blood cells and their extracellular vesicles.

1 **_Plasmodium falciparum_ infection reshapes the human microRNA profiles of red blood cells**
2 **and their extracellular vesicles**

3 Yifan Wu, Stephanie Leyk, Hanifeh Torabi, Katharina Höhn, Barbara Honecker, Maria del Pilar Martinez Tauler,
4 Dániel Cadar, Thomas Jacobs, Iris Bruchhaus, and Nahla Galal Metwally*

5 *Correspondence: metwally@bnitm.de
6

In brief

8 We found that _Plasmodium falciparum_ infection affects the expression levels of several miRNAs
9 in both human red blood cells and their secreted extracellular vesicles. We hypothesize that
10 these miRNAs may act to modulate the host immune response and in turn the outcomes of
11 malarial patients.

Highlights

13 • _Plasmodium falciparum_ infection resulted in significantly higher expression of nine
14   miRNAs in red blood cells (RBCs) and their secreted extracellular vesicles (EVs).
15 • Infection also resulted in downregulation of some members of the let-7 family of
16   miRNAs in both RBCs and their secreted EVs.
17 • Hsa-miR-451a was the most abundant secreted miRNA, but its expression level in RBCs
18   and their EVs was not affected by _P. falciparum_ infection.
19 • The miRNAs that were differentially expressed in RBCs and their EVs target genes that
20   play roles in immune responses.
21
22
23
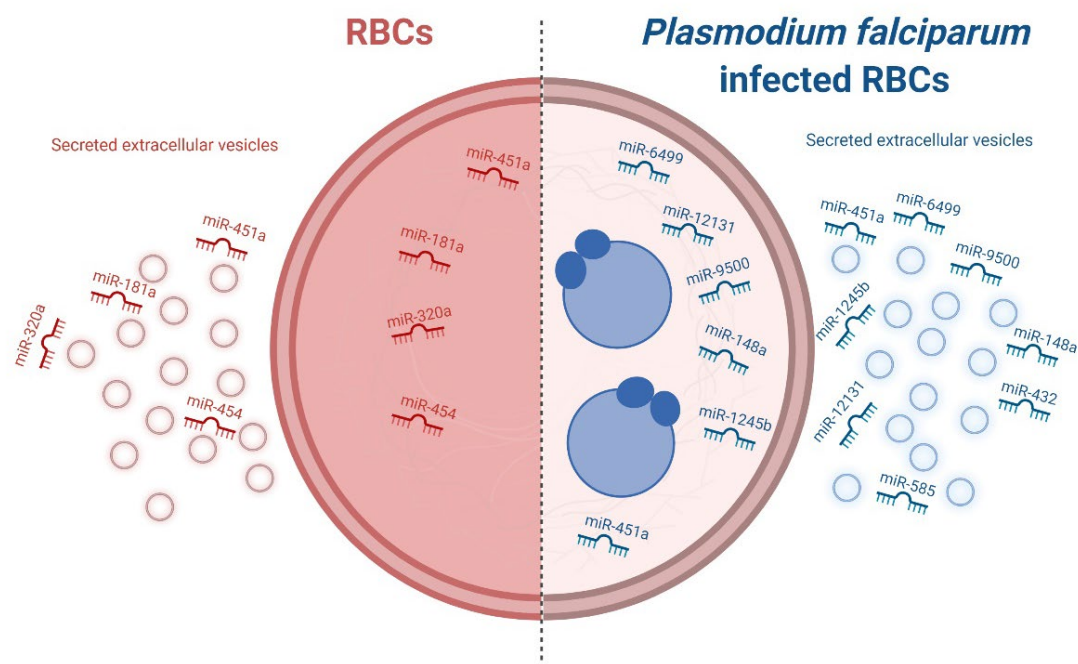
27 **_Plasmodium falciparum_ infection reshapes the human microRNA profiles of red blood cells**

28 **and their extracellular vesicles**

29 Yifan Wu[1], Stephanie Leyk[2], Hanifeh Torabi[1], Katharina Höhn[3], Barbara Honecker[1], Maria del Pilar Martinez

30 Tauler [1], Dániel Cadar[3], Thomas Jacobs[2], Iris Bruchhaus[1&5], and Nahla Galal Metwally[1, *]

31 [1] Research group Host Parasite Interaction, [2] Research group Protozoa Immunology, [3] Cellular Parasitology Department, [4]

32 Arbovirology Department, Bernhard Nocht Institute for Tropical Medicine, Hamburg, Germany. [5] Biology Department

33 University of Hamburg, Hamburg, Germany

34 *Correspondence: metwally@bnitm.de

SUMMARY

36 _Plasmodium falciparum_, a human malaria parasite, develops in red blood cells (RBCs), which

37 represent approximately 70% of all human blood cells. Additionally, RBC-derived extracellular

38 vesicles (RBC-EVs) represent 7.3% of the total EV population. The roles of miRNAs in the

39 consequences of _P. falciparum_ infection are unclear. Here, we analyzed the miRNA profiles of

40 non-infected human RBCs (niRBCs), ring-infected RBCs (riRBCs), and trophozoite-infected RBCs

41 (trRBCs), as well as those of EVs secreted from these cells. Hsa-miR-451a was the most

42 abundant miRNA in all RBC and RBC-EV populations, but its expression level was not affected

43 by _P. falciparum_ infection. Overall, the miRNA profiles of RBCs and their EVs were altered

44 significantly after infection. Most of the differentially expressed miRNAs were shared between

45 RBCs and their EVs. A target prediction analysis of the top nine common upregulated miRNAs

46 revealed the possible identity of the genes targeted by these miRNAs (such as CXCL10, OAS1,

47 IL7, and CCL5) involved in immunomodulation.

KEYWORDS:

49 _P. falciparum_, RBCs, microRNAs, NGS, Malaria, Cerebral malaria, mRNA, Extracellular vesicles,

50 Immunomodulation, miRNA profiles.

INTRODUCTION

52 Malaria has a major impact on human health worldwide. According to the World Health

53 Organization, malaria killed 627,000 people in 2020, representing a 12% increase in the death

54 rate from 2019, which was attributed to service disruption due to the COVID-19 pandemic.

55 Notably, 77% of the malaria-related deaths in 2020 were children under 5 years of age (WHO,

56 2020). In the same year, 11.6 million pregnant women were diagnosed with malaria infection,

57 resulting in 819,000 children with low birthweight (WHO, 2020). Malaria is caused by five

58 species of the genus *Plasmodium*, although *P. falciparum* is responsible for most malaria-

59 related deaths (WHO, 2020).

60 Cerebral malaria (CM) is a severe neurological complication of *P. falciparum* infection. The

61 pathogenic basis of CM is poorly understood, but cytoadhesion and the host immune response

62 are thought to be involved. Red blood cells (RBCs) have long been recognized as a perfect

63 shelter for *Plasmodium* parasitic invaders, providing them with not only abundant food

64 resources but also protection against host immune attacks. Upon entry into RBCs, *P. falciparum*

65 uses different strategies to survive. For example, the parasite changes the morphology of

66 infected RBCs (iRBCs) by inducing the production of knob-like protrusions on the cell surface

67 (Rug et al., 2006). These protrusions provide a scaffold for the correct presentation of the

68 parasite's major virulence protein, erythrocyte membrane protein 1 (*Pf*EMP1), thereby

69 stabilizing the binding of iRBCs to human endothelial cell (EC) receptors (Keyes et al., 2001;

70 Newbold et al., 1999).

71 The main function of terminally differentiated RBCs is oxygen transportation via hemoglobin.

72 During differentiation to their mature form, RBCs gradually lose cellular organelles and a lot of

73 their nucleic acid content (the long-held belief that mature RBCs lack DNA and RNA is now

74 recognized to be wrong). RNA-seq technologies have revealed that mature RBCs contain some

75 mRNAs and microRNAs (miRNAs) (Chen et al., 2008; Kannan and Atreya, 2010; Sangokoya and

76 LaMonte, 2010). Indeed, recent estimates have suggested that RBCs express approximately

77 8092 mRNAs and 359 miRNAs (Azzouzi et al., 2015; Doss et al., 2015). Many of the most highly

78 expressed RBC-mRNAs encode proteins that are associated with erythroid differentiation. In

79 addition, RBCs express mRNAs that encode proteins involved in the initiation, activation, and

80 regulation of transcription and translation (such as RNA polymerases I, II, and III; zinc/PHD

81 finger DNA-binding proteins; and cysteinyl- and lysyl-tRNA synthetases), as well as important

82 RNA-stabilizing factors (such as poly(A)-binding proteins and the antiapoptotic proteins beclin

83 1, reticulon 4, BCL2, and IAP) (Kabanova et al., 2009).

84 MiRNAs are small noncoding RNAs that inhibit the expression of approximately 60% of protein-

85 coding genes. Direct interaction of miRNAs through complementary base pairing leads to

86 cleavage of their target mRNAs (Bartel et al., 2009). In addition, a high concentration of miRNAs

87 causes hypermethylation of genes encoding target mRNAs, resulting in downregulation of gene

88 transcription (Khraiwesh et al., 2010). Under normal physiological conditions, miRNAs have

89 unique expression profiles within each organ. Pathogen invasion of host cells causes

90 dysregulation of miRNA profiles (Liang et al., 2007; Zhou et al., 2018). Some pathogens

91 preferentially invade certain tissues, leading to tissue-specific alterations in miRNA profiles

92 (Chakraborty et al., 2017) that can either lead to host protection or increase the pathogenic

93 effect of the invading organism (Ruiz-Tagel et al., 2020; SUN et al., 2020).

94 RBC-miRNAs play a key role in hematopoiesis and the maturation of RBCs (Chen et al., 2008;

95 Juzenas et al., 2017; Kannan and Atreya, 2010; Ryan and Atreya, 2011; Teruel-Montoya et al.,

96 2014), and are also involved in the development of specific diseases such as atherosclerosis (Li

97 et al., 2016). Six abundant RBC-miRNAs have been identified to date, namely, miR-451a, miR-

98 144-3p, miR-16, miR-92a, let-7, and miR-486-5p (Doss et al., 2015). RBCs of the sickle cell

99 phenotype are also enriched with specific miRNAs that lead to growth inhibition of the malaria

100 parasite through the translational repression of parasite mRNAs (LaMonte et al., 2012).

101 Chakrabarti and colleagues also reported that human miR-197-5p inhibits the *P. falciparum*

102 apicortin which affects the parasite growth (Chakrabarti et al., 2020). Adding to this, other

103 researchers postulated that, after RBCs invasion the human RISC complex is imported into the

104 parasite which might interact with the *Plasmodium* mRNA and regulate their stability and

105 translation (Dandewad et al., 2019).

106 Currently, minimal information is available on the role of miRNAs in the pathogenesis of *P.*

107 *falciparum* complications. In addition, to our knowledge, a comprehensive analysis of the

108 human RBC-miRNA profile has not yet been performed.

109 Viable cells communicate indirectly by releasing extracellular vesicles (EVs) that contain

110 miRNAs, mRNAs, and proteins. EVs are either formed inside multivesicular bodies (exosomes)

111 or directly from the plasma membrane (microvesicles). EVs released from RBCs contain miRNAs

112 coupled with Argonaute 2; these complexes can alter gene expression in other types of cells

113 upon uptake of the RBC-EVs (Arroyo et al., 2011; Mantel and Marti, 2014; Mantel et al., 2016;

114 Vu et al., 2017; Willeit et al., 2013; Zhang J. et al., 2012).

115 Here, to identify the potential roles played by miRNAs during *P. falciparum* infection, we

116 examined the expression levels of RBC-miRNAs, RBC-EV-miRNAs, and RBC-mRNAs in both non-

117 infected RBCs (niRBCs) and *P. falciparum*-infected RBCs (iRBCs). Further investigations in this

118 area could inspire the development of novel miRNAs-based therapeutics.

119 **RESULTS**

120 **Isolation of RBC-miRNAs, RBC-EV-miRNAs, and RBC-mRNAs**

121 An overview of the procedure used to isolate and characterize RBC-miRNAs, RBC-EV-miRNAs,

122 and RBC-mRNAs is shown in (Figure 1A). niRBCs and *P. falciparum* iRBCs were cultivated as

123 described previously (Trager and Jensen, 2005). The *P. falciparum* culture was tightly

124 synchronized to enrich stage specific iRBCs for the isolation of miRNA, mRNA, and EVs (ring

125 stage iRBCs (riRBCs) or trophozoite stage iRBCs (trRBCs)) (Lambros et al., 1979). RBC-miRNAs

126 and RBC-mRNAs were isolated from cells as controls. RBC-EVs were also purified from the

127 culture supernatants of niRBCs, riRBCs, and trRBCs, as described previously (Mantel et al., 2014).

128 Subsequently, RBC-EV-miRNAs were isolated. The RBC-miRNAs, RBC-EV-miRNAs, and RBC-

129 mRNAs were subjected to next-generation sequencing (NGS), and the obtained sequences

130 were aligned to the human miRNA/transcriptome reference sequences.

131 Transmission electron microscopy following incubation with an antibody targeting CD235a, a

132 membrane-bound sialoglycoprotein present on mature RBCs, confirmed that the isolated EVs

133 did indeed originate from the niRBCs, riRBCs, and trRBCs (Figure 1B). This analysis also

134 confirmed that the purified EVs displayed the expected circular morphology (Pisitkun et al.,

135 2004; Szatanek et al., 2017), with an average size of approximately 150-200 nm. In addition, a

136 nanoparticle tracking assay confirmed that the average size of all three EV populations was

137 100–250 nm (Figure 1C).

138 **Identification of abundant miRNAs in RBCs**

139 A previous study using NGS identified 287 known and 72 putative novel RBC-miRNAs (Doss et

140 al., 2015). A later study found that several miRNAs, including miR-451, miR-486-5p, and miR-

141 144-3p, are expressed at high levels in RBCs (Wu et al., 2017). Here, we found that miR-451a

142 was the most abundant miRNA in niRBCs, riRBCs, and trRBCs but was expressed at a similar

143 level in all three cell types, with average normalized expression levels of 17×10^6, 16.7×10^6, and

144 15.7×10^6, respectively. Similarly, miR-451a was abundant in the EVs isolated from niRBCs,

145 riRBCs, and trRBCs, but its expression level did not differ significantly between the three EV

146 populations, with average normalized expression levels of approximately 8.6×10^5, 6.5×10^5, and

147 6.8×10^5, respectively (Figure 2).

148

149

150
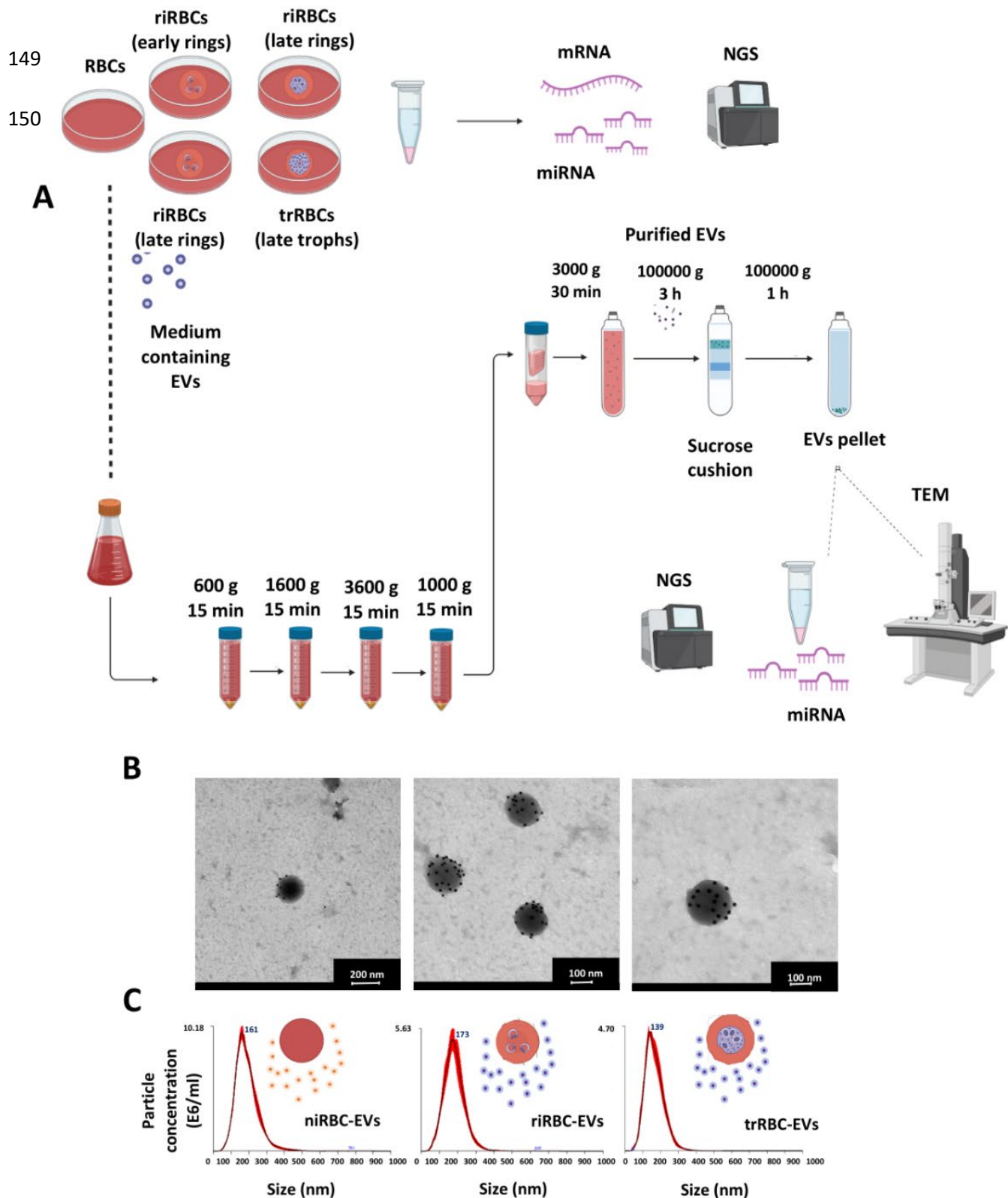
Figure 1. (A) Schematic overview of the workflow used to isolate and characterize RBC-miRNAs, RBC-EV-miRNAs, and RBC-mRNAs. RBCs infected with *P. falciparum* and their culture supernatants (containing EVs) were harvested as riRBCs and trRBCs. As a control, niRBCs were cultured in the same medium and the supernatant was also harvested. The culture supernatants were centrifuged sequentially to isolate EVs. RBC-mRNAs and RBC-miRNAs were purified from the cultivated RBCs. Finally, RBC-EV-miRNAs were purified from the isolated EVs. **(B)** Transmission electron microscopy was performed to confirm the presence of EVs after purification. niRBCs, riRBCs, and trRBCs were incubated with an antibody targeting human CD235a and then subjected to immunogold labeling. **(C)** The left, middle, and right graphs show nanoparticle tracking analyses of EVs from niRBCs, riRBCs, and trRBCs, respectively.
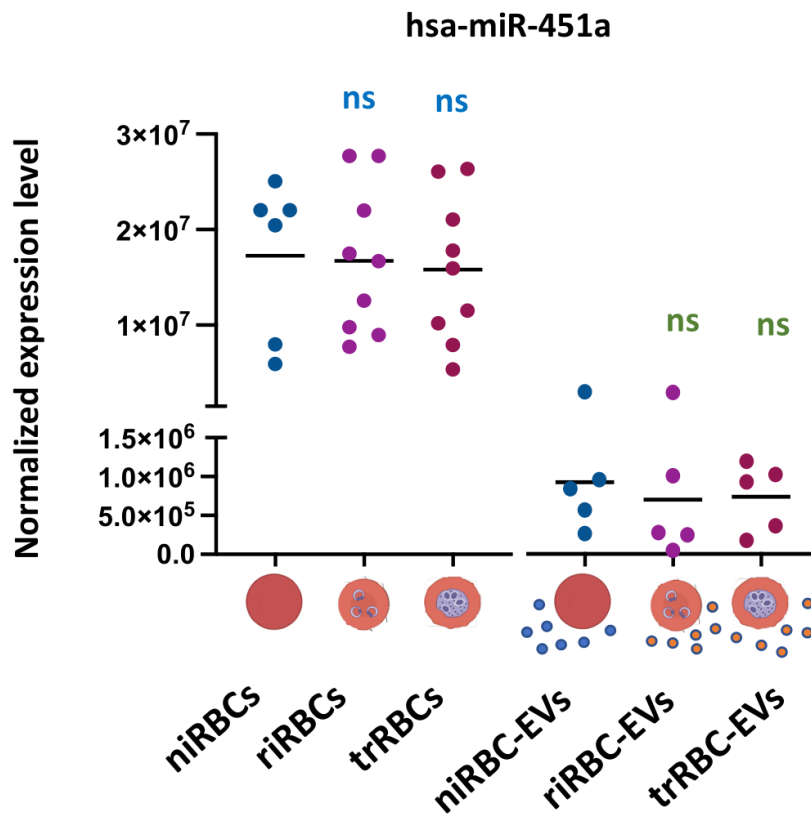
Figure 2. Expression of hsa-miR-451a in niRBCs, riRBCs, and trRBCs, as well as in EVs isolated from these cell types. The comparisons were performed using the differential expression function in the CLC genomics software V22. Statistical significance was calculated based on an FDR-adjusted P-value < 0.05 (ns = nonsignificant) (FDR = False Discovery Rate).
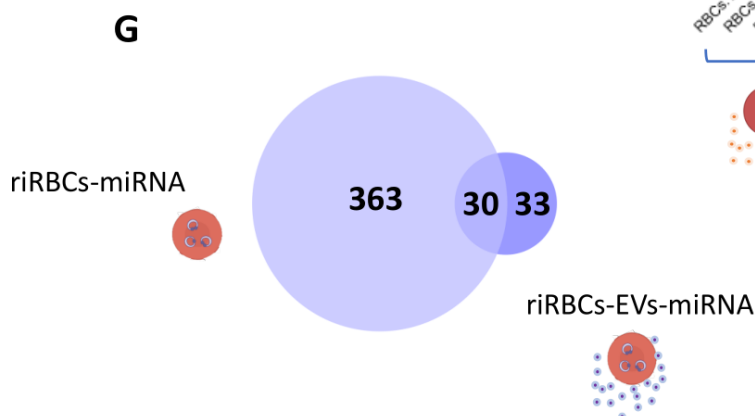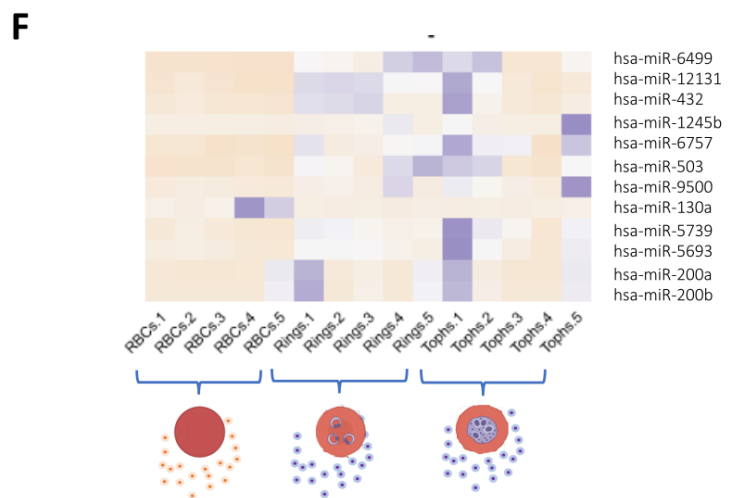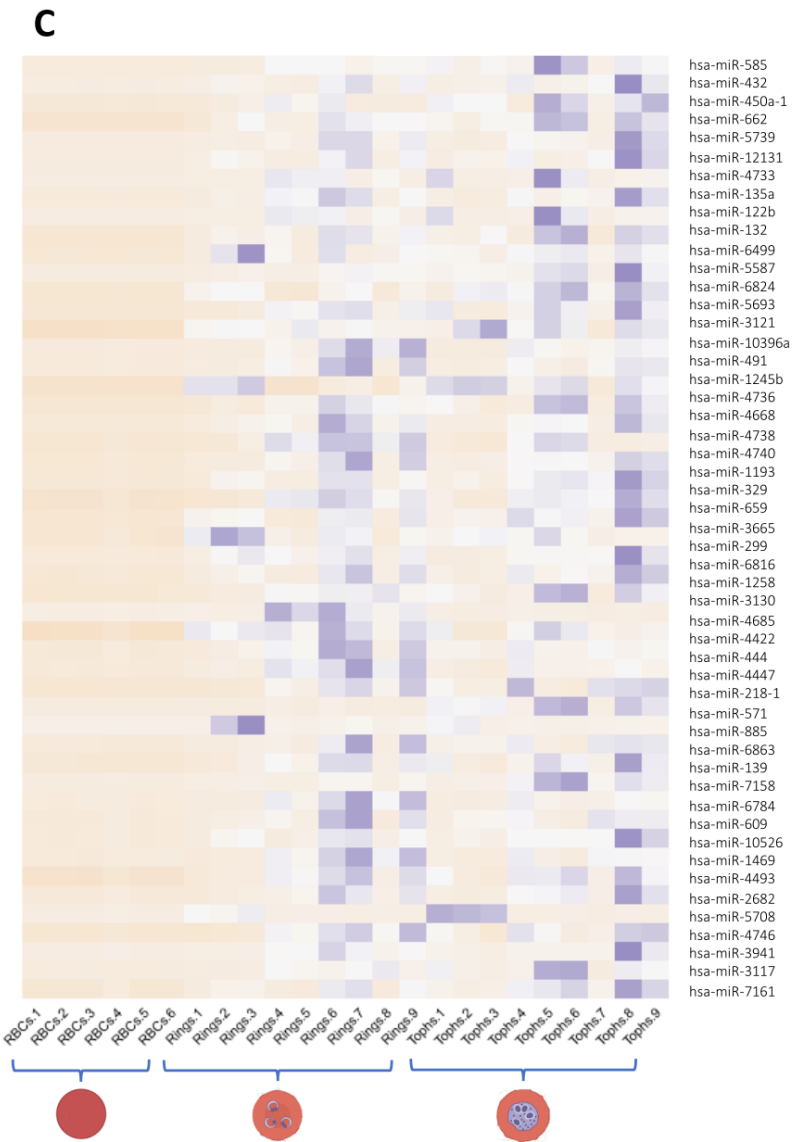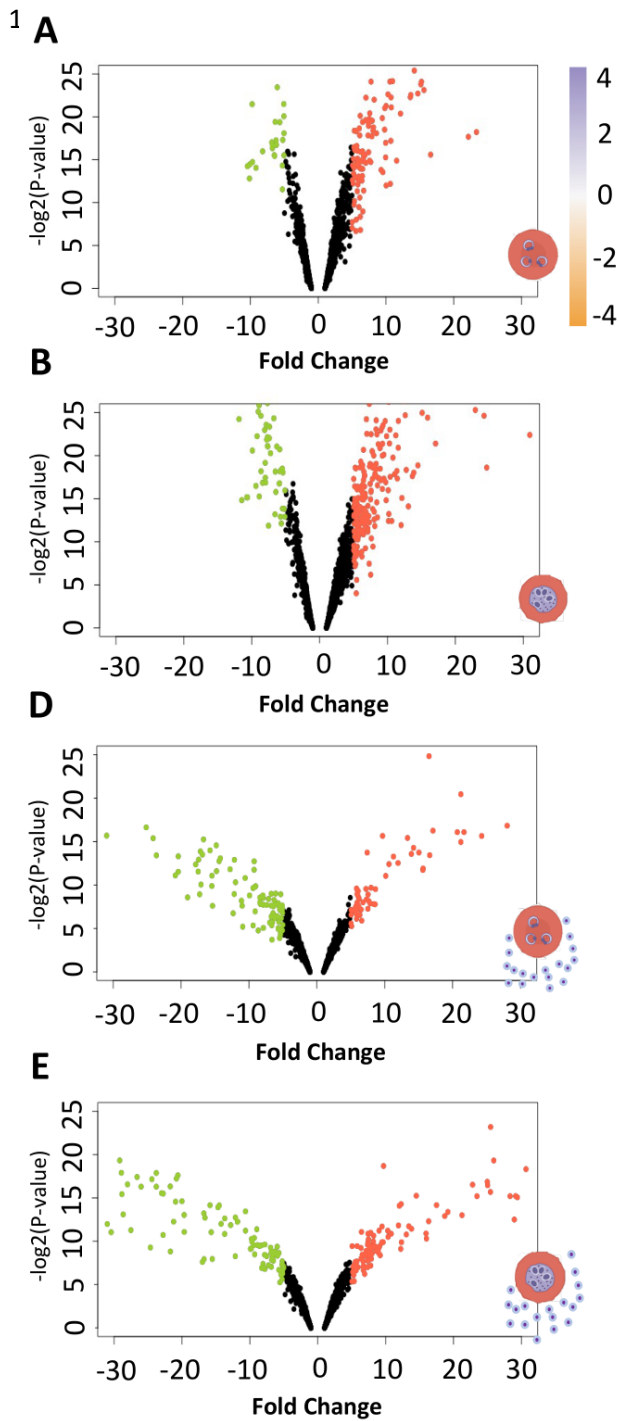
Figure 3. (A, B, D &E) Volcano plots showing the distributions of the normalized expression levels of miRNAs in riRBCs versus niRBCs (A), trRBCs versus niRBCs (B), riRBC-EVs versus niRBCs-EVs (D), and trRBC-EVs versus niRBCs-EVs (E). The volcano plots were generated using the R program (for the script, please see Supplemental Text 1). (C, F) Heat maps representing the expression levels of the top 50 miRNAs that were differentially expressed in both riRBCs and trRBCs versus niRBCs (C) and the top 12 miRNAs that were significantly highly expressed in both riRBCs-EVs and trRBCs-EVs versus niRBCs-EVs (F). The heat maps were produced using the pheatmap R package (Kolde, 2019; R Core team, 2013) (for the script, please see Supplemental Text 2). (G) A Venn diagram showing the overlap between the numbers of miRNAs that were differentially expressed in riRBCs versus niRBCs, and in riRBC-EVs versus niRBC-EVs. The miRNAs included in the comparison were highly expressed, with a fold change of at least 2 versus the uninfected control and FDR P-value < 0.05.

Differential expression of miRNAs in iRBCs versus niRBCs

Next, we used CLC Genomics software V22 to identify miRNAs that were differentially expressed in riRBCs or trRBCs versus niRBCs. Clean NGS reads were aligned to the miRbase v22 database. Overall, the expression levels of 206 and 26 miRNAs were significantly upregulated and downregulated (fold change >5), respectively, in riRBCs versus niRBCs (Figure 3A). Furthermore, 321 and 53 miRNAs were significantly upregulated and downregulated (fold change >5), respectively, in trRBCs versus niRBCs (Figure 3B). Figure 3E shows a heat map of the top 50 miRNAs that were highly expressed in both riRBCs and trRBCs versus niRBCs (see also Supplemental Table 1). To generate the heat map, we used the normalized expression values (total counts) from the differential expression function in CLC Genomics software V22, and statistical significance was calculated using a 10% FDR-adjusted P-value. The heat map showed very low, homogenous expression of these 50 miRNAs in niRBCs (RBCs 1–6 in Figure 3E). However, a marked color change in the heat map was evident for the infected populations (Rings 1–9 and Trophs 1–9 in Figure 3C), indicating increased expression of the miRNAs. In general, expression of the 50 miRNAs was increased slightly in the riRBCs harvested at 4–6 hours postinvasion (Rings 1–3 in Figure 3C) but was increased more prominently in the riRBCs harvested at 8–14 hours postinvasion (Rings 4–9 in Figure 3C). The raw reads were deposited in NCBI (Bioproject Number: PRJNA897869).
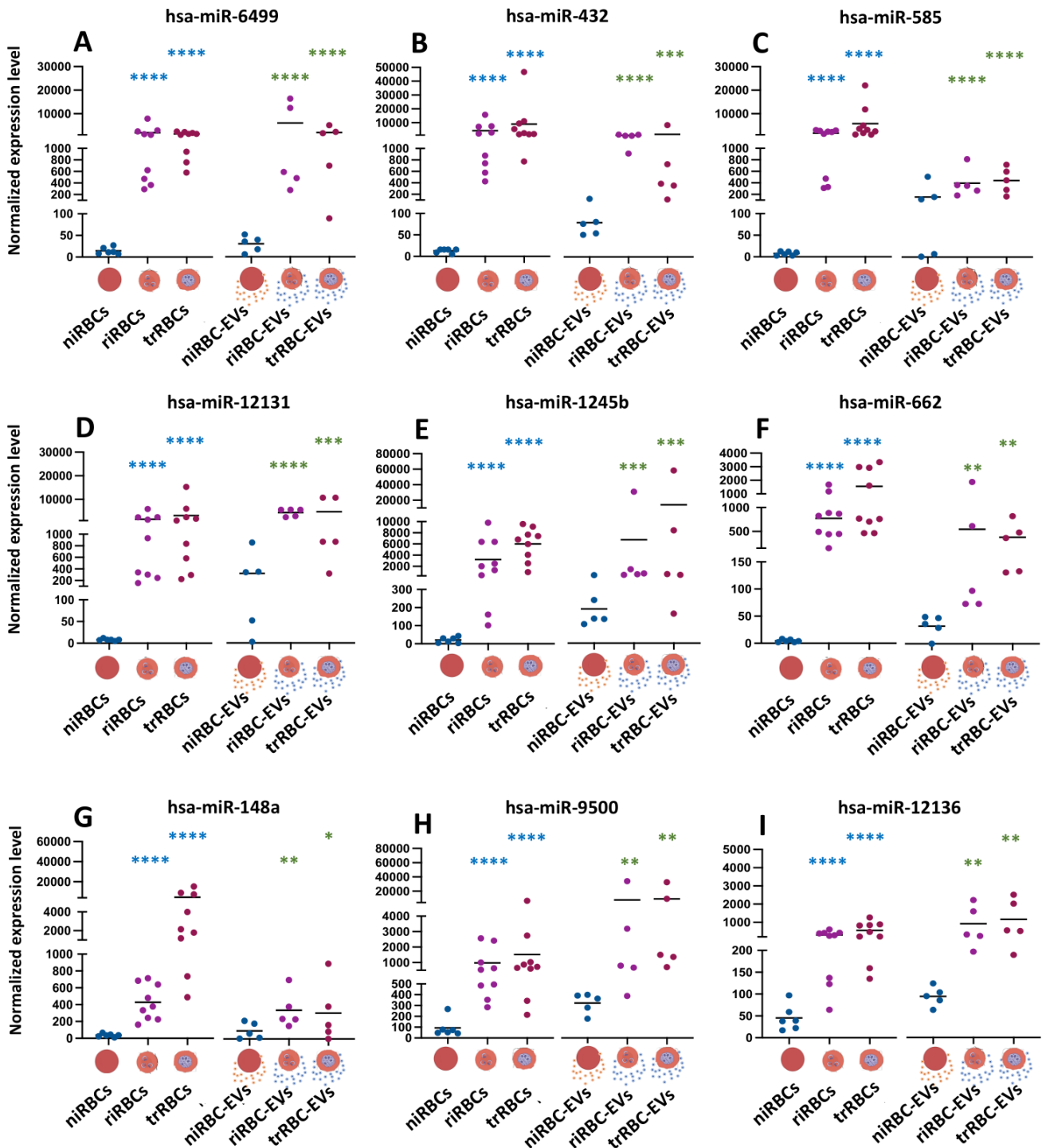
Figure 4. The expression levels of the top significantly highly expressed miRNAs in riRBCs and trRBCs versus niRBCs, and in riRBC-EVs and trRBC-EVs versus niRBC-EVs. The comparisons were performed using the differential expression function in CLC Genomics software V22. Statistical significance was calculated based on an FDR-adjusted P-value (*P < 0.05, **P < 0.01, ***P < 0.001 and ****P < 0.0001).

181

Differential expression of miRNAs in iRBC-EVs versus niRBC-EVs

A comparison of the distribution of miRNAs in the isolated EVs revealed that 63 and 53 miRNAs were significantly upregulated and downregulated, respectively, in riRBC-EVs versus niRBC-EVs (Figure 3D). Furthermore, 144 and 72 miRNAs were significantly upregulated and downregulated (fold change >5), respectively, in trRBC-EVs versus niRBC-EVs (Figure 3E). Figure 3F shows a heat map of the top 12 miRNAs that were differentially expressed in both riRBC-EVs and trRBC-EVs versus niRBC-EVs (see also Supplemental Table 2). The heat map was generated as described in the section above. As seen for the differentially expressed miRNAs in the RBCs, the majority of the top 12 miRNAs that were differentially expressed in the isolated EVs showed very low, homogenous expression in EVs from uninfected cells (RBCs 1–5 in Figure 3F), with increased expression in the infected populations (Rings 1–5 and Trophs 1–5 in Figure 3F).

Identification of common differentially expressed miRNAs in riRBCs and riRBC-EVs versus uninfected controls

Overall, the expression levels of 393 miRNAs were upregulated significantly in riRBCs versus niRBCs, and those of 63 miRNAs were upregulated significantly in riRBC-EVs versus niRBC-EVs (fold change cut off ≥ 2). An analysis of the common upregulated miRNAs revealed that 30 were highly differentially expressed in both riRBCs and riRBC-EVs (Figure 3G). The subsections below focus on the top nine common upregulated miRNAs (those with the highest statistical significance) and their target genes identified by IPA software. The top nine miRNA candidates are listed in table 1.

202 **hsa-miR-6499-3p** (Figure 4A). The *NFKBIA* gene was predicted as a target of miR-6499-3p.

203 NFKBIA is involved in acute phase response signaling, including the activation of neutrophils

204 and T-cells (Supplemental Tables 3 and 4). The gene encoding ULBP3, which is involved in

205 natural killer cell signaling, was also predicted as a target (Figures 5A & 5B) (see also

206 Supplemental Tables 3 and 4).

207 **hsa-miR-432-5p** (Figure 4B). Among others, the gene encoding interlukin-7 (IL7), which is

208 involved in both the IL7 and JAK1/JAK2 cytokine signaling pathways, was predicted as a target

209 of miR-432-5p (Figures 5A & 5B) (see also Supplemental Tables 3 and 4).

210 **hsa-miR-585-5p** (Figure 4C)**.** The interlukin-6 (*IL6ST)* gene was predicted as a target of miR-585-

211 5p. *IL6ST* is involved in the acute phase signaling pathway as well as IL6 cytokine signaling

212 (Figures 5A & 5B) (see also Supplemental Tables 3 and 4).

213 **hsa-miR-12131** (Figure 4D). No targets were predicted for this miRNA.

214 **hsa-miR-1245b-5p** (Figure 4E). The gene encoding MAPK13, which plays a role in T lymphocyte

215 and acute phase signaling, was predicted as a target of miR-1245b-5p (Figures 5A & 5B) (see

216 also Supplemental Tables 3 and 4).

217 **hsa-miR-662** (Figure 4F). The gene encoding LTBR, which is involved in intercellular crosstalk

218 between dendritic cells and natural killer cells, was predicted as a target of miR-662 (Figures 5A

219 & 5B) (see also Supplemental Tables 3 and 4).

220 **hsa-miR-148a-5p** (Figure 4G). Among others, miR-148a-5p is predicted to target the gene

221 encoding OAS1, which plays a role in interferon signaling. The interlukin-22 (*IL22*) gene was also

222 identified as a target of miR-148a-5p (Figures 5A & 5B) (Supplemental Tables 3 and 4).

223 **hsa-miR-9500** (Figure 4H). Among others, miR-9500 is predicted to target the gene encoding

224 CXCL10, which mediates communication between the innate and adaptive immune systems

225 (Figures 5A & 5B) (see also Supplemental Tables 3 and 4).

226 **hsa-miR-12136** (Figure 4I). No targets were predicted for this miRNA.

227

228

229

230

Table 1: Top highly expressed miRNA candidates in both iRBCs and iRBCs-EVs

miRNA	Accession number	Sequence	Target gene (Predicted)	Predicted relative KD	Position
hsa-miR-6499-3p	MIMAT0025451	AGCAGUGUUUGUUUUGCCCACA	*NFKBIA*	N/A	110-117 of NFKBIA 3' UTR 117-123 of NFKBIA 3' UTR
hsa-miR-432-5p	MIMAT0025450	UCGGGCGCAAGAGCACUGCAGU	IL7	-3.101 -1.124	45-52 of IL7 3' UTR 548-554 of IL7 3' UTR
hsa-miR-585-5p	MIMAT0026618	CUAGCACACAGAUACGCCCAGA	*IL6ST*	N/A	3017-3023 of IL6ST 3' UTR 5995-6002 of IL6ST 3' UTR
hsa-miR-12131	MI0039733	UCCCUGCCCUUUAUUUGGGGAGUACACCUCUCCAAAUAUACAGUUAACUGAUGUUUU ACUGUUUAUUUGGAGAGGUGUACUCCCAAAUAAAGGGCAUACCCUC	-	-	-
hsa-miR-1245b-5p	MI0017431	UUUAUAUGUAGGCCUUUAGAUCACUUAAAGAGUAUUCAACAUCAGAUGAUCUAAAG GCCUAUACAUAAA	MAPK13	-4.037 -2.503	1741-1747 of MAPK13 3' UTR 4952-4958 of MAPK13 3' UTR
hsa-miR-662	MI0003670	GCUGUUGAGGCUGCGCAGCCAGGCCCUGACGGUGGGGUGGCUGCGGGCCUUCUGAA GGUCUCCCACGUUGUGGCCCAGCAGCGCAGUCACGUUGC	LTBR	N/A	68-75 of LTBR 3' UTR
hsa-miR-148a-5p	MI0000253	GAGGCAAAGUUCUGAGACACUCCGACUCUGAGUAUGAUAGAAGUCAGUGCACUACA GAACUUUGUCUC	*IL22*	N/A	15-22 of IL22 3' UTR
hsa-miR-9500	MI0029185	AAAAGGGAAGAUGGUGACCACAUAGGAGGGACAGCGGCCUUUCCAACAGGGGACCCU UGCCAGCC	CXCL10	N/A	70-77 of CXCL10 3' UTR
hsa-miR-12136	MI0039740	GAAAAAGUCAUGGAGGCCAUGGGGUUGGCUUGAAACCAGCUUUGGGGGGUUCGAU UCCUUCCUUUUU UGUC	-	-	-

*Relative KD: values are predicted using a convolutional neural network (CNN) that predicts binding affinity between miRNA and any 12-nt sequence (Targetscan V8 Human).

Functional analysis of highly expressed miRNA candidates

IPA software was used to identify the target genes for the above-mentioned miRNA candidates. Supplementary Table 4 lists the target genes and their functions. STRING database was used to cluster the target genes. The K-means clustering method was used to allocate the proteins encoded by these genes into four main clusters according to the experimental records within different databases (Figure 5A). The blue cluster includes 19 nodes corresponding to genes related to immune-regulatory interactions. The red cluster consists of 23 nodes corresponding to genes related to plasma membrane and cell signalling. The yellow cluster contains 23 nodes corresponding to genes related to HIF-1 and phagosome pathways. Finally, the green cluster contains 18 nodes corresponding to genes encoding proteins involved in cytokine receptor activity and T-cell chemotaxis (for example: IL7, CXCL10, CCL5, and TNFSF4) (Figure 5A & 5B).

A

HIF-1 and
phagosome pathways

Cytokine receptor activity
and T- cell chemotaxis

Plasma membrane
and cell signalling

Immune - regulatory
interactions

B

Values above this threshold are capped

ID	Source	Term ID	Term Name	Padj
1	GO:MF	0004888	Transmembrane signaling receptor activity	4.156×10^{-6}
2	GO:MF	0038023	Signaling receptor activity	1.282×10^{-5}
3	GO:MF	0060089	Molecular transducer activity	1.282×10^{-5}
4	GO:BP	0023052	Signaling	1.686×10^{-15}
5	GO:BP	0007154	Cell communication	2.710×10^{-15}
6	GO:BP	0034097	Response to cytokine	1.230×10^{-11}
7	GO:CC	0005886	Plasma membrane	2.422×10^{-13}
8	GO:CC	0071944	Cell periphery	9.502×10^{-16}
9	GO:CC	1903561	Extracellular vesicle	2.507×10^{-2}
10	KEGG	04145	Phagosome	1.106×10^{-3}
11	REAC	HSA-12	Cytokine signaling in immune system	2.784×10^{-6}
12	REAC	HAS-16	Immune system	5.783×10^{-5}
13	WP	WP619	Type II interferon signaling (IFNG)	2.418×10^{-3}

Figure 5. (A) STRING clustering of the predicted target genes of the top differentially expressed miRNAs shown in Figure 4. Four clusters were identified using K-means clustering: blue cluster (immune regulatory interactions), red cluster (plasma membrane and cell signaling), yellow cluster (HIF-1 and phagosome pathways), and green cluster (cytokine receptor activity and T-cell chemotaxis). The blue and pink connector lines represent the database and experimentally confirmed interactions, respectively. (B) A g:Profiler graph showing the significant biological pathways affected by the predicted target genes. Transmembrane signaling receptor activity was the top pathway, followed by various signaling and cell communication pathways.
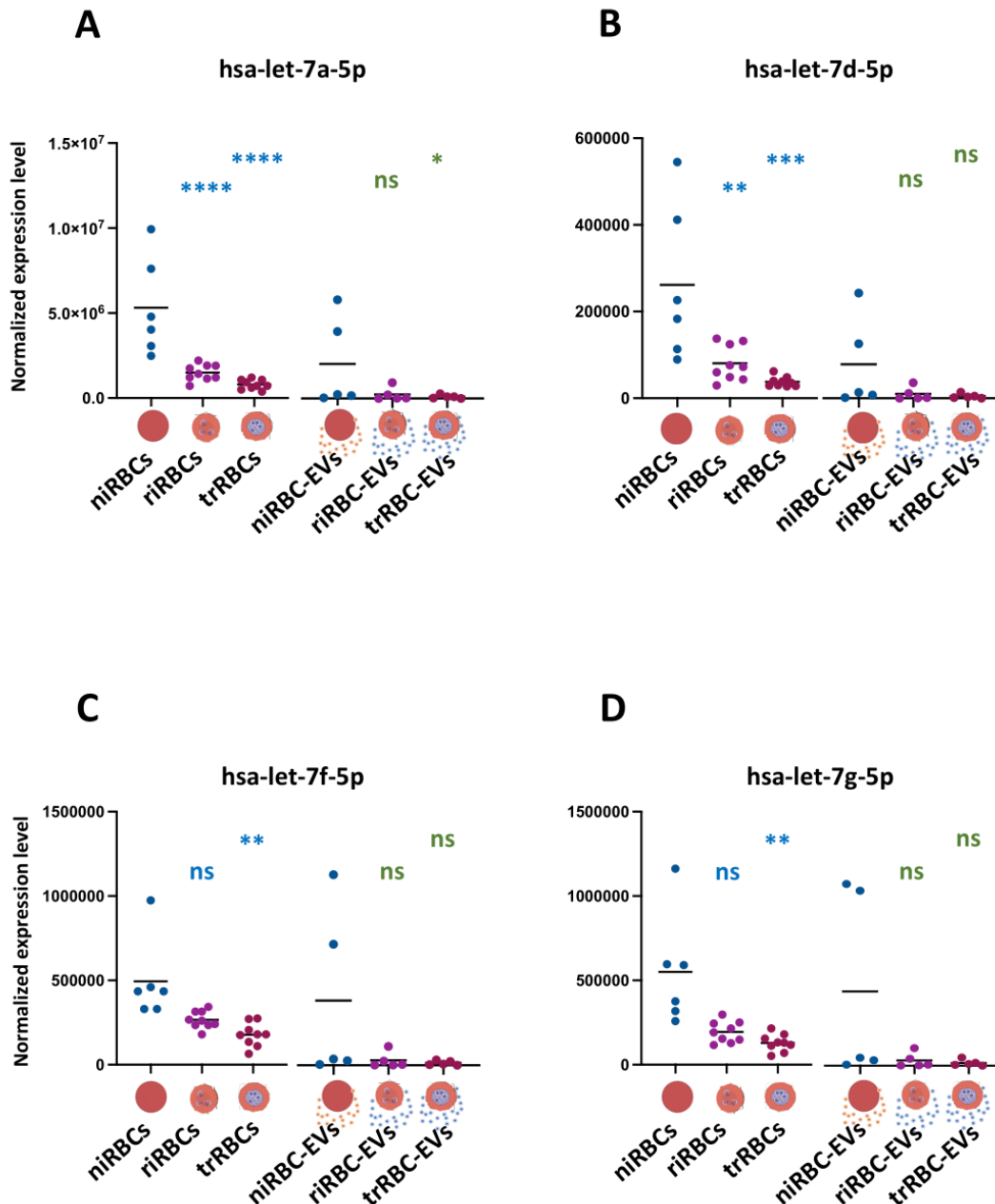
Figure 6. The expression levels of some hsa-let-7 family members in riRBCs and trRBCs versus niRBCs, and in riRBC-EVs and trRBC-EVs versus niRBC-EVs. The comparisons were done using the differential expression function in CLC Genomics software V22. Statistical significance was calculated using an FDR-adjusted P-value < 0.05 (ns = non-significant).

264 **Differential expression of the let-7 family in iRBCs**

265 Members of the let-7 family of miRNAs control cell signaling and immunomodulatory pathways.

266 Figure 6 shows the expression profiles of some let-7 family members in niRBCs, iRBCs, and their

267 EVs. The expression levels of let-7a-5p and let-7d-5p were downregulated significantly in both

268 riRBCs and trRBCs versus niRBCs (Figures 6A & 6B). Within the EVs, hsa-let-7a-5p was only

269 downregulated significantly in trRBC-EVs, and let-7d-5p expression was not affected

270 significantly by *P. falciparum* infection. The expression levels of let-7f and let-7g were

271 downregulated significantly in trRBCs (versus niRBCs), but their levels in the EVs were not

272 affected significantly by *P. falciparum* infection (Figures 6C & 6D).

273 **Differential expression of mRNAs in iRBCs versus niRBCs**

274 Our findings from the miRNA analyses prompted us to examine whether the mRNA expression

275 profile of human RBCs is also affected by *P. falciparum* infection. To this end, we performed

276 NGS of mRNAs extracted from riRBCs, trRBCs, and niRBCs. The reads were aligned to the human

277 transcriptome using the RNA-seq function of CLC Genomics software V22. FDR-adjusted P-

278 values were used to detect mRNAs that were differentially expressed in riRBCs and trRBCs

279 versus niRBCs. Figure 7A shows a heat map of the statistically significant differentially expressed

280 genes. Overall, 20 and 30 mRNAs were significantly downregulated and upregulated,

281 respectively, in the infected cells (Supplemental Table 5). We calculated the percentages of the

282 dominant transcripts in niRBCs and found that *RPS12* and *RPL41* represented 19% and 11% of

283 the total transcripts, respectively. These two genes encode cytoplasmic ribosomes. The

284 expression levels of *RPS12* and *RPL41*, as well as other genes encoding cytoplasmic ribosomes,

285 were downregulated significantly in RBCs after infection with *P. falciparum* (Figure 7B). In

286 addition, riRBCs and trRBCs showed significant increases in the expression levels of the *ATAD2*,

287 *CALM2*, and *HSP90α* mRNAs (Figure 7B). Figure 7C shows a K-means clustering analysis of the

288 genes that were downregulated significantly in riRBCs and trRBCs versus niRBCs. These

289 downregulated genes mainly encoded cytoplasmic ribosomal proteins (Figure 7D).

290

291

292

293
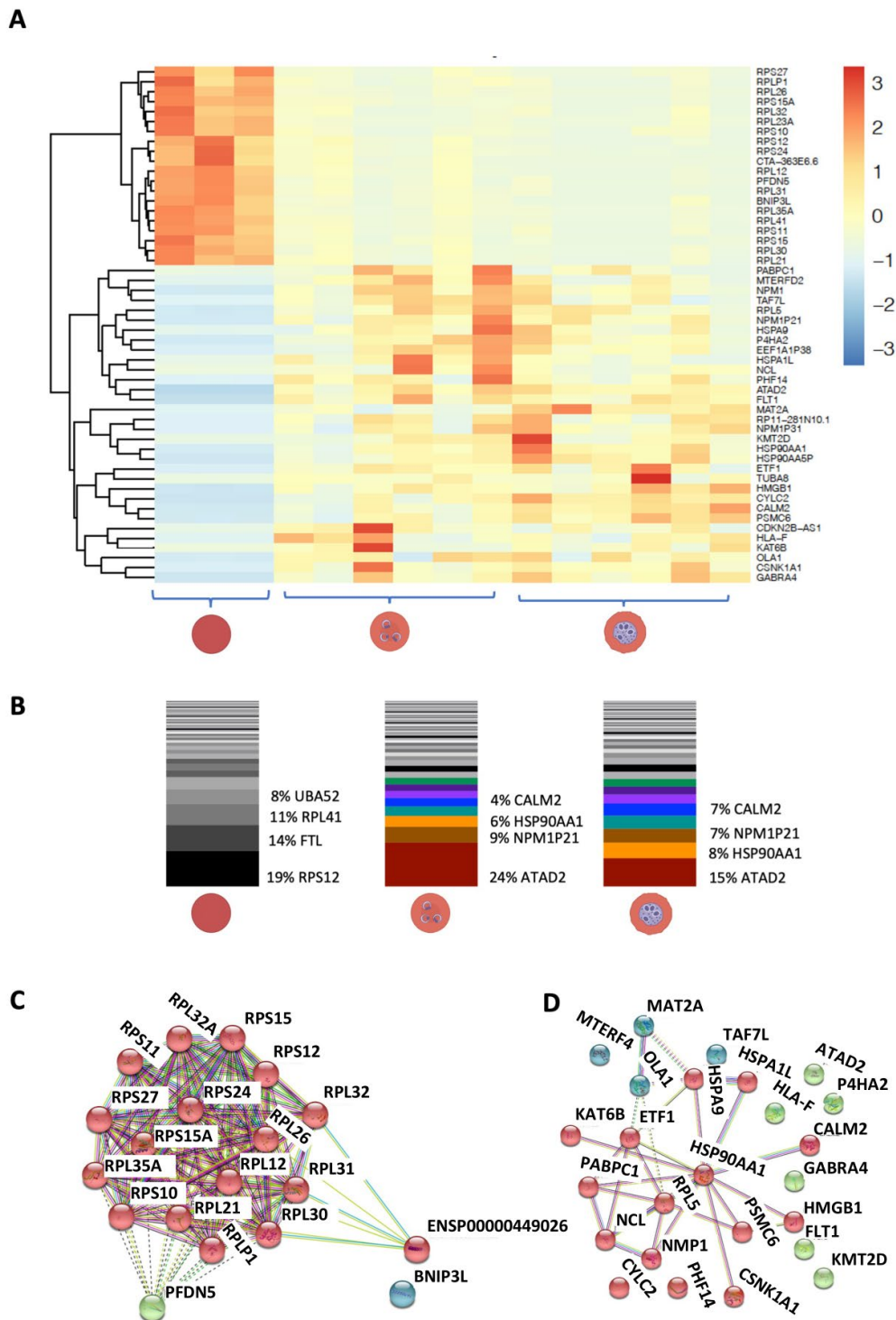
Figure 7. (A) A heat map representing the expression levels of the most highly differentially expressed mRNAs in riRBCs and trRBCs versus niRBCs. The heat map was produced using the pheatmap R package (Kolde, 2019) (for the script, please see Supplemental Text 2). (B) A graphical presentation of the dominant transcripts within the cell populations described in A. (C, D) STRING clustering analyses of the proteins encoded by the genes that were downregulated (C) or upregulated (D) in iRBCs versus niRBCs. The blue and pink connector lines represent the database and experimentally confirmed interactions, respectively.

DISCUSSION

Genetic polymorphism that affects the host's response to pathogens might explain why 2% of malaria patients develop CM. Various cellular signals, including immune signaling pathways, require fine-tuned regulation during infection, and we postulate that these regulations occur, at least in part, via miRNAs. Indeed, there is substantial evidence to support the hypothesis that human miRNAs influence the outcome and complications of *P. falciparum* infection. MiRNAs play a primary role in regulating gene expression by binding to target mRNAs and preventing their translation into proteins. Single miRNAs can bind to several genes involved in different pathways. In malaria, human miRNAs can penetrate *P. falciparum*-infected cells and form duplexes with mRNAs, preventing their translation (LaMonte et al., 2012). A previous study found that miR-150-5p was downregulated in whole blood from an adult infected with *P. falciparum* (Kaur et al., 2015). On the other hand, another study found that miR-150-5p was upregulated in plasma-derived EVs from patients infected with P. vivax (Chamnanchanunt et al., 2015). C57BL76 mice infected with *P. berghei* ANKA develop CM and have higher expression levels of miR-27a and miR-142 in their brains than *P. yoelii*-infected mice without CM (Martin-Alonso et al., 2018). In addition, recent studies have identified miRNAs as crucial host factors that regulate parasite growth (Chang and Mendell, 2007; Rubio et al., 2016).

MiRNA profiles are tissue-specific, and erythrocyte-derived miRNAs have been reported as potential biomarkers of specific diseases. A number of miRNAs that are up- or downregulated during erythropoiesis are selectively retained in mature RBCs (Chen et al., 2008; Hamilton, 2010; Ryan and Atreya, 2011). Here, we characterized the effects of *P. falciparum* infection on the miRNA profiles of human RBCs and their secreted EVs. We found that miR-451a was the most abundant miRNA in both RBCs and RBC-EVs, an observation that is consistent with other studies. For example, miR-451a is reportedly abundant in cells of the erythroid lineage, including mature RBCs (Chen et al., 2008). Chamnanchanunt et al. (2015) found that miR-451 was downregulated in plasma samples from patients with *P. vivax* infection. Mantel et al. (2013) demonstrated the internalization of iRBC-EVs within macrophages, where they initiate a strong inflammatory response. Later, the same group found that miR-451a is present in iRBC-EVs and postulated that it is transported to ECs via these vesicles and subsequently alters their function (Mantel et al., 2016). This hypothesis contradicts our current finding that miR-451a levels in

329   RBCs and RBC-EVs were the same before and after *P. falciparum* infection, suggesting that RBC-

330   EVs deliver the same amount of miR-451a to recipient cells under uninfected and infected

331   conditions. We speculate that the functional impairment of ECs in Mantel's experiments might

332   have been due to other differentially expressed miRNAs that were transported within EVs, such

333   as those identified in our current study.

334   In this study, we detected high expression of human miRNA candidates within *Plasmodium*-

335   infected iRBCs. In a study in 2012, LaMonte and colleagues reported the translocation of human

336   miRNAs to *Plasmodium falciparum* (LaMonte et al., 2012), suggesting that these miRNAs could

337   be preserved from degradation within the parasite vacuole. However, our results do not

338   support this possibility because we isolated miRNA from niRBCs and iRBCs at the same time,

339   which gives no chance for miRNA degradation within the niRBCs. This was further confirmed by

340   the results of experiments showing that miRNA profiles were not appreciably different in blood

341   samples taken from different healthy individuals over a 2-year period.

342   Based on our experiments, we hypothesize that there might be minimal transcription

343   happening within the RBCs even after enucleation. This is supported by other studies showing

344   that RBCs contain RNA polymerase I, II, and III, as well as DNA binding proteins (Kabanova et

345   al., 2009). Also, RBCs express TLR9 on their surface, which scavenge cell free CpG-DNA during

346   quiescent states to prevent non-specific inflammation (Lam et al., 2021 & Hotz et al., 2018).

347   These small DNA fragments may act as templates for transcription. Further studies are needed

348   to test this hypothesis.

349   In our study, we identified that nine miRNAs were significantly expressed at high levels in iRBCs

350   and in their EVs at both the ring and trophozoite stages. To our knowledge, there have been no

351   other reports of an association between these miRNAs and pathogenesis/severity of malaria.

352   We attribute this shortfall to the fact that most studies isolate miRNAs from serum-derived EVs,

353   which include EVs from different tissue origins (Ketprasit et al., 2020). *P. falciparum*-induced

354   dysregulation of miRNAs could affect multiple cellular functions and pathological processes,

355   depending on the target genes of the affected miRNAs. Our bioinformatic analysis uncovered

356   several interesting targets of the infection-related differentially expressed miRNAs; hence, it

357   would be useful to study the functions of these miRNAs and how they affect different recipient

358   cells in more detail. The putative target genes identified here were clustered into four main

359   groups, including cell signaling, HIF-1 and phagosome pathways, cytokine receptor activity, and

360   immune regulatory interactions. Accordingly, we plan to analyze the effects of these miRNAs

361   and target genes in different recipient cells, such as ECs and other immune cells.

362   We found that miR-200a-3p, miR-200b-3p, and miR-200c-3p were upregulated in EVs isolated

363   from both riRBCs and trRBCs (Supplemental Tables 1 & 2). A previous study demonstrated that

364   miR-200b and miR-200c mediate a proinflammatory response in patients with *Listeria* infection,

365   and that the expression levels of the protein-coding target genes are inversely correlated with

366   those of the miRNAs (Izar et al., 2012). Another study found that miR-200b and miR-200c play

367   a role in neurodegenerative diseases by targeting genes that cause progressive degeneration

368   of the structure of the central nervous system (Sundararajan et al., 2022). These results suggest

369   that RBCs contribute to modulation of the immune response during *P. falciparum* infection;

370   however, the mechanism underlying this process is currently unknown.

371   Several miRNAs in the let-7 family were downregulated significantly in both RBCs and RBC-EVs

372   after *P. falciparum* infection (Supplemental Tables 1 & 2). The let-7 family controls cell signaling

373   pathways in many living organisms. Notably, let-7 reduces the potency of the innate immune

374   response by repressing translation of the mRNA encoding Toll-like receptor 4 (TLR4), which

375   controls the activation of nuclear factor κB and the expression of a set of downstream genes

376   involved in inflammation. Downregulation of let-7 has also been reported in several viral

377   diseases. Also, *Cryptosporidium parvum* infection was reported to be associated with reduced

378   let-7i and increased TLR4 signaling. Let-7 also affects the differentiation of CD8-positive T-cells,

379   which can release effector cytokines and eliminate infected target cells (Chen et al., 2007;

380   Kumar et al., 2015; Wells et al., 2018).

381   In support of our finding that *P. falciparum* infection affects the miRNA profile of RBCs,

382   alterations in host cell miRNA profiles have also been reported for other parasites (Acuna et al.,

383   2020). For example, in *Leishmania donovani*-infected mice, the surface acid protease (gp63)

384   of the parasite targets the host's Dicer1, cleaving Dicer to downregulate pre-miR-122 and its

385   processing to miR-122, leading to reduced post-transcriptional regulation of its target mRNAs

386   and increased pathogenicity (Ghosh et al., 2013). In addition, miR-551 is reportedly upregulated

387   in dendritic cells following *L. donovani* infection and can interfere with TLR4 signaling, which

388   plays an important role in the activation of the antileishmanial immune response (Tolouei et

389   al., 2013). During *Toxoplasma gondii* infection, the expression of miR-17-92 is increased within

390   infected cells, leading to inhibition of the proapoptotic molecule BIM. This inhibition of

391   apoptosis helps Toxoplasma evade the immune system (Goebel et al., 2001; O'Connor et al.,

392   1998). Furthermore, in *Trypanosoma cruzi* infection, downregulation of miR-133 and miR-208

393   is correlated with the increased expression of cardiac genes that play a role in the

394   cardiovascular complications seen in chronic Chagas disease patients (Abel et al., 2001;

395   Nogueria et al., 2014).

396   In early studies, technological limitations may have hampered the identification of low levels

397   of mRNAs in RBCs (Lee et al., 1986; Rainen et al., 2002). In 2006, researchers detected small

398   RNAs in RBCs for the first time (Rathjen et al., 2006). This discovery was followed by the

399   confirmation that RBCs express several different types of long RNAs (~8,092 genes) (Azzouzi et

400   al., 2015; Doss et al., 2015). The RBC transcriptome originates from the remaining

401   transcriptome of differentiating erythroid cells that persists after enucleation and terminal

402   differentiation. Previous studies have demonstrated that miRNAs target genes within RBCs; for

403   example, miR-4732-3p, which targets Smad2 and Smad4 (Chen et al., 2007; Dong et al., 2014).

404   Therefore, in addition to examining the miRNA profiles of niRBCs and iRBCs, we also

405   characterized changes in the RBC mRNA profile after *P. falciparum* infection and found that the

406   levels of the dominant transcripts in niRBCs (RPS12 and RPL41) were downregulated

407   significantly after infection. We postulate that the residual translation of mRNAs in RBCs is

408   regulated by miRNAs. However, we cannot exclude the possibility that some ribosomes in RBCs

409   might be neglected due to the density of hemoglobin. A small number of ribosomes may be

410   enough to complete translation, in which case mature RBCs retain a few specific RNA species.

411   We also performed an immunofluorescence analysis of niRBCs, riRBCs, and trRBCs using anti-

412   DNA antibodies and identified tiny fragments of DNA (Supplemental Figure 1). Further studies

413   are required to validate these findings.

414   In summary, we examined the miRNA profiles of niRBCs and iRBCs, as well as their secreted EVs.

415   The miRNA profiles of RBCs and their EVs were altered significantly after *P. falciparum* infection,

416   and a bioinformatic prediction of the target genes suggested that several factors work together

417   in a tightly regulated fashion to control the immune response during infection. Evidence from

418   other studies suggests that RBC-miRNAs are transported inside EVs and taken up by various

419   cells throughout the circulatory system, thereby affecting mRNA expression in these recipient

420   cells. Further studies are required to clarify the functions of miRNAs in RBCs and RBC-EVs.

421   Nonetheless, the results presented here contribute to current understanding of the dynamics

422   of cell-cell communication during *P. falciparum* infection.

423

424   **STAR ★ METODS**

425   Detailed methods are provided in the online version of this paper and include the following:

426   • CELL CULTURE AND REAGENTS
427   • MATERIALS AND KITS
428   • DATA DEPOSIT
429   • SOFTWARES
430   • METHOD DETAILS
431   • DATA ANA LYSIS AND AVAILIABILITY

432   **SUPPLEMENTAL INFORMATION**

433   Supplemental information for this article is available online.

434

435

457 **REFERENCES**
458

459 ARROYO, J. D., CHEVILLET, J. R., KROH, E. M., RUF, I. K., PRITCHARD, C. C., GIBSON, D. F., MITCHELL, P. S., BENNETT,
460   C. F., POGOSOVA-AGADJANYAN, E. L., STIREWALT, D. L., TAIT, J. F. & TEWARI, M. 2011. Argonaute2
461   complexes carry a population of circulating microRNAs independent of vesicles in human plasma. *Proc*
462   *Natl Acad Sci U S A,* 108, 5003-8.
463 AZZOUZI, I., MOEST, H., WOLLSCHEID, B., SCHMUGGE, M., EEKELS, J. J. M. & SPEER, O. 2015. Deep sequencing and
464   proteomic analysis of the microRNA-induced silencing complex in human red blood cells. *Exp Hematol,*
465   43, 382-392.
466 BARTEL, D. P. 2009. MicroRNAs: target recognition and regulatory functions. *Cell,* 136, 215-33.
467 CHAKRABORTY, C., SHARMA, A. R., SHARMA, G., DOSS, C. G. P. & LEE, S. S. 2017. Therapeutic miRNA and siRNA:
468   Moving from Bench to Clinic as Next Generation Medicine. *Mol Ther Nucleic Acids,* 8, 132-143.
469 CHAKRABARTI M, GARG S, RAJAGOPAL A, PATI S, SINGH S. Targeted repression of Plasmodium apicortin by host
470   microRNA impairs malaria parasite growth and invasion. Dis Model Mech. 2020 Jun 3;13(6):dmm042820.
471   doi: 10.1242/dmm.042820. PMID: 32493727; PMCID: PMC7286292.
472 CHANG T.-C. and Mendell J. T. (2007). microRNAs in vertebrate physiology and human disease. Annu. Rev.
473   Genomics Hum. Genet. 8, 215-239. 10.1146/annurev.genom.8.080706.092351
474 CHAMNANCHANUNT S, KUROKI C, DESAKORN V, ENOMOTO M, THANACHARTWET V, SAHASSANANDA D,
475   SATTABONGKOT J, JENWITHISUK R, FUCHAROEN S, SVAST S, UMEMURA T. Downregulation of plasma
476   miR-451 and miR-16 in Plasmodium vivax infection. Exp Parasitol. 2015 Aug;155:19-25. doi:
477   10.1016/j.exppara.2015.04.013. Epub 2015 Apr 22. PMID: 25913668.
478 CHEN, S. Y., WANG, Y., TELEN, M. J. & CHI, J. T. 2008a. The genomic analysis of erythrocyte microRNA expression
479   in sickle cell diseases. *PLoS One,* 3, e2360.
480 CHEN, X. M., SPLINTER, P. L., O'HARA, S. P. & LARUSSO, N. F. 2007. A cellular micro-RNA, let-7i, regulates Toll-like
481   receptor 4 expression and contributes to cholangiocyte immune responses against Cryptosporidium
482   parvum infection. *J Biol Chem,* 282, 28929-28938.
483 CHEN, Y., LIU, W., CHAO, T., ZHANG, Y., YAN, X., GONG, Y., QIANG, B., YUAN, J., SUN, M. & PENG, X. 2008b.
484   MicroRNA-21 down-regulates the expression of tumor suppressor PDCD4 in human glioblastoma cell
485   T98G. *Cancer Lett,* 272, 197-205.
486 DANDEWAD V, VINDU A, JOSEPH J, SESHADRI V. Import of human miRNA-RISC complex into Plasmodium
487   falciparum and regulation of the parasite gene expression. J Biosci. 2019 Jun;44(2):50. PMID: 31180063.
488 DOSS, J. F., CORCORAN, D. L., JIMA, D. D., TELEN, M. J., DAVE, S. S. & CHI, J. T. 2015. A comprehensive joint analysis
489   of the long and short RNA transcriptomes of human erythrocytes. *BMC Genomics,* 16, 952.
490 Fu Y, Wu PH, Beane T, Zamore PD, Weng Z: Elimination of PCR duplicates in RNAseq and small RNA-seq using
491   unique molecular identifiers. BMC Genomics 2018;19:531
492 Ghosh J, Bose M, Roy S, Bhattacharyya SN. Leishmania donovani targets Dicer1 to downregulate miR-122, lower
493   serum cholesterol, and facilitate murine liver infection. Cell Host Microbe. 2013 Mar 13;13(3):277-88. doi:
494   10.1016/j.chom.2013.02.005. PMID: 23498953; PMCID: PMC3605572.
495 HAMILTON AJ. MicroRNA in erythrocytes. Biochem Soc Trans. 2010 Feb;38(Pt 1):229-31. doi: 10.1042/BST0380229.
496   PMID: 20074065.
497 Hotz MJ, Qing D, Shashaty MGS, Zhang P, Faust H, Sondheimer N, Rivella S, Worthen GS, Mangalmurti NS. Red
498   Blood Cells Homeostatically Bind Mitochondrial DNA through TLR9 to Maintain Quiescence and to
499   Prevent Lung Injury. Am J Respir Crit Care Med. 2018 Feb 15;197(4):470-480. doi: 10.1164/rccm.201706-
500   1161OC. PMID: 29053005; PMCID: PMC5821907.
501 IZAR, B., MANNALA, G. K., MRAHEIL, M. A., CHAKRABORTY, T. & HAIN, T. 2012. microRNA response to Listeria
502   monocytogenes infection in epithelial cells. *Int J Mol Sci,* 13, 1173-85.
503 JUZENAS, S., VENKATESH, G., HUBENTHAL, M., HOEPPNER, M. P., DU, Z. G., PAULSEN, M., ROSENSTIEL, P., SENGER,
504   P., HOFMANN-APITIUS, M., KELLER, A., KUPCINSKAS, L., FRANKE, A. & HEMMRICH-STANISAK, G. 2017. A
505   comprehensive, cell specific microRNA catalogue of human peripheral blood. *Nucleic Acids Res,* 45, 9290-
506   9301.
507 KABANOVA, S., KLEINBONGARD, P., VOLKMER, J., ANDREE, B., KELM, M. & JAX, T. W. 2009. Gene expression
508   analysis of human red blood cells. *Int J Med Sci,* 6, 156-9.
509 KANNAN, M. & ATREYA, C. 2010. Differential profiling of human red blood cells during storage for 52 selected
510   microRNAs. *Transfusion,* 50, 1581-8.
511 KHRAIWESH, B., ARIF, M. A., SEUMEL, G. I., OSSOWSKI, S., WEIGEL, D., RESKI, R. & FRANK, W. 2010. Transcriptional
512   control of gene expression by microRNAs. *Cell,* 140, 111-22.

Ketprasit N, Cheng IS, Deutsch F, Tran N, Imwong M, Combes V, Palasuwan D. The characterization of extracellular vesicles-derived microRNAs in Thai malaria patients. Malar J. 2020 Aug 10;19(1):285. doi: 10.1186/s12936-020-03360-z. PMID: 32778117; PMCID: PMC7418320.

KUMAR, M., SAHU, S. K., KUMAR, R., SUBUDDHI, A., MAJI, R. K., JANA, K., GUPTA, P., RAFFETSEDER, J., LERM, M., GHOSH, Z., VAN LOO, G., BEYAERT, R., GUPTA, U. D., KUNDU, M. & BASU, J. 2015. MicroRNA let-7 modulates the immune response to Mycobacterium tuberculosis infection via control of A20, an inhibitor of the NF-kappaB pathway. *Cell Host Microbe,* 17**,** 345-356.

KYES, S., HORROCKS, P. & NEWBOLD, C. 2001. Antigenic variation at the infected red cell surface in malaria. *Annu Rev Microbiol,* 55**,** 673-707.

Lam LKM, Murphy S, Kokkinaki D, Venosa A, Sherrill-Mix S, Casu C, Rivella S, Weiner A, Park J, Shin S, Vaughan AE, Hahn BH, Odom John AR, Meyer NJ, Hunter CA, Worthen GS, Mangalmurti NS. DNA binding to TLR9 expressed by red blood cells promotes innate immune activation and anemia. Sci Transl Med. 2021 Oct 20;13(616):eabj1008. doi: 10.1126/scitranslmed.abj1008. Epub 2021 Oct 20. PMID: 34669439; PMCID: PMC9065924.

LAMBROS, C. & VANDERBERG, J. P. 1979. Synchronization of Plasmodium falciparum erythrocytic stages in culture. *J Parasitol,* 65**,** 418-20.

LAMONTE, G., PHILIP, N., REARDON, J., LACSINA, J. R., MAJOROS, W., CHAPMAN, L., THORNBURG, C. D., TELEN, M. J., OHLER, U., NICCHITTA, C. V., HAYSTEAD, T. & CHI, J. T. 2012. Translocation of sickle cell erythrocyte microRNAs into Plasmodium falciparum inhibits parasite translation and contributes to malaria resistance. *Cell Host Microbe,* 12**,** 187-99.

LETAFATI, A., NAJAFI, S., MOTTAHEDI, M., KARIMZADEH, M., SHAHINI, A., GAROUSI, S., ABBASI-KOLLI, M., SADRI NAHAND, J., TAMEHRI ZADEH, S. S., HAMBLIN, M. R., RAHIMIAN, N., TAGHIZADIEH, M. & MIRZAEI, H. 2022. MicroRNA let-7 and viral infections: focus on mechanisms of action. *Cell Mol Biol Lett,* 27**,** 14.

LI, K. Y., ZHENG, L., WANG, Q. & HU, Y. W. 2016. Characteristics of erythrocyte-derived microvesicles and its relation with atherosclerosis. *Atherosclerosis,* 255**,** 140-144.

LIANG, Y., RIDZON, D., WONG, L. & CHEN, C. 2007. Characterization of microRNA expression profiles in normal human tissues. *BMC Genomics,* 8**,** 166.

MANTEL, P. Y., HJELMQVIST, D., WALCH, M., KHAROUBI-HESS, S., NILSSON, S., RAVEL, D., RIBEIRO, M., GRURING, C., MA, S., PADMANABHAN, P., TRACHTENBERG, A., ANKARKLEV, J., BRANCUCCI, N. M., HUTTENHOWER, C., DURAISINGH, M. T., GHIRAN, I., KUO, W. P., FILGUEIRA, L., MARTINELLI, R. & MARTI, M. 2016. Infected erythrocyte-derived extracellular vesicles alter vascular function via regulatory Ago2-miRNA complexes in malaria. *Nat Commun,* 7**,** 12727.

MANTEL, P. Y. & MARTI, M. 2014. The role of extracellular vesicles in Plasmodium and other protozoan parasites. *Cell Microbiol,* 16**,** 344-54.

NEWBOLD, C., CRAIG, A., KYES, S., ROWE, A., FERNANDEZ-REYES, D. & FAGAN, T. 1999. Cytoadherence, pathogenesis and the infected red cell surface in Plasmodium falciparum. *Int J Parasitol,* 29**,** 927-37.

PISITKUN, T., SHEN, R. F. & KNEPPER, M. A. 2004. Identification and proteomic profiling of exosomes in human urine. *Proc Natl Acad Sci U S A,* 101**,** 13368-73.

RYAN P., ATREYA C. (2011). Blood cell microRNAs: what are they and what future do they hold? Transfus. Med. Rev. 25 247–251. 10.1016/j.tmrv.2011.01.005

RUBIO M., BASSAT Q., ESTIVILL X. and MAYOR A. (2016). Tying malaria and microRNAs: from the biology to future diagnostic perspectives. Malar. J. 15, 167 10.1186/s12936-016-1222-9

RUG, M., PRESCOTT, S. W., FERNANDEZ, K. M., COOKE, B. M. & COWMAN, A. F. 2006. The role of KAHRP domains in knob formation and cytoadherence of P falciparum-infected human erythrocytes. *Blood,* 108**,** 370-8.

RUIZ-TAGLE, C., NAVES, R. & BALCELLS, M. E. 2020. Unraveling the Role of MicroRNAs in Mycobacterium tuberculosis Infection and Disease: Advances and Pitfalls. *Infect Immun,* 88.

RYAN, P. & ATREYA, C. 2011. Blood cell microRNAs: what are they and what future do they hold? *Transfus Med Rev,* 25**,** 247-51.

SANGOKOYA, C., LAMONTE, G. & CHI, J. T. 2010. Isolation and characterization of microRNAs of human mature erythrocytes. *Methods Mol Biol,* 667**,** 193-203.

SHAH, M. D., BERGERON, A. L., DONG, J. F. & LOPEZ, J. A. 2008. Flow cytometric measurement of microparticles: pitfalls and protocol modifications. *Platelets,* 19**,** 365-72.

Sun L, YU Y, NIU B, WANG D. Red Blood Cells as Potential Repositories of MicroRNAs in the Circulatory System. Front Genet. 2020 Jun 3;11:442. doi: 10.3389/fgene.2020.00442. PMID: 32582273; PMCID: PMC7286224

SUNDARARAJAN, V., BURK, U. C. & BAJDAK-RUSINEK, K. 2022. Revisiting the miR-200 Family: A Clan of Five Siblings with Essential Roles in Development and Disease. *Biomolecules,* 12.

569 SZATANEK, R., BAJ-KRZYWORZEKA, M., ZIMOCH, J., LEKKA, M., SIEDLAR, M. & BARAN, J. 2017. The Methods of
570   Choice for Extracellular Vesicles (EVs) Characterization. *Int J Mol Sci,* 18.
571 TERUEL-MONTOYA, R., KONG, X., ABRAHAM, S., MA, L., KUNAPULI, S. P., HOLINSTAT, M., SHAW, C. A., MCKENZIE,
572   S. E., EDELSTEIN, L. C. & BRAY, P. F. 2014. MicroRNA expression differences in human hematopoietic cell
573   lineages enable regulated transgene expression. *PLoS One,* 9**,** e102259.
574 TERUEL-MONTOYA, R., ROSENDAAL, F. R. & MARTINEZ, C. 2015. MicroRNAs in hemostasis. *J Thromb Haemost,* 13**,**
575   170-81.
576 TRAGER, W. & JENSEN, J. B. 2005. Human malaria parasites in continuous culture. 1976. *J Parasitol,* 91**,** 484-6.
577 Vu L, Ragupathy V, Kulkarni S, Atreya C. Analysis of Argonaute 2-microRNA complexes in ex vivo stored red blood
578   cells. Transfusion. 2017 Dec;57(12):2995-3000. doi: 10.1111/trf.14325. Epub 2017 Sep 20. PMID:
579   28940437.
580 WELLS, A. C., DANIELS, K. A., ANGELOU, C. C., FAGERBERG, E., BURNSIDE, A. S., MARKSTEIN, M., ALFANDARI, D.,
581   WELSH, R. M., POBEZINSKAYA, E. L. & POBEZINSKY, L. A. 2017. Modulation of let-7 miRNAs controls the
582   differentiation of effector CD8 T cells. *Elife,* 6.
583 WILLEIT P, ZAMPETAKI A, DUDEK K, KAUDEWITZ D, KING A, KIRKBY NS, Crosby-Nwaobi R, Prokopi M, Drozdov I,
584   Langley SR, Sivaprasad S, et al. Circulating microRNAs as novel biomarkers for platelet activation. Circ Res.
585   2013;112(4):595–600
586 WU, C. W., CAO, X., BERGER, C. K., FOOTE, P. H., MAHONEY, D. W., SIMONSON, J. A., ANDERSON, B. W., YAB, T. C.,
587   TAYLOR, W. R., BOARDMAN, L. A., KISIEL, J. B. & AHLQUIST, D. A. 2017. Novel Approach to Fecal Occult
588   Blood Testing by Assay of Erythrocyte-Specific microRNA Markers. *Dig Dis Sci,* 62**,** 1985-1994.
589 ZHANG Y., ROCCARO A. M., ROMBAOA C., FLORES L., OBAD S., FERNANDES S. M., et al. (2012). LNA-mediated anti-
590   miR-155 silencing in low-grade B-cell lymphomas. Blood 120, 1678–1686 10.1182/blood-2012-04-425207
591 ZHOU, M. H., ZHANG, L., SONG, M. J. & SUN, W. J. 2018. MicroRNA-218 prevents lung injury in sepsis by inhibiting
592   RUNX2. *Eur Rev Med Pharmacol Sci,* 22**,** 8438-8446.

593

594

STAR ★ METODS

- ### CELL CULTURE AND REAGENTS

Plasmodium falciparum isolate and culture

IT4 (FCR3S1.2)	August 1976, 1 ml of patient blood (MRCL, Fajara-Gambia, West Africa) was diluted in 10 ml of RPMI 1640 and 10% FCS and shipped on wet ice to New York, NY, USA. Parasites were cultured directly in continuous cultures using the Petri-dish-candle jar technique (Jensen und Trager, 1978), giving line FCR3 or IT4. Although it was suspected to be mixed with another Brazilian isolate, it only contained one genome. This isolate was supplied by Mo Klinkert, BNITM, Hamburg.
Human Serum	Human Serum (A$^+$) Interstate Blood Bank, Inc (Memphis, USA).
Human red blood cells (RBCs)	Human Blood (0+) University Clinic-Eppedorf-Hamburg-Germany. Freshly isolated blood cells were used in the experiments. They were kept in a fridge at 4°C for a maximum of 2 weeks.

Reagents

Reagent	Source	Identifier
RPMI 1640	Applichem	A1538,9010
Hypoxanthine	Sigma	H9636-56
Gelatin from porcine skin-175 g bloom type A	Sigma	G2625
D-Sorbitol	Sigma	S1876

- ### KITS AND MATERIALS

Reagent/Material	Source
QUbit ^{TM} Protein Assay Kit #Q33211	ThermoFisher Scientific, Waltham, USA
Ultrafiltration units 100,000 MWCO PES	Sartorius, Göttingen, Germany
miRNeasy mini-Kit	Qiagen, Hilden, Germany
Agilent 2100® bioanalyzer Pico-Kit	Agilent
QIAseq Standard mRNA Select Kit (96) #180775	Qiagen
NextSeq 500/550 Mid Output Kit v.25 (150 Cycles) #20024904	illumina

Reagent	Source	Identifier
α human CD235a -HI264	Biolegend, San Diego, USA	#349103
goat-anti mouse colloidal gold-conjugated secondary antibody	Jackson Immuno Research, Cambridge shire, UK	-
CALM2 monoclonal antibody	MyBiosource.com	#MBS200093
Anti-HSP90α	Merck	#CA1023-50UG
ALEXA FLUOR 488	Thermo Fisher Scientific	#A28175
QuDye dsDNA HS Assay Kit	Lumiprobe	# 12102

- ### SOFTWARES

Software	Version	Source
NanoSight Software	(NTA3 0064)	-
Agilent 2100® bioanalyzer software	-	Santa Clara, USA
CLC genomics work bench	version 21	Qiagen, Aarhus
IPA	-	Qiagen, Aarhus
Graphpad Prism	Version 9.4.1	San Diego, California

606

- **DATA DEPOSIT**

Contact for reagent and resource sharing

612

- **METHOD DETAILS**

P. falciparum culture

The IT4 (FCR3S1.2) isolate was cultivated in RPMI medium in the presence of 10% human serum
A+ (Interstate Blood Bank, Inc. Memphis, TN, USA) and human O+ erythrocytes (5% hematocrit;
UKE, Hamburg, Germany) according to standard procedures (Trager & Jensen 1976). Parasite
cultures were synchronized once per week using 5% sorbitol (Lambros et al 1979). Trophozoites
were enriched using 1% gelatine solution on the day of harvest to remove niRBCs. Then, the
80-90% trRBCs were lysed in 4X Trizol and stored at -80°C until the miRNA/mRNA purification
step. Part of the enriched trRBC sample was cultivated with sufficient medium and niRBCs to
allow approximately 70-90% riRBCs to be reached on the day after initiating cultivation. The
riRBCs were lysed in 4X Trizol and kept at -80°C until the miRNA/mRNA purification step. niRBCs
were also incubated in vesicle-free medium for two days before miRNA/mRNA purification as
a control.

Extracellular vesicles purification

iRBCs-EVs were isolated from IT4 *P. falciparum* cell culture with 10% parasitemia as previously
described (Mantel and Marti, 2014). In brief, the medium was changed to vesicle-depleted
RPMI medium (depletion was done by centrifugation at 100,000 rcf for 90 min at 4°C). On the
next day, (28 h after changing the medium), the cell culture supernatants (100 ml from 10 Petri
dishes) were collected and sequentially centrifuged at 600 g, 1600 g, 3600 g and 10,000 g for
15 min each. After each step, the respective supernatant was collected for the next
centrifugation step. To concentrate the EVs, the suspension was passed through ultrafiltration
units (100,000 MWCO PES; Sartorius, Göttingen, Germany) for 30 min at 3000 g. The EVs
contained in the concentrated supernatant were dissolved in PBS, layered on top of a 60 %
sucrose cushion, and centrifuged at 100,000 g for 16 h at 4°C. The interphase was collected and
washed with PBS twice at 100,000 g for 60 min at 4°C. EVs were resuspended and pooled in

638 1000 µL PBS (0.2 µm filtered) and stored in 200 µL aliquots at -80°C. For isolation of EVs from

639 uninfected RBCs (RBC-EV), which were used as negative controls in subsequent experiments,

640 10 petri dishes of 500 µL human blood 0+ (UKE Hamburg, Germany) and 10 ml *P. falciparum*

641 culture medium for EV isolation were incubated at 37 °C. After 28 h supernatants were

642 collected and processed as described above. Protein concentration of EV samples was

643 determined using the QUBIT Protein Assay Kit (ThermoFisher Scientific, Waltham, USA)

644 according to manufacturer's instructions and by measuring the A_{280} content on a

645 Nanodrop2000 (ThermoFisher Scientific, Waltham, USA).

646 **Electron microscopy**

647 Glow-discharged carbon- and formvar-coated nickel grids (Plano GmbH, Wetzlar, Germany)

648 were incubated with aliquots of freshly isolated EVs. After washing with PBS and incubation in

649 the blocking buffer (0.5% BSA in PBS), the EVs on the grids were labelled with the primary

650 antibody (α human CD235a -HI264, Biolegend, San Diego, USA) at a concentration of 1:100 v/v

651 in PBS (PAA-Laboratories GmbH, Pasching, Austria) containing 0.5% BSA (Sigma-Aldrich,

652 Steinheim, Germany) for at least 21 h at 4°C. The controls for antibody specificity included

653 omitting the primary antibody from the incubating solution. After the incubation period, the

654 grids were rinsed in buffer and further incubated with a goat-anti mouse colloidal gold-

655 conjugated secondary antibody (12 nm gold particles from Jackson Immuno Research,

656 Cambridgeshire, UK) at a dilution of 1:100 v/v for at least 21 h at 4°C. Nickel grids were rinsed

657 in buffer and stained with 2% aqueous uranyl acetate (Electron Microscopy Sciences, Hatfield,

658 USA) for 15 sec. Grids were finally observed under a Tecnai Spirit electron microscope (Thermo

659 Fisher Scientific, Waltham, USA) operating at 80 kV, and images were recorded with a digital

660 CCD camera.

661 **Nano particle tracking analysis (NTA) with Nanosight NS300**

662 Purified EVs pellet were diluted 1:300 in PBS. The following settings were set according to the

663 manufacturer's software manual (NanoSight LM10 User Manual, MAN0510-04-EN, 2015): the

664 camera level was increased until all particles were distinctly visible (level16 and gain=20). A

665 total number of 900 frames was recorded in each session (camera: CCD). The autofocus was

666 adjusted to avoid indistinct particles. For each measurement, five 1-min videos were captured

667 under the following conditions: cell temperature: 25°C; Frame rate/FBS: 30. After capture, the

668 videos were analyzed by the in-build NanoSight Software (NTA3 0064) with a detection
669 threshold of 6 and screen gain of 10.

670

671 **Immunofluorescence assays**

672 Blood smears (10 μl) were taken from IT4 *P. falciparum* cultures with 1–3 % parasitaemia. The smears
673 were fixed in acetone for 30 min and then rehydrated with 1x PBS for 5 min. The first antibody (1:20 in
674 3% BSA/PBS; CALM2 monoclonal antibody #MBS200093 (MyBiosource.com) or anti-HSP90α #CA1023-
675 50UG (Merck) was then added and the slides were incubated for one hour in a humid dark box. The
676 smears were washed 5x with 1X PBS and then labelled with AlexaFluor (1:1000) (Thermo Fisher #
677 A28175) and DAPI (1mg/ml) (1:1000) (Roche # 10236276001) for 1 h in a humid dark box. After a 5x
678 wash with 50 μl 1x PBS, the smears were air dried and Moviol was added before they were covered with
679 a plastic cover slip. Images were taken through a EVOS FL auto-inverted microscope (Thermo Fisher
680 Scientific, Waltham, USA) and analysed using ImageJ 1.53K. To calculate the corrected total cell
681 fluorescence (CTCF), the following formula was used: Integrated Density – (Area of selected cell X Mean
682 fluorescence of background readings).

683

684 **mRNA purification and sequencing**

685 Samples in Trizol were thawed before adding 200 μl chloroform and centrifugation for 30 min
686 at 4°C and 12000 rpm. The miRNeasy mini-Kit- (Qiagen, Hilden, Germany) was used according
687 to the manufacturer's instructions. The quality of mRNA/miRNA was assessed using the Agilent
688 2100® bioanalyzer system. According to the manufacturer's instructions, Ribosomal RNA was
689 removed using QIAseq FastSelect RNA Removal Kit. The QIAseq Stranded mRNA Select Kit was
690 used for mRNA enrichment. mRNA was sequenced using NextSeq 500/550 Mid Output Kit v2.5
691 (150 Cycles).

692 **miRNA purification and sequencing**

693 Samples in Trizol were thawed before adding 140 μl chloroform and centrifugation for 15 min
694 at 4°C and 12000 rpm. The miRNeasy mini-Kit- (Qiagen, Hilden, Germany) was used according
695 to the manufacturer's instructions. The quality of mRNA/miRNA was assessed using the Agilent
696 2100® bioanalyzer system. miRNA library preparation was performed in BGI Genomics – China.
697 The small RNAs (18-30 nt) were purified by PAGE. For adapter ligation, the purified RNA was
698 incubated with 3' adapter followed by the 5' adapter. Reverse transcription PCR was then
699 performed and the PCR product was purified by PAGE. After denaturating and circularizing the

700   DNA product, single-stranded circular DNA molecules were replicated via rolling cycle

701   amplification, and a DNA nanoball (DNB) containing multiple copies of DNA was generated.

702   DNBseq-UMI was then performed and about 18 M reads were generated per sample. UMI is

703   known to correct the quantitative bias caused by PCR amplification of more than 70% small

704   RNAs (Fu et al., 2018).

705   • **DATA ANALYSIS**

706   Bioinformatics analysis was conducted using CLC genomics work bench version 22 (Qiagen,

707   Aarhus). Clean reads were imported, and miRNA was quantified and annotated on the miRbase

708   v22. Differential expression was performed, and P-values were adjusted using FDR 10%. hsg19

709   was used as a mRNA reference.

710   **CLC Parameters(miRNA-Quantification):**
711
712   miRBase: miRBase-Release_v22 / Prioritized species = Homo sapiens / Allow length based isomiRs = Yes /
713   Additional upstream bases = 2 / Maximum mismatches = 2 / Strand specific = Yes / Minimum sequence length =
714   18 / Maximum sequence length = 25
715
716   **CLC differential expression Parameters (miRNA/mRNA):**
717
718   Whole transcriptome RNA-seq / Normalization Method = TMM / Filter on Average expression for FDR correction
719   / Result Handling = Save
720
721   **CLC Trim Parameters(mRNA):**
722
723   Trim using quality scores = Yes / Quality limit = 0.05 / Trim ambiguous nucleotides = Yes / Maximum number of
724   ambiguities = 2 / Automatic read-through adapter trimming = Yes / Remove 5' terminal nucleotides = No / Remove
725   3' terminal nucleotides = No / Trim to a fixed length = No / Maximum length = 150 / Trim end = Trim from 3'-end
726   / Discard short reads = No / Discard long reads = No / Save discarded sequences = No / Save broken pairs = No /
727   Create report = Yes
728
729   **CLC RNA-seq Parameters (mRNA):**
730
731   Enable spike-ins = No / Database files = Homo sapiens (hg19) sequence / Maximum cost = 2 / Similarity fraction =
732   0.8 / Auto-detect paired distances = Yes / Maximum number of hits for a read = 10 / Strand setting = Both /
733   Minimum supporting count = 5 / Create report = Yes / Unmapped reads = No / Expression value = Total count
734

735   **Data availability**

736   The raw reads were deposited in NCBI (Bioproject Number: PRJNA897869).

737
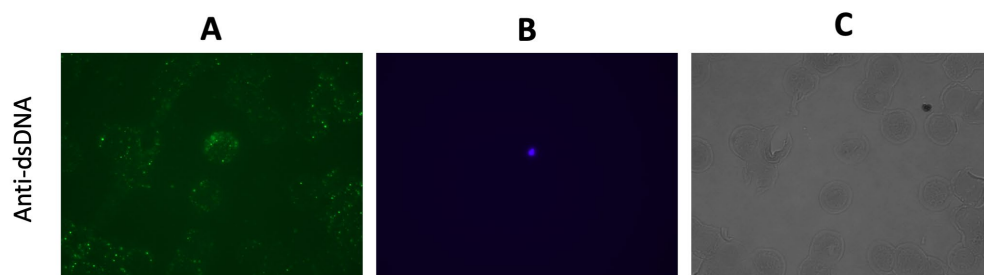
Supplemental Fig 1. Human red blood cells were labelled using anti-dsDNA antibody (Lumiprobe), which was then conjugated to Alexa-Fluor-488 (Thermo Fisher Scientific) as a secondary antibody (No reaction was observed with the secondary antibody alone). Nuclei of infected red blood cells were stained with Hoechst-33342 (1:1000) (Sigma) (A) Green (GFP) channel (B) Blue channel and (C) Phase channel. Images were taken at 20x magnification using an EVOS FL Auto inverted microscope (Thermo Fisher Scientific, Waltham, USA).

2.2 Analysis of the interaction between *Plasmodium falciparum*-infected erythrocytes and human endothelial cells using a laminar flow system, bioinformatic tracking and transcriptome analysis.

Chapter 11

Analysis of the Interaction Between *Plasmodium falciparum*-Infected Erythrocytes and Human Endothelial Cells Using a Laminar Flow System, Bioinformatic Tracking and Transcriptome Analysis

Yifan Wu, Philip Bouws, Stephan Lorenzen, Iris Bruchhaus, and Nahla Galal Metwally

Abstract

During malaria infection, the endothelial lining of the small blood vessels of the brain and other vital organs is strongly stimulated. This leads to fatal complications and poor prognosis of the infection. It is believed that two main reasons are responsible for this pathology, namely the cytoadhesion of *Plasmodium falciparum*-infected erythrocytes (IEs) on the one hand and the proinflammatory products released by the IEs which activate the endothelial cells (ECs) on the other hand. Until recently, most of the studies that characterized the activation of ECs were performed under static conditions, which do not reflect the real sequelae in vivo. In this chapter, we present a system, which allows authentic simulation of the IEs–ECs interactions during *P. falciparum* infection.

The main idea of the system is to provide an adequate shear stress over the ECs during the cytoadhesion and stimulation with IEs, which provides a better basis for the investigation of the cytoadhesion pathology through analyzing the ECs' transcriptome after stimulation. On the other hand, analyzing the transcriptome of the IEs might also give deeper analysis of their response to shear stress. Deep understanding of these events might help in the development of novel treatment strategies that interfere with this cell–cell interaction.

Key words Endothelial cells, Shear stress, Cytoadhesion, *P. falciparum*, Cerebral malaria

1 Introduction

Plasmodium falciparum causes the most severe form of malaria. This is thought to be mainly due to the cytoadherence of *P. falciparum*-infected erythrocytes (IEs) on the endothelial lining of microvessels and activation of endothelial cells (ECs) due to

---

Yifan Wu and Philip Bouws contributed equally to this work.

inflammatory products secreted by the IEs [1]. For the cytoadhesion interactions, several interactive parasite ligands and host receptors were identified. The most well-described parasite ligand is *P. falciparum* erythrocyte membrane protein 1 (*Pf*EMP1). *Pf*EMP1 proteins are encoded by the *var* gene family, there are about 60 *var* genes per parasite genome [2–4]. *Pf*EMP1 is known to impose domains which bind to different receptors on human ECs such as CD36, ICAM-1 (intracellular adhesion molecule-1), EPCR (endothelial protein C receptor), and CSA (chondroitin sulfate A) [4–7]. Cytoadhesion leads to accumulation of IEs in the vascular bed of vital organs which might obstruct the vessels and stop the blood supply. *Pf*EMP1 is composed of variable domains with great amino acid sequence diversity among different parasite isolates. The complexity of the *Pf*EMP1 composition on the surface of IEs makes it difficult to target these proteins to inhibit the cytoadhesion [4–7].

EC activation is defined as changes that occur in both morphology and behavior of ECs due to exposure to a cytokine, chemokine, cellular ligand, or soluble factor [8, 9]. During infection with *P. falciparum* much remained unknown in signaling initiation within the ECs. ECs are thought to be activated by inflammatory cytokines and other material released during the rupture of IEs (such as hemoglobin and histones) and by the cytoadhesion of IEs [10–12]. This leads to a proinflammatory state of the ECs, activation of the clotting mechanisms that impairs the barrier function. Vascular leak will be followed and accordingly direct interaction of the cytokines and toxins with the host tissue and finally organ damage. Cytoadhesion and EC activation are tightly linked. Cytoadhesion can cause EC activation and on the other hand EC activation enhances cytoadhesion to receptors such as ICAM-1 (a vicious circle). This link between the two pathways makes it difficult to determine the primary initiating event [12].

The endothelium actively maintains about 60,000 miles of blood vessels in the human body. It used to be thought that ECs had only a barrier function, as a "cellophane wrapper" of the vascular tree. Several years of research have shown that ECs have variable functions [13]. These include blood vessel tone, blood flow, hemostasis, recruitment of neutrophils, hormone trafficking, and filtration [14, 15]. ECs are normally under different shear stresses depending on the dimension of vessels. Shear stress is defined as the dragging frictional force generated by flowing blood. ECs respond to shear stress through structural alignment of the cells and the secretion of subsets of proteins [16]. Normal physiological flow is a laminar flow, associated with physiological phenotype of the ECs. Recently, it has been described that, a subset of miRNAs in the ECs called "mechano-microRNAs (miRNAs)" respond to flow [16]. The exposure of ECs to different shear
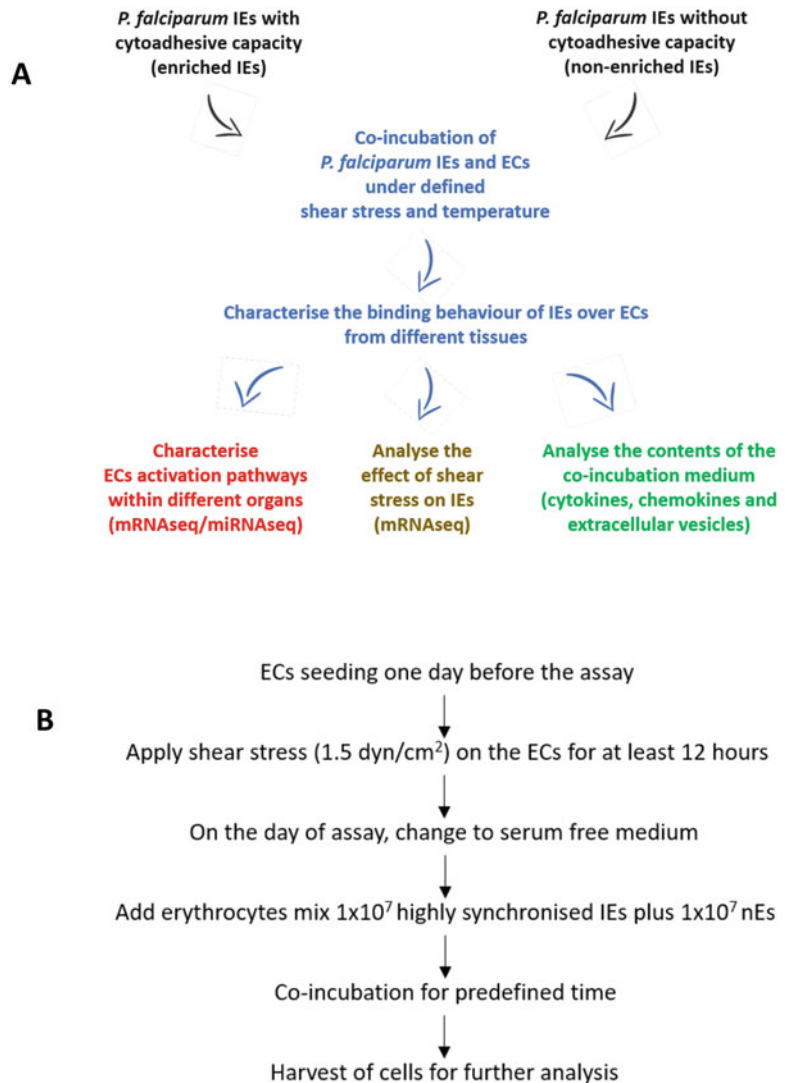
Fig. 1 (**a**) shows the main idea of the experimental design and the different outputs of the study. (**b**) explains the main steps of the co-incubation experiment

stresses leads to various intracellular responses that modulated the expression of some receptors on the cell surface [16].

Authentic stimulation of the ECs is important to monitor in detail the first signal of the proinflammatory response and the following cascades. We, therefore, set out to examine the initiating signal for the activation of ECs during interaction with *P. falciparum* IEs (Fig. 1). We present a novel experimental design, which will provide data that will close some of our knowledge gaps. First, we use a laminar flow system (with a predefined shear stress value, flow rate, and temperature) to mimic the human blood circulation, which enabled us to obtain an in vivo-like situation of

IEs within the human circulation. Using next-generation sequencing (NGS) technology in transcriptome sequencing and analysis of different ECs from different tissues will help in dissecting both molecular and cellular aspects of inflammatory response to *P. falciparum* infection.

2   Materials

2.1   Cells

1. Endothelial cells: HBEC-5i (ATCC® CRL-3245™) cultivated in DMEM F12 according to ATCC® guidelines. HULEC (ATCC® CRL -3244™) cultivated in MCDB131 according to ATCC® guidelines.

2. *P. falciparum* isolate IT4/FCR3S1.2 (long-term laboratory adapted), cultivated in RPMI medium with 10% human serum (A⁺) and 5% hematocrit (0⁺). The culture was incubated at 37 °C in 5% CO_2, 1% O_2, and 94% N_2. Medium was changed daily and the culture was split according to the experiments' requirements [17]. Gelatine flotation was used on the day of flow experiments to isolate *P. falciparum* knobby IEs.

2.2   Laminar Flow System

1. Ibidi Pump system (ibidi, Gräfelfing, Germany).

2. Yellow green perfusion set (ibidi, Gräfelfing, Germany).

3. µ-Slide-0.8 Luer ibiTreat channel (ibidi, Gräfelfing, Germany).

2.3   Lab Equipment

1. 37 °C incubator (or other temperature) and 5% CO_2.

2. Laptop to control the pump.

3. Inverted microscope with camera for video recording (we used EVOS FL Auto-inverted microscope (Thermo Fisher Scientific, Waltham, USA).

4. Temperature controlling hood for inverted microscope.

5. Agilent 2100® bioanalyzer system (Agilent, Santa Clara, USA).

2.4   Kits

1. Qiagen RNA Mini Kit (Qiagen, Hilden Germany).

2. Agilent RNA 6000 Pico Kit (Agilent, Santa Clara, USA).

3. QIAseq FastSelect RNA Removal Kit (Qiagen, Hilden Germany).

4. QIAseq Stranded RNA Library Kits (Qiagen, Hilden Germany).

5. NextSeq 500/550 Mid Output Kit v2.5 (150 Cycles) (Illumina, San Diego, USA).

   (a) **Buffers and enzymes**
   - RPMI culture medium: the following components were mixed and sterile filtrated: 16.4 g RPMI 1640 powder dissolved in 800 mL distilled water; 0.05 g hypoxanthine dissolved in 70 mL distilled water;

100 mL human serum (A$^+$) inactivated two times for 30 min at 56 °C; 30 mL 7.5% NaHCO$_3$; 250μL gentamycin (40 mg/mL).

- PBS 10× (pH 7.4): 80 g (1.37 M); NaCl$_2$ g (27 mM) KCl; 14.4 g (101 mM) Na$_2$HPO$_4$ (anhydrous); 18 mM KH$_2$PO$_4$.

- Accutase cell detachment solution with 0.5 mM EDTA.

- TRIzol™ Reagent (Thermo Fisher Scientific, Waltham, MA, USA).

3 Methods

3.1 Co-Incubation of IEs and ECs Using a Laminar Flow System

1. For the co-incubation of IEs and ECs using a laminar flow system, seed a total of 2×10^5 ECs in one laminar flow slide.

2. Allow the ECs to adhere for about 2 h.

3. During this, add 14 mL of ECs culture medium into the fluidic unit.

4. Connect the perfusion set and run "remove air bubbles" demo.

5. Connect the slides to the perfusion set and the fluidic unit and start the flow with shear stress 1.5 dyn/cm^2 [18].

6. Incubate the fluidic unit and slides at 37 °C for at least 12 h.

7. On the day of the assay, stop the run and change the medium to serum-free RPMI medium.

8. IEs must be highly synchronized (ring/trophozoite/schizont stage). Gelatine flotation [19] is used to select the trophozoite/schizont stages on the day of assay or 1 day before the assay to obtain synchronized ring stages IEs. For this, the following steps are followed:

    (a) Pellet the culture in a 15 mL falcon for 5 min at 800 ×g.

    (b) Resuspend the culture pellet in 1 volume of prewarmed RPMI medium.

    (c) Add two volumes of prewarmed 1% gelatin and mix gently.

    (d) Incubate for 20 min at 37 °C.

    (e) Remove the supernatant carefully and transfer it to a 15 mL reaction tube. Pellet the enriched IEs for 5 min at 800 ×g. Follow with washing with serum-free RPMI one time and then pellet again. Finally, resuspend the pellet in 1 mL serum-free RMPI medium to estimate the cell count.

9. Transfer in total 2×10^7 IEs from **step 8** to the fluidic unit (50% IEs and 50% non-infected erythrocytes (nEs)).

10. As a control, nEs should be used in a separate fluidic unit.

11. Set the shear stress to 1.5 dyn/cm^2 (physiologically relevant shear force).

12. Set up the co-incubation period to 8 or 12 h.

13. After the co-incubation period, stop the experiment and disconnect the fluidic unit.

14. Wash the ECs with PBS and add 200μL Accutase, incubate for 2 min at 37 °C.

15. Collect the detached ECs using serum-free medium.

16. Centrifuge the cell suspension, aspirate the supernatant, add 500μL TRIzol™, and keep at −80 °C until further isolation of RNA/miRNA.

17. Collect the medium (containing IEs/nEs) from the unit in a 15 mL reaction tube.

18. Centrifuge the medium, the supernatant might be frozen for further investigations at −80 °C.

19. Collect the IEs/nEs after centrifugation, add 500μL TRIzol™, and keep at −80 °C until the further isolation of RNA/miRNA.

3.2 Isolation of RNA/miRNA and NGS Sequencing of ECs

1. Qiagen® miRNeasy Mini Kit according to manufacturer's instructions follow these steps:

    (a) Thaw the samples from **step 19** at room temperature.

    (b) For every 500μL, add 140μL chloroform and shake strongly for 15 s then incubate at room temperature for 2 min. This is followed by 15 min centrifugation at 4 °C and 12,000 ×g.

    (c) Transfer the upper aqueous phase in a new tube, add 500μL of 10% ethanol, and mix gently. Then transfer the mixture into an RNeasy Mini spin column and centrifuge at 8000 ×g for 15 s at room temperature. Discard the flow-through.

    (d) Wash with 700μL Buffer RWT and centrifuge for 15 s at 8000 ×g and discard the flow-through.

    (e) Perform two times wash with 500μL Buffer RPE and centrifuge for 15 s at 8000 ×g and discard the flow-through.

    (f) To elute the RNA, transfer the RNeasy Mini spin column to a new 1.5 mL collection tube. Pipet 25μL RNase-free water directly onto the RNeasy Mini spin column membrane incubate for 2 min at room temperature. Centrifuge for 1 min at 8000 ×g. Repeat the elution step again to finally have 50μL solution.

    (g) Determine the RNA concentration using Nanodrop.

2. Evaluate the quality and quantity of the isolated RNA using Agilent 2100®bioanalyzer system. For this, we use Agilent RNA 6000® Pico kit.

    (a) Prepare the ladder according to the manufacturer's instructions and freeze it at −80 °C.

    (b) The gel dye mix is preferred to be prepared on the day of assay. Start by pipetting 550μL of the RNA 6000 Pico gel matrix over the supplied spin filter. Centrifuge for 10 min at 1500 ×g at room temperature. For the gel dye, mix pipette 65μL from the filtered gel into a new 1.5 mL RNAse-free tube. Add 1μL of RNA 6000 Pico dye and vortex. Centrifuge for 10 min at 13000 ×g at room temperature.

    (c) Put a new RNA 6000 Pico chip on the chip priming station. Add 9.0μL of gel dye in the corresponding well. Close chip priming station. Press plunger until it is held by the clip. Wait for exactly 30 s then release clip. Pipette 9.0μL of gel dye mix in the other two gel wells.

    (d) Pipette 9.0μL of the RNA 6000 Pico conditioning solution in the corresponding well. Pipette 5μL of RNA 6000 Pico marker in all 12 wells.

    (e) Pipette 1μL of the heat denatured and aliquoted ladder in the corresponding well. Pipette 1μL of sample in each of the 11 sample wells. Put the chip in the vortexer (IKA - Model MS3) and vortex for 1 min at the indicated setting (2400 rpm). Run the chip in the Agilent 2100 bioanalyzer within 5 min.

    (f) Evaluate the RIN value of each sample (we send for sequencing the samples with 7–10 RIN values).

3. For mRNAseq, we use IlluminaNextseq® platform (per transcriptome between 6 and 10 million reads should be enough). Considering miRNAseq, we usually send the samples to BGI Genomics Co (Shenzhen, China). Libraries were prepared using unique molecular identifiers (UMI)followed by NGS sequencing [20, 21].

3.3 Bioinformatics Data Analysis

1. Evaluate the quality of the reads using FastQC. This can be downloaded from (https://www.bioinformatics.babraham.ac.uk/projects/fastqc/). It is recommended to include only reads with ≥30 Phred quality score.

2. Remove the low-quality reads and sequencing adaptors. Then the clean reads are aligned to reference transcriptomes for ECs reads using RSEM and Bowtie2 [22]. Finally, identification of the differentially expressed genes can be performed using DEseq2 R package [23, 24] as follows:

```
#Trim:
 TrimmomaticPE raw_1.fq.gz raw_2.fq.gz trim_1.fq.gz /dev/null
trim_2.fq.gz /dev/null ILLUMINACLIP:TruSeq3-PE-2.fa:2:30:10:8:
true LEADING:5 TRAILING:10 SLIDINGWINDOW:4:15 MINLEN:36

 #RSEM:
 rsem-calculate-expression --bowtie2 --paired-end trim_1.fq.gz
trim_2.fq.gz reference sampleName

 #DESeq:
 suppressMessages(library(tximport))
suppressMessages(library(DESeq2))
LIST=c("ctrl1", "ctrl2", "ctrl3", "treat1", "treat2",
"treat3")
txi <- tximport(paste(LIST, ".genes.results", sep=""), type =
"rsem", txIn = FALSE, txOut = FALSE)
txi$length[txi$length==0]=1
what=c(rep("ctrl", 3), rep("treat",3))
colData=data.frame(row.names=LIST, what=what)
dds=DESeqDataSetFromTximport(txi, colData=colData, design=~-
what)
dds=DESeq(dds)
res=results(dds)
tab=data.frame(
   counts(dds, norm=T),
   baseMean=res[,"baseMean"],
   baseMeanA=rowMeans(counts(dds, norm=T)[,1:3]),
   baseMeanB=rowMeans(counts(dds, norm=T)[,4:6]),
   foldChange=2^(res[,"log2FoldChange"]),
   res[,c("log2FoldChange", "pvalue", "padj")])
tab=tab[order(tab$pval),]
write.table(tab, file="results.csv")
```

3. Statistical significance can be evaluated using the Benjamini-Hochberg method with a false discovery rate of 10%.

3.4 Imaging

To be able to characterize the binding behavior of IEs to ECs, movies could be recorded. In this case, different set-ups could be used, such as controlling the temperature of the assay or stimulating the ECs with different cytokines (TNF-α for example). After recording the image sequence (at least one every 3 s), trackdem R package could be used to track the IEs and record their exact binding behavior under different conditions as described in Subheading 3.5 [18–25].

3.5 R Tracking Script Used for bioinformatics Analysis

```
library(trackdem)
dir <- 'newtrack/404016'
class(dir) <- c('TrDm')
str (dir)
allFullImages <- loadImages(dirPictures=dir, nImages=1:201)
allFullImages
class(allFullImages)
## Detect background
stillBack <- createBackground(allFullImages,method='mean')
plot(stillBack)
## Subtract background
allImages <- subtractBackground(bg=stillBack)
plot(allImages)
## Identify moving particles
##findThreshold(allmages)
partIden <- identifyParticles(sbg=allImages, pixelRange=c
(3,500),select='both', autoThres=FALSE,threshold=0.1)
pit<-summary(partIden)
capture.output(pit, file = "sum_partIden-404016-6a.txt")
## Reconstruct trajectories
records <- trackParticles(partIden,L=50,R=1,weight=c(1,1,1))
ic<-summary(records, incThres = 10)
capture.output(ic, file = "records-404016-6a.txt")
## plots
plot(records,type='animation',incThres=10,name='animation_
404016-6a') # create animation
plot(records,type='trajectories',incThres=10,name='animation-
404016-6a')
# create tracks
## population count
icn<-summary (records, incThres = 10)$N
capture.output(icn, file = "sum_popcount-404016-6a.txt")
####### total displacement in pixels
dip<-summary(records,incThres=10)$particles[,"Total    move-
ment"]
capture.output(dip, file = "pix--404016-6a.txt")
S <- dip * 0.4572 #########pixels to um distance in um
write.table(S, "um-404016-6a.csv", sep="\t", row.name=FALSE)
capture.output(S, file = "um--404016-6a.txt")
```

4 Notes

1. For every experiment, at least two slides of ECs should be prepared to be able to isolate enough amount of RNA.

2. One fluidic unit can be used for 2–6 slides seeded with the same cell line. Slides could be connected with connectors supplied by ibidi®.

3. We have tried to use three fluidic units at the same time to perform three different parallel experiments, but we noticed that the flow might not be equally distributed among all three units, so we recommend using only two fluidic units per experiment.

4. In the software settings of pump controlling program, we set up the calibration factor to value of 1. This ensures the binding of IEs to ECs.

5. Using this method, ECs activation could be analyzed in the presence/absence of cytoadhesion. This is achieved by using IEs enriched for binding to the used ECs [26]. This can be performed through panning of the IEs with high binding capacity for 4–5 times. Other experiments could also be performed with the non-enriched IEs which have minimal binding capacity.

6. For deeper and two-way analysis, we recommend using one kit to isolate both RNA and miRNA at the same time.

References

1. Margaret A, Phillips JNB, Manyando C, van Huijsduijnen RH, Van Voorhis WC, Wells TNC (2017) Malaria. Nat Rev Dis Primers 3:17050

2. Cunnington AJ, Walther M, Riley EM (2013) Piecing together the puzzle of severe malaria. Sci Transl Med 5(211):211ps18

3. Taylor TE, Fu WJ, Carr RA, Whitten RO, Mueller JS, Fosiko NG, Lewallen S, Liomba NG, Molyneux ME (2004) Differentiating the pathologies of cerebral malaria by postmortem parasite counts. Nat Med 10(2):143–145. https://doi.org/10.1038/nm986

4. Craig AG, Khairul MF, Patil PR (2012) Cytoadherence and severe malaria. Malays J Med Sci 19(2):5–18

5. Rowe JA, Claessens A, Corrigan RA, Arman M (2009) Adhesion of Plasmodium falciparum-infected erythrocytes to human cells: molecular mechanisms and therapeutic implications. Expert Rev Mol Med 11:e16. https://doi.org/10.1017/S1462399409001082

6. Turner L, Lavstsen T, Berger SS, Wang CW, Petersen JE, Avril M, Brazier AJ, Freeth J, Jespersen JS, Nielsen MA, Magistrado P, Lusingu J, Smith JD, Higgins MK, Theander TG (2013) Severe malaria is associated with parasite binding to endothelial protein C receptor. Nature 498(7455):502–505. https://doi.org/10.1038/nature12216

7. Kyes S, Horrocks P, Newbold C (2001) Antigenic variation at the infected red cell surface in malaria. Annu Rev Microbiol 55:673–707. https://doi.org/10.1146/annurev.micro.55.1.673

8. Drexler H, Hornig B (1999) Endothelial dysfunction in human disease. J Mol Cell Cardiol 31(1):51–60. https://doi.org/10.1006/jmcc.1998.0843

9. Pate M, Damarla V, Chi DS, Negi S, Krishnaswamy G (2010) Endothelial cell biology: role in the inflammatory response. Adv Clin Chem 52:109–130

10. Cunnington AJ, Riley EM, Walther M (2013) Stuck in a rut? Reconsidering the role of parasite sequestration in severe malaria syndromes. Trends Parasitol 29(12):585–592. https://doi.org/10.1016/j.pt.2013.10.004

11. Kim H, Higgins S, Liles WC, Kain KC (2011) Endothelial activation and dysregulation in malaria: a potential target for novel therapeutics. Curr Opin Hematol 18(3):177–185. https://doi.org/10.1097/MOH.0b013e328345a4cf

12. Grau GE, Craig AG (2012) Cerebral malaria pathogenesis: revisiting parasite and host

contributions. Future Microbiol 7 (2):291–302. https://doi.org/10.2217/fmb. 11.155

13. Rajendran P, Rengarajan T, Thangavel J et al (2013) The vascular endothelium and human diseases. Int J Biol Sci 9(10):1057–1069. Published 2013 Nov 9. https://doi.org/10.7150/ijbs.7502

14. Wu F, Liu L, Zhou H (2017) Endothelial cell activation in central nervous system inflammation. J Leukoc Biol 101(5):1119–1132. https://doi.org/10.1189/jlb.3RU0816-352RR

15. Drexler H (1997) Endothelial dysfunction: clinical implications. Prog Cardiovasc Dis 39 (4):287–324

16. Rashad S, Han X, Saqr K, Tupin S, Ohta M, Niizuma K, Tominaga T (2020) Epigenetic response of endothelial cells to different wall shear stress magnitudes: a report of new mechano-miRNAs. J Cell Physiol 235 (11):7827–7839. https://doi.org/10.1002/jcp.29436

17. Trager W, Jensen JB (1976) Human malaria parasites in continuous culture. Science 193 (4254):673–675. https://doi.org/10.1126/science.781840

18. Lubiana P, Bouws P, Roth LK, Dorpinghaus M, Rehn T, Brehmer J, Wichers JS, Bachmann A, Hohn K, Roeder T, Thye T, Gutsmann T, Burmester T, Bruchhaus I, Metwally NG (2020) Adhesion between *P. falciparum* infected erythrocytes and human endothelial receptors follows alternative binding dynamics under flow and febrile conditions. Sci Rep 10(1):4548. https://doi.org/10.1038/s41598-020-61388-2

19. Waterkeyn JG, Cowman AF, Cooke BM (2001) *Plasmodium falciparum*: gelatin enrichment selects for parasites with full-length chromosome 2. Implications for cytoadhesion assays. Exp Parasitol 97(2):115–118. https://doi.org/10.1006/expr.2000.4593

20. Fu Y, Wu PH, Beane T, Zamore PD, Weng Z (2018) Elimination of PCR duplicates in RNA-seq and small RNA-seq using unique molecular identifiers. BMC Genomics 19:531

21. Raabe CA, Tang TH, Brosius J, Rozhdestvensky TS (2014) Biases in small RNA deep sequencing data. Nucleic Acids Res 42 (3):1414–1426. https://doi.org/10.1093/nar/gkt1021

22. Langmead B, Salzberg SL (2012) Fast gapped-read alignment with Bowtie 2. Nat Methods 9:357–359

23. R: a language and environment for statistical computing, R Core Team, R Foundation for Statistical Computing, Vienna, Austria. https://www.R-project.org

24. Love MI, Huber W, Anders S (2014) Moderated estimation of fold change and dispersion for RNA-seq data with DESeq2. Genome Biol 15(12):550. https://doi.org/10.1186/s13059-014-0550-8

25. Bruijning M, Visser MD, Hallmann CA, Jongejans E (2018) Trackdem: automated particle tracking to obtain population counts and size distributions from videos in R. Methods Ecol Evol 9(4):965–973

26. Metwally NG, Tilly AK, Lubiana P, Roth LK, Dorpinghaus M, Lorenzen S, Schuldt K, Witt S, Bachmann A, Tidow H, Gutsmann T, Burmester T, Roeder T, Tannich E, Bruchhaus I (2017) Characterisation of *Plasmodium falciparum* populations selected on the human endothelial receptors P-selectin, E-selectin, CD9 and CD151. Sci Rep 7(1):4069. https://doi.org/10.1038/s41598-017-04241-3

2.3 CD36-a host receptor necessary for malaria parasites to establish and maintain infection.

Review

CD36—A Host Receptor Necessary for Malaria Parasites to Establish and Maintain Infection

Anna Bachmann [1,2,3,4,†], Nahla Galal Metwally [1,†], Johannes Allweier [1,5], Jakob Cronshagen [1], Maria del Pilar Martinez Tauler [1], Agnes Murk [1], Lisa Katharina Roth [1], Hanifeh Torabi [1], Yifan Wu [1], Thomas Gutsmann [5] and Iris Bruchhaus [1,2,*]

1   Bernhard Nocht Institute for Tropical Medicine, 20359 Hamburg, Germany
2   Biology Department, University of Hamburg, 22601 Hamburg, Germany
3   Centre for Structural Systems Biology, 22607 Hamburg, Germany
4   German Center for Infection Research (DZIF), Partner Site Hamburg-Borstel-Lübeck-Riems, 20359 Hamburg, Germany
5   Division of Biophysics, Research Center Borstel-Leibniz Lung Center, 23845 Borstel, Germany
*   Correspondence: bruchhaus@bnitm.de
†   These authors contributed equally to this work.

Abstract: *Plasmodium falciparum*-infected erythrocytes (*Pf*IEs) present *P. falciparum* erythrocyte membrane protein 1 proteins (*Pf*EMP1s) on the cell surface, via which they cytoadhere to various endothelial cell receptors (ECRs) on the walls of human blood vessels. This prevents the parasite from passing through the spleen, which would lead to its elimination. Each *P. falciparum* isolate has about 60 different *Pf*EMP1s acting as ligands, and at least 24 ECRs have been identified as interaction partners. Interestingly, in every parasite genome sequenced to date, at least 75% of the encoded *Pf*EMP1s have a binding domain for the scavenger receptor CD36 widely distributed on host endothelial cells and many other cell types. Here, we discuss why the interaction between *Pf*IEs and CD36 is optimal to maintain a finely regulated equilibrium that allows the parasite to multiply and spread while causing minimal harm to the host in most infections.

Keywords: *Plasmodium falciparum*; malaria; sequestration; cytoadhesion; endothelial cell receptor; CD36

1. Introduction

Despite progress in malaria control, malaria remains one of the most important infectious diseases worldwide. In 2020, about 267 million malaria cases, including 409,000 deaths, were recorded [1]. Concerning all malaria parasites, the deadliest, *Plasmodium falciparum*, has a complex life cycle that alternates between *Anopheles* mosquitoes and humans. The asexual cycle that takes place in humans consists of the liver stage (multiplication of the parasite in hepatocytes) and the intraerythrocytic cycle (multiplication of the parasite in erythrocytes). Each intraerythrocytic cycle lasts approximately 48 h, during which the merozoite that invaded the erythrocyte develops through the ring stage to the trophozoite and finally the schizont. At the end of the intraerythrocytic cycle, the newly formed merozoites are released, ready to invade new erythrocytes. Some merozoites develop into gametocytes, which must be taken up by female Anopheles mosquitoes to complete their sexual development. The complexity of the parasite's life cycle and its masterful ability to evade its elimination by the host immune system challenge our efforts to combat the disease.

To survive in the human host, *P. falciparum* has evolved unique mechanisms, two of which, called sequestration and antigenic variation, rely mainly on a highly diverse protein family, the *P. falciparum* erythrocyte membrane protein 1 (*Pf*EMP1). The *Pf*EMP1s, which the parasite exposes on the surface of its host cell from the trophozoite stage onwards, have

at least a dual function. First, they bind to various endothelial cell receptors (ECRs) on the walls of blood vessels (sequestration), thereby disappearing from the peripheral circulation and bypassing removal by the spleen. Unlike other plasmodial species, the deformability of *P. falciparum* infected erythrocytes (*Pf*IEs) decreases as the parasite matures, so that circulating trophozoites and schizonts would be retained in the spleen and removed from circulation by resident macrophages [2–6]. Second, *Pf*EMP1 represents the main target of the humoral immune response [7], but due to the presence of numerous copies of *var* genes encoding *Pf*EMP1, the parasite can sequentially present different *Pf*EMP1 variants on the surface of its host cell and use them for sequestration. The ability to alter the presented *Pf*EMP1 by antigenic variation enables the parasite to stay one step ahead of the immune system and maintain long-lasting, chronic infections, e.g., for bridging dry seasons [8–12].

2. The *Pf*EMP1 Family

The *Pf*EMP1 family is encoded by about 45–90 *var* genes per parasite genome [12]. Expression of the *var* genes is mutually exclusive in ring-stage parasites, such that only a single *Pf*EMP1 variant is present on the surface of trophozoite- or schizont-stage *Pf*IEs at any given time [13,14] for review [10]. Mutually exclusive expression relies on very complex mechanisms. These are based on both epigenetic regulation and cis-acting DNA elements and RNA transcripts involved in *var* gene activation and silencing (for review [10]).

The *var* genes and their encoding *Pf*EMP1s vary greatly from parasite to parasite, and recombination constantly generates new variants, so there is an enormous repertoire of *var* genes in nature [13–16]. The molecular masses of *Pf*EMP1s range from 150 to 400 kDa. These proteins consist of an intracellular acidic terminal segment (ATS domain), a transmembrane domain, and a variable, extracellularly exposed region responsible for receptor binding. This extracellular region contains a single N-terminal segment (NTS; main classes A, B, and pam) and a variable number of different Duffy binding-like domains (DBL; main classes α–ζ and pam) and cysteine-rich interdomain regions (CIDR; main classes α–δ and pam) [17–20]. Approximately two-thirds of *var* genes localize in the subtelomeric regions of the chromosomes. Most of the subtelomeric and central localized *var* genes are located in regions of electron-dense heterochromatin at the nuclear periphery, with the active *var* gene shifting to the region of lower electron density [14]. Depending on the chromosomal localization, the upstream sequence, and the direction of transcription of the *var* genes, *Pf*EMP1s can be classified as A, B, C, or E [17,21–23].

A few conserved, strain-transcendent *var* variants have been described: *var1*, *var2csa* (group E), and *var3*. The *var1* gene occurs in two variants in the parasite population, *var1-3D7* and *-IT*, is often conserved as a pseudogene, and the encoded protein may not be presented on the erythrocyte surface [12,24]. VAR2CSA has an atypical domain architecture, mediates binding to chondroitin sulfate A (CSA) in the placenta, and is, thus, important in pregnancy-associated malaria [25]. VAR3 proteins are very short *Pf*EMP1s with unknown receptor binding phenotypes [26]. Analysis of 399 different *Pf*EMP1 sequences from seven *P. falciparum* genomes allowed the identification of 23 domain cassettes (DCs) that could be important for protein folding and binding to human ECRs, as well as for reflecting recombination breakpoints [17]. About 10% of *Pf*EMP1s variants belong to group A and are usually longer proteins with a head structure that includes a DBLα1 and either a CIDRα1 domain (CIDRα1.4–7) that binds to the endothelial protein C receptor (EPCR) or a CIDRβ/γ/δ domain with unknown receptor binding phenotype [12]. Groups B and C make up the majority of *Pf*EMP1s (at least 75%) and typically have DBLα0-CIDRα2–6 head structures that bind to CD36, followed by only two additional extracellular domains (DBLδ1, CIDRβ/γ). A subset of chimeric B-type proteins (group B/A, also known as DC8-containing proteins) has a DBLα2 domain (chimeric DBLα0/1 domain) and an EPCR-binding CIDRα1.1 or CIDRα1.8 domain typically attached to a complement component C1q receptor (C1qR)-binding DBLβ12 domain [27–34]. Thus, the head structure confers mutually exclusive binding properties to either EPCR (14%), CD36 (72%), CSA (3%), or to one or more unknown ECRs via the CIDRβ/γ/δ domains (10%) or VAR3 (1%) [35]. Con-

cerning the C-terminal to the head structure, most *Pf*EMP1s have additional DBL domains, of which certain subsets of the DBLβ domains bind intercellular adhesion molecule-1 (ICAM-1) [36,37] or C1qR [38]. As an example, the *Pf*EMP1 repertoire of the *P. falciparum* isolate IT4 is shown in Figure 1.
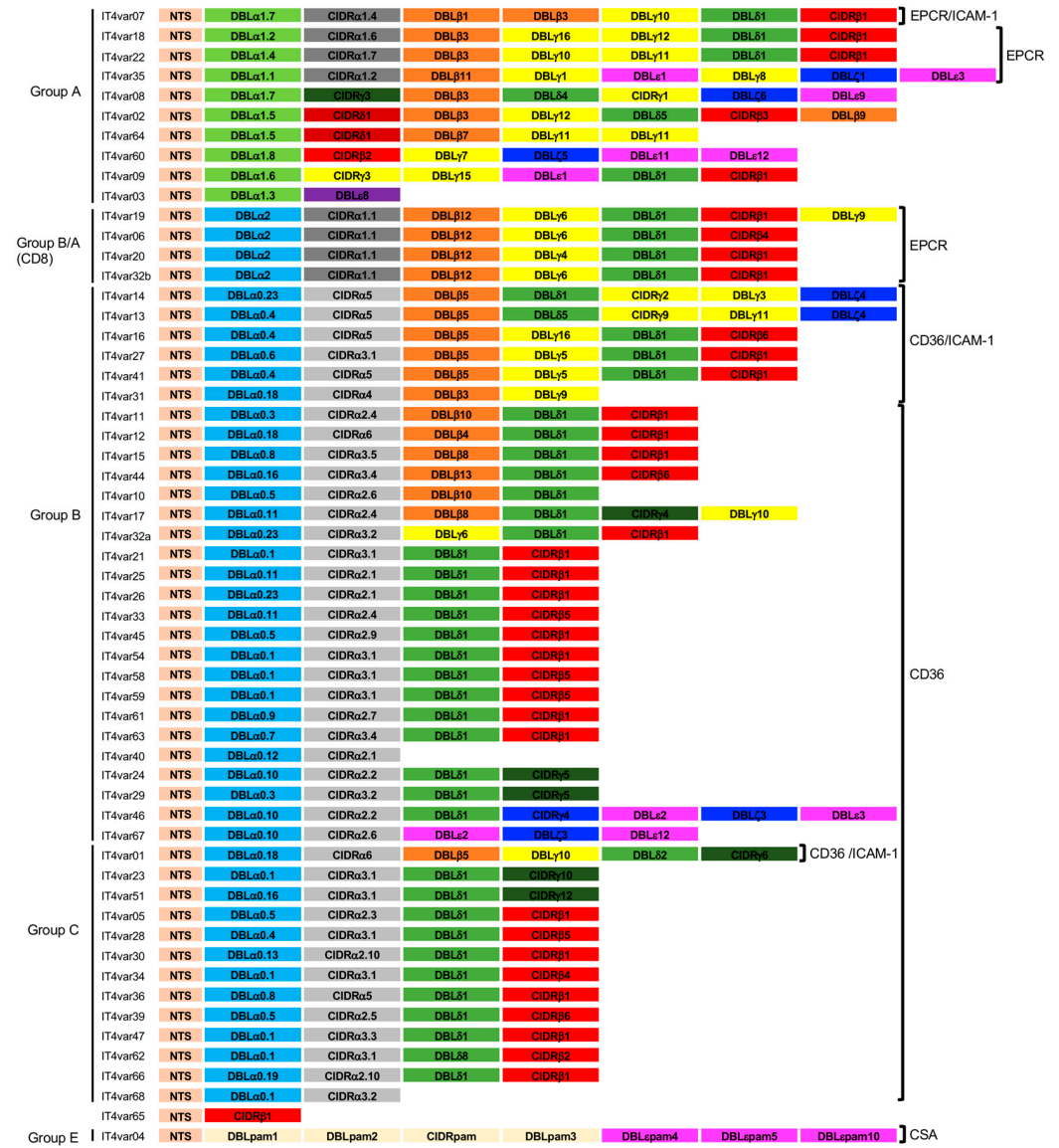
Figure 1. *Pf*EMP1 repertoire of the *P. falciparum* isolate IT4, adapted from [17]. ECR binding phenotype [36]. Color code: light brown: N-terminal segment (NTS); bright green: Duffy binding-like (DBL)α1; light blue: DBLα2, DBLα0; dark grey: Cys rich inter-domain regions (CIDR)α1; light grey: CIDRα2–6; dark green: CIDRγ; orange: DBLβ; yellow: DBLγ; green: DBLδ; pink: DBLε; blue: DBLζ; purple: DBLε; IT4var04: light yellow: DBL/CIDRpam: pink: DBLεpam.

3. Knobs—Anchor Point for *Pf*EMP1s

*Pf*EMP1s are concentrated in nanoscale, electron-dense protrusions of the plasma membrane of *Pf*IEs, the so-called knobs. They are formed in erythrocytes about 16 h after parasite invasion and reach their highest density 20 h after infection [39,40]. Single knobs have a hemispherical ellipsoid shape with a minor axis of 20 nm and a major axis of 120 nm [41]. Knobs are composed of various submembrane structural proteins, including the major protein of this structure, knob-associated histidine-rich protein (KAHRP). These consist of *Pf*EMP3, the ring-infected red cell antigen (RESA), the mature parasite-infected red cell surface antigen (MESA)/*Pf*EMP2, and *Pf*332 [41,42]. The knobs consist of a highly

organized skeleton made of a spiral structure located beneath specialized areas of the erythrocyte membrane (Figure 2) [43]. The arrangement of *Pf*EMP1s in a cluster near the top of the knobs is assumed to increase the binding capacity of *Pf*IEs, especially under flow conditions (see below) [44–47].
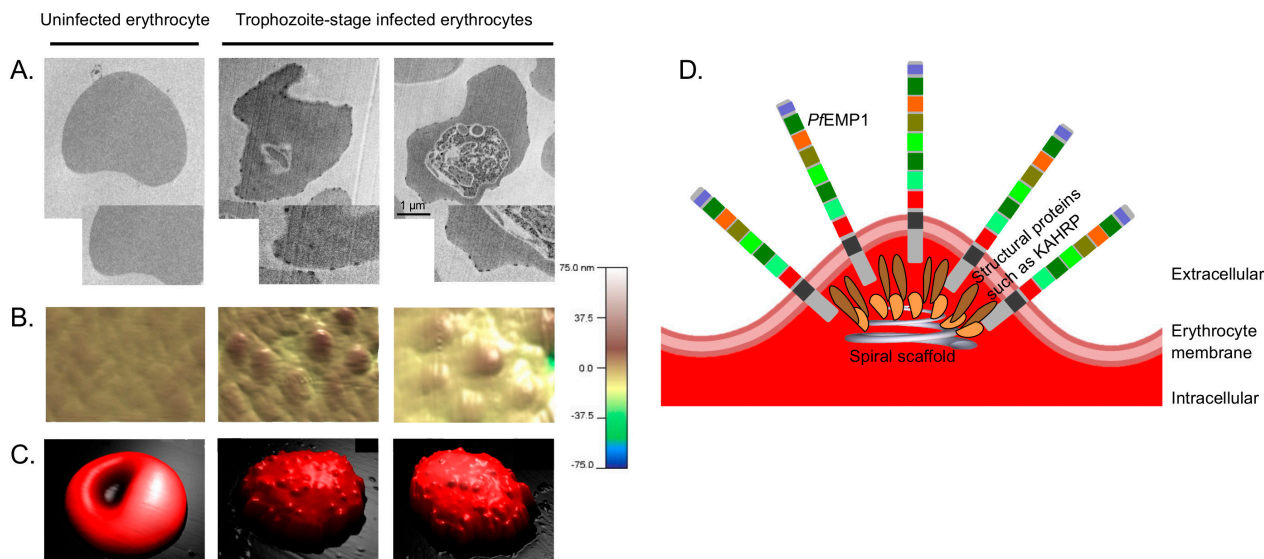
Figure 2. The knobs of *Pf*IEs. (**A**) Transmission electron micrographs of uninfected and synchronised trophozoite-stage *P. falciparum* culture 24–28 h post-infection. The parasites were cultivated in the presence of human serum (10%), and the *Pf*IEs were subjected to gelatin sedimentation to enrich knobby *Pf*IEs [40,48]. (**B**,**C**) atomic force microscopic three-dimensional images of the surface of uninfected and trophozoite-stage *Pf*IEs [40]. Images in (**B**) show magnifications directly from the membrane surface of the erythrocytes shown in (**C**). (**D**) Simplified schematic illustration of the structure of knobs.

4. Endothelial Cell Receptors (ECRs)

At least 24 ECRs were described as binding partners for *Pf*IEs. These include EPCR, gC1qR, ICAM-1, and CD36, mentioned above, as well as platelet endothelial cell adhesion molecule-1 (PECAM-1), CSA (adhesion to placental epithelium) [49], heparan sulphate, hyaluronic acid, neuronal cell adhesion molecule (NCAM), P-selectin, E-selectin, vascular cell adhesion molecule-1 (VCAM-1), thrombospondin, fractalkine, $\alpha v \beta 3$- and $\alpha V \beta 6$-integrin, fibronectin, CD9, CD151, multidrug resistance protein 1 and 2, erythropoietin receptor 1, and tumour necrosis factor receptor (TNFR) 1 and 2 [6,33,37,48,50–53]. To date, only a few ECRs have been shown to interact via *Pf*EMP1, and *Pf*EMP1 binding domains have only been identified for CD36, ICAM-1, EPCR, PECAM-1, and gC1qR [18,27,32,33,54].

5. Cytoadhesion of *Pf*IEs

Cytoadhesion of *Pf*IEs to ECRs in the vascular bed of organs, such as the brain, heart, lung, stomach, skin, and kidney is a central component of the pathogenesis of malaria [3–6,55–57]. In addition to the blockage of capillaries by the cytoadhesion of the *Pf*IEs, there is also an increased production of inflammatory cytokines, endothelial dysfunction, and increased vascular permeability in the affected tissue [58,59]. As a result of the immune response triggered by the growth and sequestration of the parasites, patients develop fever, headache, muscle pain, and rigor [3,60–63]. Depending on the age and immune status of the patient, severe, fatal complications such as cerebral malaria (CM), lung damage, kidney failure, acidosis, and severe anemia may occur [3,62,63]. Both children and adults can be affected by cerebral malaria, but while severe malaria puts children at higher risk for anemia and convulsions, liver dysfunction and kidney failure are more

common in adults. In addition, the clinical picture of severe malaria clearly depends on age, with mortality increasing significantly with age [64].

6. Pathology Induced by Cytoadhesion

Different *Pf*EMP1s have different binding properties to ECRs and are associated with different clinical outcomes (see review [4]). Several studies have shown that severe malaria is associated with the expression of group A and B/A *Pf*EMP1s and, in particular, with variants possessing EPCR binding capacities [65–69]. In contrast, infections dominated by CD36-binding parasites show mild disease courses [33,35,68,70–72].

Since *Pf*EMP1s are multi-domain proteins, it has already been shown that some variants can mediate adhesion to multiple ECRs (dual binder) [36,37,73,74]. Examples include *Pf*EMP1 variants that interact with ICAM-1 and EPCR or CD36. Dual binding to ICAM-1 and EPCR specifically enhances the binding of *Pf*IEs to endothelial cells (ECs) under physiologically higher shear stresses. Expression of these variants has been associated with an increased risk of developing CM, including induction of brain swelling and disruption of the blood-brain barrier [36,74–76]. Less is known about the role of dual ICAM-1 and CD36 binding *Pf*EMP1s, mainly of group B, but ICAM-1 and CD36 have been shown to work together to enhance the binding of *Pf*IEs to microvascular cells [27,37,66,77,78].

7. ECR-Specific Expression in Relation to the Origin of the Endothelial Cells

ECs derived from different organs presenting different ECRs on their cell surface. It is known that EPCR and ICAM-1 are presented on brain ECs and are mainly bound by DC8- and group A *Pf*EMP1s [33,36,74,75,79]. Ortolan and colleagues have recently shown that the same *Pf*EMP1s that cytoadhere to brain ECs also bind EPCR intestinal and renal ECs. In this context, it is suggested that a binding axis between the brain, gut, and kidney may contribute to the multi-organ complications of severe malaria [80]. In contrast, CD36 is not presented on brain ECs, or only in very low amounts, and was also not detected on intestinal and peritubular renal ECs [81,82]. Thus, in contrast to EPCR, CD36 seems to occur mainly in the microvascular beds of non-vital organs. As mentioned above, several studies have linked EPCR- or dual EPCR- and ICAM-1-binding *Pf*EMP1s to severe malaria, which most likely occurs in individuals without preformed immunity [33,68,72,79,83–85]. For example, Wichers and colleagues recently demonstrated a clear association between the expression of *Pf*EMP1s, which have an EPCR-binding phenotype, with first-time infection and severe malaria [84]. Transcripts for CD36-binding variants were found more frequently in parasites from non-severely infected and pre-exposed patients.

Interestingly, however, in the same study, CD36-binding variants are overrepresented in all groups of adult malaria patients analyzed, even in severe cases and in first-time infected individuals [84], which is in stark contrast to the pattern seen in severely ill children [70]. The authors speculate that this could be the reason for multisystemic disease symptoms in adult malaria patients. Alternatively, parasites in these less ill adult patients compared to children could have a less dominant expression of EPCR-binding *Pf*EMP1 [84]. Further studies also showed that parasite cytoadhesion to CD36 correlates with the development of mild malaria [70,85,86]. Accordingly, both factors, the already acquired immunity and the age of patients, seem to favor the expression of CD36-binding variants.

8. Hierarchy of *var* Expression during the Human Blood Phase

Independent analyses of first-generation blood-stage parasites from malaria-naive human volunteers infected with *P. falciparum* sporozoites have shown remarkably consistent expression of a broad repertoire of *var* genes, primarily type B (*P. falciparum* strain NF54: [87–90]; unpublished data for *P. falciparum strain* 7G8). This broad expression pattern is modulated by existing host immunity. In African pre-exposed individuals, the expression of many variants at the parasite population level is reduced to very few or a single B-type, possibly reflecting gaps in the host antibody repertoire [91]. In severe disease, expression of *var* genes shifts toward group A or A/B for unknown reasons, resulting in expression

of *Pf*EMP1 with EPCR and/or ICAM-1 or a yet unknown binding domain [65,84,92–96]. Group A *Pf*EMP1s are therefore thought to possess binding phenotypes that confer a selective advantage for parasites to replicate asexually, e.g., by decreasing splenic clearance, but at the same time favors the development of severe malaria [31]. In this context, it has been shown that antibodies for the EPCR binding domains (CIDRα1.1/4–8) are acquired faster and earlier in life than those to the CD36 binding domains (CIDRα2–6) in endemic areas and that this is associated with protection against severe malaria, including CM [31,65,95,97,98]. This raises the question of the evolutionary advantage of A-type expression for the parasite since cytoadhesion in vital organs via EPCR and ICAM-1 may lead to rapid death of infected individuals and thus not to transmission of the parasite to the mosquito. On the other hand, the rapid development of the protection of individuals from severe malaria could therefore be an advantage for the parasites, as they would be less likely to harm their hosts in the event of re-infection [93]. Later in the course of asymptomatic infection, *Pf*IEs appear to have altered cytoadherence properties, as more developed, "older" parasites circulate in the blood than in symptomatic cases. This observation suggests that these parasites either express a lower total amount of *Pf*EMP1 on the host cell surface or a different set of *Pf*EMP1 variants with less adhesive binding domains [99]. Since it is already known that chromosomal location determines the on-and-off rate of *var* genes [100], it would be plausible that parasites in primary infections initiate expression of the most telomeric B-type *var* genes, then tend to express A-types during severe disease, but in the case of long-lasting asymptomatic infections may then express centrally located C-types, which are known to have very slow off rates in comparison to subtelomeric *var* genes. The concept of an initial high *var* gene switching rate to establish infection and a slower switching rate of later expressed genes to maintain infection was already proposed 20 years ago [101,102].

9. *P. falciparum* and CD36

Looking at the *Pf*EMP1 family, the question arises why, depending on the parasite genome, between 75–85% of *var* genes encode *Pf*EMP1s, which have a CIDRα2–6 domain for CD36 binding [17,27,31]. Interestingly, the CIDRα domains were shown to be present only in the *P. falciparum*-containing branch (clade B) of the *Laverania* subgenus. This could indicate that the binding to CD36 provides a selective advantage for *P. falciparum* [103]. What kind of selection advantage this was is yet unclear.

What advantage does the parasite have in retaining this large number of CD36-binding *Pf*EMP1 variants in its genome? Additionally, what is the difference between the individual variants or, more generally, between CD36 binding mediated by group B or C *Pf*EMP1s?

10. CD36

CD36 is a pattern recognition receptor (PRR) that belongs to the class B scavenger receptor family. It is a glycoprotein present in many tissues and involved in several key processes. These include lipid processing and uptake, thrombostasis, glucose metabolism, immune function, angiogenesis, and fat taste (for review [104–108]. CD36 is found on platelets, mononuclear phagocytes, adipocytes, hepatocytes, myocytes, some epithelia and, as mentioned above, expressed on the endothelia of liver, spleen, skin, lung, muscle, and adipose tissue [81,82,109]. On microvascular ECs, CD36 is a receptor for thrombospondin-1 and related proteins and functions as a negative regulator of angiogenesis. At least 60 variants have been described in the coding region of the *CD36* gene. The mutations of CD36 caused by gene variants can also influence the adhesion of *Pf*IEs and ECs. This could directly influence the severity of a malaria infection via the degree of cytoadhesion. There are several studies on this, but with contradictory results [110]).

11. CD36 Binding *Pf*EMP1 Variants—Benefits for Parasite and Host

Several observations may help explain why a large number of CD36-binding *Pf*EMP1 variants is not only beneficial for parasite development, but may also be an advantage for the infected host.

A. The parasite targets a region of CD36 that is essential for its physiological role in fatty acid uptake because mutation of F153 disrupts the interaction of CD36 with CIDRα2–6 but also abolishes the binding of CD36 to oxidized LDL particles. This reduces the likelihood that the human host can escape from *Pf*EMP1 binding by altering its CD36 [28].

B. In contrast to the EPCR binding surface of CIDRα1 domains, which protrudes and is a structure that is likely to be well recognized by antibodies, the CD36 binding site is concave, and the conserved hydrophobic residues are hidden in a pocket, so maybe they are less easily recognized. In addition, the binding site is surrounded by a sequence-diverse protein surface containing a flexible loop that may make antibody recognition less likely. This unique interaction site of the parasite with CD36, which protects essential residues from exposure to the immune system, appears to allow the parasite to utilize an antigenically diverse set of CIDRα2–6 for cytoadhesion to CD36 to be protected from splenic clearance [28].

C. CD36 is found in cells of the innate and adaptive immune system [104–108]. It has been shown that *Pf*IEs can adhere to dendritic cells (DCs). This attachment inhibits maturation of these cells and their ability to stimulate T cells. Thus, the parasite can trigger dysregulation of the immune system. This favors the development of the parasite by impairing the host immune system's ability to clear the infection [108,111–114]. However, there is also an observation that the mechanism of DC inhibition by *Pf*IEs may be independent of *Pf*EMP1 and CD36 [115].

D. The previously determined hierarchy of *var* expression upon parasite entry into human blood begins with group B and suggests that most parasites bind to CD36, as they all encode a CD36-binding phenotype. Most infected individuals, including those who are not immune, do not develop severe malaria, and cytoadhesion of *Pf*IEs occurs in extensive microvascular beds in tissues other than the brain (skin, muscle, adipose tissue). Therefore, cytoadhesion in such non-vital tissues could promote survival and transmission of the parasite while minimizing host damage and death [87–90].

E. Antibody-induced selective binding and internalization of CD36 do not result in proinflammatory cytokine production by human macrophages. Interestingly, CD36-mediated phagocytosis of *Pf*IEs also did not result in cytokine secretion by primary macrophages [116]. However, CD36-mediated binding of *Pf*IEs increases the likelihood of phagocytosis by macrophages. This can lead to a reduction in parasitemia, but also allows the parasite to maintain a viable infection without causing too much damage to the host through high parasitemia [108,114,117,118].

F. DCs react to *P. falciparum* very early during infection and can, thus, influence the development of immunity. Internalization of *Pf*IEs by DCs and subsequent proinflammatory cytokine production of DCs, NK, and T cells depends on CD36. Notably, plasmacytoid DCs regulate innate and adaptive immunity to malaria via the production of proinflammatory cytokines. As this effect is particularly evident at low levels of parasitemia, the role of CD36 for malaria immunity appears to take place early during infection and to promote the development of protective immunity against malaria [118,119].

All these observations underline the importance of CD36 for malaria. During long co-evolution, a fine balance has evolved between host and parasite, allowing the parasite to multiply but harming the host as little as possible.

12. Binding Phenotypes of *Pf*IEs

Cytoadhesion of *Pf*IEs is divided into the three phases: "tethering", "rolling", and "immobilization", comparable to leukocyte diapedesis [120–122]. However, the dynamics of cytoadhesion of *Pf*IEs to the vascular endothelium is controversial. For example, some authors describe cytoadhesion to ICAM-1 as rolling, and to CD36 as stationary, or vice versa [123–127]. However, there is increasing evidence that *Pf*IEs are very likely to roll over

CD36 [126–131]. Recently, the binding phenotype for different ECRs was investigated using a laminar flow system with transgenic Chinese hamster ovary (CHO) cells carrying different ECRs on their surface [127]. Rolling was observed upon interaction with CD36, and the rolling behavior of disc-shaped *Pf*IEs at the trophozoite stage (flipping) differed from the rolling behavior of round-shaped *Pf*IEs at the schizont stage (continuous rolling) (Figure 3). Moreover, *Pf*IEs in the schizont stage roll more stably than *Pf*IEs in the trophozoite stage at different shear stresses [127]. The rolling motion of *Pf*IEs was also seen on transgenic mouse fibroblasts presenting CD36 [128] and on recombinant CD36 instead of transgenic eukaryotic cells [129]. As described above, the dermal endothelium has large amounts of CD36. Rolling movements of *Pf*IEs have also been found on dermal ECs, as well as on human skin grafts, on which large amounts of CD36 are found [126,128,130,131]. Additionally, last but not least, the rolling CD36 binding phenotype was also confirmed by in silico modeling [132,133]. However, depending on the experimental setup, the parasite isolates used, and the parasite stage, different velocities were measured at similar shear forces. For trophozoite-stage parasites confronted with recombinant CD36, average velocities between 140 μm/min to 680 μm/min were measured at a shear force of 1.6 Pa, depending on the isolate [129]. When transgenic CHO cells presenting CD36 on the surface were used instead of recombinant CD36 in a similar experimental setup, average velocities ranging from 11 μm/min to 33 μm/min, i.e., a 12–20 fold lower value, were measured, also depending on the parasite stage and isolate [127]. If *Pf*IEs cytoadhere for approximately 30 h during their intraerythrocytic development, they travel distances between 25–122 cm or 2–6 cm, respectively, depending on the experimental setup [127,129]. In both cases, however, the probability of passing over the spleen and being removed accordingly is low.
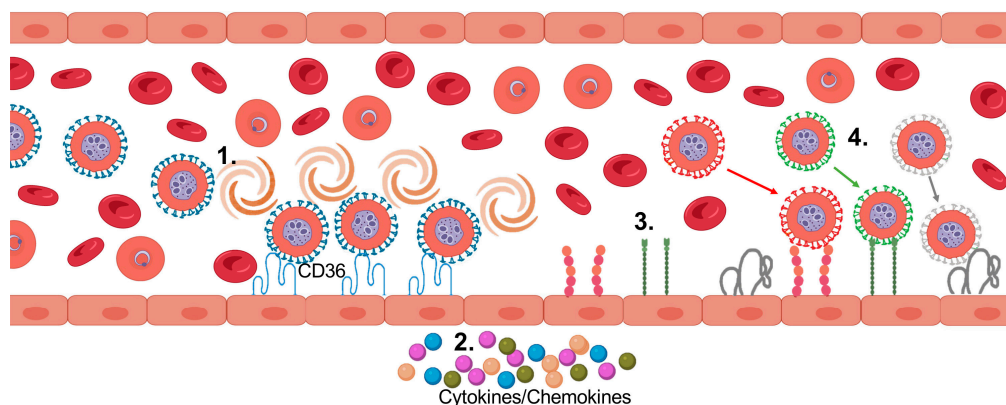
Figure 3. Presumed sequence of sequestration of *Pf*IEs to the vascular endothelium. 1. Adhesion and rolling over CD36. 2. Over time: endothelial activation, cytokine release. 3. Cytokine/chemokine-induced presentation of various receptors (e.g., ICAM-1, P-selectin, CD9). 4. Adhesion of *Pf*EMP1s with different binding phenotypes (created with BioRender).

Further studies showed that initial contact of *Pf*IEs to CD36 under flow conditions activates Scr-family kinases, leading to dephosphorylation of CD36 via p130CAS signaling. This increases the binding affinity of *Pf*IEs to CD36 and, thus, leads to increased adhesion of the *Pf*IEs. This mechanism also leads to actin cytoskeletal remodeling and subsequent CD36 clustering, which further increases *Pf*IE adhesion [128,131,134]. It is postulated that a small number of strongly adherent *Pf*IEs activate the endothelium, and thus enhance the cytoadhesion of most parasites [131]. However, the binding mode of *Pf*IEs also seems to be strongly dependent on the respective ECR. For ICAM-1, CD9, P-selectin, as well as CSA, stationary binding, instead of rolling, was observed under flow conditions [127] (Figure 3). Stationary binding to ICAM-1 was also demonstrated in an earlier study [126]. However, while binding to CD36 occurred at shear forces below 4 dyn/cm^2, binding to ICAM-1, CD9, P-selectin, and CSA occurred mostly at lower shear forces (from 2 dyn/cm^2) [127].

Of note, the origin and environment of the ECR studied (recombinant or presented on eukaryotic cells) also seems to be important for characterising the binding phenotype. Antia and colleagues observed a rolling binding type for *Pf*IEs, with an average rolling velocity of about 10 μm/s at 1–2 kPa and of 1–3 μm/s when recombinant ICAM-1 or CD36 was used, respectively [123]. Interestingly, in the same study, stationary binding of *Pf*IEs, as also described by Lubiana and colleagues [127], was observed on transgenic CHO cells presenting ICAM-1 [123]. However, the binding showed large variations. Thus, the *Pf*IEs came to a standstill for a few seconds, but were then also able to detach from the CHO cells again [123].

13. Importance of Knobs for Cytoadhesion

It is well established that knobs play a crucial role in the cytoadhesion of *P. falciparum* [45,47,48,127,135]. Among other findings, *Pf*IEs from patients with hemoglobin S (HbS) or hemoglobin C (HbC; both hemoglobin mutations protect against severe complications and death from malaria [136–138]) have been found to exhibit reduced cytoadhesion to microvascular endothelial cells [139,140]. The results suggest that HbS and HbC alter the erythrocyte membrane in a manner that inhibits the transport and/or docking of parasite proteins and impairs the ability of the parasite to remodel the surface of its host cell. This also leads to the fact that the knobs can no longer be formed correctly, and *Pf*EMP1 is also no longer presented correctly [139,140].

In the absence of knobs, parasite adhesion to CD36 was observed only under static conditions, but not under flow conditions simulating the situation in human blood [47,141]. In the absence of knobs on the surface of *Pf*IEs, the rolling distance is shortened compared to knob-positive *Pf*IEs [127]. The more stable rolling described above, and the rolling over longer distances of the schizont stage, is most likely related to the uniform coverage of the surface with knobs [130]. Furthermore, the adhesion force seems to be lower in the schizonts than in the trophozoites [142]. The comparison of knob-negative and knob-positive *Pf*IEs suggests that the presence of knobs stabilises the ligand-receptor interaction due to the concentrated amount of *Pf*EMP1 on the knob surface (Figure 4) [46,127].
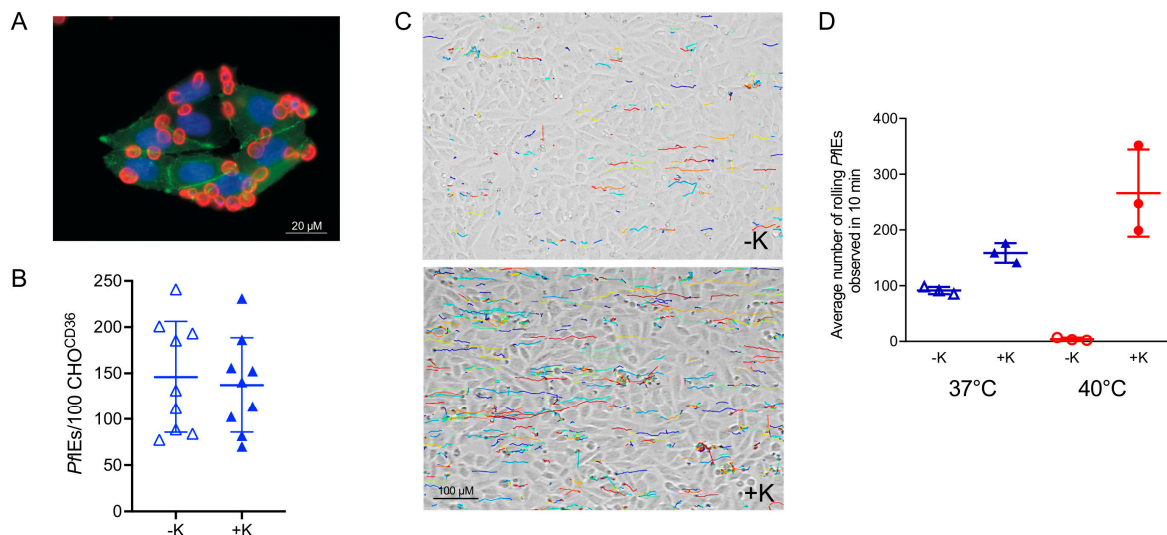
Figure 4. Cytoadhesion of knobby and knobless *Pf*IEs to transgenic CHO cells presenting CD36 on the cell surface (CHO^{CD36}) under static and flow conditions and at different temperatures. (**A**) Adhesion of *Pf*IEs (red; anti-glycophorin A) to CHO^{CD36} cells (blue: nucleus (DAPI), green: cell surface (CD36-GFP fusion protein) under static binding conditions. (**B**) Cytoadhesion of knobless (−K) and knobby (+K) *Pf*IEs to CHO^{CD36} cells. (**C**) Trajectories showing the rolling binding behavior of knobless (−K) and knobby (+K) *Pf*IEs to CHO^{CD36} cells. (**D**) Average number of knobless (−K) and knobby (+K) *Pf*IEs adhering to CHO^{CD36} cells at 37 °C (blue) and 40 °C (red) at a shear stress of 0.9 dyn/cm^2 [127].

Another important observation could be made under fever conditions. Only knob-positive *Pf*IEs were able to bind to different ECRs (CSA, CD36) at 40 °C with preserved ECR-specific binding mode (rolling or stationary) (Figure 4) [48,127]. Measurement of the binding force between *Pf*IEs and CSA by force spectroscopy showed a decrease in binding force at febrile temperatures, but the number of bound *Pf*IEs increased. It was hypothesized that this increase in binding is due to non-specific binding despite the decrease in force [143]. Again, however, a study showed that, at febrile temperatures, binding affinities to CD36 and ICAM-1 decreased [144].

In summary, there is strong evidence that the presence of knobs on the surface of *Pf*IEs is an essential prerequisite for the parasite circulating in the bloodstream to adhere to the endothelium even under febrile conditions. An evolutionary pressure for the formation of knobs on *Pf*IEs in the human host is therefore operative.

14. Conclusions

CD36 is the main receptor for *Pf*IE cytoadhesion to the vascular endothelium. Due to the rolling behavior and the resulting short contact of parasites with CD36 on the ECs, these ECs may not or are only slightly activated. Likely, only B group *Pf*EMP1s with a particularly strong binding affinity to CD36 or dual binding properties, as well as the increase in parasitemia and the accompanying stimulation of the immune system and the release of proinflammatory cytokines, lead to an activation of the endothelium and thus also to the presentation of other ECRs such as ICAM-1 or P-selectin. Finally, *Pf*IEs with different binding phenotypes can also adhere, with static binding leading to further activation of the endothelium and the immune system.

Further observations highlight the role of CD36 in *P. falciparum* infection. (i) A large number of *Pf*EMP1s containing a CD36 binding domain [17,27,31]; (ii) the binding of *Pf*IEs to DCs via CD36, which inhibits their cell maturation and ability to stimulate NK and T cells [108,111–114]; (iii) CD36-mediated phagocytosis of *Pf*IEs does not result in cytokine secretion by macrophages [116] (however, it may result in a reduction in parasitemia [108,114,117,118]); (iv) in the early stage of infection, internalization of CD36-binding *Pf*IEs by DCs leads to increased cytokine production and activation of NK and T cells, which promotes the establishment of protective immunity [118,119].

Thus, CD36 is of great importance for establishing a finely regulated equilibrium between the parasite and the host, whereby the parasite can multiply and spread while the host experiences little damage.

References

1. WHO. *World Malaria Report 2021*; WHO: Geneva, Switzerland, 2021.
2. Saul, A. The role of variant surface antigens on malaria-infected red blood cells. *Parasitol. Today* **1999**, *15*, 455–457. [CrossRef] [PubMed]
3. Phillips, M.A.; Burrows, J.N.; Manyando, C.; van Huijsduijnen, R.H.; Van Voorhis, W.C.; Wells, T.N.C. Malaria. *Nat. Rev. Dis. Prim.* **2017**, *3*, 17050. [CrossRef] [PubMed]
4. Craig, A.G.; Khairul, M.F.; Patil, P.R. Cytoadherence and severe malaria. *Malays. J. Med. Sci.* **2012**, *19*, 5–18. [PubMed]
5. Newbold, C.; Craig, A.; Kyes, S.; Rowe, A.; Fernandez-Reyes, D.; Fagan, T. Cytoadherence, pathogenesis and the infected red cell surface in *Plasmodium falciparum*. *Int. J. Parasitol.* **1999**, *29*, 927–937. [CrossRef] [PubMed]

6. Rowe, J.A.; Claessens, A.; Corrigan, R.A.; Arman, M. Adhesion of *Plasmodium falciparum*-infected erythrocytes to human cells: Molecular mechanisms and therapeutic implications. *Expert Rev. Mol. Med.* **2009**, *11*, e16. [CrossRef] [PubMed]

7. Chan, J.A.; Howell, K.B.; Reiling, L.; Ataide, R.; Mackintosh, C.L.; Fowkes, F.J.; Petter, M.; Chesson, J.M.; Langer, C.; Warimwe, G.M.; et al. Targets of antibodies against *Plasmodium falciparum*-infected erythrocytes in malaria immunity. *J. Clin. Investig.* **2012**, *122*, 3227–3238. [CrossRef]

8. Miller, L.H.; Good, M.F.; Milon, G. Malaria pathogenesis. *Science* **1994**, *264*, 1878–1883. [CrossRef]

9. Nyarko, P.B.; Claessens, A. Understanding Host-Pathogen-Vector Interactions with Chronic Asymptomatic Malaria Infections. *Trends Parasitol.* **2021**, *37*, 195–204. [CrossRef]

10. Deitsch, K.W.; Dzikowski, R. Variant Gene Expression and Antigenic Variation by Malaria Parasites. *Annu. Rev. Microbiol.* **2017**, *71*, 625–641. [CrossRef] [PubMed]

11. Petter, M.; Duffy, M.F. Antigenic Variation in *Plasmodium falciparum*. *Results Probl. Cell Differ.* **2015**, *57*, 47–90. [CrossRef] [PubMed]

12. Otto, T.D.; Assefa, S.A.; Bohme, U.; Sanders, M.J.; Kwiatkowski, D.; Pf3k, c.; Berriman, M.; Newbold, C. Evolutionary analysis of the most polymorphic gene family in *falciparum* malaria. *Wellcome Open Res.* **2019**, *4*, 193. [CrossRef] [PubMed]

13. Voss, T.S.; Healer, J.; Marty, A.J.; Duffy, M.F.; Thompson, J.K.; Beeson, J.G.; Reeder, J.C.; Crabb, B.S.; Cowman, A.F. A var gene promoter controls allelic exclusion of virulence genes in *Plasmodium falciparum* malaria. *Nature* **2006**, *439*, 1004–1008. [CrossRef] [PubMed]

14. Kyes, S.A.; Kraemer, S.M.; Smith, J.D. Antigenic variation in *Plasmodium falciparum*: Gene organization and regulation of the var multigene family. *Eukaryot. Cell* **2007**, *6*, 1511–1520. [CrossRef] [PubMed]

15. Pasternak, N.D.; Dzikowski, R. PfEMP1: An antigen that plays a key role in the pathogenicity and immune evasion of the malaria parasite *Plasmodium falciparum*. *Int. J. Biochem. Cell Biol.* **2009**, *41*, 1463–1466. [CrossRef] [PubMed]

16. Kraemer, S.M.; Smith, J.D. A family affair: Var genes, PfEMP1 binding, and malaria disease. *Curr. Opin. Microbiol.* **2006**, *9*, 374–380. [CrossRef]

17. Rask, T.S.; Hansen, D.A.; Theander, T.G.; Gorm Pedersen, A.; Lavstsen, T. *Plasmodium falciparum* erythrocyte membrane protein 1 diversity in seven genomes—Divide and conquer. *PLoS Comput. Biol.* **2010**, *6*, e1000933. [CrossRef] [PubMed]

18. Smith, J.D.; Craig, A.G.; Kriek, N.; Hudson-Taylor, D.; Kyes, S.; Fagan, T.; Pinches, R.; Baruch, D.I.; Newbold, C.I.; Miller, L.H. Identification of a *Plasmodium falciparum* intercellular adhesion molecule-1 binding domain: A parasite adhesion trait implicated in cerebral malaria. *Proc. Natl. Acad. Sci. USA* **2000**, *97*, 1766–1771. [CrossRef] [PubMed]

19. Smith, J.D.; Subramanian, G.; Gamain, B.; Baruch, D.I.; Miller, L.H. Classification of adhesive domains in the *Plasmodium falciparum* erythrocyte membrane protein 1 family. *Mol. Biochem. Parasitol.* **2000**, *110*, 293–310. [CrossRef] [PubMed]

20. Gardner, M.J.; Hall, N.; Fung, E.; White, O.; Berriman, M.; Hyman, R.W.; Carlton, J.M.; Pain, A.; Nelson, K.E.; Bowman, S.; et al. Genome sequence of the human malaria parasite *Plasmodium falciparum*. *Nature* **2002**, *419*, 498–511. [CrossRef] [PubMed]

21. Kraemer, S.M.; Smith, J.D. Evidence for the importance of genetic structuring to the structural and functional specialization of the *Plasmodium falciparum var* gene family. *Mol. Microbiol.* **2003**, *50*, 1527–1538. [CrossRef] [PubMed]

22. Kraemer, S.M.; Kyes, S.A.; Aggarwal, G.; Springer, A.L.; Nelson, S.O.; Christodoulou, Z.; Smith, L.M.; Wang, W.; Levin, E.; Newbold, C.I.; et al. Patterns of gene recombination shape var gene repertoires in *Plasmodium falciparum*: Comparisons of geographically diverse isolates. *BMC Genom.* **2007**, *8*, 45. [CrossRef]

23. Lavstsen, T.; Salanti, A.; Jensen, A.T.; Arnot, D.E.; Theander, T.G. Sub-grouping of *Plasmodium falciparum* 3D7 *var* genes based on sequence analysis of coding and non-coding regions. *Malar. J.* **2003**, *2*, 27. [CrossRef]

24. Kyes, S.A.; Christodoulou, Z.; Raza, A.; Horrocks, P.; Pinches, R.; Rowe, J.A.; Newbold, C.I. A well-conserved *Plasmodium falciparum var* gene shows an unusual stage-specific transcript pattern. *Mol. Microbiol.* **2003**, *48*, 1339–1348. [CrossRef]

25. Rowe, J.A.; Kyes, S.A. The role of *Plasmodium falciparum var* genes in malaria in pregnancy. *Mol. Microbiol.* **2004**, *53*, 1011–1019. [CrossRef]

26. Wang, C.W.; Lavstsen, T.; Bengtsson, D.C.; Magistrado, P.A.; Berger, S.S.; Marquard, A.M.; Alifrangis, M.; Lusingu, J.P.; Theander, T.G.; Turner, L. Evidence for in vitro and in vivo expression of the conserved VAR3 (type 3) *Plasmodium falciparum* erythrocyte membrane protein 1. *Malar. J.* **2012**, *11*, 129. [CrossRef]

27. Robinson, B.A.; Welch, T.L.; Smith, J.D. Widespread functional specialization of *Plasmodium falciparum* erythrocyte membrane protein 1 family members to bind CD36 analysed across a parasite genome. *Mol. Microbiol.* **2003**, *47*, 1265–1278. [CrossRef] [PubMed]

28. Hsieh, F.L.; Turner, L.; Bolla, J.R.; Robinson, C.V.; Lavstsen, T.; Higgins, M.K. The structural basis for CD36 binding by the malaria parasite. *Nat. Commun.* **2016**, *7*, 12837. [CrossRef] [PubMed]

29. Mo, M.; Lee, H.C.; Kotaka, M.; Niang, M.; Gao, X.; Iyer, J.K.; Lescar, J.; Preiser, P. The C-terminal segment of the cysteine-rich interdomain of *Plasmodium falciparum* erythrocyte membrane protein 1 determines CD36 binding and elicits antibodies that inhibit adhesion of parasite-infected erythrocytes. *Infect. Immun.* **2008**, *76*, 1837–1847. [CrossRef]

30. Miller, L.H.; Hudson-Taylor, D.; Gamain, B.; Saul, A.J. Definition of the minimal domain of CIDR1alpha of *Plasmodium falciparum* PfEMP1 for binding CD36. *Mol. Biochem. Parasitol.* **2002**, *120*, 321–323. [CrossRef]

31. Smith, J.D.; Rowe, J.A.; Higgins, M.K.; Lavstsen, T. Malaria's deadly grip: Cytoadhesion of *Plasmodium falciparum*-infected erythrocytes. *Cell Microbiol.* **2013**, *15*, 1976–1983. [CrossRef] [PubMed]

32. Lau, C.K.; Turner, L.; Jespersen, J.S.; Lowe, E.D.; Petersen, B.; Wang, C.W.; Petersen, J.E.; Lusingu, J.; Theander, T.G.; Lavstsen, T.; et al. Structural conservation despite huge sequence diversity allows EPCR binding by the PfEMP1 family implicated in severe childhood malaria. *Cell Host Microbe* **2015**, *17*, 118–129. [CrossRef] [PubMed]

33. Turner, L.; Lavstsen, T.; Berger, S.S.; Wang, C.W.; Petersen, J.E.; Avril, M.; Brazier, A.J.; Freeth, J.; Jespersen, J.S.; Nielsen, M.A.; et al. Severe malaria is associated with parasite binding to endothelial protein C receptor. *Nature* **2013**, *498*, 502–505. [CrossRef] [PubMed]

34. Baruch, D.I.; Ma, X.C.; Singh, H.B.; Bi, X.; Pasloske, B.L.; Howard, R.J. Identification of a region of PfEMP1 that mediates adherence of *Plasmodium falciparum* infected erythrocytes to CD36: Conserved function with variant sequence. *Blood* **1997**, *90*, 3766–3775. [CrossRef]

35. Mkumbaye, S.I.; Wang, C.W.; Lyimo, E.; Jespersen, J.S.; Manjurano, A.; Mosha, J.; Kavishe, R.A.; Mwakalinga, S.B.; Minja, D.T.R.; Lusingu, J.P.; et al. The Severity of *Plasmodium falciparum* Infection Is Associated with Transcript Levels of var Genes Encoding Endothelial Protein C Receptor-Binding *P. falciparum* Erythrocyte Membrane Protein 1. *Infect. Immun.* **2017**, *85*. [CrossRef]

36. Lennartz, F.; Adams, Y.; Bengtsson, A.; Olsen, R.W.; Turner, L.; Ndam, N.T.; Ecklu-Mensah, G.; Moussiliou, A.; Ofori, M.F.; Gamain, B.; et al. Structure-Guided Identification of a Family of Dual Receptor-Binding PfEMP1 that Is Associated with Cerebral Malaria. *Cell Host Microbe* **2017**, *21*, 403–414. [CrossRef]

37. Janes, J.H.; Wang, C.P.; Levin-Edens, E.; Vigan-Womas, I.; Guillotte, M.; Melcher, M.; Mercereau-Puijalon, O.; Smith, J.D. Investigating the host binding signature on the *Plasmodium falciparum* PfEMP1 protein family. *PLoS Pathog.* **2011**, *7*, e1002032. [CrossRef] [PubMed]

38. Magallon-Tejada, A.; Machevo, S.; Cistero, P.; Lavstsen, T.; Aide, P.; Rubio, M.; Jimenez, A.; Turner, L.; Valmaseda, A.; Gupta, H.; et al. Cytoadhesion to gC1qR through *Plasmodium falciparum* Erythrocyte Membrane Protein 1 in Severe Malaria. *PLoS Pathog.* **2016**, *12*, e1006011. [CrossRef] [PubMed]

39. Quadt, K.A.; Barfod, L.; Andersen, D.; Bruun, J.; Gyan, B.; Hassenkam, T.; Ofori, M.F.; Hviid, L. The density of knobs on *Plasmodium falciparum*-infected erythrocytes depends on developmental age and varies among isolates. *PLoS ONE* **2012**, *7*, e45658. [CrossRef]

40. Tilly, A.K.; Thiede, J.; Metwally, N.; Lubiana, P.; Bachmann, A.; Roeder, T.; Rockliffe, N.; Lorenzen, S.; Tannich, E.; Gutsmann, T.; et al. Type of in vitro cultivation influences cytoadhesion, knob structure, protein localization and transcriptome profile of *Plasmodium falciparum*. *Sci. Rep.* **2015**, *5*, 16766. [CrossRef]

41. Alampalli, S.V.; Grover, M.; Chandran, S.; Tatu, U.; Acharya, P. Proteome and Structural Organization of the Knob Complex on the Surface of the *Plasmodium* Infected Red Blood Cell. *Proteom. Clin. Appl.* **2018**, *12*, e1600177. [CrossRef]

42. Maier, A.G.; Cooke, B.M.; Cowman, A.F.; Tilley, L. Malaria parasite proteins that remodel the host erythrocyte. *Nat. Rev. Microbiol.* **2009**, *7*, 341–354. [CrossRef]

43. Watermeyer, J.M.; Hale, V.L.; Hackett, F.; Clare, D.K.; Cutts, E.E.; Vakonakis, I.; Fleck, R.A.; Blackman, M.J.; Saibil, H.R. A spiral scaffold underlies cytoadherent knobs in *Plasmodium falciparum*-infected erythrocytes. *Blood* **2016**, *127*, 343–351. [CrossRef]

44. Gruenberg, J.; Allred, D.R.; Sherman, I.W. Scanning electron microscope-analysis of the protrusions (knobs) present on the surface of *Plasmodium falciparum*-infected erythrocytes. *J. Cell Biol.* **1983**, *97*, 795–802. [CrossRef]

45. Cutts, E.E.; Laasch, N.; Reiter, D.M.; Trenker, R.; Slater, L.M.; Stansfeld, P.J.; Vakonakis, I. Structural analysis of *P. falciparum* KAHRP and PfEMP1 complexes with host erythrocyte spectrin suggests a model for cytoadherent knob protrusions. *PLoS Pathog.* **2017**, *13*, e1006552. [CrossRef] [PubMed]

46. Sanchez, C.P.; Karathanasis, C.; Sanchez, R.; Cyrklaff, M.; Jager, J.; Buchholz, B.; Schwarz, U.S.; Heilemann, M.; Lanzer, M. Single-molecule imaging and quantification of the immune-variant adhesin VAR2CSA on knobs of *Plasmodium falciparum*-infected erythrocytes. *Commun. Biol.* **2019**, *2*, 172. [CrossRef] [PubMed]

47. Crabb, B.S.; Cooke, B.M.; Reeder, J.C.; Waller, R.F.; Caruana, S.R.; Davern, K.M.; Wickham, M.E.; Brown, G.V.; Coppel, R.L.; Cowman, A.F. Targeted gene disruption shows that knobs enable malaria-infected red cells to cytoadhere under physiological shear stress. *Cell* **1997**, *89*, 287–296. [CrossRef] [PubMed]

48. Dorpinghaus, M.; Furstenwerth, F.; Roth, L.K.; Bouws, P.; Rakotonirinalalao, M.; Jordan, V.; Sauer, M.; Rehn, T.; Pansegrau, E.; Hohn, K.; et al. Stringent Selection of Knobby *Plasmodium falciparum*-Infected Erythrocytes during Cytoadhesion at Febrile Temperature. *Microorganisms* **2020**, *8*, 174. [CrossRef] [PubMed]

49. Boeuf, P.; Hasang, W.; Hanssen, E.; Glazier, J.D.; Rogerson, S.J. Relevant assay to study the adhesion of *Plasmodium falciparum*-infected erythrocytes to the placental epithelium. *PLoS ONE* **2011**, *6*, e21126. [CrossRef] [PubMed]

50. Esser, C.; Bachmann, A.; Kuhn, D.; Schuldt, K.; Forster, B.; Thiel, M.; May, J.; Koch-Nolte, F.; Yanez-Mo, M.; Sanchez-Madrid, F.; et al. Evidence of promiscuous endothelial binding by *Plasmodium falciparum*-infected erythrocytes. *Cell Microbiol.* **2014**, *16*, 701–708. [CrossRef]

51. Chesnokov, O.; Merritt, J.; Tcherniuk, S.O.; Milman, N.; Oleinikov, A.V. *Plasmodium falciparum* infected erythrocytes can bind to host receptors integrins alphaVbeta3 and alphaVbeta6 through DBLdelta1_D4 domain of PFL2665c PfEMP1 protein. *Sci. Rep.* **2018**, *8*, 17871. [CrossRef] [PubMed]

52. Siano, J.P.; Grady, K.K.; Millet, P.; Wick, T.M. Short report: *Plasmodium falciparum*: Cytoadherence to alpha(v)beta3 on human microvascular endothelial cells. *Am. J. Trop. Med. Hyg.* **1998**, *59*, 77–79. [CrossRef] [PubMed]

53. Metwally, N.G.; Tilly, A.K.; Lubiana, P.; Roth, L.K.; Dorpinghaus, M.; Lorenzen, S.; Schuldt, K.; Witt, S.; Bachmann, A.; Tidow, H.; et al. Characterisation of *Plasmodium falciparum* populations selected on the human endothelial receptors P-selectin, E-selectin, CD9 and CD151. *Sci. Rep.* **2017**, *7*, 4069. [CrossRef] [PubMed]

54. Bengtsson, A.; Joergensen, L.; Rask, T.S.; Olsen, R.W.; Andersen, M.A.; Turner, L.; Theander, T.G.; Hviid, L.; Higgins, M.K.; Craig, A.; et al. A novel domain cassette identifies *Plasmodium falciparum* PfEMP1 proteins binding ICAM-1 and is a target of cross-reactive, adhesion-inhibitory antibodies. *J. Immunol.* **2013**, *190*, 240–249. [CrossRef] [PubMed]

55. Milner, D.A., Jr.; Valim, C.; Carr, R.A.; Chandak, P.B.; Fosiko, N.G.; Whitten, R.; Playforth, K.B.; Seydel, K.B.; Kamiza, S.; Molyneux, M.E.; et al. A histological method for quantifying *Plasmodium falciparum* in the brain in fatal paediatric cerebral malaria. *Malar. J.* **2013**, *12*, 191. [CrossRef] [PubMed]

56. Milner, D.A., Jr.; Lee, J.J.; Frantzreb, C.; Whitten, R.O.; Kamiza, S.; Carr, R.A.; Pradham, A.; Factor, R.E.; Playforth, K.; Liomba, G.; et al. Quantitative Assessment of Multiorgan Sequestration of Parasites in Fatal Pediatric Cerebral Malaria. *J. Infect. Dis.* **2015**, *212*, 1317–1321. [CrossRef]

57. Taylor, T.E.; Fu, W.J.; Carr, R.A.; Whitten, R.O.; Mueller, J.S.; Fosiko, N.G.; Lewallen, S.; Liomba, N.G.; Molyneux, M.E. Differentiating the pathologies of cerebral malaria by postmortem parasite counts. *Nat. Med.* **2004**, *10*, 143–145. [CrossRef]

58. Lyke, K.E.; Burges, R.; Cissoko, Y.; Sangare, L.; Dao, M.; Diarra, I.; Kone, A.; Harley, R.; Plowe, C.V.; Doumbo, O.K.; et al. Serum levels of the proinflammatory cytokines interleukin-1 beta (IL-1beta), IL-6, IL-8, IL-10, tumor necrosis factor alpha, and IL-12(p70) in Malian children with severe *Plasmodium falciparum* malaria and matched uncomplicated malaria or healthy controls. *Infect. Immun.* **2004**, *72*, 5630–5637. [CrossRef] [PubMed]

59. Raacke, M.; Kerr, A.; Dorpinghaus, M.; Brehmer, J.; Wu, Y.; Lorenzen, S.; Fink, C.; Jacobs, T.; Roeder, T.; Sellau, J.; et al. Altered Cytokine Response of Human Brain Endothelial Cells after Stimulation with Malaria Patient Plasma. *Cells* **2021**, *10*, 1656. [CrossRef] [PubMed]

60. Hasday, J.D.; Bannerman, D.; Sakarya, S.; Cross, A.S.; Singh, I.S.; Howard, D.; Drysdale, B.E.; Goldblum, S.E. Exposure to febrile temperature modifies endothelial cell response to tumor necrosis factor-alpha. *J. Appl. Physiol.* **2001**, *90*, 90–98. [CrossRef] [PubMed]

61. Oakley, M.S.; Gerald, N.; McCutchan, T.F.; Aravind, L.; Kumar, S. Clinical and molecular aspects of malaria fever. *Trends Parasitol.* **2011**, *27*, 442–449. [CrossRef]

62. Cunnington, A.J.; Riley, E.M.; Walther, M. Microvascular dysfunction in severe *Plasmodium falciparum* Malaria. *J. Infect. Dis.* **2013**, *207*, 369–370. [CrossRef] [PubMed]

63. Gazzinelli, R.T.; Kalantari, P.; Fitzgerald, K.A.; Golenbock, D.T. Innate sensing of malaria parasites. *Nat. Rev. Immunol.* **2014**, *14*, 744–757. [CrossRef]

64. Dondorp, A.M.; Lee, S.J.; Faiz, M.A.; Mishra, S.; Price, R.; Tjitra, E.; Than, M.; Htut, Y.; Mohanty, S.; Yunus, E.B.; et al. The relationship between age and the manifestations of and mortality associated with severe malaria. *Clin. Infect. Dis.* **2008**, *47*, 151–157. [CrossRef]

65. Jensen, A.T.; Magistrado, P.; Sharp, S.; Joergensen, L.; Lavstsen, T.; Chiucchiuini, A.; Salanti, A.; Vestergaard, L.S.; Lusingu, J.P.; Hermsen, R.; et al. *Plasmodium falciparum* associated with severe childhood malaria preferentially expresses PfEMP1 encoded by group A var genes. *J. Exp. Med.* **2004**, *199*, 1179–1190. [CrossRef] [PubMed]

66. Avril, M.; Tripathi, A.K.; Brazier, A.J.; Andisi, C.; Janes, J.H.; Soma, V.L.; Sullivan, D.J., Jr.; Bull, P.C.; Stins, M.F.; Smith, J.D. A restricted subset of var genes mediates adherence of *Plasmodium falciparum*-infected erythrocytes to brain endothelial cells. *Proc. Natl. Acad. Sci. USA* **2012**, *109*, E1782–E1790. [CrossRef] [PubMed]

67. Claessens, A.; Adams, Y.; Ghumra, A.; Lindergard, G.; Buchan, C.C.; Andisi, C.; Bull, P.C.; Mok, S.; Gupta, A.P.; Wang, C.W.; et al. A subset of group A-like var genes encodes the malaria parasite ligands for binding to human brain endothelial cells. *Proc. Natl. Acad. Sci. USA* **2012**, *109*, E1772–E1781. [CrossRef] [PubMed]

68. Lavstsen, T.; Turner, L.; Saguti, F.; Magistrado, P.; Rask, T.S.; Jespersen, J.S.; Wang, C.W.; Berger, S.S.; Baraka, V.; Marquard, A.M.; et al. *Plasmodium falciparum* erythrocyte membrane protein 1 domain cassettes 8 and 13 are associated with severe malaria in children. *Proc. Natl. Acad. Sci. USA* **2012**, *109*, E1791–E1800. [CrossRef]

69. Duffy, F.; Bernabeu, M.; Babar, P.H.; Kessler, A.; Wang, C.W.; Vaz, M.; Chery, L.; Mandala, W.L.; Rogerson, S.J.; Taylor, T.E.; et al. Meta-analysis of *Plasmodium falciparum var* Signatures Contributing to Severe Malaria in African Children and Indian Adults. *mBio* **2019**, *10*, e00217-19. [CrossRef]

70. Jespersen, J.S.; Wang, C.W.; Mkumbaye, S.I.; Minja, D.T.; Petersen, B.; Turner, L.; Petersen, J.E.; Lusingu, J.P.; Theander, T.G.; Lavstsen, T. *Plasmodium falciparum var* genes expressed in children with severe malaria encode CIDRalpha1 domains. *EMBO Mol. Med.* **2016**, *8*, 839–850. [CrossRef] [PubMed]

71. Bertin, G.I.; Lavstsen, T.; Guillonneau, F.; Doritchamou, J.; Wang, C.W.; Jespersen, J.S.; Ezimegnon, S.; Fievet, N.; Alao, M.J.; Lalya, F.; et al. Expression of the domain cassette 8 *Plasmodium falciparum* erythrocyte membrane protein 1 is associated with cerebral malaria in Benin. *PLoS ONE* **2013**, *8*, e68368. [CrossRef] [PubMed]

72. Bernabeu, M.; Danziger, S.A.; Avril, M.; Vaz, M.; Babar, P.H.; Brazier, A.J.; Herricks, T.; Maki, J.N.; Pereira, L.; Mascarenhas, A.; et al. Severe adult malaria is associated with specific PfEMP1 adhesion types and high parasite biomass. *Proc. Natl. Acad. Sci. USA* **2016**, *113*, E3270–E3279. [CrossRef] [PubMed]

73. Chen, Q.; Heddini, A.; Barragan, A.; Fernandez, V.; Pearce, S.F.; Wahlgren, M. The semiconserved head structure of *Plasmodium falciparum* erythrocyte membrane protein 1 mediates binding to multiple independent host receptors. *J. Exp. Med.* **2000**, *192*, 1–10. [CrossRef] [PubMed]

74. Avril, M.; Bernabeu, M.; Benjamin, M.; Brazier, A.J.; Smith, J.D. Interaction between Endothelial Protein C Receptor and Intercellular Adhesion Molecule 1 to Mediate Binding of *Plasmodium falciparum*-Infected Erythrocytes to Endothelial Cells. *mBio* **2016**, *7*, e00615-16. [CrossRef]

75. Bernabeu, M.; Gunnarsson, C.; Vishnyakova, M.; Howard, C.C.; Nagao, R.J.; Avril, M.; Taylor, T.E.; Seydel, K.B.; Zheng, Y.; Smith, J.D. Binding Heterogeneity of *Plasmodium falciparum* to Engineered 3D Brain Microvessels Is Mediated by EPCR and ICAM-1. *mBio* **2019**, *10*, e00420-19. [CrossRef] [PubMed]

76. Adams, Y.; Olsen, R.W.; Bengtsson, A.; Dalgaard, N.; Zdioruk, M.; Satpathi, S.; Behera, P.K.; Sahu, P.K.; Lawler, S.E.; Qvortrup, K.; et al. *Plasmodium falciparum* erythrocyte membrane protein 1 variants induce cell swelling and disrupt the blood-brain barrier in cerebral malaria. *J. Exp. Med.* **2021**, *218*, e20201266. [CrossRef] [PubMed]

77. McCormick, C.J.; Craig, A.; Roberts, D.; Newbold, C.I.; Berendt, A.R. Intercellular adhesion molecule-1 and CD36 synergize to mediate adherence of *Plasmodium falciparum*-infected erythrocytes to cultured human microvascular endothelial cells. *J. Clin. Investig.* **1997**, *100*, 2521–2529. [CrossRef]

78. Gray, C.; McCormick, C.; Turner, G.; Craig, A. ICAM-1 can play a major role in mediating *P. falciparum* adhesion to endothelium under flow. *Mol. Biochem. Parasitol.* **2003**, *128*, 187–193. [CrossRef] [PubMed]

79. Storm, J.; Jespersen, J.S.; Seydel, K.B.; Szestak, T.; Mbewe, M.; Chisala, N.V.; Phula, P.; Wang, C.W.; Taylor, T.E.; Moxon, C.A.; et al. Cerebral malaria is associated with differential cytoadherence to brain endothelial cells. *EMBO Mol. Med.* **2019**, *11*, e9164. [CrossRef] [PubMed]

80. Ortolan, L.S.; Avril, M.; Xue, J.; Seydel, K.B.; Zheng, Y.; Smith, J.D. *Plasmodium falciparum* Parasite Lines Expressing DC8 and Group A PfEMP1 Bind to Brain, Intestinal, and Kidney Endothelial Cells. *Front. Cell Infect. Microbiol.* **2022**, *12*, 813011. [CrossRef]

81. Swerlick, R.A.; Lee, K.H.; Wick, T.M.; Lawley, T.J. Human dermal microvascular endothelial but not human umbilical vein endothelial cells express CD36 in vivo and in vitro. *J. Immunol.* **1992**, *148*, 78–83.

82. Turner, G.D.; Morrison, H.; Jones, M.; Davis, T.M.; Looareesuwan, S.; Buley, I.D.; Gatter, K.C.; Newbold, C.I.; Pukritayakamee, S.; Nagachinta, B.; et al. An immunohistochemical study of the pathology of fatal malaria. Evidence for widespread endothelial activation and a potential role for intercellular adhesion molecule-1 in cerebral sequestration. *Am. J. Pathol.* **1994**, *145*, 1057–1069.

83. Kessler, A.; Dankwa, S.; Bernabeu, M.; Harawa, V.; Danziger, S.A.; Duffy, F.; Kampondeni, S.D.; Potchen, M.J.; Dambrauskas, N.; Vigdorovich, V.; et al. Linking EPCR-Binding PfEMP1 to Brain Swelling in Pediatric Cerebral Malaria. *Cell Host. Microbe* **2017**, *22*, 601–614.e605. [CrossRef] [PubMed]

84. Wichers, J.S.; Tonkin-Hill, G.; Thye, T.; Krumkamp, R.; Kreuels, B.; Strauss, J.; von Thien, H.; Scholz, J.A.; Smedegaard Hansson, H.; Weisel Jensen, R.; et al. Common virulence gene expression in adult first-time infected malaria patients and severe cases. *eLife* **2021**, *10*, e69040. [CrossRef]

85. Tuikue Ndam, N.; Moussiliou, A.; Lavstsen, T.; Kamaliddin, C.; Jensen, A.T.R.; Mama, A.; Tahar, R.; Wang, C.W.; Jespersen, J.S.; Alao, J.M.; et al. Parasites Causing Cerebral *Falciparum* Malaria Bind Multiple Endothelial Receptors and Express EPCR and ICAM-1-Binding PfEMP1. *J. Infect. Dis* **2017**, *215*, 1918–1925. [CrossRef] [PubMed]

86. Ochola, L.B.; Siddondo, B.R.; Ocholla, H.; Nkya, S.; Kimani, E.N.; Williams, T.N.; Makale, J.O.; Liljander, A.; Urban, B.C.; Bull, P.C.; et al. Specific receptor usage in *Plasmodium falciparum* cytoadherence is associated with disease outcome. *PLoS ONE* **2011**, *6*, e14741. [CrossRef] [PubMed]

87. Bachmann, A.; Petter, M.; Krumkamp, R.; Esen, M.; Held, J.; Scholz, J.A.; Li, T.; Sim, B.K.; Hoffman, S.L.; Kremsner, P.G.; et al. Mosquito Passage Dramatically Changes var Gene Expression in Controlled Human *Plasmodium falciparum* Infections. *PLoS Pathog.* **2016**, *12*, e1005538. [CrossRef] [PubMed]

88. Wang, C.W.; Hermsen, C.C.; Sauerwein, R.W.; Arnot, D.E.; Theander, T.G.; Lavstsen, T. The *Plasmodium falciparum* var gene transcription strategy at the onset of blood stage infection in a human volunteer. *Parasitol. Int.* **2009**, *58*, 478–480. [CrossRef]

89. Milne, K.; Ivens, A.; Reid, A.J.; Lotkowska, M.E.; O'Toole, A.; Sankaranarayanan, G.; Munoz Sandoval, D.; Nahrendorf, W.; Regnault, C.; Edwards, N.J.; et al. Mapping immune variation and *var* gene switching in naive hosts infected with *Plasmodium falciparum*. *eLife* **2021**, *10*, e62800. [CrossRef]

90. Pickford, A.K.; Michel-Todo, L.; Dupuy, F.; Mayor, A.; Alonso, P.L.; Lavazec, C.; Cortes, A. Expression Patterns of *Plasmodium falciparum* Clonally Variant Genes at the Onset of a Blood Infection in Malaria-Naive Humans. *mBio* **2021**, *12*, e0163621. [CrossRef]

91. Bachmann, A.; Bruske, E.; Krumkamp, R.; Turner, L.; Wichers, J.S.; Petter, M.; Held, J.; Duffy, M.F.; Sim, B.K.L.; Hoffman, S.L.; et al. Controlled human malaria infection with *Plasmodium falciparum* demonstrates impact of naturally acquired immunity on virulence gene expression. *PLoS Pathog.* **2019**, *15*, e1007906. [CrossRef]

92. Kyriacou, H.M.; Stone, G.N.; Challis, R.J.; Raza, A.; Lyke, K.E.; Thera, M.A.; Kone, A.K.; Doumbo, O.K.; Plowe, C.V.; Rowe, J.A. Differential *var* gene transcription in *Plasmodium falciparum* isolates from patients with cerebral malaria compared to hyperparasitaemia. *Mol. Biochem. Parasitol.* **2006**, *150*, 211–218. [CrossRef] [PubMed]

93. Warimwe, G.M.; Keane, T.M.; Fegan, G.; Musyoki, J.N.; Newton, C.R.; Pain, A.; Berriman, M.; Marsh, K.; Bull, P.C. *Plasmodium falciparum var* gene expression is modified by host immunity. *Proc. Natl. Acad. Sci. USA* **2009**, *106*, 21801–21806. [CrossRef] [PubMed]

94. Bachmann, A.; Predehl, S.; May, J.; Harder, S.; Burchard, G.D.; Gilberger, T.W.; Tannich, E.; Bruchhaus, I. Highly co-ordinated *var* gene expression and switching in clinical *Plasmodium falciparum* isolates from non-immune malaria patients. *Cell Microbiol.* **2011**, *13*, 1397–1409. [CrossRef] [PubMed]

95. Cham, G.K.; Turner, L.; Lusingu, J.; Vestergaard, L.; Mmbando, B.P.; Kurtis, J.D.; Jensen, A.T.; Salanti, A.; Lavstsen, T.; Theander, T.G. Sequential, ordered acquisition of antibodies to *Plasmodium falciparum* erythrocyte membrane protein 1 domains. *J. Immunol.* **2009**, *183*, 3356–3363. [CrossRef] [PubMed]

96. Obeng-Adjei, N.; Larremore, D.B.; Turner, L.; Ongoiba, A.; Li, S.; Doumbo, S.; Yazew, T.B.; Kayentao, K.; Miller, L.H.; Traore, B.; et al. Longitudinal analysis of naturally acquired PfEMP1 CIDR domain variant antibodies identifies associations with malaria protection. *JCI Insight* **2020**, *5*. [CrossRef] [PubMed]

97. Cabrera, A.; Neculai, D.; Kain, K.C. CD36 and malaria: Friends or foes? A decade of data provides some answers. *Trends Parasitol.* **2014**, *30*, 436–444. [CrossRef]

98. Turner, L.; Lavstsen, T.; Mmbando, B.P.; Wang, C.W.; Magistrado, P.A.; Vestergaard, L.S.; Ishengoma, D.S.; Minja, D.T.; Lusingu, J.P.; Theander, T.G. IgG antibodies to endothelial protein C receptor-binding cysteine-rich interdomain region domains of *Plasmodium falciparum* erythrocyte membrane protein 1 are acquired early in life in individuals exposed to malaria. *Infect. Immun.* **2015**, *83*, 3096–3103. [CrossRef]

99. Andrade, C.M.; Fleckenstein, H.; Thomson-Luque, R.; Doumbo, S.; Lima, N.F.; Anderson, C.; Hibbert, J.; Hopp, C.S.; Tran, T.M.; Li, S.; et al. Increased circulation time of *Plasmodium falciparum* underlies persistent asymptomatic infection in the dry season. *Nat. Med.* **2020**, *26*, 1929–1940. [CrossRef]

100. Frank, M.; Dzikowski, R.; Amulic, B.; Deitsch, K. Variable switching rates of malaria virulence genes are associated with chromosomal position. *Mol. Microbiol.* **2007**, *64*, 1486–1498. [CrossRef]

101. Paget-McNicol, S.; Gatton, M.; Hastings, I.; Saul, A. The *Plasmodium falciparum var* gene switching rate, switching mechanism and patterns of parasite recrudescence described by mathematical modelling. *Parasitology* **2002**, *124*, 225–235. [CrossRef]

102. Gatton, M.L.; Cheng, Q. Investigating antigenic variation and other parasite-host interactions in *Plasmodium falciparum* infections in naive hosts. *Parasitology* **2004**, *128*, 367–376. [CrossRef] [PubMed]

103. Otto, T.D.; Gilabert, A.; Crellen, T.; Bohme, U.; Arnathau, C.; Sanders, M.; Oyola, S.O.; Okouga, A.P.; Boundenga, L.; Willaume, E.; et al. Genomes of all known members of a *Plasmodium* subgenus reveal paths to virulent human malaria. *Nat. Microbiol.* **2018**, *3*, 687–697. [CrossRef] [PubMed]

104. Pepino, M.Y.; Kuda, O.; Samovski, D.; Abumrad, N.A. Structure-function of CD36 and importance of fatty acid signal transduction in fat metabolism. *Annu. Rev. Nutr.* **2014**, *34*, 281–303. [CrossRef] [PubMed]

105. Silverstein, R.L.; Febbraio, M. CD36, a scavenger receptor involved in immunity, metabolism, angiogenesis, and behavior. *Sci. Signal.* **2009**, *2*, re3. [CrossRef]

106. Chen, Y.; Zhang, J.; Cui, W.; Silverstein, R.L. CD36, a signaling receptor and fatty acid transporter that regulates immune cell metabolism and fate. *J. Exp. Med.* **2022**, *219*, e20211314. [CrossRef] [PubMed]

107. Yang, M.; Silverstein, R.L. CD36 signaling in vascular redox stress. *Free Radic. Biol. Med.* **2019**, *136*, 159–171. [CrossRef]

108. Serghides, L.; Smith, T.G.; Patel, S.N.; Kain, K.C. CD36 and malaria: Friends or foes? *Trends Parasitol.* **2003**, *19*, 461–469. [CrossRef]

109. Canton, J.; Neculai, D.; Grinstein, S. Scavenger receptors in homeostasis and immunity. *Nat. Rev. Immunol.* **2013**, *13*, 621–634. [CrossRef]

110. Xu, X.; Zheng, X.; Zhu, F. CD36 gene variants and their clinical relevance: A narrative review. *Ann. Blood* **2021**, *6*, 34. [CrossRef]

111. Urban, B.C.; Willcox, N.; Roberts, D.J. A role for CD36 in the regulation of dendritic cell function. *Proc. Natl. Acad. Sci. USA* **2001**, *98*, 8750–8755. [CrossRef]

112. Urban, B.C.; Ferguson, D.J.; Pain, A.; Willcox, N.; Plebanski, M.; Austyn, J.M.; Roberts, D.J. *Plasmodium falciparum*-infected erythrocytes modulate the maturation of dendritic cells. *Nature* **1999**, *400*, 73–77. [CrossRef] [PubMed]

113. Wu, X.; Gowda, N.M.; Gowda, D.C. *Plasmodium falciparum*: Differential merozoite dose requirements for maximal production of various inflammatory cytokines. *Exp. Parasitol.* **2011**, *127*, 202–207. [CrossRef] [PubMed]

114. Patel, S.N.; Serghides, L.; Smith, T.G.; Febbraio, M.; Silverstein, R.L.; Kurtz, T.W.; Pravenec, M.; Kain, K.C. CD36 mediates the phagocytosis of *Plasmodium falciparum*-infected erythrocytes by rodent macrophages. *J. Infect. Dis.* **2004**, *189*, 204–213. [CrossRef] [PubMed]

115. Elliott, S.R.; Spurck, T.P.; Dodin, J.M.; Maier, A.G.; Voss, T.S.; Yosaatmadja, F.; Payne, P.D.; McFadden, G.I.; Cowman, A.F.; Rogerson, S.J.; et al. Inhibition of dendritic cell maturation by malaria is dose dependent and does not require *Plasmodium falciparum* erythrocyte membrane protein 1. *Infect. Immun.* **2007**, *75*, 3621–3632. [CrossRef]

116. Erdman, L.K.; Cosio, G.; Helmers, A.J.; Gowda, D.C.; Grinstein, S.; Kain, K.C. CD36 and TLR interactions in inflammation and phagocytosis: Implications for malaria. *J. Immunol.* **2009**, *183*, 6452–6459. [CrossRef]

117. McGilvray, I.D.; Serghides, L.; Kapus, A.; Rotstein, O.D.; Kain, K.C. Nonopsonic monocyte/macrophage phagocytosis of *Plasmodium falciparum*-parasitized erythrocytes: A role for CD36 in malarial clearance. *Blood* **2000**, *96*, 3231–3240. [CrossRef]

118. Gowda, N.M.; Wu, X.; Kumar, S.; Febbraio, M.; Gowda, D.C. CD36 contributes to malaria parasite-induced pro-inflammatory cytokine production and NK and T cell activation by dendritic cells. *PLoS ONE* **2013**, *8*, e77604. [CrossRef]

119. Thylur, R.P.; Wu, X.; Gowda, N.M.; Punnath, K.; Neelgund, S.E.; Febbraio, M.; Gowda, D.C. CD36 receptor regulates malaria-induced immune responses primarily at early blood stage infection contributing to parasitemia control and resistance to mortality. *J. Biol. Chem.* **2017**, *292*, 9394–9408. [CrossRef]

120. Simon, S.I.; Goldsmith, H.L. Leukocyte adhesion dynamics in shear flow. *Ann. Biomed. Eng.* **2002**, *30*, 315–332. [CrossRef]

121. Kunkel, E.J.; Dunne, J.L.; Ley, K. Leukocyte arrest during cytokine-dependent inflammation in vivo. *J. Immunol.* **2000**, *164*, 3301–3308. [CrossRef]

122. Helms, G.; Dasanna, A.K.; Schwarz, U.S.; Lanzer, M. Modeling cytoadhesion of *Plasmodium falciparum*-infected erythrocytes and leukocytes-common principles and distinctive features. *FEBS Lett.* **2016**, *590*, 1955–1971. [CrossRef] [PubMed]

123. Antia, M.; Herricks, T.; Rathod, P.K. Microfluidic modeling of cell-cell interactions in malaria pathogenesis. *PLoS Pathog.* **2007**, *3*, e99. [CrossRef]

124. Flatt, C.; Mitchell, S.; Yipp, B.; Looareesuwan, S.; Ho, M. Attenuation of cytoadherence of *Plasmodium falciparum* to microvascular endothelium under flow by hemodilution. *Am. J. Trop. Med. Hyg.* **2005**, *72*, 660–665. [CrossRef] [PubMed]

125. Li, A.; Lim, T.S.; Shi, H.; Yin, J.; Tan, S.J.; Li, Z.; Low, B.C.; Tan, K.S.; Lim, C.T. Molecular mechanistic insights into the endothelial receptor mediated cytoadherence of *Plasmodium falciparum*-infected erythrocytes. *PLoS ONE* **2011**, *6*, e16929. [CrossRef]

126. Yipp, B.G.; Hickey, M.J.; Andonegui, G.; Murray, A.G.; Looareesuwan, S.; Kubes, P.; Ho, M. Differential roles of CD36, ICAM-1, and P-selectin in *Plasmodium falciparum* cytoadherence in vivo. *Microcirculation* **2007**, *14*, 593–602. [CrossRef] [PubMed]

127. Lubiana, P.; Bouws, P.; Roth, L.K.; Dorpinghaus, M.; Rehn, T.; Brehmer, J.; Wichers, J.S.; Bachmann, A.; Hohn, K.; Roeder, T.; et al. Adhesion between *P. falciparum* infected erythrocytes and human endothelial receptors follows alternative binding dynamics under flow and febrile conditions. *Sci. Rep.* **2020**, *10*, 4548. [CrossRef] [PubMed]

128. Ho, M.; Hoang, H.L.; Lee, K.M.; Liu, N.; MacRae, T.; Montes, L.; Flatt, C.L.; Yipp, B.G.; Berger, B.J.; Looareesuwan, S.; et al. Ectophosphorylation of CD36 regulates cytoadherence of *Plasmodium falciparum* to microvascular endothelium under flow conditions. *Infect. Immun.* **2005**, *73*, 8179–8187. [CrossRef] [PubMed]

129. Herricks, T.; Avril, M.; Janes, J.; Smith, J.D.; Rathod, P.K. Clonal variants of *Plasmodium falciparum* exhibit a narrow range of rolling velocities to host receptor CD36 under dynamic flow conditions. *Eukaryot. Cell* **2013**, *12*, 1490–1498. [CrossRef] [PubMed]

130. Dasanna, A.K.; Lansche, C.; Lanzer, M.; Schwarz, U.S. Rolling Adhesion of Schizont Stage Malaria-Infected Red Blood Cells in Shear Flow. *Biophys. J.* **2017**, *112*, 1908–1919. [CrossRef] [PubMed]

131. Yipp, B.G.; Robbins, S.M.; Resek, M.E.; Baruch, D.I.; Looareesuwan, S.; Ho, M. Src-family kinase signaling modulates the adhesion of *Plasmodium falciparum* on human microvascular endothelium under flow. *Blood* **2003**, *101*, 2850–2857. [CrossRef] [PubMed]

132. Fedosov, D.A.; Caswell, B.; Karniadakis, G.E. Wall shear stress-based model for adhesive dynamics of red blood cells in malaria. *Biophys. J.* **2011**, *100*, 2084–2093. [CrossRef] [PubMed]

133. Fedosov, D.A.; Lei, H.; Caswell, B.; Suresh, S.; Karniadakis, G.E. Multiscale modeling of red blood cell mechanics and blood flow in malaria. *PLoS Comput. Biol.* **2011**, *7*, e1002270. [CrossRef] [PubMed]

134. Davis, S.P.; Amrein, M.; Gillrie, M.R.; Lee, K.; Muruve, D.A.; Ho, M. *Plasmodium falciparum*-induced CD36 clustering rapidly strengthens cytoadherence via p130CAS-mediated actin cytoskeletal rearrangement. *FASEB J.* **2012**, *26*, 1119–1130. [CrossRef] [PubMed]

135. Horrocks, P.; Pinches, R.A.; Chakravorty, S.J.; Papakrivos, J.; Christodoulou, Z.; Kyes, S.A.; Urban, B.C.; Ferguson, D.J.; Newbold, C.I. PfEMP1 expression is reduced on the surface of knobless *Plasmodium falciparum* infected erythrocytes. *J. Cell Sci.* **2005**, *118*, 2507–2518. [CrossRef]

136. May, J.; Evans, J.A.; Timmann, C.; Ehmen, C.; Busch, W.; Thye, T.; Agbenyega, T.; Horstmann, R.D. Hemoglobin variants and disease manifestations in severe *falciparum* malaria. *JAMA* **2007**, *297*, 2220–2226. [CrossRef] [PubMed]

137. Modiano, D.; Luoni, G.; Sirima, B.S.; Simpore, J.; Verra, F.; Konate, A.; Rastrelli, E.; Olivieri, A.; Calissano, C.; Paganotti, G.M.; et al. Haemoglobin C protects against clinical *Plasmodium falciparum* malaria. *Nature* **2001**, *414*, 305–308. [CrossRef] [PubMed]

138. Agarwal, A.; Guindo, A.; Cissoko, Y.; Taylor, J.G.; Coulibaly, D.; Kone, A.; Kayentao, K.; Djimde, A.; Plowe, C.V.; Doumbo, O.; et al. Hemoglobin C associated with protection from severe malaria in the Dogon of Mali, a West African population with a low prevalence of hemoglobin S. *Blood* **2000**, *96*, 2358–2363. [CrossRef]

139. Fairhurst, R.M.; Baruch, D.I.; Brittain, N.J.; Ostera, G.R.; Wallach, J.S.; Hoang, H.L.; Hayton, K.; Guindo, A.; Makobongo, M.O.; Schwartz, O.M.; et al. Abnormal display of PfEMP-1 on erythrocytes carrying haemoglobin C may protect against malaria. *Nature* **2005**, *435*, 1117–1121. [CrossRef]

140. Cholera, R.; Brittain, N.J.; Gillrie, M.R.; Lopera-Mesa, T.M.; Diakite, S.A.; Arie, T.; Krause, M.A.; Guindo, A.; Tubman, A.; Fujioka, H.; et al. Impaired cytoadherence of *Plasmodium falciparum*-infected erythrocytes containing sickle hemoglobin. *Proc. Natl. Acad. Sci. USA* **2008**, *105*, 991–996. [CrossRef] [PubMed]

141. Arman, M.; Adams, Y.; Lindergard, G.; Rowe, J.A. A method for positive and negative selection of *Plasmodium falciparum* platelet-mediated clumping parasites and investigation of the role of CD36. *PLoS ONE* **2013**, *8*, e55453. [CrossRef]

142. Xu, X.; Efremov, A.K.; Li, A.; Lai, L.; Dao, M.; Lim, C.T.; Cao, J. Probing the cytoadherence of malaria infected red blood cells under flow. *PLoS ONE* **2013**, *8*, e64763. [CrossRef] [PubMed]

143. Carvalho, P.A.; Diez-Silva, M.; Chen, H.; Dao, M.; Suresh, S. Cytoadherence of erythrocytes invaded by *Plasmodium falciparum*: Quantitative contact-probing of a human malaria receptor. *Acta Biomater.* **2013**, *9*, 6349–6359. [CrossRef] [PubMed]

144. Lim, Y.B.; Thingna, J.; Cao, J.; Lim, C.T. Single molecule and multiple bond characterization of catch bond associated cytoadhesion in malaria. *Sci. Rep.* **2017**, *7*, 4208. [CrossRef] [PubMed]

2.4 Altered cytokine response of human brain endothelial cells after stimulation with malaria patient plasma.

Altered Cytokine Response of Human Brain Endothelial Cells after Stimulation with Malaria Patient Plasma

Michaela Raacke [1,†], Amy Kerr [1,†], Michael Dörpinghaus [1], Jana Brehmer [1], Yifan Wu [1], Stephan Lorenzen [1], Christine Fink [2], Thomas Jacobs [1], Thomas Roeder [2,3], Julie Sellau [1], Anna Bachmann [1], Nahla Galal Metwally [1] and Iris Bruchhaus [1,4,*]

1   Bernhard Nocht Institute for Tropical Medicine, 20359 Hamburg, Germany; michaela.raacke@web.de (M.R.); a.kerr@freenet.de (A.K.); michael.doerpinghaus@web.de (M.D.); jana.brehmer@bnitm.de (J.B.); wu.yifan@bnitm.de (Y.W.); lorenzen@bnitm.de (S.L.); tjacobs@bnitm.de (T.J.); sellau@bnitm.de (J.S.); bachmann@bnitm.de (A.B.); metwally@bnitm.de (N.G.M.)
2   Department of Molecular Physiology, Kiel University, 24118 Kiel, Germany; cfink@zoologie.uni-kiel.de (C.F.); troeder@zoologie.uni-kiel.de (T.R.)
3   Airway Research Center North (ARCN), Member of the German Center for Lung Research (DZL), 24118 Kiel, Germany
4   Department of Biology, University of Hamburg, 20148 Hamburg, Germany
*   Correspondence: bruchhaus@bnitm.de; Tel.: +49-404-281-8472
†   Contributed equally.

Abstract: Infections with the deadliest malaria parasite, *Plasmodium falciparum*, are accompanied by a strong immunological response of the human host. To date, more than 30 cytokines have been detected in elevated levels in plasma of malaria patients compared to healthy controls. Endothelial cells (ECs) are a potential source of these cytokines, but so far it is not known if their cytokine secretion depends on the direct contact of the *P. falciparum*-infected erythrocytes (IEs) with ECs in terms of cytoadhesion. Culturing ECs with plasma from malaria patients (27 returning travellers) resulted in significantly increased secretion of IL-11, CXCL5, CXCL8, CXCL10, vascular endothelial growth factor (VEGF) and angiopoietin-like protein 4 (ANGPTL4) if compared to matching controls (22 healthy individuals). The accompanying transcriptome study of the ECs identified 43 genes that were significantly increased in expression (≥1.7 fold) after co-incubation with malaria patient plasma, including *cxcl5* and *angptl4*. Further bioinformatic analyses revealed that biological processes such as cell migration, cell proliferation and tube development were particularly affected in these ECs. It can thus be postulated that not only the cytoadhesion of IEs, but also molecules in the plasma of malaria patients exerts an influence on ECs, and that not only the immunological response but also other processes, such as angiogenesis, are altered.

Keywords: *Plasmodium falciparum*; malaria; endothelial cells; cytokines

1. Introduction

Despite the advances in malaria control programs, malaria remains one of the most detrimental infectious diseases worldwide. In 2019, about 229 million cases of malaria were recorded, including 409,000 cases of deaths [1]. Within the five species that cause malaria in humans, *Plasmodium falciparum* is the most clinically relevant one and responsible for most deaths. The complications caused by malaria infection are multifactorial; both the parasite and the host contribute. A central part of the pathogenesis is the cytoadhesion of *P. falciparum*-infected erythrocytes (IEs) within the vascular bed of vitally important organs, such as the brain, heart, lung, stomach, skin and kidney [2–4]. Besides blockage of capillaries due to the cytoadhesion of the IEs, increased inflammatory cytokine production, endothelial dysfunction and increased vascular permeability also occur in the affected tissue [5–7]. As a result of the immune response induced by parasite growth and cytoadhesion to the endothelium, patients develop fever, headaches, muscle aches and rigors [8–12].

According to the age and immune status of the patient, severe lethal complications, such as cerebral malaria (CM), lung injury, renal failure, acidosis and severe anaemia, may develop [11–13]. Not only the acute complications affect the patients, but also one third of survivors (African children and adult travellers) were found to suffer from long-term health problems, such as cognitive and neurological impairments [14–16].

Several in vitro studies have shown that interaction of the IEs with endothelial cells (ECs) increase the expression of various genes encoding proinflammatory cytokines, such as IL-6, IL-1 and tumor necrosis factor-alpha (TNF-α), and chemokines, such as CXCL8, CCL2, CCL20, CXCL1, CXCL2 and CCL5, which are important for the recruitment of leukocytes to the endothelium during inflammation [17–19].

Diverse plasmodial antigens and released components, as well as endogenous metabolites associated with danger signals, have repeatedly been shown to stimulate the immune system. Glycosylphosphadidylinositol anchors of *P. falciparum* proteins have been the first ones described [20], leading to production of the proinflammatory cytokines in macrophages [21]. It was also shown that in monocytes fed with hemozoin, expression of genes encoding for cytokines and chemokines was increased [22]. In macrophages, incubation with hemozoin resulted in an increase in various chemokine transcripts, including CCL3, CCL4, CXCL1 and CCL2 [23], but phagocytosis of hemozoin leads to impairment of macrophage function [24]. Thus, *P. falciparum* malaria is accompanied by a strong immunological reaction of the host. This considerable increase in systemic and local inflammation contributes significantly to the pathogenesis of malaria. The immune response triggered by *P. falciparum* is a very complex event. To date, well over 30 cytokines have been described, which can be detected in serum or plasma of malaria patients in larger quantities compared to healthy controls. These include CCL2, CCL4, CXCL4, CXCL8, CXCL10, CCL3, IL-1β, IL-6, CXCL2, TNF-α, interferon-gamma (INF-γ), IL-1α, IL-12, IL-17A, IL-15, IL-10, IL1-RA, CCL20, vascular endothelial growth factor (VEGF), IL-13, IL-31, IL-33, CXCL9, IL-9, CCL28 and granulocyte-colony stimulating factor (G-CSF) [5,25–38]. Significantly increased amounts of CCL2, CCL4, CXCL4, CXCL8, CXCL10, IL-1RA, IL-6, TNF-α and G-CSF were detected in patients with CM [27,29,39,40] and the amount of some cytokines (CCL2, CCL4, CXCL4, CXCL8, CXCL10 and CCL3) directly correlates with the severity of a malaria infection [25,26,29,30,36].

Plasma levels of 29 biomarkers, including various chemokines and cytokines, were investigated in patients with CM and non-CM. However, significantly increased levels in patients with CM compared to non-CM were only found for IL-6, CXCL8 and IL-1RA [26]. A positive correlation with parasitaemia was described for CCL20 and CXCL9 [36].

To date, there are no studies comparing the levels of different cytokines in the plasma of *P. falciparum*-infected returning travellers and, in parallel, elucidating the influence of these plasmas on the stimulation of ECs and the associated secretion of these factors into the cell culture supernatant as well as their influence on EC gene expression.

Our studies showed that co-incubation of brain ECs with plasma from malaria patients resulted in significantly increased secretion of IL-11, CXCL5, CXCL10, VEGF and angiopoietin-like protein 4 (ANGPTL4). A comparative transcriptome analysis revealed that, in addition to an inflammatory response, biological processes such as cell migration, cell proliferation and tube development, as well as the KEGG 'IL-17 signalling pathway', were particularly affected.

2. Materials and Methods

2.1. Blood Plasma of Malaria Patients and Healthy Control Individuals

The study was performed on 27 EDTA-plasma samples from patients diagnosed with *P. falciparum* malaria, with parasitaemia between <1% and 11%. All patients were adult tropical returnees and were treated as in- or outpatients in Hamburg, Germany. Patients were either seen in the outpatient clinic of the University Medical Center Hamburg-Eppendorf (UKE) at the Bernhard Nocht Institute for Tropical Medicine, treated as inpatients at the UKE, or at the Bundeswehrkrankenhaus Hamburg. As controls, 22 plasma samples from

healthy individuals were used. The study was approved by the relevant ethics committee (Ethical Review Board of the Medical Association of Hamburg, reference numbers PV3828 and PV4539) (Supplementary Table S1).

2.2. HBEC-5i Brain Endothelial Cell Line

This project was carried out using human brain endothelial cells HBEC-5i, derived from the cerebral cortex and immortalized with the SV40 large T antigen (American Type Culture Collection (ATCC), Manassas, VA, USA; no. CRL-3245). HBEC-5i cells were seeded in 0.1% gelatin-coated T25 culture flasks. For normal cell culture, DMEM/F-12 complete growth medium (Gibco, Thermo Fisher Scientific, Bremen, Germany) containing 40 µg/mL endothelial cell growth supplement (ECGS; Merck Millipore, Darmstadt, Germany), 10% heat-inactivated foetal calf serum (Capricorn Scientific, Ebsdorfergrund, Germany) and 9 µg/mL gentamycin (Sigma–Aldrich Merck, Darmstadt, Germany) was used. The endothelial cells (ECs) were cultivated at 37 °C and 5% CO_2 atmosphere and split every 2–4 days when a confluence of 70–90% is reached.

2.3. Stimulation Assay of ECs with Plasma of Malaria Patients and Healthy Control Individuals

The 96-well plates were coated with 50 µL of 0.1% gelatin (Sigma–Aldrich Merck, Darmstadt, Germany) in Dulbecco's Phosphate-Buffered Saline (DPBS; PAN, Biotech, Germany) per well and incubated at 37 °C for 30 min. After incubation, the gelatin was aspirated and 50 µL DMEM/F-12 medium was placed in each well and incubated at 37 °C for 15 min to adjust the pH value. After removal of the DMEM/F-12 medium, 1×10^4 ECs in 200 µL DMEM/F-12 medium were added to each well. The cells were cultivated for two days with a medium change after the first day.

For the stimulation assay, the cells were washed twice with 100 µL/well DMEM/F-12 medium each before addition of the human plasma. In total, 80 µL of a plasma mixture consisting of 58 µL DMEM/F-12/gentamycin medium, 2 µL heparin (10,000 units/mL; Braun, Melsungen, Germany) and 20 µL human plasma were added per well. Each plasma sample was analysed in quadruple. The 96-well plate was then incubated for 6 h at 37 °C (5% CO_2). After completion of the 6 h incubation, the supernatant was removed, and the wells were washed 4 times with DMEM/F-12/gentamycin medium. Then 100 µL of DMEM/F-12 complete growth medium was added and the cells were incubated for another 42 h before the cell culture supernatant was removed; after a total amount of 48 h, the four replicates were pooled, centrifuged and the supernatant immediately frozen at −80 °C.

For the transcriptome analyses, the ECs were incubated in T25 cell culture flasks (monolayer 70–90%) containing 4.5 mL DMEM/F-12/gentamycin medium, 50 µL heparin (10,000 units/mL; Braun, Melsungen, Germany) and 500 µL plasma of malaria patients and healthy controls, respectively (plasma concentration 10%), for 7 h. Afterwards, the cells were washed and lysed with 200 µL Trizol (Invitrogen, Thermo Fisher Scientific, Bremen, Germany) and stored at −80 °C until the RNA was isolated.

2.4. LEGENDplex^{TM} Assay

The LEGENDplex Kits used were multiplex bead-based assay panels manufactured by BioLegend, Inc. (San Diego, CA, USA). The two bead panels that were chosen for measurement of cytokine concentration in every sample included the pro-inflammatory cytokines IL-1α and IL-1β, the pro- and anti-inflammatory cytokines IL-6, IL-7, IL-12 and IFN-β, the anti-inflammatory cytokines IL-1RA, IL-10 and IL-11, and the proinflammatory chemokines CCL3, CCL20, CXCL1, CXCL5, CXCL8, CXCL10 and VEGF. The bead-assays were performed following instructions provided by the manufacturer in duplicates. After completion of the reaction, the samples were transferred to FACS tubes to be read on a flow cytometer (BD Accuri® C6 Flow Cytometer, Thermo Fisher Scientific, Bremen, Germany).

The concentration of a particular analyte was determined by the provided LEGEND-plexTM Software v8 based on a known standard curve. Values with evident methodical

errors were excluded. After calculating the mean of the two replicated values for each analyte, statistical analyses were performed using GraphPad Prism (version 9.02 (134) GraphPad Software Inc, San Diego, CA, USA). A Mann–Whitney *U* test was run to determine differences in cytokine concentration between groups. Exact *p*-values corrected for ties were calculated and differences considered significant for *p*-values ≤ 0.05. In case of normally distributed data, an independent samples *t*-test was performed to support the results (data not shown). Patient's plasma samples were divided into three subgroups, based on parasitaemia. Kendall's tau b correlation was run to determine the relationship between the analyte concentration and level of parasitaemia. The correlation between the cytokines and parasitaemia was performed by means of a correlation analysis using the nonparametric Spearman correlation (GraphPad Prism, version 9.02 (134)). For multiple testing, the Benjamini–Hochberg adjustment and conservative Bonferroni correction were applied [41].

2.5. ANGPTL4 and TNF-α ELISA

Human ANGPTL4 and TNF-α was measured using ELISA after respective dilution of the sample in a reagent dilution buffer following the instructions of the manufacturers (R&D Systems, Minneapolis, MN, USA). Significance was evaluated using the Mann–Whitney *U* test.

2.6. RNA Isolation

RNA was isolated using a PureLink RNA Mini Kit (Thermo Fisher Scientific, Bremen, Germany) according to the manufacturer's instructions. Genomic DNA contamination was removed using the TURBO DNA-free Kit (Invitrogen, Thermo Fisher Scientific, Bremen, Germany) followed by a magnetic bead enzymatic wash using Agencourt RNAClean XP (Beckman Coulter, Krefeld, Germany). The concentration and quality of isolated RNA were assessed using an Agilent 2100 Bioanalyser System with the Agilent RNA 6000 Pico Kit (Agilent Technologies, Ratlingen, Germany). The RNA was sent to BGI (Shenzhen, China), where RNAseq was performed using the Illumina HiSeq 4000 PE100 platform (approximately 11 M PE reads per samples). Reads were quality and adapter trimmed using Trimmomatic [42] and aligned to the human transcriptome by RSEM [43] using Bowtie2 [44] as an aligner. Differential expression was determined using DESeq2 [45].

3. Results

3.1. Determination of Concentrations of Different Cytokines in Plasmas of Malaria Patients and Healthy Controls

In the first part of this study, the plasmas of 27 patients infected with *P. falciparum* with a parasitaemia between <1% and 11% and of 22 healthy individuals were analysed for the presence of 16 different cytokines. All 27 patients were adult tropical returnees with symptomatic *P. falciparum* malaria (Supplementary Table S1). In this study, the proinflammatory cytokines IL-1α and IL-1β, the pro- and anti-inflammatory cytokines IL-6, IL-7, IL-11, IL-12 and IFN-β, the anti-inflammatory cytokines IL-1RA and IL-10 and the proinflammatory chemokines CCL3, CCL20, CXCL1, CXCL5, CXCL8 and CXCL10, as well as the growth factor VEGF, were analysed using a customized LEGENDplex assay (Supplementary Table S2).

For cytokines IL-6, IL-1RA, IL-10 and IL-11 and chemokines CXCL1, CXCL8, CXCL10, CCL3 and CCL2, significantly higher concentrations were found in plasma samples of malaria patients compared to healthy controls (Figure 1A). For IL-6, IL-1RA, CCL3, CCL20 and CXCL10, the significant difference was already detected at a parasitaemia < 1.0%. For CXCL8, IL-10 and CXCL1, a significantly higher value was found at a parasitaemia $\geq 1\%$ and for IL-11 and CXCL5 only at a parasitaemia > 2.5% (Figure 1A).
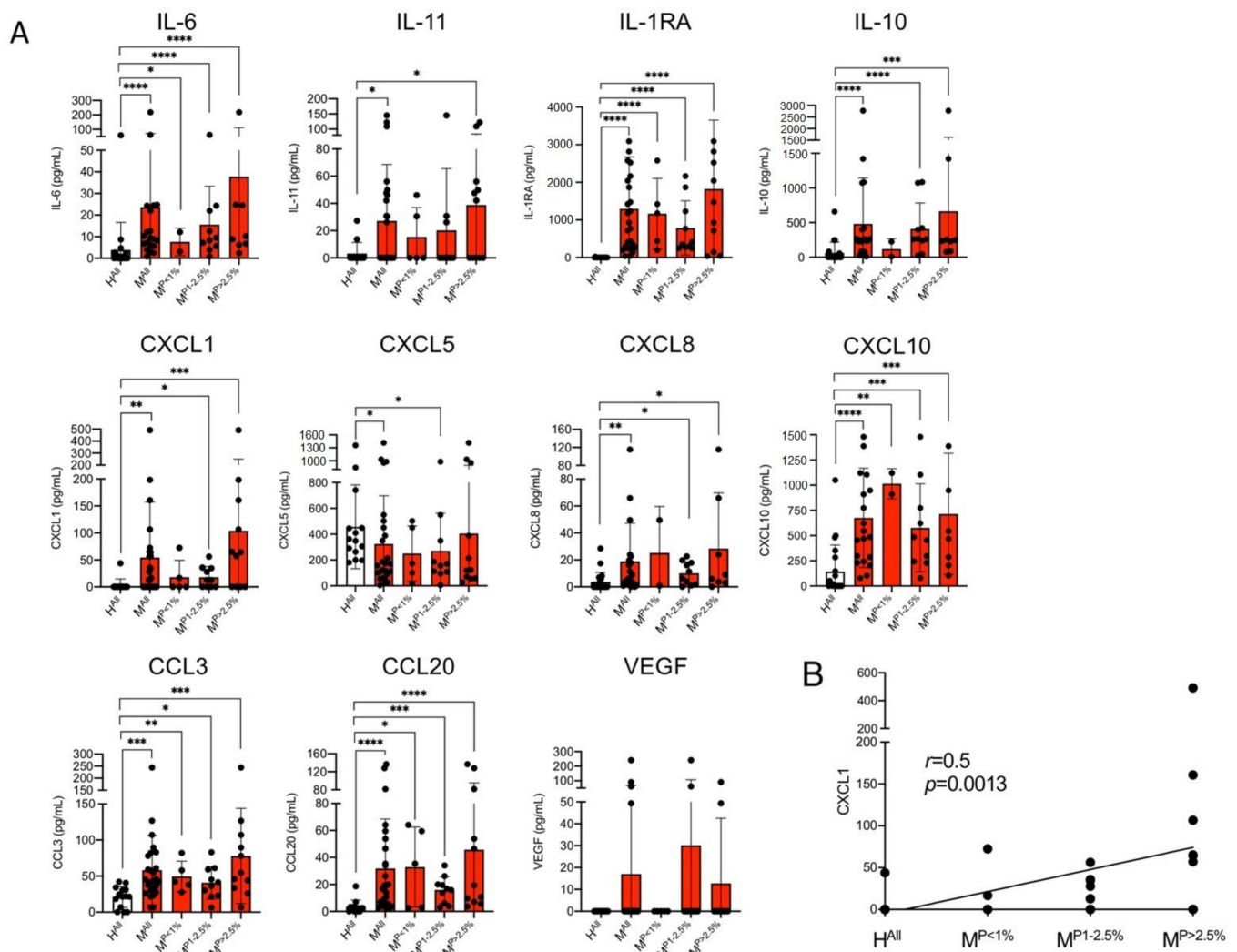
Figure 1. Levels of cytokines in plasma derived from malaria patients (M) and healthy control individuals (H). (**A**) The amount of cytokines was measured with a bead-based LEGENDplex assay (*n* = 13–26, Supplementary Tables S2 and S3). Data are expressed as the mean ± standard deviation (SD). Statistical analyses were performed using the Mann–Whitney *U* test (* *p* < 0.05; ** *p* < 0.01; *** *p* < 0.001; **** *p* < 0.0001). (**B**) For CXCL1, the correlation between the amount of cytokine and parasitaemia was performed by means of a nonparametric Spearman correlation using GraphPad Prism (version 9.0.2 (134)). Abbreviations: Healthy controls (H^{All}); malaria patients (M^{All}); malaria patients with a parasitaemia < 1% (M$^{P<1\%}$), 1–2.5% (M$^{P1-2.5\%}$) and >2.5% (M$^{P>2.5\%}$).

The greatest increase in the amount in the plasmas of malaria patients compared to healthy controls was observed for IL-1RA (H^{All}: 1.8 ± 6.9 pg/m, M^{All}: 1296 ± 1378 pg/m; 720-fold increase), followed by CXCL1 (H^{All}: 3.1 ± 11.7 pg/mL, M^{All}: 54.4 ± 103.0 pg/mL; 17.5-fold increase), CCL20 (H^{All}: 3.5 ± 5.0 pg/mL, M^{All}: 31.8 ± 36.6 pg/mL; 9.1-fold increase) and IL-11 (H^{All}: 3.2 ± 8.2 pg/mL, M^{All}: 27.1 ± 41.5 pg/mL; 8.5-fold increase) (Figure 1A, Supplementary Table S3). For CXCL1, there is a correlation between the amount of cytokine detected and the different levels of parasitaemia (*p* = 0.0013, *r* = 0.5) (Figure 1B). For none of the other cytokines could a correlation with parasitemia be demonstrated. Interestingly, CXCL5 is the only chemokine that was detected at significantly lower levels in plasma malaria patients than in plasma of healthy controls (Figure 1A). For VEGF, no significant difference was found between patients with malaria infection and the healthy controls, but four malaria plasma samples showed an increase of the VEGF amount, while all remaining individuals had levels beyond the detection limit of the LEGENDplex assay

(Figure 1A). The amounts of IL-1 α, IL-1β, IL-7, IL-12 and IFN-β were also below the detection limit of the LEGENDplex assay.

Thus, for nine of the 16 cytokines examined, a significantly increased amount and for one (CXCL5) a lower amount was found in the plasma of infected individuals compared to healthy controls. Five cytokines were below the detection level of the assay (Figure 1A, Supplementary Table S3).

The amount of TNF-α in the plasmas of malaria patients and healthy controls was determined separately by ELISA. On average, significantly less TNF-α is present in the plasmas of malaria patients compared to controls (H^{All}: 3770 ± 11,925 pg/mL, M^{All}: 75 ± 160 pg/mL; however, this was not significant (p = 0.0531) (Figure 2, Supplementary Table S4).
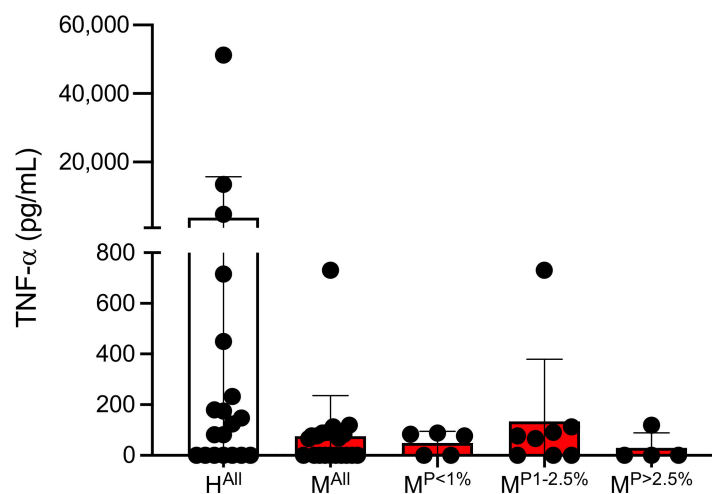
Figure 2. Amount of TNF-α in plasmas of malaria patients and healthy individuals (Supplementary Table S4). Abbreviations: Healthy controls (H^{All}); malaria patients (M^{All}); malaria patients with a parasitaemia < 1% ($M^{P<1\%}$), 1–2.5% ($M^{P1-2.5\%}$) and >2.5% ($M^{P>2.5\%}$).

3.2. Determination of Concentrations of Various Cytokines in the Culture Supernatant of ECs Stimulated with Plasma from Malaria Patients and Healthy Controls

The next step was to investigate whether the plasma of malaria patients and non-infected, healthy individuals have an influence on EC cytokine secretion. It must be mentioned here that, of course, not only cytokines present in plasma, but also various plasmodial antigens and released components, as well as endogenous metabolites, can stimulate ECs. For this purpose, ECs of the brain EC line HBEC-5i were stimulated for six hours with human plasma using a concentration of 25%. Afterwards, the plasma-containing culture supernatant was removed, and the ECs were cultivated in DMEM/F-12 complete growth medium. Cell culture supernatants were collected 48 h after starting the stimulation and the level of cytokines secreted was analysed. Subsequently, the culture medium was removed, and the level of cytokines secreted in the culture supernatant was analysed (Supplementary Table S2). Preliminary studies have shown that significant effects could only be measured 48 h after stimulation.

Stimulation of ECs with plasma from malaria patients resulted in significantly increased levels of IL-11, CXCL5, CXCL8, CXCL10 and VEGF in comparison to stimulation of ECs using plasma from healthy controls (Figure 2). In all cases, the measured difference was significant; but, in contrast to the results from the plasma samples, only a 1.5–2.3-fold increase was detected (IL-11: H^{All}: 346.4 ± 157.3 pg/mL, M^{All}: 526.9 ± 219.3 pg/mL, 1.5-fold; CXCL5: H^{All}: 152.5 ± 128.6 pg/mL, M^{All}: 263.5 ± 117.8 pg/mL, 1.7-fold; CXCL8: H^{All}: 7085 ± 7065 pg/mL, M^{All}: 11,681 ± 6360 pg/mL, 1.6-fold; CXCL10: H^{All}: 30.4 ± 34.2 pg/mL, M^{All}: 69.2 ± 53.6 pg/mL, 2.3-fold; VEGF: H^{All}: 112.1 ± 56.2 pg/mL, M^{All}: 170.1 ± 59.3 pg/mL, 1.5-fold) (Figure 3, Supplementary Table S3).
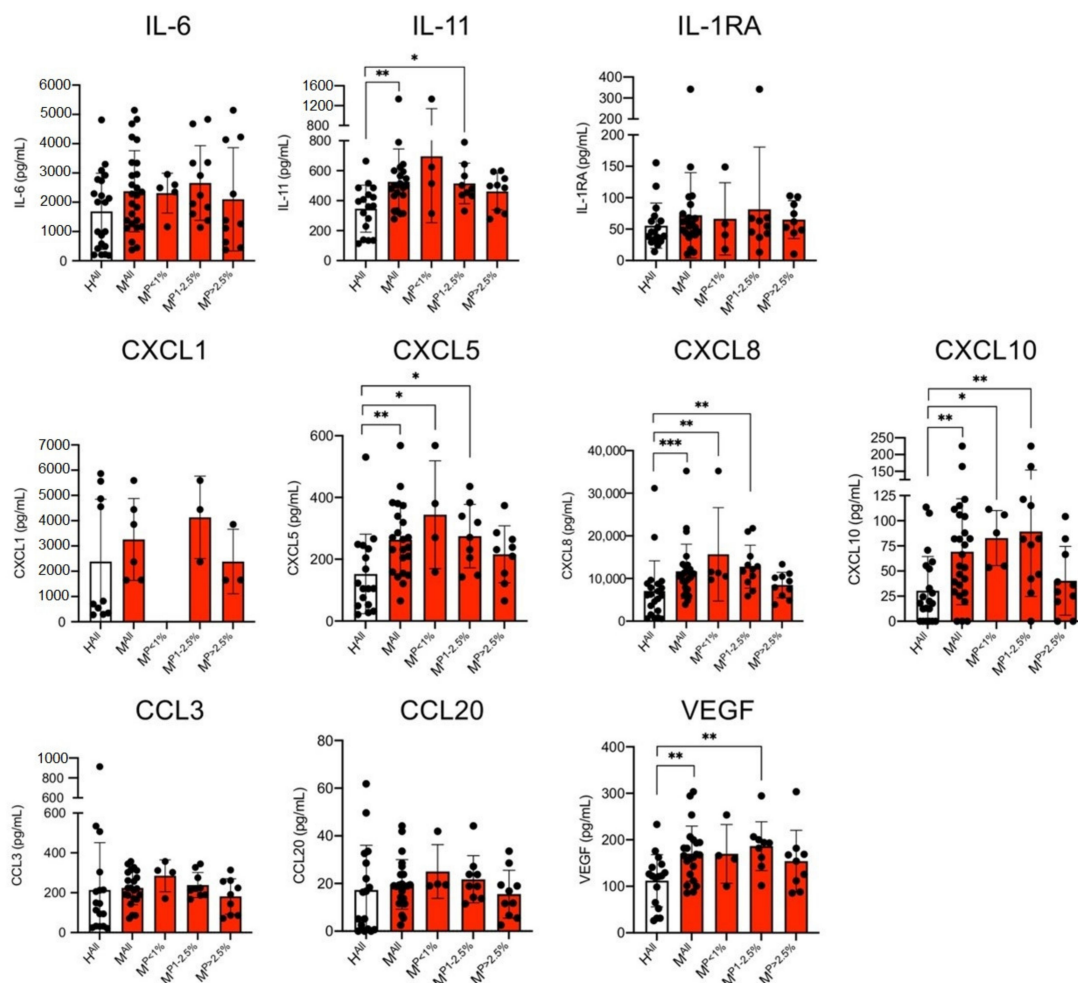
Figure 3. Level of cytokines in the culture supernatants of endothelial cells (HBEC-5i) stimulated with plasma derived from malaria patients (M) and healthy control individuals (H) were analysed with a bead-based LEGENDplex assay (n = 6–26; Supplementary Tables S2 and S3). Data are expressed as the mean ± SD. Statistical analyses were performed using the Mann–Whitney U test (* $p < 0.05$; ** $p < 0.01$; *** $p < 0.001$). Abbreviations: Healthy controls (H[All]); malaria patients (M[All]); malaria patients with a parasitaemia < 1% (M[P<1%]), 1–2.5% (M[P1−2.5%]) and >2.5% (M[P>2.5%]).

Again, the amount of IL-1α, IL-1β, IL-7, IL-12 and IFN-β were below the detection limit of the LEGENDplex assay, in this case also of IL-10. In contrast to the CC levels in the plasmas, no differences were detected for the cytokines IL-6, IL-1RA and the chemokines CCL3, CCL20 and CXCL1 in the cell culture supernatants of HBEC-5i cells stimulated with plasma from malaria patients and healthy controls (Figure 3).

If we corrected for multiple testing and included all cytokines with measurable values, most of the reported differences (supernatant and plasma) are still be significant (Figures 1 and 3, Supplementary Table S5). For the supernatants, there is no different result with either the Benjamini–Hochberg adjustment or the conservative Bonferroni correction. For plasma, CXCL5 and IL-11 fail the Bonferroni correction, while with the Benjamini–Hochberg adjustment CXCL5 proves significant and IL-11 just misses the cut-off ($p = 0.0457$, cut-off = 0.0455).

No TNF-α was detected in the supernatants of endothelial cells after stimulation with plasma from the malaria patients or with plasma from the healthy controls, respectively.

3.3. Amount of Secreted Angiopoietin-like Protein 4 (ANGPTL4) in Culture Supernatant of ECs Stimulated with Plasma Derived from Malaria Patients and Healthy Individuals

Studies suggest a synergistic effect of ANGPTL4 and VEGF [46,47]. Therefore, both the plasmas as well as the culture supernatants of the ECs stimulated with plasma were

examined for the presence of ANGTPL4 using an ELISA assay. On average, there was less ANGPTL4 in the plasmas of the malaria patients than in the plasmas of the controls (H^{All}: 656.8 ± 1108.7 ng/mL, M^{All}: 149.9 ± 93.4 ng/mL); however, this was not significant (Figure 4A). When the ECs were stimulated with the plasmas, the reverse was observed. Stimulation with plasma from malaria patients resulted in an increase in the measured amount of ANGPTL4 in comparison to the controls (H^{All}: 13.8 ± 3.4 ng/mL, M^{All}: 16.4 ± 5.6 ng/mL, $p = 0.0691$). However, the measured amounts were 10–50 times lower than in the plasmas. Considering the different parasitaemia levels separately, only plasma from patients with a parasitaemia of >2.5% has significantly higher levels of ANGPTL4 (20.7 ± 8.5 ng/mL, $p = 0.0071$) in the supernatant compared to the controls (Figure 4B, Supplementary Table S6).
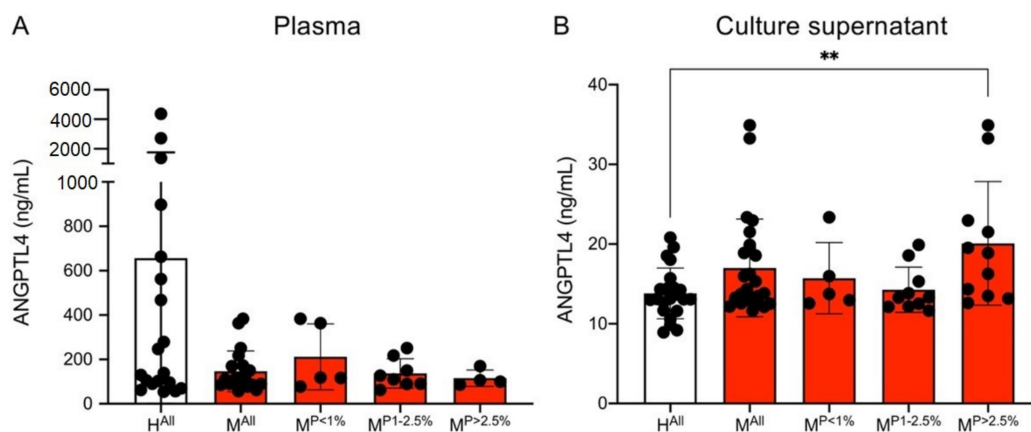
Figure 4. Amount of ANGPTL4 in plasma (**A**) and culture supernatants (**B**) of endothelial cells (HBEC-5i) co-incubated with plasma from malaria patients and healthy individuals. Statistical analyses were performed using the Mann–Whitney *U* test (** $p < 0.01$) (Supplementary Table S6). Abbreviations: Healthy controls (H^{All}); malaria patients (M^{All}); malaria patients with a parasitaemia < 1% ($M^{P<1\%}$), 1–2.5% ($M^{P1-2.5\%}$) and >2.5% ($M^{P>2.5\%}$).

3.4. Comparative Transcriptome Analyses of ECs Stimulated with Plasma of Malaria Patients and Healthy Individuals

Next, we analysed whether the differences observed on the protein level in the culture supernatant after stimulation of the ECs with plasma of malaria patients could also be found on the RNA level. For this purpose, the HBEC-5i cells were stimulated with the plasma of four malaria patients and of three healthy control individuals for seven hours and subsequently their transcriptomes were analysed. The malaria patients had a parasitaemia between 2.5 and 4% (Supplementary Tables S1, S7 and S8).

After seven hours of stimulation, a significant increase was observed for *il1β* ($p = 0.0042$), *cxcl1* ($p = 0.0029$), *cxcl5* ($p = 0.0059$) and *angptl4* ($p = 0.0002$) after stimulation with patient plasma. A tendency was only observed for *vegf* ($p = 0.05$). This is due to the measured expression level of the control H8. This deviates significantly from the expression level of the other two controls (expression level: 5820 vs. 860–935). A decrease in expression, albeit non-significant, after stimulation with plasma from malaria patients compared to the controls was observed for *il11* expression ($p = 0.05$), which is in contrast to the LEGENDplex results (Figure 5, Supplementary Table S9). Using qPCR analysis for *angptl4* and *vegf*, the difference in gene expression detected after 7 h could no longer be observed 48 h after stimulation (data not shown).
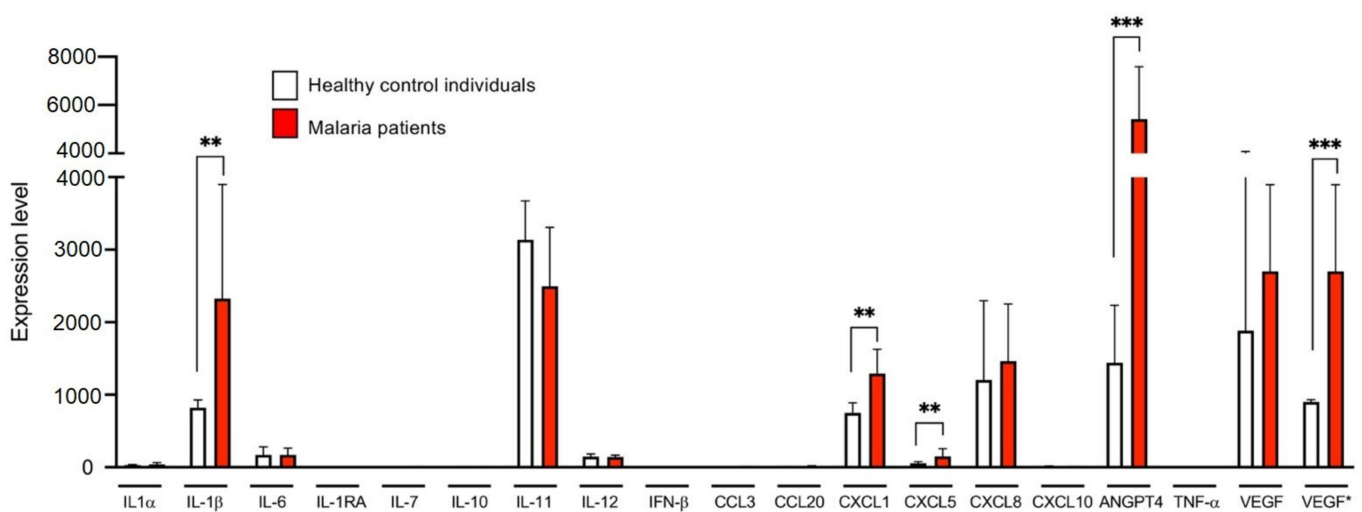
Figure 5. Expression levels of genes coding for the examined cytokines of endothelial cells (HBEC-5i) stimulated with plasma from three healthy control individual and four malaria patients. HBEC-5i cells were incubated for 7 h in the presence of 10% plasma derived from three control individuals and four malaria patients (Supplementary Tables S1, S3, S7 and S8). Subsequently, RNA was isolated from the HBEC-5i cells and a comparative transcriptome analysis was performed (Supplementary Table S9). VEGF*: Analysis excluding sample H8. M6, M9, M10, and M11: 4 biological replicates each; H5 and H10: 2 biological replicates each; H8: 1 biological replicate. Statistical analyses were performed using the Mann–Whitney *U* test (** $p < 0.01$; *** $p < 0.001$).

Transcriptome analysis also provides an overall view of the changes in EC gene expression after stimulation with patient plasma. For this analysis, genes with a base mean level ≥ 40, a differential expression with a fold change $\leq 0.6/\geq 1.7$ and a padj ≤ 0.05 were included. Only thirteen genes were identified that were expressed between 1.7- and 3-fold higher after stimulation with the plasma of healthy control individuals compared to stimulation with the patient plasma (Supplementary Tables S9 and S10). On the other hand, 43 genes are expressed between 1.7- and 4.5-fold higher in ECs after stimulation with plasma from malaria patients than after stimulation with plasma from healthy controls (Table 1, Supplementary Tables S9 and S11).

To identify the biological processes in which the proteins encoded by the identified genes but also the cytokines identified by LEGENDplex and ELISA are involved, a gene set enrichment analyses (GSEA) was performed using g:Profiler analysis [48] (Table 1). The g:Profiler analyses shows that within the gene ontology term biological processes (GO:BP), 'positive regulation of cell migration', 'blood vessel development' and 'inflammatory response' are significantly regulated (padj = 7.602×10^{-5}, 2.542×10^{-4} and 2.474×10^{-4}, respectively). The KEGG pathways 'rheumatoid arthritis (padj = 4.499×10^{-4}) and 'IL-17 signaling pathway' (padj = 3.436×10^{-4}) also were found to be upregulated (Table 1). To identify protein–protein interaction networks, a Markov Clustering (MCL) analyses was performed using the program STRING, version 11.0 [49,50]. This analysis yields four clusters, the largest comprising 20 proteins, which are involved in 'positive regulation of cell population proliferation' (padj 4.312×10^{-8}) and 'tube development' (padj 1.948×10^{-5}). The cluster 'cholesterol metabolic process' (padj 3.1×10^{-6}) contains four proteins and the cluster 'negative regulation of cell differentiation' (padj 3.4×10^{-2}) contains three proteins. In addition, an unassigned cluster (three proteins) was predicted (Figure 6, Table 1).

Table 1. Genes differentially higher expressed (≥1.7 fold) in endothelial cells incubated with plasma from malaria patients (M6, M9, M10, and M11) compared to incubation with plasma from healthy controls (H5, H10, and H8).

	Gene	Expression Level		Fold Change	padj	GO:BP			KEGG		MCL	Name
		H[5,10,8]	M[6,9,10,11]			1	2	3	4	5		
1	CSF3	16	73	4.5	0.016				light blue		red	Colony Stimulating Factor 3
2	ANGPTL4	1442	5419	3.8	4.17×10^{-6}		green				red	Angiopoietin Like 4
3	IL1B	821	2324	2.8	0.019	light green	green	dark green	light blue	blue	red	Interleukin 1b
4	CXCL5	55	149	2.7	0.049			dark green	light blue	blue	red	Chemokine cxcl5
5	FOXS1	18	47	2.7	0.002		green					Forkhead Box S1
6	HMOX1	410	1083	2.6	0.033	light green	green	dark green			red	Heme Oxygenase 1
7	GDNF	39	98	2.5	0.044		green				red	Glial Cell Derived Neurotrophic Factor
8	OPCML	29	71	2.4	3.1×10^{-5}						blue	Opioid Binding Protein/Cell Adhesion Mol. Like
9	GPR68	23	57	2.4	0.015							G Protein-Coupled Receptor 68
10	INSIG1	1065	2543	2.4	0.002						yellow	Insulin Induced Gene 1
11	TNFAIP6	21	49	2.3	0.026	light green					red	TNF Alpha Induced Protein 6
12	IGFBP5	3873	8901	2.3	3.15×10^{-7}	light green					red	Insulin Like Growth Factor Binding Protein 5
13	ESM1	809	1783	2.2	0.022		green				red	Endothelial Cell Specific Molecule 1
14	POSTN	920	1922	2.1	5.43×10^{-5}	light green					green	Periostin
15	SERPINA9	57	116	2	3.75×10^{-5}							Serpin Family A Member 9
16	ADTRP	49	100	2	0.023		green					Androgen Dependent TFPI Regulating Protein
17	MSMO1	1097	2235	2	0.0002		green				yellow	Methylsterol Monooxygenase 1
18	HAS2	1299	2642	2	0.041	light green					red	Hyaluron Synthase 2
19	LDLR	1491	3030	2	0.0012		green	dark green			yellow	Low Density Lipoprotein Receptor
20	SHANK1	25	51	2	0.0036						blue	SH3 And Multiple Ankyrin Repeat Domains 1_2
21	RFX8	38	76	2	0.0031							RFX Family Member 8, Lacking RFX DNA bd.
22	CHST2	305	606	2	0.0012		green	dark green				Carbohydrate Sulfotransferase 2
23	EREG	128	253	2	0.0126		green				red	Epiregulin
24	PTX3	6486	12598	1.9	0.00012			dark green			red	Pentraxin 3
25	PTGS1	66	128	1.9	0.0123			dark green				Prostaglandin-Endoperoxide Synthase 1
26	RPSAP52	69	133	1.9	1.2×10^{-7}							Ribosomal Protein SA Pseudogene 52
27	FAM84A	241	455	1.9	0.0012							LRAT Domain Containing 1
28	LAMC2	1258	2329	1.9	0.0341	light green						Laminin Subunit Gamma 2
29	SERPINE1	57674	106566	1.8	0.0002	light green	green	dark green			red	Serpin Family E Member 1
30	TMEM158	752	1377	1.8	3.63×10^{-5}							Transmembrane Protein 158
31	FRMPD4	54	97	1.8	0.023						blue	FERM And PDZ Domain Containing
32	B3GNT5	150	267	1.8	0.0099							UDP-GlcNAc:BetaGal Beta-1,3-N-Acetylglucosaminyltransferase 5
33	CAMK1G	111	197	1.8	4.31×10^{-5}							Calcium/Calmodulin Dependent Protein Kinase IG
34	HMGCS1	1014	1798	1.8	0.016						yellow	3-Hydroxy-3-Methylglutaryl-CoA Synthase 1
35	PQLC2L	37	65	1.7	0.0176							Solute Carrier Family 66 Member 1 Like
36	CD93	114	197	1.7	0.00764							CD93 Molecule
37	TWIST2	122	212	1.7	0.0095	light green					green	Twist Family BHLH Transcription Factor 2
38	IRX3	82	143	1.7	0.0035							Iroquois Homeobox 3
39	CXCL1	749	1293	1.7	0.0017			dark green	light blue	blue	red	C-X-C Motif Chemokine Ligand 1
40	RRAD	146	251	1.7	0.0301							Ras Related Glycolysis Inhibitor/ Calcium Channel Reg.
41	POU2F2	104	180	1.7	0.0065							POU Class 2 Homeobox 2
42	HSPA1B	3762	6447	1.7	0.0055							Heat Shock Protein Family A (Hsp70) Member 1B
43	PLIN2	2740	4688	1.7	0.0022						red	Perilipin 2
44 *	VEGF	1884	2700	1.4	ns	light green	green		light blue			Vascular Epidermal Growth Factor
45 *	IL11	3135	2494	0.8	ns				light blue			Interleukin 11
46 *	CXCL10	7.3	5.2	0.67	ns	light green	green	dark green		blue		C-X-C Motif Chemokine Ligand 10
47 *	CXCL8	1203	1462	1.2	ns	light green	green	dark green	light blue	blue	red	C-X-C Motif Chemokine Ligand 8

* Differential amount detected in LegendPlex assay. Abbreviations and color code: GO term: Biological Processes (GO:BP): (1) positive regulation of cell migration (padj 8.301×10^{-6}); (2) blood vessel development (padj 3.601×10^{-5}); (3) inflammatory response (padj 3.497×10^{-5}); KEGG pathway: (4) rheumatoid arthritis (padj 1.537×10^{-5}); (5) IL-17 signalling pathway (padj 2.131×10^{-5}); MCL-Clustering (GO:BP): red—positive regulation of cell population proliferation (padj 4.312×10^{-8}) and tube development (padj 1.948×10^{-5}); green—negative regulation of cell differentiation (padj 3.4×10^{-2}); yellow—cholesterol metabolic process (padj 3.1×10^{-6}); blue—unassigned cluster.
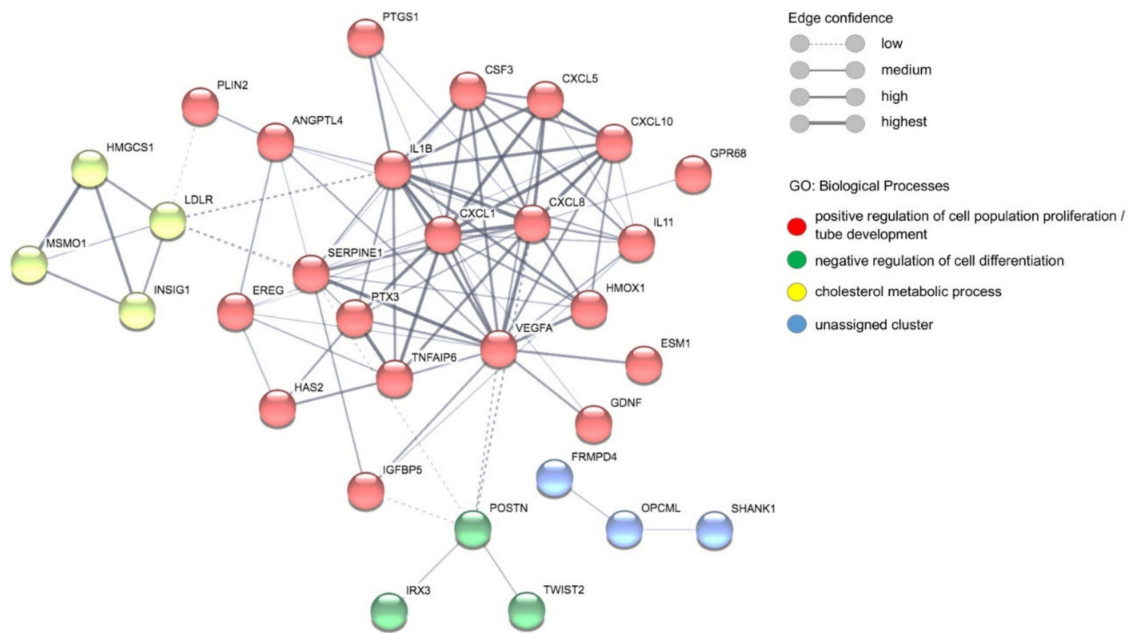
Figure 6. Detection of protein–protein networks through Markov Clustering (MCL) using STRING: functionalprotein association networks [49,50]. Proteins that have not been assigned to a network are not included in the figure. The proteins with a red circle can be assigned to 'positive regulation of cell population proliferation' and 'tube development', proteins with a green circle can be assigned to 'negative regulation of cell differentiation', and proteins with a yellow circle can be assigned to 'cholesterol metabolic process' within the gene ontology terms biological processes (GO:BP). Proteins with a blue circle belong to an unassigned cluster.

4. Discussion

Previously, more than 30 cytokines have been identified whose production is increased due to *P. falciparum* infection and that, as a result, can be detected in higher amounts in plasma of malaria patients compared to healthy controls. For some of them, such as CXCL8 and CXCL10, a correlation with severity of the disease was observed [7,25,30,36,37,51]. Classical immune cells, such as macrophages/monocytes and dendritic cells, are well known for their cytokine production in malaria [22,23,52]. The role of ECs in this context is only fragmentarily understood although they are in constant contact with circulating cytokines and among the first to detect pathogens and they express receptors for pathogen and cytokine recognition (for a review, see [53]). They are the interface between the circulatory system and surrounding tissue, regulating the diapedesis of immune cells (for a review, see [54]) and transporting cytokines from the tissue to the circulatory system [55,56]. Furthermore, they were recently shown to internalize IEs, possibly leading to blood–brain barrier (BBB) breakdown [57]. However, they are also active players in innate and adaptive immune response (for a review, see [54]) and capable of cytokine secretion themselves [58,59]. It is well studied that cytoadhesion of IEs in the capillaries of various organs not only causes blockage of blood flow, which can lead to organ hypoxia and thus organ failure, but also activates ECs. This leads to increased cytokine production, which can induce endothelial dysfunction and thereby contribute to pathogenesis of CM [5–7]. An increase in gene expression induced by cytoadhesion has been demonstrated for a number of cytokine-encoding genes [17–19]. However, it is not only cytoadhesion of IEs that leads to an increase in cytokine production. This could also be demonstrated for *Plasmodium* antigens. It was shown that hemozoin leads to an increased secretion of CXCL8 and CCL5 from the endothelium [60]. Similarly, isolated *P. falciparum* histones stimulate the production of CXCL8 [61].

There is general agreement that EC activation is important in the pathogenesis of complicated forms of malaria. However, different approaches to identify the underlying

mechanisms in EC activation by *P. falciparum* or its metabolites have so far not been able to reach a unified conclusion [62]. One explanation for the divergent results could lie in the tissue-specific variations of the endothelia, which cause different patterns of immune response [63]. However, one should also keep in mind that the immortalised cell lines used, but also the primary endothelial cells, can show different reaction types. In view of the variability in protein expression and chemokine secretion, it is of utmost importance to determine the response of ECs from human brain microvasculature to *P. falciparum* infection if new approaches in the treatment of cerebral malaria are to be pursued.

The aim of the study presented here was to investigate the immunostimulatory potential of plasma samples drawn from *P. falciparum*-infected patients on ECs in absence of adhering IEs. All 27 malaria patients included in the study were adults with symptomatic malaria. However, the severity of infection according to the WHO criteria could only be determined in a subgroup of the samples included in our study (*n* = 17) [64]; for the rest (*n* = 10), the clinical manifestation is unknown. Within these 17 patients, only three patients could be assigned to severe malaria. As a subgroup of three severe malaria patients is too small for statistical analyses with the corresponding corrections for multiple comparisons, it was decided not to distinguish between clinical manifestations in this study.

In plasmas of the 27 travel returnees infected with *P. falciparum* examined in this study, a LEGENDplex assay detected significantly higher concentrations for 9 of the 16 cytokines analysed compared to the corresponding healthy controls, namely, IL-6, IL-1RA, IL-10, IL-11, CCL3, CCL20, CXCL1, CXCL8 and CXCL10. Interestingly, the concentration of CXCL5 in the plasma of malaria patients was below the detected levels in controls. This is consistent with the observation made by a study conducted in Cameroon, which shows decreased serum levels of CXCL5 in *P. falciparum*-infected individuals. The reason for the lower amount of CXCL5 in plasma of malaria patients is not yet clear [35]. A similar observation was made for TNF-a. Again, there was a tendency for greater amounts to be present in the plasmas of the healthy controls compared to the malaria patients, which was nevertheless not significant.

The dysfunction of ECs and the associated development of vascular damage in the brain, resulting in impairment of the BBB, is one of the consequences of a malaria infection. Oggungwan and colleagues demonstrated that sera from malaria patients are able to increase cell permeability in vitro [65]. Increased endothelial permeability associated with malaria has also been shown elsewhere [66–69]. One trigger of endothelial dysfunction may be stimulation by various cytokines. They could be circulating in the blood stream or produced within the surrounding tissues or by the ECs themselves, acting in an autocrine or paracrine manner. ECs can produce pro-inflammatory and anti-inflammatory cytokines and chemokines as well as growth factors in response to various stimuli, including IL-1α, IL-1β, IL-3, IL-5, IL-6, IL-10, IL-11, CXCL8, CXCL10, IL-11 and VEGF ([70]; for a review, see [71]).

After stimulation of ECs with plasma from malaria patients, we could measure an increased amount in the culture supernatants for IL-11, CXCL5, CXCL8, CXCL10, VEGF and ANGPTL4 (only if plasma of malaria patients with a parasitaemia >2.5% were used) compared to stimulation with plasma from healthy individuals. For all other cytokines examined, the prevalence of a malaria infection in the plasma donor led to no significant differences in cytokine secretion by ECs stimulated with the plasma. This is also the case for TNF-α, which was not detectable in the supernatants of endothelial cells stimulated with both plasma from the control and malaria patients. Furthermore, no expression of the TNF-α coding gene could be detected. This is in contrast to the described increased expression of TNF-α after direct interaction of IEs with endothelial cells [17–19].

However, it must be emphasized here that the stimulation experiments were carried out with the immortalised brain endothelial cell line HBEC-5i. Although this exhibits essential features of cerebral ECs, there are also deviations. EC proteins, such as CD51, ICAM-1 and VCAM-1, are presented on the surface, while others, such as CD31, CD36 and CD62E, are absent [72]. In addition, HBEC-5i cells carry chondroitin sulfate A (CSA) as a

dominant molecule on its surface [73]. Nevertheless, HBEC-5i exhibits essential features of cerebral EC, including tight junction structures in particular [72].

CXCL8 binds to CXCR1 and CXCR2, the most important receptor for chemotaxis and mostly expressed on neutrophils. In models of ischemic brain injury, blockage of CXCL8 shows neuroprotective effects and leads to a reduction in infarct volume. In traumatic brain injury, elevated CXCL8 levels in cerebrospinal fluids are connected to BBB damage and increased mortality (for a review, see [74]). Additionally, CXCL8 is involved in angiogenesis. It has been shown that recombinant human CXCL8 can induce EC proliferation and is also involved in capillary tube organization [75,76].

As mentioned above, stimulation with plasma from malaria patients resulted in a significantly increased concentration of CXCL8 in the culture supernatant of ECs. Thus, it can be postulated that plasmodial antigens present in plasma might stimulate this secretion, which has also been described in other studies [60,61].

CXCL5, like CXCL8, is important for neutrophil recruitment and activation. The importance of CXCL5 in malaria pathology is unknown. However, CXCL5 has been described to play a role in ischemia–reperfusion-induced injury in human brain microvascular ECs associated with BBB disruption. CXCL5 has been shown to be upregulated in ischemic stroke and this correlates positively with brain injury. In addition, CXCL5 appears to interfere with brain EC function by regulating the p38 MAP kinase signalling pathway [77]. CXCL5-induced impairment of brain endothelial barrier function has also been demonstrated in other contexts [78]. In rats, pretreatment of ECs with IL-10 inhibited CXCL5-mediated cytokine gene transcription [79]. This is consistent with IL-10 functioning as a crucial anti-inflammatory and protective cytokine in experimental cerebral malaria [80,81]. Elevated plasma concentrations of IL-10 are detected in both mild and cerebral malaria, which is compatible with our findings, but for non-survivors of cerebral malaria a decrease in IL-10 levels was shown [27,82]. An inverted ratio in cytokine concentration between the malaria and control group in plasma and supernatant, as observed in CXCL5 and ANGPTL4, does not constitute a contradiction. Instead, it highlights the need to assess cytokine profiles at the cellular level, if aiming to understand the complex interactions taking place in CM. Brain swelling due to the disruption of the BBB and (cytokine-containing) fluid influx was found to occur in 84% of children dying due to cerebral malaria, but only in 27% of the survivors [83]. However, no correlation between peripheral blood cytokine concentrations and the occurrence of brain swelling in these children could be detected, implying a more local event [84]. Cytokine concentrations measured in peripheral blood represent only the systemic effects and are affected by receptor binding, degradation and excretion. The crucial site of cytokine impact is the cell-surrounding micromilieu [85]. HBECs can secrete cytokines in an apical or basolateral direction (for review [86]). Apically released cytokines would be diluted in the circulating blood, creating a locally acting gradient.

VEGF is a key regulator of physiological angiogenesis. VEGF (i) can promote proliferation and migration of ECs; (ii) serve as a survival factor for ECs; and (iii) is known as a vascular permeability factor, based on its ability to induce vascular leakage [87–91]. VEGF is known to bind to vascular endothelial growth factor receptor 1 (VEGFR-1) (Flt-1) and vascular endothelial growth factor receptor 2 (VEGFR-2) (KDR/FlK-1) on ECs, resulting in a mitogen-activated protein kinase (MAPK) signalling cascade [92]. VEGF seems to play a particularly important role in the repair of brain tissue and wound healing ([93], for a review, see [94]). Increased levels of VEGF can be detected in malaria patients and an increased expression of VEGF was also observed in astrocytes of patients who died of CM [90,95]. However, the role that VEGF plays in CM in particular is still not clear. There is evidence of both a protective and a pathogenic influence for VEGF in the pathology in CM (for a review, see [94]). In our study, VEGF could not be detected in any of the 14 samples examined from the healthy individuals and in the malaria patients VEGF could only be detected in four of the 26 plasma samples analysed. This result contrasts with the findings of Furuta and colleagues mentioned above, where elevated VEGF levels were found in malaria patients compared to patients with febrile illnesses or healthy adults [90]. However,

Armah and colleagues also found no difference in the VEGF levels between Ghanaian children with CM, severe malaria or not infected with *Plasmodium* [25]. One explanation for these divergent results in malaria research in general might lie within genetic differences. *P. falciparum* is the strongest known force of evolutionary selection in the recent history of humankind. Diverse adaptions led to differences in resistance, reactions and susceptibility to plasmodial infections between ethnic groups and individuals (for a review, see [96]). A different picture emerges for the amount of secreted VEGF in the culture supernatants of plasma-stimulated ECs. Here, we could detect significantly ($p = 0.0044$) higher concentrations in the supernatants of ECs stimulated with plasma from malaria patients compared to controls. In vitro studies also show that parasite antigens (crude extract of IEs) can induce VEGF secretion from, in this case, human mast cell lines [90].

An interplay between VEGF and ANGPTL4 has been described in different diseases, such as obesity and diabetic macular oedema [46,47]. As mentioned above, significantly lower amounts of ANGPTL4 can be detected in the plasma of malaria patients compared to the plasma of healthy individuals. This picture is reversed, however, if one considers the amounts of ANPTL4 in the culture supernatants of ECs stimulated with plasma. Here, just as for VEGF, significantly higher concentrations can be detected in the culture supernatants after simulation with plasma from the malaria patients (with a parasitaemia >2.5%) compared to plasma from the healthy individuals. Both VEGF and ANGPTL4 are proangiogenic molecules. Besides angiogenesis, ANGPTL4 is involved in several other processes, such as lipid metabolism, wound healing, inflammation, and redox regulation (for a review, see [97]). For ANGPTL4, but also VEGF, it has been shown that expression is also strongly increased by hypoxia, thereby leading to induction of angiogenesis [98–100].

CXCL10, like VEGF and ANGPTL4, is present in significantly higher concentrations in culture supernatants of ECs stimulated with plasma from malaria patients compared to plasma from healthy individuals. While VEGF and ANGPTL4 have angiogenic and proliferative effects, CXCL10 has angiostatic and anti-proliferative effects [101–103]. The important role of CXCL10 is illustrated in a study by Wilson and colleagues. Here, significantly elevated levels of CXCL10 and CXCL4 were found in patients who had died from CM compared to patients who had survived CM or patients with mild malaria [29]. CXCL10 produced by endothelial cells was shown to play a key role in inducing firm adhesion of T cells and preventing cell detachment from the brain vasculature. The induction of CXCL10 was completely dependent on IFN-γ receptor signalling and played a crucial role in mediating the T-cell–endothelial cell adhesion events that initiate the inflammatory processes that damage the endothelium and promote the development of CM [104]. Bodnar and colleagues showed that incubation of ECs with CXCL10 also significantly reduced tube formation [105].

That the angiogenesis of ECs is strongly influenced by the plasma of malaria patients also becomes clear when looking at the differential gene expression after stimulation of ECs with plasma from malaria patients in comparison to healthy individuals (Table 1). In particular, GO terms such as 'positive regulation of cell migration', 'blood vessel/tube development', 'negative regulation of cell differentiation' and 'inflammatory response' were significantly upregulated in ECs stimulated with patients' plasma in comparison to the controls. Based on these results, it can be postulated that there must be a very delicate balance between these molecules to stimulate proliferation of ECs on the one hand and to limit angiogenesis as well as endothelial dysfunction.

5. Conclusions

Our results clearly show that not only cytoadhesion of IEs can lead to stimulation of ECs, inducing the production of various cytokines, but also the plasma of malaria patients, specifically, the parasite and host molecules contained therein, which trigger these processes and thus cause a different cytokine profile than the plasma of healthy controls. IL-11, CXCL5, CXCL8, CXCL10, VEGF and ANGPTL4 have been secreted in significantly higher amounts. This is consistent with the pre-existing finding that plasma

from malaria patients impairs endothelial barrier integrity in human umbilical vein ECs [65]. We were able to demonstrate the activation of ECs derived from the microvasculature of the human brain and specify their response. However, we did not identify the plasma factors responsible for this effect and thus cannot say whether they are of parasitic or host-specific origin.

Supplementary Materials: The following are available online at https://www.mdpi.com/article/ 10.3390/cells10071656/s1. Table S1—List of plasmas examined, indicating the donor's parasitaemia; Table S2—Number of plasmas analysed from malaria patients and healthy individuals and number of culture supernatants analysed from HBEC-5i cells stimulated with individual plasma samples from malaria patients and healthy individuals. Table S3—Levels of various cytokines determined using a LEGENDplex assay in plasma from malaria patients and control individuals and in culture supernatant of endothelial cells (HBEC-5i) stimulated with these plasmas. Table S4—Levels of TNF-α in plasma from malaria patients and control individuals. Table S5—Adjustment for multiple comparison (cut-offs that are met for the corresponding analyte are shown in bolt). Table S6—Levels of ANGPTL4 in plasma from malaria patients and control individuals and in culture supernatant of endothelial cells (HEBEC-5i) stimulated with these plasmas. Table S7—Levels of cytokines in the plasma of three control individuals (H5, H8, H10) and of four malaria patients (M6, M9, M10, M11), which were used to stimulated endothelial cells (HBEC-5i) for transcriptome analysis. Table S8—Levels of cytokines in the culture supernatant of endothelial cells (HBEC-5i), stimulated with plasma of three control individuals (H5, H8, H10) and of four malaria patients (M6, M9, M10, M11). Table S9—Transcriptome analyses of endothelial cells (HBEC-5i) stimulated with plasma from three healthy control individuals (H5, H10, H8) and from four malaria patients (M6, M9, M10, M11). Table S10—Genes whose expression is significantly decreased after co-incubation of endothelial cells (HBEC-5i) with plasma from malaria patients (M) compared to the healthy controls (H). Table S11—Genes whose expression is significantly increased after co-incubation of endothelial cells (HBEC-5i) with plasma from malaria patients (M) compared to the healthy controls (H).

References

1. WHO. *World Malaria Report 2020*; WHO Team, Global Malaria Programme: Geneva, Switzerland, 2020; ISBN 978-92-4-001579-1.
2. Milner, D.A., Jr.; Lee, J.J.; Frantzreb, C.; Whitten, R.O.; Kamiza, S.; Carr, R.A.; Pradham, A.; Factor, R.E.; Playforth, K.; Liomba, G.; et al. Quantitative assessment of multiorgan sequestration of parasites in fatal pediatric cerebral malaria. *J. Infect. Dis.* **2015**, *212*, 1317–1321. [CrossRef] [PubMed]
3. Milner, D., Jr.; Factor, R.; Whitten, R.; Carr, R.A.; Kamiza, S.; Pinkus, G.; Molyneux, M.; Taylor, T. Pulmonary pathology in pediatric cerebral malaria. *Hum. Pathol.* **2013**, *44*, 2719–2726. [CrossRef] [PubMed]

4.   Taylor, T.E.; Fu, W.J.; Carr, R.A.; Whitten, R.O.; Mueller, J.S.; Fosiko, N.G.; Lewallen, S.; Liomba, N.G.; Molyneux, M.E. Differentiating the pathologies of cerebral malaria by postmortem parasite counts. *Nat. Med.* **2004**, *10*, 143–145. [CrossRef] [PubMed]

5.   Lyke, K.E.; Burges, R.; Cissoko, Y.; Sangare, L.; Dao, M.; Diarra, I.; Kone, A.; Harley, R.; Plowe, C.V.; Doumbo, O.K.; et al. Serum levels of the proinflammatory cytokines interleukin-1 beta (IL-1beta), IL-6, IL-8, IL-10, tumor necrosis factor alpha, and IL-12(p70) in Malian children with severe *Plasmodium falciparum* malaria and matched uncomplicated malaria or healthy controls. *Infect. Immun.* **2004**, *72*, 5630–5637. [CrossRef]

6.   Nishanth, G.; Schluter, D. Blood-brain barrier in cerebral malaria: Pathogenesis and therapeutic intervention. *Trends Parasitol.* **2019**, *35*, 516–528. [CrossRef]

7.   Dunst, J.; Kamena, F.; Matuschewski, K. Cytokines and chemokines in cerebral malaria pathogenesis. *Front. Cell. Infect. Microbiol.* **2017**, *7*, 324. [CrossRef]

8.   Hasday, J.D.; Bannerman, D.; Sakarya, S.; Cross, A.S.; Singh, I.S.; Howard, D.; Drysdale, B.E.; Goldblum, S.E. Exposure to febrile temperature modifies endothelial cell response to tumor necrosis factor-alpha. *J. Appl. Physiol.* **2001**, *90*, 90–98. [CrossRef]

9.   Oakley, M.S.; Gerald, N.; McCutchan, T.F.; Aravind, L.; Kumar, S. Clinical and molecular aspects of malaria fever. *Trends Parasitol.* **2011**, *27*, 442–449. [CrossRef]

10. Oakley, M.S.; Kumar, S.; Anantharaman, V.; Zheng, H.; Mahajan, B.; Haynes, J.D.; Moch, J.K.; Fairhurst, R.; McCutchan, T.F.; Aravind, L. Molecular factors and biochemical pathways induced by febrile temperature in intraerythrocytic *Plasmodium falciparum* parasites. *Infect. Immun.* **2007**, *75*, 2012–2025. [CrossRef]

11. Phillips, M.A.; Burrows, J.N.; Manyando, C.; van Huijsduijnen, R.H.; Van Voorhis, W.C.; Wells, T.N.C. Malaria. *Nat. Rev. Dis. Primers* **2017**, *3*, 17050. [CrossRef]

12. Cunnington, A.J.; Riley, E.M.; Walther, M. Microvascular dysfunction in severe *Plasmodium falciparum* malaria. *J. Infect. Dis.* **2013**, *207*, 369–370. [CrossRef]

13. Gazzinelli, R.T.; Kalantari, P.; Fitzgerald, K.A.; Golenbock, D.T. Innate sensing of malaria parasites. *Nat. Rev. Immunol.* **2014**, *14*, 744–757. [CrossRef]

14. Boivin, M.J.; Bangirana, P.; Byarugaba, J.; Opoka, R.O.; Idro, R.; Jurek, A.M.; John, C.C. Cognitive impairment after cerebral malaria in children: A prospective study. *Pediatrics* **2007**, *119*, e360–e366. [CrossRef]

15. Idro, R.; Marsh, K.; John, C.C.; Newton, C.R. Cerebral malaria: Mechanisms of brain injury and strategies for improved neurocognitive outcome. *Pediatric Res.* **2010**, *68*, 267–274. [CrossRef]

16. Roze, E.; Thiebaut, M.M.; Mazevet, D.; Bricaire, F.; Danis, M.; Deseilligny, C.P.; Caumes, E. Neurologic sequelae after severe falciparum malaria in adult travelers. *Eur. Neurol.* **2001**, *46*, 192–197. [CrossRef]

17. Chakravorty, S.J.; Carret, C.; Nash, G.B.; Ivens, A.; Szestak, T.; Craig, A.G. Altered phenotype and gene transcription in endothelial cells, induced by *Plasmodium falciparum*-infected red blood cells: Pathogenic or protective? *Int. J. Parasitol.* **2007**, *37*, 975–987. [CrossRef] [PubMed]

18. Tripathi, A.K.; Sha, W.; Shulaev, V.; Stins, M.F.; Sullivan, D.J., Jr. *Plasmodium falciparum*-infected erythrocytes induce NF-kappaB regulated inflammatory pathways in human cerebral endothelium. *Blood* **2009**, *114*, 4243–4252. [CrossRef] [PubMed]

19. Viebig, N.K.; Wulbrand, U.; Forster, R.; Andrews, K.T.; Lanzer, M.; Knolle, P.A. Direct activation of human endothelial cells by *Plasmodium falciparum*-infected erythrocytes. *Infect. Immun.* **2005**, *73*, 3271–3277. [CrossRef]

20. Schofield, L.; Hackett, F. Signal transduction in host cells by a glycosylphosphatidylinositol toxin of malaria parasites. *J. Exp. Med.* **1993**, *177*, 145–153. [CrossRef]

21. Zhu, J.; Krishnegowda, G.; Gowda, D.C. Induction of proinflammatory responses in macrophages by the glycosylphosphatidylinositols of *Plasmodium falciparum*: The requirement of extracellular signal-regulated kinase, p38, c-Jun N-terminal kinase and NF-kappaB pathways for the expression of proinflammatory cytokines and nitric oxide. *J. Biol. Chem.* **2005**, *280*, 8617–8627. [CrossRef] [PubMed]

22. Giribaldi, G.; Prato, M.; Ulliers, D.; Gallo, V.; Schwarzer, E.; Akide-Ndunge, O.B.; Valente, E.; Saviozzi, S.; Calogero, R.A.; Arese, P. Involvement of inflammatory chemokines in survival of human monocytes fed with malarial pigment. *Infect. Immun.* **2010**, *78*, 4912–4921. [CrossRef]

23. Jaramillo, M.; Godbout, M.; Olivier, M. Hemozoin induces macrophage chemokine expression through oxidative stress-dependent and -independent mechanisms. *J. Immunol.* **2005**, *174*, 475–484. [CrossRef]

24. Schwarzer, E.; Bellomo, G.; Giribaldi, G.; Ulliers, D.; Arese, P. Phagocytosis of malarial pigment haemozoin by human monocytes: A confocal microscopy study. *Parasitology* **2001**, *123*, 125–131. [CrossRef]

25. Armah, H.B.; Wilson, N.O.; Sarfo, B.Y.; Powell, M.D.; Bond, V.C.; Anderson, W.; Adjei, A.A.; Gyasi, R.K.; Tettey, Y.; Wiredu, E.K.; et al. Cerebrospinal fluid and serum biomarkers of cerebral malaria mortality in Ghanaian children. *Malar. J.* **2007**, *6*, 147. [CrossRef] [PubMed]

26. Dieye, Y.; Mbengue, B.; Dagamajalu, S.; Fall, M.M.; Loke, M.F.; Nguer, C.M.; Thiam, A.; Vadivelu, J.; Dieye, A. Cytokine response during non-cerebral and cerebral malaria: Evidence of a failure to control inflammation as a cause of death in African adults. *PeerJ* **2016**, *4*, e1965. [CrossRef]

27. Jain, V.; Armah, H.B.; Tongren, J.E.; Ned, R.M.; Wilson, N.O.; Crawford, S.; Joel, P.K.; Singh, M.P.; Nagpal, A.C.; Dash, A.P.; et al. Plasma IP-10, apoptotic and angiogenic factors associated with fatal cerebral malaria in India. *Malar. J.* **2008**, *7*, 83. [CrossRef] [PubMed]

28. Herbert, F.; Tchitchek, N.; Bansal, D.; Jacques, J.; Pathak, S.; Becavin, C.; Fesel, C.; Dalko, E.; Cazenave, P.A.; Preda, C.; et al. Evidence of IL-17, IP-10, and IL-10 involvement in multiple-organ dysfunction and IL-17 pathway in acute renal failure associated to *Plasmodium falciparum* malaria. *J. Transl. Med.* **2015**, *13*, 369. [CrossRef]

29. Wilson, N.O.; Jain, V.; Roberts, C.E.; Lucchi, N.; Joel, P.K.; Singh, M.P.; Nagpal, A.C.; Dash, A.P.; Udhayakumar, V.; Singh, N.; et al. CXCL4 and CXCL10 predict risk of fatal cerebral malaria. *Dis. Markers* **2011**, *30*, 39–49. [CrossRef] [PubMed]

30. Berg, A.; Patel, S.; Gonca, M.; David, C.; Otterdal, K.; Ueland, T.; Dalen, I.; Kvaloy, J.T.; Mollnes, T.E.; Aukrust, P.; et al. Cytokine network in adults with falciparum malaria and HIV-1: Increased IL-8 and IP-10 levels are associated with disease severity. *PLoS ONE* **2014**, *9*, e114480. [CrossRef] [PubMed]

31. Prakash, D.; Fesel, C.; Jain, R.; Cazenave, P.A.; Mishra, G.C.; Pied, S. Clusters of cytokines determine malaria severity in *Plasmodium falciparum*-infected patients from endemic areas of Central India. *J. Infect. Dis.* **2006**, *194*, 198–207. [CrossRef]

32. Colborn, J.M.; Ylostalo, J.H.; Koita, O.A.; Cisse, O.H.; Krogstad, D.J. Human gene expression in uncomplicated *Plasmodium falciparum* malaria. *J. Immunol. Res.* **2015**, *2015*, 162639. [CrossRef]

33. Bwanika, R.; Kato, C.D.; Welishe, J.; Mwandah, D.C. Cytokine profiles among patients co-infected with *Plasmodium falciparum* malaria and soil borne helminths attending Kampala International University Teaching Hospital, in Uganda. *Allergy Asthma Clin. Immunol.* **2018**, *14*, 10. [CrossRef]

34. Thuma, P.E.; van Dijk, J.; Bucala, R.; Debebe, Z.; Nekhai, S.; Kuddo, T.; Nouraie, M.; Weiss, G.; Gordeuk, V.R. Distinct clinical and immunologic profiles in severe malarial anemia and cerebral malaria in Zambia. *J. Infect. Dis.* **2011**, *203*, 211–219. [CrossRef]

35. Che, J.N.; Nmorsi, O.P.; Nkot, B.P.; Isaac, C.; Okonkwo, B.C. Chemokines responses to *Plasmodium falciparum* malaria and co-infections among rural Cameroonians. *Parasitol. Int.* **2015**, *64*, 139–144. [CrossRef]

36. Ayimba, E.; Hegewald, J.; Segbena, A.Y.; Gantin, R.G.; Lechner, C.J.; Agosssou, A.; Banla, M.; Soboslay, P.T. Proinflammatory and regulatory cytokines and chemokines in infants with uncomplicated and severe *Plasmodium falciparum* malaria. *Clin. Exp. Immunol.* **2011**, *166*, 218–226. [CrossRef] [PubMed]

37. Burgmann, H.; Hollenstein, U.; Wenisch, C.; Thalhammer, F.; Looareesuwan, S.; Graninger, W. Serum concentrations of MIP-1 alpha and interleukin-8 in patients suffering from acute *Plasmodium falciparum* malaria. *Clin. Immunol. Immunopathol.* **1995**, *76*, 32–36. [CrossRef] [PubMed]

38. Otterdal, K.; Berg, A.; Michelsen, A.E.; Patel, S.; Gregersen, I.; Sagen, E.L.; Halvorsen, B.; Yndestad, A.; Ueland, T.; Langeland, N.; et al. Plasma levels of interleukin 27 in falciparum malaria is increased independently of co-infection with HIV: Potential immune-regulatory role during malaria. *BMC Infect. Dis.* **2020**, *20*, 65. [CrossRef]

39. John, C.C.; Panoskaltsis-Mortari, A.; Opoka, R.O.; Park, G.S.; Orchard, P.J.; Jurek, A.M.; Idro, R.; Byarugaba, J.; Boivin, M.J. Cerebrospinal fluid cytokine levels and cognitive impairment in cerebral malaria. *Am. J. Trop. Med. Hyg.* **2008**, *78*, 198–205. [CrossRef] [PubMed]

40. John, C.C.; Park, G.S.; Sam-Agudu, N.; Opoka, R.O.; Boivin, M.J. Elevated serum levels of IL-1ra in children with *Plasmodium falciparum* malaria are associated with increased severity of disease. *Cytokine* **2008**, *41*, 204–208. [CrossRef] [PubMed]

41. Benjamini, Y.; Hochberg, Y. Controlling the false discovery rate—A practical and powerful approach to multiple testing. *J. R. Stat. Soc. Ser. B Stat. Methodol.* **1995**, *57*, 289–300. [CrossRef]

42. Bolger, A.M.; Lohse, M.; Usadel, B. Trimmomatic: A flexible trimmer for Illumina sequence data. *Bioinformatics* **2014**, *30*, 2114–2120. [CrossRef]

43. Li, B.; Dewey, C.N. RSEM: Accurate transcript quantification from RNA-Seq data with or without a reference genome. *BMC Bioinform.* **2011**, *12*, 323. [CrossRef]

44. Langmead, B.; Salzberg, S.L. Fast gapped-read alignment with Bowtie 2. *Nat. Methods* **2012**, *9*, 357–359. [CrossRef] [PubMed]

45. Love, M.I.; Huber, W.; Anders, S. Moderated estimation of fold change and dispersion for RNA-seq data with DESeq2. *Genome Biol.* **2014**, *15*, 550. [CrossRef] [PubMed]

46. Sodhi, A.; Ma, T.; Menon, D.; Deshpande, M.; Jee, K.; Dinabandhu, A.; Vancel, J.; Lu, D.; Montaner, S. Angiopoietin-like 4 binds neuropilins and cooperates with VEGF to induce diabetic macular edema. *J. Clin. Investig.* **2019**, *129*, 4593–4608. [CrossRef]

47. Gealekman, O.; Burkart, A.; Chouinard, M.; Nicoloro, S.M.; Straubhaar, J.; Corvera, S. Enhanced angiogenesis in obesity and in response to PPARgamma activators through adipocyte VEGF and ANGPTL4 production. *Am. J. Physiol. Endocrinol. Metab.* **2008**, *295*, E1056–E1064. [CrossRef] [PubMed]

48. Raudvere, U.; Kolberg, L.; Kuzmin, I.; Arak, T.; Adler, P.; Peterson, H.; Vilo, J. g:Profiler: A web server for functional enrichment analysis and conversions of gene lists (2019 update). *Nucleic Acids Res.* **2019**, *47*, W191–W198. [CrossRef]

49. Szklarczyk, D.; Gable, A.L.; Lyon, D.; Junge, A.; Wyder, S.; Huerta-Cepas, J.; Simonovic, M.; Doncheva, N.T.; Morris, J.H.; Bork, P.; et al. STRING v11: Protein-protein association networks with increased coverage, supporting functional discovery in genome-wide experimental datasets. *Nucleic Acids Res.* **2019**, *47*, D607–D613. [CrossRef] [PubMed]

50. Snel, B.; Lehmann, G.; Bork, P.; Huynen, M.A. STRING: A web-server to retrieve and display the repeatedly occurring neighbourhood of a gene. *Nucleic Acids Res.* **2000**, *28*, 3442–3444. [CrossRef]

51. Ioannidis, L.J.; Nie, C.Q.; Hansen, D.S. The role of chemokines in severe malaria: More than meets the eye. *Parasitology* **2014**, *141*, 602–613. [CrossRef]

52. Wu, X.; Gowda, N.M.; Kumar, S.; Gowda, D.C. Protein-DNA complex is the exclusive malaria parasite component that activates dendritic cells and triggers innate immune responses. *J. Immunol.* **2010**, *184*, 4338–4348. [CrossRef]

53. Opitz, B.; Hippenstiel, S.; Eitel, J.; Suttorp, N. Extra- and intracellular innate immune recognition in endothelial cells. *Thromb. Haemost.* **2007**, *98*, 319–326. [CrossRef]

54. Nourshargh, S.; Alon, R. Leukocyte migration into inflamed tissues. *Immunity* **2014**, *41*, 694–707. [CrossRef]

55. Middleton, J.; Patterson, A.M.; Gardner, L.; Schmutz, C.; Ashton, B.A. Leukocyte extravasation: Chemokine transport and presentation by the endothelium. *Blood* **2002**, *100*, 3853–3860. [CrossRef]

56. Mordelet, E.; Davies, H.A.; Hillyer, P.; Romero, I.A.; Male, D. Chemokine transport across human vascular endothelial cells. *Endothelium* **2007**, *14*, 7–15. [CrossRef] [PubMed]

57. Adams, Y.; Olsen, R.W.; Bengtsson, A.; Dalgaard, N.; Zdioruk, M.; Satpathi, S.; Behera, P.K.; Sahu, P.K.; Lawler, S.E.; Qvortrup, K.; et al. *Plasmodium falciparum* erythrocyte membrane protein 1 variants induce cell swelling and disrupt the blood-brain barrier in cerebral malaria. *J. Exp. Med.* **2021**, *218*. [CrossRef]

58. Nilsen, E.M.; Johansen, F.E.; Jahnsen, F.L.; Lundin, K.E.; Scholz, T.; Brandtzaeg, P.; Haraldsen, G. Cytokine profiles of cultured microvascular endothelial cells from the human intestine. *Gut* **1998**, *42*, 635–642. [CrossRef]

59. Briones, M.A.; Phillips, D.J.; Renshaw, M.A.; Hooper, W.C. Expression of chemokine by human coronary-artery and umbilical-vein endothelial cells and its regulation by inflammatory cytokines. *Coron. Artery Dis.* **2001**, *12*, 179–186. [CrossRef] [PubMed]

60. Basilico, N.; Corbett, Y.; D'Alessandro, S.; Parapini, S.; Prato, M.; Girelli, D.; Misiano, P.; Olliaro, P.; Taramelli, D. Malaria pigment stimulates chemokine production by human microvascular endothelium. *Acta Trop.* **2017**, *172*, 125–131. [CrossRef] [PubMed]

61. Gillrie, M.R.; Lee, K.; Gowda, D.C.; Davis, S.P.; Monestier, M.; Cui, L.; Hien, T.T.; Day, N.P.J.; Ho, M. *Plasmodium falciparum* histones induce endothelial proinflammatory response and barrier dysfunction. *Am. J. Pathol.* **2012**, *180*, 1028–1039. [CrossRef]

62. Chakravorty, S.J.; Hughes, K.R.; Craig, A.G. Host response to cytoadherence in *Plasmodium falciparum*. *Biochem. Soc. Trans.* **2008**, *36*, 221–228. [CrossRef] [PubMed]

63. Hillyer, P.; Mordelet, E.; Flynn, G.; Male, D. Chemokines, chemokine receptors and adhesion molecules on different human endothelia: Discriminating the tissue-specific functions that affect leucocyte migration. *Clin. Exp. Immunol.* **2003**, *134*, 431–441. [CrossRef]

64. Wichers, J.S.; Tonkin-Hill, G.; Thye, T.; Krumkamp, R.; Kreuels, B.; Strauss, J.; von Thien, H.; Scholz, J.A.; Smedegaard Hansson, H.; Weisel Jensen, R.; et al. Common virulence gene expression in adult first-time infected malaria patients and severe cases. *Elife* **2021**, *10*. [CrossRef]

65. Oggungwan, K.; Glaharn, S.; Ampawong, S.; Krudsood, S.; Viriyavejakul, P. FTY720 restores endothelial cell permeability induced by malaria sera. *Sci. Rep.* **2018**, *8*, 10959. [CrossRef]

66. Tripathi, A.K.; Sullivan, D.J.; Stins, M.F. *Plasmodium falciparum*-infected erythrocytes increase intercellular adhesion molecule 1 expression on brain endothelium through NF-kappaB. *Infect. Immun.* **2006**, *74*, 3262–3270. [CrossRef]

67. Mohan, A.; Sharma, S.K.; Bollineni, S. Acute lung injury and acute respiratory distress syndrome in malaria. *J. Vector Borne Dis.* **2008**, *45*, 179–193. [PubMed]

68. Pal, P.; Daniels, B.P.; Oskman, A.; Diamond, M.S.; Klein, R.S.; Goldberg, D.E. *Plasmodium falciparum* histidine-rich protein II compromises brain endothelial barriers and may promote cerebral malaria pathogenesis. *mBio* **2016**, *7*. [CrossRef]

69. Gallego-Delgado, J.; Basu-Roy, U.; Ty, M.; Alique, M.; Fernandez-Arias, C.; Movila, A.; Gomes, P.; Weinstock, A.; Xu, W.; Edagha, I.; et al. Angiotensin receptors and beta-catenin regulate brain endothelial integrity in malaria. *J. Clin. Investig.* **2016**, *126*, 4016–4029. [CrossRef] [PubMed]

70. Luster, A.D.; Unkeless, J.C.; Ravetch, J.V. Gamma-interferon transcriptionally regulates an early-response gene containing homology to platelet proteins. *Nature* **1985**, *315*, 672–676. [CrossRef] [PubMed]

71. Mai, J.; Virtue, A.; Shen, J.; Wang, H.; Yang, X.F. An evolving new paradigm: Endothelial cells—Conditional innate immune cells. *J. Hematol. Oncol.* **2013**, *6*, 61. [CrossRef]

72. Wassmer, S.C.; Combes, V.; Candal, F.J.; Juhan-Vague, I.; Grau, G.E. Platelets potentiate brain endothelial alterations induced by *Plasmodium falciparum*. *Infect. Immun.* **2006**, *74*, 645–653. [CrossRef]

73. Dorpinghaus, M.; Furstenwerth, F.; Roth, L.K.; Bouws, P.; Rakotonirinalalao, M.; Jordan, V.; Sauer, M.; Rehn, T.; Pansegrau, E.; Hohn, K.; et al. Stringent selection of knobby *Plasmodium falciparum*-infected erythrocytes during cytoadhesion at febrile temperature. *Microorganisms* **2020**, *8*, 174. [CrossRef] [PubMed]

74. Semple, B.D.; Kossmann, T.; Morganti-Kossmann, M.C. Role of chemokines in CNS health and pathology: A focus on the CCL2/CCR2 and CXCL8/CXCR2 networks. *J. Cereb. Blood Flow Metab.* **2010**, *30*, 459–473. [CrossRef]

75. Li, A.; Dubey, S.; Varney, M.L.; Dave, B.J.; Singh, R.K. IL-8 directly enhanced endothelial cell survival, proliferation, and matrix metalloproteinases production and regulated angiogenesis. *J. Immunol.* **2003**, *170*, 3369–3376. [CrossRef]

76. Heidemann, J.; Ogawa, H.; Dwinell, M.B.; Rafiee, P.; Maaser, C.; Gockel, H.R.; Otterson, M.F.; Ota, D.M.; Lugering, N.; Domschke, W.; et al. Angiogenic effects of interleukin 8 (CXCL8) in human intestinal microvascular endothelial cells are mediated by CXCR2. *J. Biol. Chem.* **2003**, *278*, 8508–8515. [CrossRef]

77. Yu, M.; Ma, X.; Jiang, D.; Wang, L.; Zhan, Q.; Zhao, J. CXC chemokine ligand 5 (CXCL5) disrupted the permeability of human brain microvascular endothelial cells via regulating p38 signal. *Microbiol. Immunol.* **2021**, *65*, 40–47. [CrossRef] [PubMed]

78. Haarmann, A.; Schuhmann, M.K.; Silwedel, C.; Monoranu, C.M.; Stoll, G.; Buttmann, M. Human brain endothelial CXCR2 is inflammation-inducible and mediates CXCL5- and CXCL8-triggered paraendothelial barrier breakdown. *Int. J. Mol. Sci.* **2019**, *20*, 602. [CrossRef]

79. Chandrasekar, B.; Melby, P.C.; Sarau, H.M.; Raveendran, M.; Perla, R.P.; Marelli-Berg, F.M.; Dulin, N.O.; Singh, I.S. Chemokine-cytokine cross-talk. The ELR+ CXC chemokine LIX (CXCL5) amplifies a proinflammatory cytokine response via a phosphatidyli-nositol 3-kinase-NF-kappa B pathway. *J. Biol. Chem.* **2003**, *278*, 4675–4686. [CrossRef]

80. Kossodo, S.; Monso, C.; Juillard, P.; Velu, T.; Goldman, M.; Grau, G.E. Interleukin-10 modulates susceptibility in experimental cerebral malaria. *Immunology* **1997**, *91*, 536–540. [CrossRef]

81. Sanni, L.A.; Jarra, W.; Li, C.; Langhorne, J. Cerebral edema and cerebral hemorrhages in interleukin-10-deficient mice infected with *Plasmodium chabaudi*. *Infect. Immun.* **2004**, *72*, 3054–3058. [CrossRef] [PubMed]

82. Mandala, W.L.; Msefula, C.L.; Gondwe, E.N.; Drayson, M.T.; Molyneux, M.E.; MacLennan, C.A. Cytokine profiles in Malawian children presenting with uncomplicated malaria, severe malarial anemia, and cerebral malaria. *Clin. Vaccine Immunol.* **2017**, *24*. [CrossRef]

83. Seydel, K.B.; Kampondeni, S.D.; Valim, C.; Potchen, M.J.; Milner, D.A.; Muwalo, F.W.; Birbeck, G.L.; Bradley, W.G.; Fox, L.L.; Glover, S.J.; et al. Brain swelling and death in children with cerebral malaria. *N. Engl. J. Med.* **2015**, *372*, 1126–1137. [CrossRef] [PubMed]

84. Harawa, V.; Njie, M.; Kessler, A.; Choko, A.; Kumwenda, B.; Kampondeni, S.; Potchen, M.; Kim, K.; Jaworowski, A.; Taylor, T.; et al. Brain swelling is independent of peripheral plasma cytokine levels in Malawian children with cerebral malaria. *Malar. J.* **2018**, *17*, 435. [CrossRef]

85. Jason, J.; Archibald, L.K.; Nwanyanwu, O.C.; Byrd, M.G.; Kazembe, P.N.; Dobbie, H.; Jarvis, W.R. Comparison of serum and cell-specific cytokines in humans. *Clin. Diagn. Lab. Immunol.* **2001**, *8*, 1097–1103. [CrossRef]

86. Worzfeld, T.; Schwaninger, M. Apicobasal polarity of brain endothelial cells. *J. Cereb. Blood Flow Metab.* **2016**, *36*, 340–362. [CrossRef]

87. Ferrara, N.; Chen, H.; Davis-Smyth, T.; Gerber, H.P.; Nguyen, T.N.; Peers, D.; Chisholm, V.; Hillan, K.J.; Schwall, R.H. Vascular endothelial growth factor is essential for corpus luteum angiogenesis. *Nat. Med.* **1998**, *4*, 336–340. [CrossRef] [PubMed]

88. Gerber, H.P.; Dixit, V.; Ferrara, N. Vascular endothelial growth factor induces expression of the antiapoptotic proteins Bcl-2 and A1 in vascular endothelial cells. *J. Biol. Chem.* **1998**, *273*, 13313–13316. [CrossRef]

89. Yuan, F.; Chen, Y.; Dellian, M.; Safabakhsh, N.; Ferrara, N.; Jain, R.K. Time-dependent vascular regression and permeability changes in established human tumor xenografts induced by an anti-vascular endothelial growth factor/vascular permeability factor antibody. *Proc. Natl. Acad. Sci. USA* **1996**, *93*, 14765–14770. [CrossRef] [PubMed]

90. Furuta, T.; Kimura, M.; Watanabe, N. Elevated levels of vascular endothelial growth factor (VEGF) and soluble vascular endothelial growth factor receptor (VEGFR)-2 in human malaria. *Am. J. Trop. Med. Hyg.* **2010**, *82*, 136–139. [CrossRef]

91. Leung, D.W.; Cachianes, G.; Kuang, W.J.; Goeddel, D.V.; Ferrara, N. Vascular endothelial growth factor is a secreted angiogenic mitogen. *Science* **1989**, *246*, 1306–1309. [CrossRef] [PubMed]

92. Azzouz, M.; Ralph, G.S.; Storkebaum, E.; Walmsley, L.E.; Mitrophanous, K.A.; Kingsman, S.M.; Carmeliet, P.; Mazarakis, N.D. VEGF delivery with retrogradely transported lentivector prolongs survival in a mouse ALS model. *Nature* **2004**, *429*, 413–417. [CrossRef] [PubMed]

93. Krum, J.M.; Khaibullina, A. Inhibition of endogenous VEGF impedes revascularization and astroglial proliferation: Roles for VEGF in brain repair. *Exp. Neurol.* **2003**, *181*, 241–257. [CrossRef]

94. Canavese, M.; Spaccapelo, R. Protective or pathogenic effects of vascular endothelial growth factor (VEGF) as potential biomarker in cerebral malaria. *Pathog. Glob. Health* **2014**, *108*, 67–75. [CrossRef] [PubMed]

95. Deininger, M.H.; Winkler, S.; Kremsner, P.G.; Meyermann, R.; Schluesener, H.J. Angiogenic proteins in brains of patients who died with cerebral malaria. *J. Neuroimmunol.* **2003**, *142*, 101–111. [CrossRef]

96. Kwiatkowski, D.P. How malaria has affected the human genome and what human genetics can teach us about malaria. *Am. J. Hum. Genet.* **2005**, *77*, 171–192. [CrossRef]

97. La Paglia, L.; Listi, A.; Caruso, S.; Amodeo, V.; Passiglia, F.; Bazan, V.; Fanale, D. Potential role of ANGPTL4 in the cross talk between metabolism and cancer through PPAR signaling pathway. *PPAR Res.* **2017**, *2017*, 8187235. [CrossRef] [PubMed]

98. Le Jan, S.; Amy, C.; Cazes, A.; Monnot, C.; Lamande, N.; Favier, J.; Philippe, J.; Sibony, M.; Gasc, J.M.; Corvol, P.; et al. Angiopoietin-like 4 is a proangiogenic factor produced during ischemia and in conventional renal cell carcinoma. *Am. J. Pathol.* **2003**, *162*, 1521–1528. [CrossRef]

99. Liu, Y.; Cox, S.R.; Morita, T.; Kourembanas, S. Hypoxia regulates vascular endothelial growth factor gene expression in endothelial cells. Identification of a 5' enhancer. *Circ. Res.* **1995**, *77*, 638–643. [CrossRef] [PubMed]

100. Park, M.K.; Ko, E.J.; Jeon, K.Y.; Kim, H.; Jo, J.O.; Baek, K.W.; Kang, Y.J.; Choi, Y.H.; Hong, Y.; Ock, M.S.; et al. Induction of angiogenesis by malarial infection through hypoxia dependent manner. *Korean J. Parasitol.* **2019**, *57*, 117–125. [CrossRef]

101. Angiolillo, A.L.; Sgadari, C.; Taub, D.D.; Liao, F.; Farber, J.M.; Maheshwari, S.; Kleinman, H.K.; Reaman, G.H.; Tosato, G. Human interferon-inducible protein 10 is a potent inhibitor of angiogenesis in vivo. *J. Exp. Med.* **1995**, *182*, 155–162. [CrossRef] [PubMed]

102. Strieter, R.M.; Kunkel, S.L.; Arenberg, D.A.; Burdick, M.D.; Polverini, P.J. Interferon gamma-inducible protein 10 (IP-10), a member of the C-X-C chemokine family, is an inhibitor of angiogenesis. *Biochem. Biophys. Res. Commun.* **1995**, *210*, 51–57. [CrossRef]

103. Campanella, G.S.; Colvin, R.A.; Luster, A.D. CXCL10 can inhibit endothelial cell proliferation independently of CXCR3. *PLoS ONE* **2010**, *5*, e12700. [CrossRef] [PubMed]

104. Sorensen, E.W.; Lian, J.; Ozga, A.J.; Miyabe, Y.; Ji, S.W.; Bromley, S.K.; Mempel, T.R.; Luster, A.D. CXCL10 stabilizes T cell-brain endothelial cell adhesion leading to the induction of cerebral malaria. *JCI Insight* **2018**, *3*. [CrossRef] [PubMed]

105. Bodnar, R.J.; Yates, C.C.; Wells, A. IP-10 blocks vascular endothelial growth factor-induced endothelial cell motility and tube formation via inhibition of calpain. *Circ. Res.* **2006**, *98*, 617–625. [CrossRef] [PubMed]

3. Chapter II: Effect of *Plasmodium falciparum* cytoadhesion stimulation signal on human brain microvascular endothelial cells.

This chapter includes all the unpublished data. The material and method used in this chapter are attached in the supplement section.

3.1 Enrichment of *P. falciparum* over resting HBMEC:

In order to harvest the parasite population with high binding property to HBMECs, we started with the lab adapted *P. falciparum* IT4 isolate. Highly synchronized trophozoites were coincubated with HBMECs for 90 min at 37°C and 5% CO_2. Afterwards, unbound parasites that were floating in the media were removed by careful washing and attached parasites were kept in culture. Pictures were taken to record the binding behavior (Figure 1, A-D). The next day, selected trophozoites developed into rings were harvested and cultured as normal. When the parasitemia reached 5%, next rounds of enrichment were performed till a stronger binding pattern was observed. For the enrichment of IT4 over resting HBMEC, a relatively strong binding was observed on 7th round of enrichment.
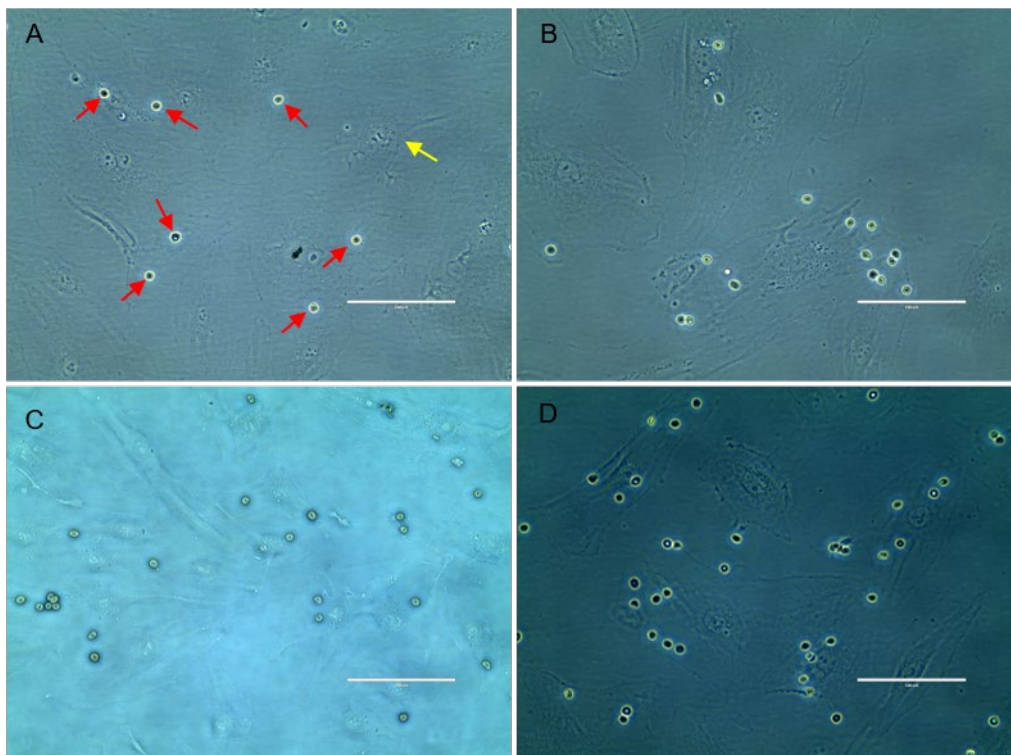
Figure 1: Enrichment of IT4 over resting HBMECs. Synchronized trophozoites were co-incubated with HBMECs for 90 mins and unbound iRBCs were washed later on. Pictures were taken after washing steps with EVOS XL inverted microscope at a 400 × magnification. The number of attached iRBCs were observed. A stronger binding behavior was obtained in the 4th round of enrichment (**A**). Adherent iRBCs were observed as in the 5th (**B**), 6th (**C**) and 7th (**D**) rounds of enrichment, respectively. Yellow arrow indicates HBMECs and red arrows indicate the attached iRBCs after washing. Scale bars = 100 μm.

3.2 Gene expression profiles of initial IT4 population and IT4 enriched over resting HBMECs:

To investigate the *Pf*EMP1s that responsible for binding to resting HBMECs on the enriched IT4 population, the transcriptomes of three independent initial IT4 cultures and seven enriched IT4 were analyzed by NGS. The normalized expression level of *Pf*EMP1-encoding *var* genes were calculated (Figure 2, A). Transcriptomic analysis of initial IT4 revealed that a wide range of *var* genes are expressed with IT4_var66 being the most dominant population which accounts for 79.26% of the total expression. The rest proportion encompassed IT4_var23 (2.73%), IT4_var65 (1.91%), IT4_var59 (1.74%), IT4_var13 (1.17%) as well as the other kinds of *var* genes with minimal expression levels (Figure 2, B). However, after the enrichment over resting HBMECs, the whole *var* profile switched remarkably. In the enriched IT4 culture, IT4_var23 represented 25.51% of the total expression and replaced IT4_var66 (25.10%) as the most abundant population. The expression level of IT4_var62 increased significantly and accounted for 17.75% in the enriched culture compared to the expression level in initial culture, which only constituted a percentage of 0.52% (Figure 2, C). The percentage of IT4_var13 also increased from 1.17% in the initial culture up to 2.57% after enrichment, although the normalized expression level showed a downregulation (Figure 2, A-C). In addition, we investigated the predicted extracellular domain structure of *Pf*EMP1s encoded by highly expressed IT4_var66, IT4_var62, IT4_var23, and IT4_var13. Most of these genes belong to group B and group C, which are considered low-virulent. However, one exception is the *Pf*EMP1 encoded by IT4_var13, which contains a DBLβ domain responsible for binding to ICAM-1 (Figure 2, D).
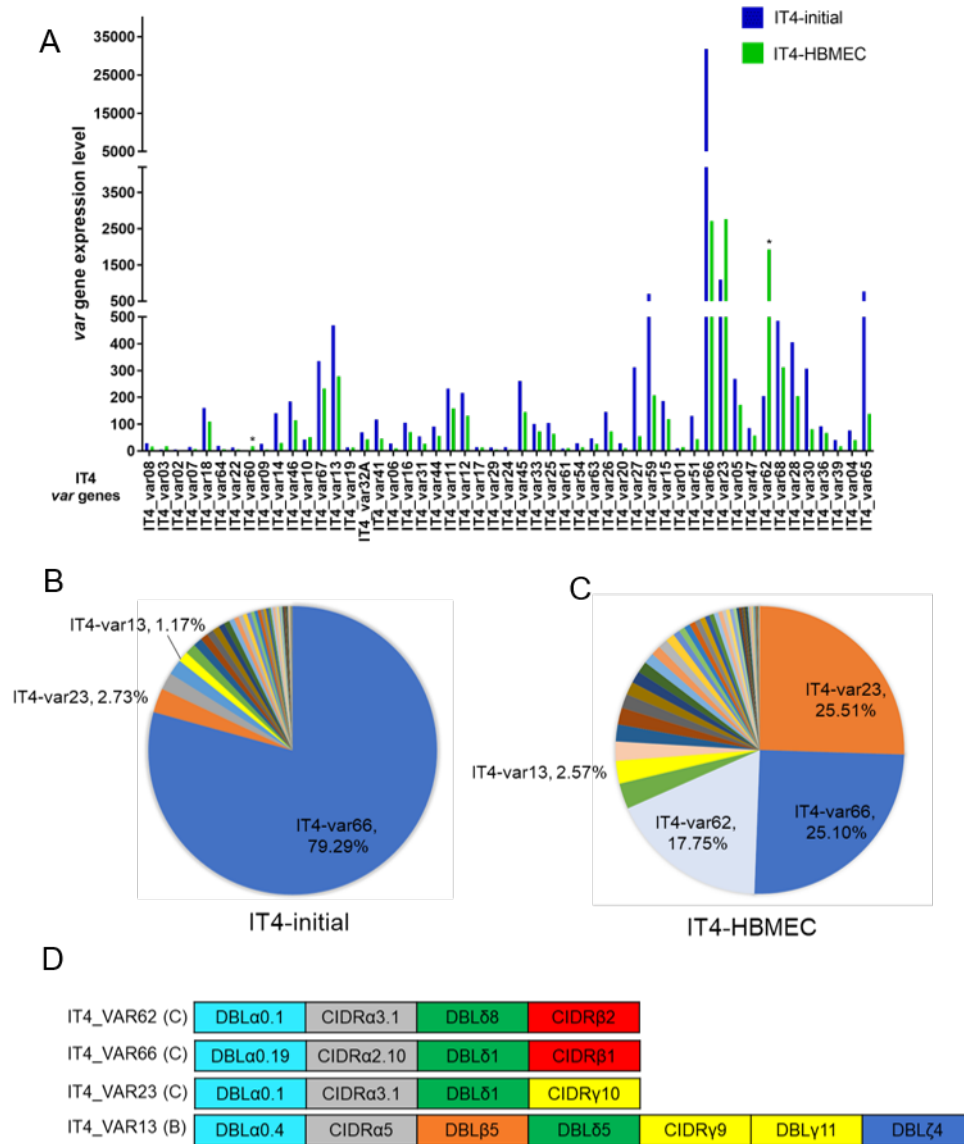
Figure 2: Gene expression profiles of initial IT4 population and IT4 enriched over resting HBMECs. (**A**) The expression level of an array of *var* genes in IT4 enriched on resting HBMECs (IT4-HBMEC) in comparison with the initial IT4 culture (IT4-initial). The expression level is calculated as average of the normalized read counts. Significantly upregulated *var* genes in IT4-HBMEC are marked by black stars (adjusted *p*-value (padj) < 0.05). (**B**) Fraction of *var* gene in IT4-initial culture. (**C**) Fraction of *var* genes in IT4-HBMEC culture. (**D**) Schematic representation of the extracellular structure of *Pf*EMP1 proteins encoded by IT4_var62, IT4_var66, IT4_var23 and IT4_var13.

3.3   Enrichment of *P. falciparum* over TNF-α-activated HBMECs:

It took seven rounds to obtain a relatively stable binding capacity when the initial IT4 was enriched over resting HBMECs, and transcriptomic data revealed only parasites expressing low-virulent *Pf*EMP1 proteins were harvested after enrichment. Therefore, in order to accomplish an immense binding phenotype and collect parasites expressing high-virulent *Pf*EMP1, TNF-α was used to activate HBMECs by expressing adhesion receptors on the surface. TNF-α (10 ng/ml) were added into HBMEC culture 24 hours before the enrichment procedure. On the following day, the same process was carried out as in the previous steps for enriching initial IT4 over resting HBMECs. Remarkably, a clear binding picture was obtained just in the first time of enrichment over TNF-α-activated HBMECs. The 3rd panning exhibited an immense number of iRBCs attached to TNF-α-activated HBMECs (Figure 3, A-C).
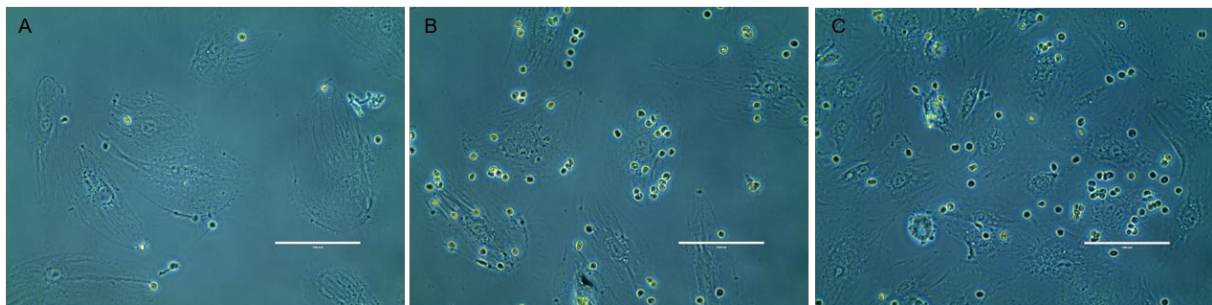
Figure 3: Enrichment of IT4 over TNF-α-activated HBMEC. HBMECs were treated with TNF-α (10 ng/ml) 24 hours prior to the assay. Trophozoites from initial IT4 population were co-cultured with HBMECs for 90 mins. Floating iRBCs were discarded by thorough washing and pictures were captured with EVOS XL inverted microscope at a 400 × magnification. An evident binding was achieved after first time of enrichment (**A**). The number of bound iRBCs increased dramatically as in the 2nd (**B**) and 3rd (**C**) times of enrichment. Scale bars = 100 μm.

3.4   Gene expression profiles of IT4 enriched over TNF-α-activated HBMECs:

In order to unravel the *Pf*EMP1 proteins responsible for binding to TNF-α-activated HBMECs, *var* gene profiles were compared between the initial IT4 culture and IT4 enriched over TNF-α-activated HBMECs (Figure 4, A). Of note, the expression level of IT4-var19 increased

33

significantly in IT4 enriched over TNF-α-activated HBMECs compared to initial culture. Group B/A IT4-var19 only represented 0.12% in the initial IT4 culture but spiked to 8.58% after the enrichment over TNF-α-activated HBMECs. Another upregulated *var* gene is IT4_var13 which increased from 1.17% in the initial culture up to 2.57% after enrichment over TNF-α-activated HBMECs. Moreover, IT4_var66 was still the overwhelmingly superior in both initial IT4 and the IT4 enriched over TNF-α-activated HBMECs (Figure 4, B). In addition, the *Pf*EMP1 variant encoded by IT4-var19 contains a functional Domain Cassette 8 (DBLα2-CIDRα1.1-DBLβ12-DBLγ4/6) structure in the extracellular part (Figure 4, C).
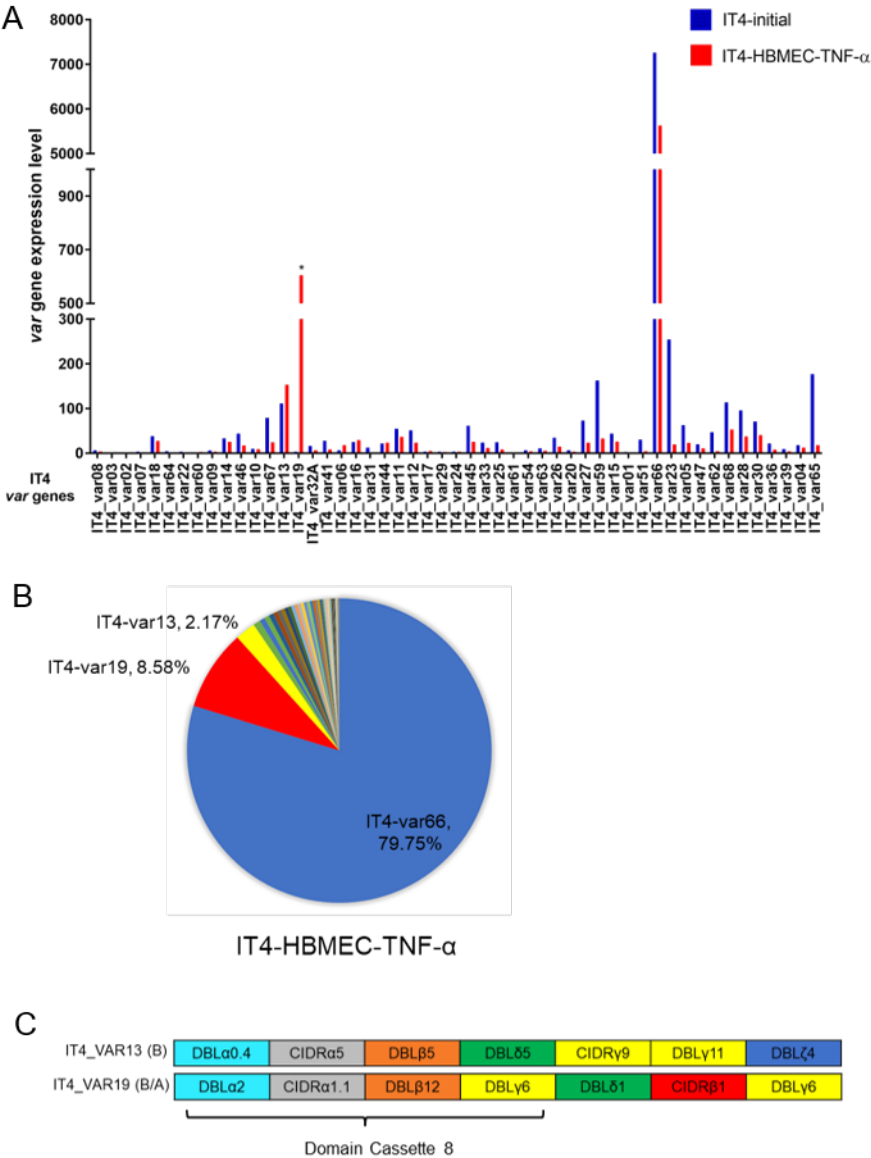
Figure 4: Gene expression profiles of IT4 enriched over TNF-α-activated HBMECs. (A) The *var* gene expression levels of IT4 enriched over TNF-α-activated HBMECs (IT4-HBMEC-TNF-α) were compared to the initial IT4 culture (IT4-initial). Significantly upregulated *var* genes in IT4-HBMEC are marked by black stars (adjusted *p*-

value (padj) < 0.05). (**B**) Fraction of *var* gene in IT4--HBMEC-TNF-α culture. (**C**) Schematic representation of the extracellular structure of *Pf*EMP1 proteins encoded by IT4_var13 and IT4_var19. A typical domain cassette 8 structure is present in the extracellular part of IT4_var19.

3.5 Surface receptors on resting HBMECs and TNF-α-activated HBMECs:

To further identify the surface receptors that are involved in cytoadhesion, the surface localization of intercellular adhesion molecule 1 (ICAM-1) and endothelial protein C receptor (EPCR), which play vital roles in cerebral malaria, were detected by flow cytometry. Resting HBMECs treated without any antibody were designed as negative control and located in Quarter 4 (Figure 5 A). After treated with anti-ICAM-1 or anti-EPCR, 72.08% and 99.92% resting HBMECs shifted to the positive Quarter 2 and 3, indicating the massive presence of ICAM-1 and EPCR on HBMECs surface (Figure 5 B, C). However, TNF-α-activated HBMECs exhibited 99.96% positivity for ICAM-1 and 99.93% positivity for EPCR (Figure 5 D, E, F). In order to better understand the receptor expression level induced by TNF-α, normalized median fluorescence intensity (nMFI) was calculated as dividing the MFI of antibody-stained cells by the MFI of unstained cells (Figure 5 G). The ICAM-1 positivity of resting HBMECs increased from 72.08% to 99.96% after TNF-α stimulation and ICAM-1 expression level upregulated significantly with a fold change of 140. Almost all resting HBMECs and TNF-α-activated HBMECs expressed EPCR on the surface. Of note, nMFI comparison indicated that a significant down-regulation of EPCR expression level was observed with a fold change of 2.78 after TNF-α stimulation (Figure 5 H).
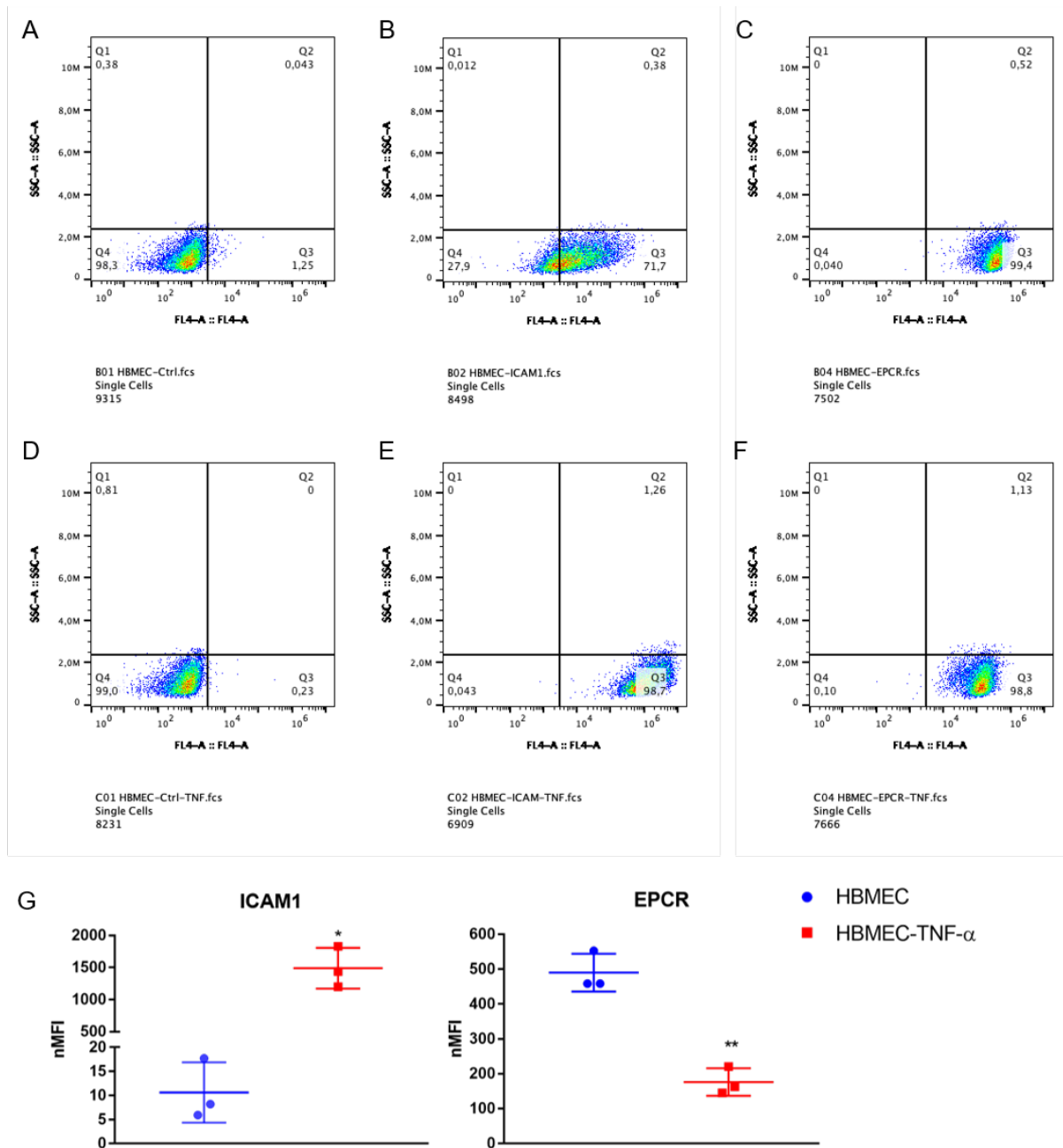
Figure 5: Detection of surface receptor expression by flow cytometry. (**A**) Unstained resting HBMECs were used as negative control. (**B**) Resting HBMECs stained with anti-ICAM-1. (**C**) Resting HBMECs stained with anti-EPCR. (**D**) Unstained TNF-α-activated HBMECs. (**E**) TNF-α-activated HBMECs stained with anti-ICAM-1. (**F**) TNF-α-activated HBMECs stained with anti-EPCR. (**G**) Comparison of ICAM-1 and EPCR expression level between resting HBMECs (HBMEC) and TNF-α-activated HBMECs (HBMECs-TNF-α) by normalized median fluorescence intensity (nMFI), calculated as dividing the MFI of stained sample by the MFI of unstained control sample. Data are shown as Mean ± SD and analyzed by unpaired t-test. *, $p < 0.05$; **, $p < 0.01$. n = 3.

3.6 Binding priority of IT4 enriched over TNF-α-activated HBMECs:

Since TNF-α-activated HBMECs exhibited the presence of both ICAM-1 and EPCR, we seek to investigate which clusters in IT4-HBMEC-TNF-α are responsible for binding to ICAM-1 and EPCR. At first, two more rounds of panning were performed and harvested a population which also showed high binding affinity to TNF-α-activated HBMECs, deemed IT4-HBMEC-P5'. Transcriptomic analysis revealed IT4-HBMEC-P5' encompassed higher percentage of IT4_var19 (15.36%) and IT4_var13 (5.45%) (Figure 7, A). Then, Chinese hamster ovary (CHO)-745 cells overexpressing ICAM-1 (CHO-745-ICAM-1) and CHO-K1 cells overexpressing EPCR (CHO-K1-EPCR) were utilized for testing the binding priority of IT4-HBMEC-P5'. IT4-HBMEC-P5' was separately enriched over CHO-745-ICAM-1 (P5'-ICAM-1) and CHO-K1-EPCR (P5'-EPCR) and adherent parasites were collected next day. IT4-HBMEC-P5' displayed intensive binding properties to both CHO-745-ICAM-1 and CHO-K1-EPCR (Figure 6, A, B). In addition, analysis of *var* profile suggested that IT4_var13 substituted IT4_var66 as the most expressed *var* gene in P5'-ICAM-1 with the proportion increased from 5.45% in IT4-HBMEC-P5' up to 62.03% in P5'-ICAM-1, followed by IT4_var16 (7.26%), IT4_var27 (5.61%), IT4_var66 (5.21%) and IT4_var31 (3.72%) (Figure 7, B, D). All these upregulated *var* genes in P5'-ICAM-1 contain either DBLβ3 or DBLβ5 in the extracellular part of their encoded *Pf*EMP1 proteins (Figure 7, F). However, IT4_var19 had the highest expression level in P5'-EPCR, accounting for 51.75% of the whole population. IT4_var13 also showed a dramatic upregulation in P5'-EPCR as well as the expression level of IT4_var4 (Figure 7, C, E).

CHO-745-ICAM-1
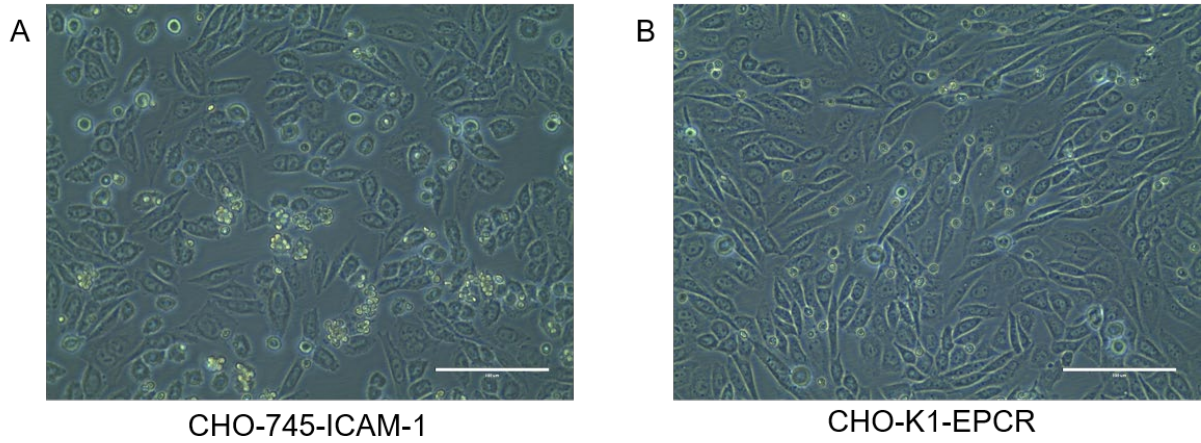
CHO-K1-EPCR

Figure 6: Binding capacity of IT4-HBMEC-P5' enriched over CHO-745-ICAM-1 and CHO-K1-EPCR. **(A)** IT4-HBMEC-P5' was enriched over CHO-745-ICAM-1. **(B)** IT4-HBMEC-P5' was enriched over CHO-K1-EPCR. Pictures were captured with EVOS XL inverted microscope at a 400 × magnification. Scale bars = 100 μm.
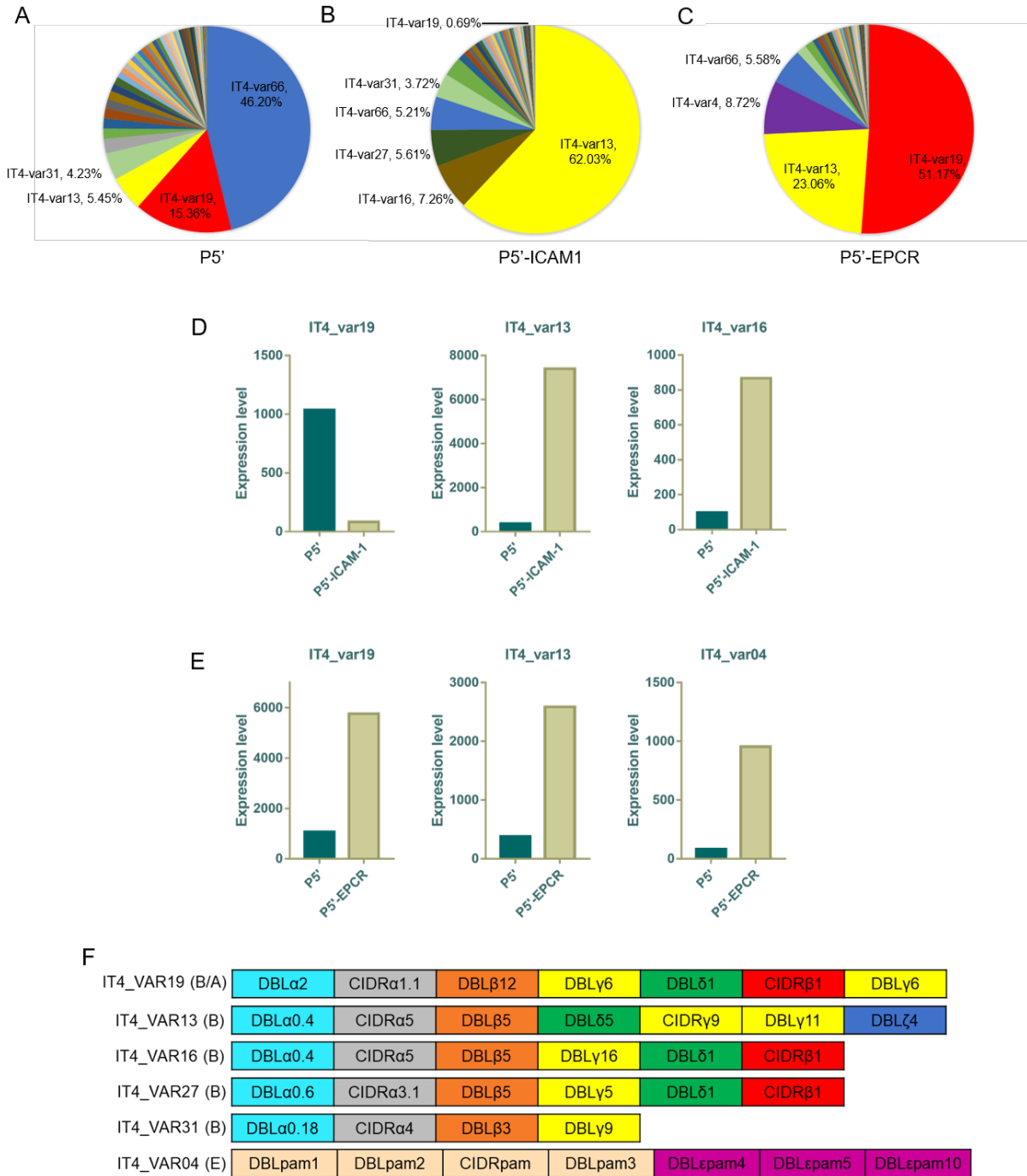
Figure 7: Gene expression profiles of IT4-HBMEC-P5', P5'-ICAM-1 and P5'-EPCR. **(A)** Fraction of *var* gene in IT4-HBMEC-P5', which was generated after continual enrichment. **(B)** Fraction of *var* gene in P5'-ICAM-1, which was generated by enriching P5' over CHO-745-ICAM-1. **(C)** Fraction of *var* gene in P5'-EPCR, which was generated by enriching P5' over CHO-K1-EPCR. **(D)** Expression level of IT4_var19, IT4_var13 and IT4_var16 in IT4-HBMEC-P5' and P5'-ICAM-1. **(E)** Expression level of IT4_var19, IT4_var13 and IT4_var4 in IT4-HBMEC-P5' and P5'-EPCR. **(F)** Schematic representation of the extracellular architecture of *Pf*EMP1 proteins encoded by IT4_var19, IT4_var13, IT4_var16, IT4_var27, IT4_var31 and IT4_var04.

3.7   Cytoadhesion-mediated effect on HBMECs:

To investigate the endothelial response induced by cytoadhesion, resting HBMECs were co-incubated with a IT4-HBMEC-TNF-α population (P4) for 4 h and 8 h separately. Afterwards, HBMECs were detached and mRNAs were isolated for NGS. The reads from NGS data were mapped to *Homo sapiens* (CRCh38) as a reference sequence and gene expression levels were calculated and normalized based on counts per million (CPM). HBMECs co-incubated with uninfected RBCs was established as negative control. A massive number of regulated genes were observed in HBMECs co-incubated with P4 compared to HBMECs co-incubated with RBCs and genes with padj < 0.05 were selected as differentially expressed genes (DEGs). In total, 101 DEGs were detected in P4-HBMEC-4h versus RBC-HBMEC-4h and 51 DEGs were detected in P4-HBMEC-8h versus RBC-HBMEC-8h (Figure 8, A). There are 16 common genes between the two differential expression comparison (Figure 8, B). Reactome pathway analysis revealed that the 101 DEGs from 4 hours of comparison were mainly clustered into cytokine signaling in immune system, including interferon induced signaling and signaling by interleukins (Figure 8, C). In addition, 12 DEGs candidates involved in this cluster were shown in Figure 8. Interestingly, the expression levels of most genes were significantly regulated after 4 hours of co-incubation (padj < 0.05) and the significance declined by reaching 8 hours of co-incubation (Figure 9).
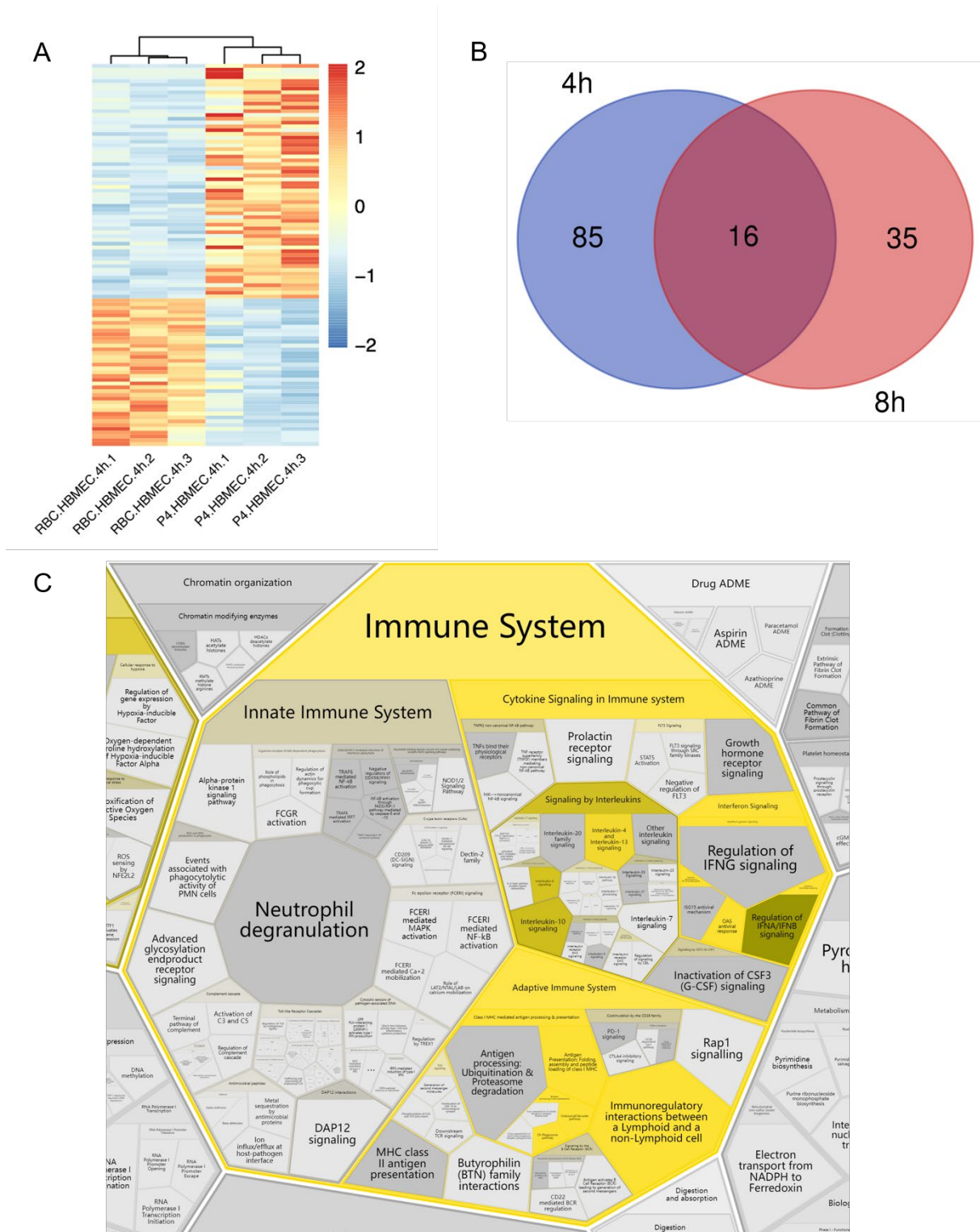
Figure 8: Cytoadhesion-mediated effect on HBMECs. **(A)** Heat map representing the expression of 101 DEGs within P4-HBMEC-4h versus RBC-HBMEC-4h. **(B)** Venn diagram illustrating the shared DEGs between 4 h of comparison and 8 h of comparison. **(C)** Reactome pathway analysis representing the functions of 101 DEGs within P4-HBMEC-4h versus RBC-HBMEC-4h.
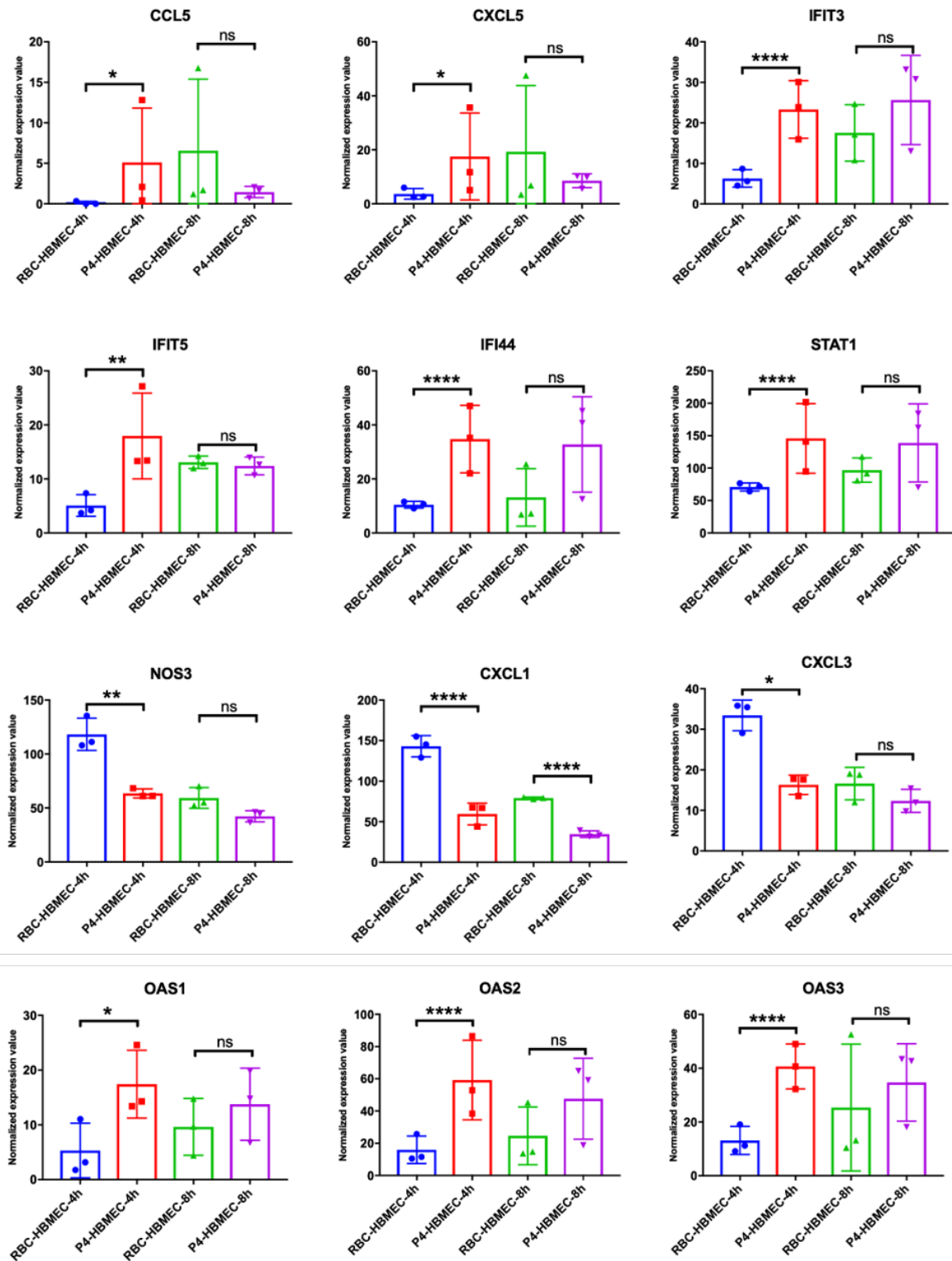
Figure 9: Differential expression of genes that were clustered into cytokine signaling in immune system pathway. The statistics significance was calculated using FDR-P value < 0.05. CCL: C-C Motif Chemokine Ligand. CXCL: C-X-C Motif Chemokine Ligand. IFIT: Interferon Induced Protein with Tetratricopeptide Repeats. STAT1: Signal Transducer and Activator of Transcription 1. NOS3: Nitric Oxide Synthase 3. OAS: 2'-5'-Oligoadenylate Synthetase.

4. Discussion:

4.1 Hsa-miR-451a as the most abundant miRNA candidate in both RBCs and EVs:

A comprehensive understanding of host-parasite interaction is still far from complete. Many players are involved in this process. MiRNA, as a small non-coding RNA, is known for mediating transcriptional and post-transcriptional gene regulation and plays a role in a vary of biological processes[113]. In order to survive and proliferate in a hostile environment, the gene expression of *Plasmodium* is tightly and elaborately regulated at each stage to ensure successful propagation[52]. This has aroused our interest on exploring the potential role of miRNA during malaria infection.

We started with uncovering the miRNA profile of niRBCs, riRBCs, trRBCs as well as their secreted EVs. Hsa-miR-451a presented as the dominant miRNA candidate in all RBC and EV populations. Hsa-miR-451a is the primary miRNA detected in erythrocytes whereas absent in progenitors of fetal liver erythroid and bone marrow erythroid, suggesting it might be involved in erythroid cells differentiation and maturation[126]. Since the expression level of Hsa-miR-451a showed no significant between healthy RBCs and *P. falciparum*-infected RBCs as well as in the secreted EVs, we believe Hsa-miR-451a expression is independent of *P. falciparum* infection. Mantel *et al.* investigated the role of miR-451a in human brain endothelium by incubating iRBC-derived EVs with brain endothelial cells. The results suggested that EV-derived miR-451a may alter endothelial barrier integrity by downregulating target genes expression such as caveolin-1 (Cav-1) and activating transcription factor 2 (ATF2)[109]. Further study need unravel the effect of miR-451a derived from niRBC-EVs and illustrate whether the observed impairment of brain endothelium integrity is specifically related to *P. falciparum* infection.

4.2 Differential expression of miRNAs in RBCs and EVs:

The comparison of miRNA profiles between iRBCs and niRBCs, as well as iRBC-EVs and niRBCs-EVs revealed that *P. falciparum* infection might modify the miRNA profile of host

erythrocytes and the secreted EVs after invasion. In addition, the putative target genes of differentially expressed miRNAs were enriched into four main function categories, containing cell signaling, HIF-1 and phagosome pathway, cytokine receptor activity, and immune regulatory interactions. Since a series of studies have suggested that iRBC-derived EVs may trigger immune response in monocytes, macrophages and brain endothelial cells and interfere cellular functions, our study further nailed down miRNAs, the main cargo in EVs, might be active players responsible for the observed effects.

Our study found that three miR-200 family members, miR-200a-3p, miR-200b-3p and miR-200c-3p, were upregulated in the EVs derived from riRBCs and trRBCs. Although the function of the cluster of miR-200 in malaria infection remains unknown, it is well-studied in other kind of infectious diseases. One study has proved that miR-200 family plays an important role in shaping the memory CD8$^+$ T cell response and determining the fate of activated T cells during lymphocytic choriomeningitis virus infection[127]. In herpes simplex virus type 1 (HSV-1) induced encephalitis animal model, miR-200 family are upregulated in various type of neuron cells and co-localized to regions of the brain with severe encephalitis-related pathology, suggesting their effect on central nervous system infection[128]. The precise function of miR-200 family in malaria infection, particularly in cerebral malaria, requires more exploration.

In contrast, s subset of downregulated miRNAs is detected in both *P. falciparum* infected RBCs and RBC-EVs, including the miR-let-7 family. Repression of miR-let-7 is also observed as researchers infected macrophages with *Salmonella*. In addition, researchers focused on the target genes of let-7 family members, including IL-6 and IL-10, two crucial cytokines in innate immune reaction. The 3' UTR region in the mRNA sequence of IL-6 and IL-10 contain the complimentary binding site of miR-let-7. Mouse embryonic fibroblast cells transfected with let-7-expressing vectors showed significantly increased expression level of IL-6 and IL-10 and this phenotype can be reversed by miRNA inhibitors[129]. Moreover, EVs derived from *P. falciparum* infected RBCs also boosted the production of IL-6 and IL-10 in macrophages[110]. Therefore, it is of great interest to clarify whether miR-let-7 repression is related to IL-6 and IL-10 production and subsequent immune response.

4.3 Differential expression of mRNAs in RBCs:

An array of mRNAs was detected in uninfected erythrocyte, with ribosomal protein S12 (RPS12), ferritin light chain (FTL) and ribosomal protein L41 (RPL41) as the three most dominant transcripts. The presence of mRNAs that encode ribosomal proteins implies that there are ongoing translation activities in the erythrocytes. Ferritin is responsible for iron storage in a soluble and nontoxic form[130]. We postulate that FTL translation process is actively regulated by unknown mechanism in erythrocyte in order to maintain iron homeostasis.

Conversely, *P. falciparum* infection substantially modified the mRNA profile in erythrocytes, with high expression levels of ATPase family AAA domain-containing protein 2 (ATAD2) and heat shock protein 90 alpha family class A member 1 (HSP90AA1). ATAD2 functions as transcription coactivator and regulates a subset of estradiol target genes[131]. The upregulation of HSP90AA1 has been seen in response to numerous cellular stresses and correlated with various infectious diseases and cancers[132]. Nevertheless, their distinct functions during malaria infection need further investigation.

4.4 The origin of regulated miRNAs and RNAs:

It is typically believed that there are no nucleic acids in mature erythrocytes as they are terminally differentiated cells and short of nuclei and organelles for transcription and translation[133]. However, multiple sources of evidence have identified the existence of miRNAs and mRNAs in both human mature erythrocytes and parasitized erythrocytes[129, 134]. The miRNA profile in mature erythrocytes showed a high degree of similarity as the miRNA profile in earlier stage of erythroid, indicating that the detected miRNAs in mature erythrocytes might originate from early-stage erythroid which still contain the transcription and translation machinery and persist even after enucleation and terminal differentiation[134].

In spite of the clear explanation that the presence of miRNAs and mRNAs in mature erythrocytes, it is still unknown why the expression level altered after *P. falciparum* infection. The first possibility is that there are certain RNA-binding proteins or other factors in erythrocytes that are able to regulate miRNA expression level by protecting them from

degradation. Some miRNA might selectively retain and have a longer half-life due to slower decay kinetics, and vice versa. Hence, after the invasion by *P. falciparum*, erythrocytes may utilize this coordination mechanism to preferentially regulate the miRNA and mRNA content and facilitate profound biological functions.

The second explanation is *P. falciparum*-infected erythrocytes actively and selectively exchange substances from the surrounding environment. This process might be accomplished by EVs that function as crucial communicators between cells and vehicles for intercellular components. Our results support this hypothesis as we observed 30 miRNAs were significantly upregulated in both riRBCs and ri-RBC-EVs. We exclude the possibility that EVs involved in this process are mainly from human serum of the culture medium, because we used different batches of human serum for erythrocyte and *P. falciparum* culture but still observed a massive number of significantly regulated miRNAs. In addition, both erythrocyte and *P. falciparum* culture were supplied with human serum-depleted medium for 12 hours in order to further diminish the effect from contaminating human serum-derived EVs.

On the other hand, it is more likely that *P. falciparum*-infected erythrocytes may actively EVs that secreted from uninfected RBCs and alter their miRNA and mRNA profiles. Interestingly, one study illustrated the mechanism of sickle erythrocyte resistance to *P. falciparum*. In sickle cells, miR-451 can incorporate into the mRNA transcript of cAMP-dependent protein kinase (PKA-R) and hamper the translation process[135]. PKA-R is a key molecule for *P. falciparum* in modulating sporozoite motility, erythrocyte invasion process and gametocytogenesis[136-138].

The intricate network of EVs remains a mystery in malaria infection. Further investigations are needed to distinguish the specific properties and contributions of EVs separately from uninfected erythrocytes and *P. falciparum*-infected erythrocytes and unravel the miRNAs degradation mechanism in erythrocytes.

4.5 IT4_var66-mediated cytoadhesion:

Our transcriptome analysis revealed that IT4-var66 had the highest expression level in the initial *P. falciparum* culture, which are long-term cultured under laboratory condition. IT4_var66 belongs to group C and contains CIDRα2.10, a CD36-binding domain[51]. IT4_var66 is commonly observed in starting culture prior to selection. In one study, researchers generated different *P. falciparum* parasite lines from long-term cultured laboratory line by limited dilution cloning and found out IT4_var66 accounted for the highest proportion in one of the clones, suggesting the growth advantage of IT4_var66 in *P. falciparum* proliferation[72]. It is conceivable that parasites tend to express CD36-binding *Pf*EMP1 proteins in patients which benefit both the host for causing limited tissue damage as well as the parasites for promoting survival and transmission. However, further study needs to explore the mechanism of *var* gene switching priority to IT4_var66 compared to other group C *var* genes.

The function of IT4_var66 remains unknown although containing a CD36-binding domain. Marion *et al.* selected initial *P. falciparum* culture over different endothelial cells. Their results showed that the expression level of IT4_var66 remained stable after enriched over human pulmonary microvascular endothelial cells and cardiac microvascular endothelial cells but decreased after enriched over bone marrow endothelial cells[139]. Combined with these results, we believe IT4_var66 has the advantages in *P. falciparum* proliferation compared to other group C *var* genes. In our study, IT4_var66 remained predominant after enriching IT4 over TNF-α-activated HBMECs. Although IT4_var66 encoded *Pf*EMP1 doesn't contain a EPCR or ICAM-1 binding domain, we speculate that there are unknown receptors on TNF-α-activated HBMECs responsible for binding to IEs expressing IEs IT4_var66.

4.6 IT4_var19-mediated cytoadhesion:

Our study indicated that IT4_var19, which encodes a *Pf*EMP1 protein containing DC8 (DBLα2-CIDRα1.1-DBLβ12-DBLγ4/6) structure, binds avidly to TNF-α-activated HBMECs. DC8 and EPCR interaction was well-characterized by various approaches. Turner *et al.* generated individual recombinant protein domains from DC8 and tested their binding capacity to recombinant EPCR (rEPCR) using enzyme-linked immunosorbent assay (ELISA). They found

out it is the CIDRα1.1 domain within the DC8 that are responsible for binding to rEPCR. Then, surface plasmon resonance were used to investigate the binding affinity between DC8 and EPCR. CIDRα1.1-EPCR interaction displayed ~29 nM dissociation constant (Kd), which is equivalent to the interaction between EPCR and its physiological ligand, APC (~32 Kd)[73]. In another study, researchers generated a parasite line mainly expressing IT4_var19. Adhesion assay revealed that IT4_var19-expressing IEs showed evident binding phenotype to HBMECs and immortalized human brain endothelial cells (HBEC-5i). Moreover, the observed binding signature can be inhibited by EPCR antibodies, soluble rEPCR and recombinant CIDRα1.1 domain proteins. IT4_var19-expressing IEs showed reduced binding ability to HBEC-5i transfected with EPCR siRNA[140]. In summary, these results have clarified the interaction between EPCR and CIDRα1.1 domain within DC8.

Our results keep in line with these studies since IT4_var19 showed a remarkable binding capacity to TNF-α-activated HBMECs, which express EPCR on surface. The interplay of IT4_var19 and EPCR was further confirmed as IT4_var19 was predominant after enriching IT4-HBMEC-P5' over CHO-K1-EPCR. Therefore, our study illustrated a clear binding picture between IT4_var19 and EPCR on HBMECs.

Besides, IT4_var19 can bind to various adhesion receptors. Complement C1q receptor (gC1qR) is expressed on a number of tissues and cell types and serve as a cytoadhesion receptor for *P. falciparum* IEs. It has been illustrated that DBLβ12 domain within DC8 is the binding site for gC1qR[141]. Beads coupling with individual domains of IT4_var19 exhibited widespread binding activity to different origins of endothelial cells, suggesting each domain within IT4_var19 are actively involved in cytoadhesion[139]. Therefore, even we observed the strong binding ability of IT4_var19-expressing IEs to HBMECs which was probably mediated by EPCR, we cannot exclude the possibility that other unknown receptors were also involved in the binding behavior.

4.7 EPCR-binding and CM:

EPCR has been recognized as the key adhesion receptor that plays a pivotal role in cerebral malaria development. *P. falciparum* parasites directly isolated from children with cerebral malaria can immensely bind to HBMECs and the presence of soluble rEPCR significantly inhibited the binding phenotype, suggesting EPCR might be the key anchor receptor for IE-mediated cytoadhesion[73]. Transcript levels of DC8-encoding *var* genes are significantly elevated in children hospitalized with CM compared to individuals with uncomplicated malaria[142]. In addition, the transcript levels of EPCR-binding *Pf*EMP1 proteins in malaria patients increased with malaria disease severity, with higher expression level in children with CM and severe malaria anemia than children with CM alone[143].

EPCR is known for maintaining the integrity of BBB, the regulation of coagulation and cytoprotective effects on endothelial cells. However, IEs may interfere the delicate homeostasis maintained by EPCR and give rise to excessive secretion of pro-inflammatory cytokines, upregulation of ICAM-1 which in turn worsen vascular occlusion, disruption of BBB and endothelial leakage[142]. Brain swelling is a critical prognostic factor for mortality in pediatric CM. One study evaluated brain swelling severity by magnetic resonance imaging in malaria patients and revealed that DC8 CIDRα1.1 transcripts were enriched in cases of CM with severe brain swelling and fatal outcomes[144]. This reinforces the possibility that DC8-expressing IEs might disrupt EPCR-mediated barrier-protective properties on brain endothelial cells and cause detrimental effects on BBB.

4.8 DBLβ5-mediated cytoadhesion:

IT4_var13 encodes a group B *Pf*EMP1 containing CIDRα5 as a CD36 binder and DBLβ5 as an ICAM-1 binder[51]. In our study, the expression level of IT4_var13 was increased in both IT4-HBMEC and IT4-HBMEC-TNF-α. Since both resting HBMEC and TNF-α-activated HBMEC expressed ICAM-1 on surface, we speculate that ICAM-1 played roles in the cytoadherence of IT4_var13-expressing IEs to HBMECs. The high proportion of IT4_var13 in P5'-ICAM-1 further confirmed the evident association between ICAM-1 and IT4_var13. In addition, IT4_var16, IT4_var27 and IT4_var31 were all upregulated in P5'-ICAM-1. One common

character of these *var* genes is they all belong to group B and encode *Pf*EMP1 proteins containing CIDRα3.1/4/5 as CD36 binder and DBLβ3/5 as ICAM-1 binder[51].

Although some group A *Pf*EMP1 proteins also contain DBLβ domains for binding to ICAM-1, the binding behavior mediated by group A DBLβ domains are distinct from group B DBLβ domains. Lennartz *et al.* performed phylogenetic analysis based on 59 DBLβ domain sequences and found out DBLβ domains from Group A *Pf*EMP1 are conserved whereas DBLβ domains from Group A *Pf*EMP1 are highly variable in sequence. Crystallography study revealed that group A DBLβ domains and group B DBLβ domains differ in the conformation of ICAM-1 binding site and angle[85]. Given that most group A *Pf*EMP1s are dual binder for ICAM-1 and EPCR while some group B *Pf*EMP1s are dual binder for ICAM-1 and CD36, the different DBLβ binding angles might influence how the adjacent domains within *Pf*EMP1 proteins interact with adhesion receptors. This might explain why only group B *var* genes were enriched instead of group A *var* genes. Although CHO-745 wild-type cell line doesn't express CD36, we suspect that some unknown receptors interfered the interaction of DBLβ and ICAM-1 and provided advantageous architecture for Group B *Pf*EMP1 to adhere to CHO-745-ICAM-1.

4.9   ICAM-1 binding and CM:

The importance of ICAM-1 mediated cytoadhesion has been illustrated in the pathogenesis of CM from several lines of evidence based on autopsy examination and *in vitro* binding studies. The plasma levels of circulating ICAM-1 (cICAM-1) were significantly higher in a group of 246 children with acute malaria compared to a group of 156 children with non-malarial illnesses. In addition, the levels of circulating cICAM-1 were correlate with the levels of TNF-α, IL-α and IFN-γ in the study, suggesting the upregulation of ICAM-1 might be attributed to the pro-inflammatory effects of cytokines on endothelial cells[145].

IEs that express ICAM-1 binding domains have been found associated with CM. The transcript levels of group A DBLβ1/3 domains and group B DBLβ5 domains were significantly elevated in CM malaria patients in comparison of individuals with uncomplicated malaria[84]. However, the contribution of group A DBLβ1/3 domains in CM pathophysiology remains controversial.

Another study revealed that there is no difference in the expression level of ICAM-1-binding DBL1/3 domain in RT-qPCR between CM and mild malaria cohorts[146]. Besides, DBLβ-specific IgG isolated from the plasma of CM patients exhibited the ability to opsonize IEs for antibody-dependent cellular phagocytosis. The opsonization of IEs by DBLβ-specific IgG enhances their recognition and uptake by immune cells, leading to the clearance of infected cells and potentially contributing to the control of malaria infection. This study indicated that ICAM-1-binding *Pf*EMP1 proteins are crucial targets of protective antibodies against malaria[147].

4.10 The effect of cytoadhesion on HBMECs:

Although the association between CM and cytoadhesion mediated by EPCR and ICAM-1 has been confirmed by several lines of evidence, little is known about the effects of cytoadhesion signal in the pathophysiology of CM. Endothelial dysfunction is a prominent characteristic of *P. falciparum* malaria and is associated with the severity of the disease, particularly in CM[148]. In the present study, HBMECs were utilized to investigate cytoadhesion-mediated endothelial response. Compared to immortalized endothelial cell line such as HBEC-5i, primary HBMEC is a better tool to illustrate the host cytoadherence signature on different *Pf*EMP1 variants as they are absent of CSA, a distinct receptor related to placental malaria. Therefore, HBMEC is an ideal model to research the effects of cytoadhesion signal on endothelial cells mediated by brain adhesion receptors such as EPCR and ICAM-1.

Some studies have already co-incubated IEs with endothelial cells to investigate the immune reaction induced by IEs[149-151]. However, these studies didn't look into the *Pf*EMP1 variants expression level of their IEs. This might cause discrepancy in their results because *Pf*EMP1 is considered the most important virulence factor and related to pathogenicity. The reaction of endothelial cells to IEs might differ depending on the virulence of the *Pf*EMP1 protein. Moreover, most study only detected a restricted number of cytokines and chemokines in endothelial cells which only reflects part of the landscape of endothelial immune response.

In our enrichment experiment, we have successfully selected a parasite line, IT4-HBMEC-TNF-α, which encompasses subpopulations of IEs that express IT4_var19 (8.58%) and IT4_var13 (2.17%). Binding experiment revealed that this parasite line can bind to both EPCR and ICAM-1 mediated by different *Pf*EMP1s. In our study, this parasite line was used to co-incubate with HBMECs for 4 h and 8 h and their transcriptomes were analyzed by NGS. In total of 101 DEGs were detected in HBMECs after 4 h of co-incubation and 51 DEGs were detected in HBMECs after 8 h of co-incubation. More DEGs were observed at 4h post coincubation compared to 8 h post coincubation, indicating the effects induced by cytoadhesion on HBMECs were more intense at 4 h timepoint. We believe that the time point at which the cytoadhesion-induced immune response reached its peak was closer to the 4-hour time point than 8-hour time point. The functions of the 101 DEGs after 4 h of co-incubation are related to cytokine signaling in immune system, including interferon induced signaling and signaling by interleukins.

4.11 Chemokines and malaria:

Chemokines are a group of small signaling proteins that play an important function in the immune system by orchestrating the movement and positioning of immune cells in response to inflammation and infection. Upon tissue damage, chemokines recruit leukocytes from the circulation and guide them into the site of damaged tissue[152]. The function of CCL5 has been characterized in JHM strain of mouse hepatitis virus infection (JHMV). During JHMV infection, the upregulation of CCL5 on endothelial surface can recruit monocytes into CNS. Accumulating neutrophils and monocytes can degrade the BBB facilitated by the secretion of matrix metalloproteinase MMP-9. Consequently, the breakdown of the BBB gives rise to the excessive infiltration of virus-specific lymphocytes into the CNS and impact the progression and severity of the infection[153].

In malaria, the reduced levels of circulating CCL5 have been observed in severe anemia malaria patients and linked to erythropoiesis inhibition and malaria-induced thrombocytopenia[154]. In our study, significantly upregulated CCL5 was detected in HBMECs upon 4 hours of co-incubation. We postulate that CCL5 might play protective effects in the early stage of infection. By comparison, the expression levels of CXCL1 and CXCL3 showed an opposite tendency

compared to CCL5 upon 4 h of co-incubation. Although chemokines mainly serve as chemoattractants to attract immune cells to the site of inflammation, they exhibit overlapping but distinct biological activities. Their specific function and the types of recruited effect cells might differ depending on the mediated signal pathways[152]. Future research efforts should prioritize the examination of effect cell types recruited by different chemokines and elucidate their immune-regulatory functions. Nevertheless, our results demonstrated the active involvement of endothelial cells in response to IEs stimulation by regulating the expression of a series of chemokines.

4.12 Interferon and malaria:

Type I interferons (IFN-Is) are a group of crucial cytokines that play significant roles in a wide range of diseases including infections, autoimmune diseases, and cancer. IFN-α and IFN-β are the most abundant and well-characterized subtypes among all IFN-Is members[155]. IFN-Is are among the most frequently produced cytokines by the host in response to malaria parasite infections. During malaria infection, parasite-derived PAMPs are recognized by host PRR such as TLR2 and TLR4 and activate downstream signal pathway effectors including IRF3 and IRF7. IRF3 and IRF7 function as transcription factors and induce the production of IFN-Is. Subsequently, IFN-Is bind to interferon α and β receptor subunit 1 and eventually induce the expression of a wide range of interferon-stimulated genes (ISGs), such as IFIT3, STAT1, OAS1, etc. ISGs can either directly target parasites, impeding their replication and survival, or modulate host immune reactions to combat *P. falciparum* infection[156]. IFN-Is can be released by a varies of cells including peripheral blood mononuclear cell (PBMC), plasmacytoid dendritic cells (pDC), macrophages as well as endothelial cells[157, 158].

A clinical study has proved the protective role of IFN-Is in malaria progression. The administration of constant human recombinant IFN-α leads to the enhanced survival in a malaria mouse model[159]. We didn't observe a significant regulation of IFN-Is in HBMECs after co-incubating with IEs. However, a number of ISGs exhibited remarkable upregulation in HBMECs after 4 h of co-incubation with IEs. In summary, our study emphasized the importance of IFN-Is signal pathway in response to IEs stimulation.

Of note, we noticed the family of OAS genes were significantly upregulated in HBMECs after 4 h of co-incubation with IEs. The OAS expression is primarily regulated by IFN-Is. The distinct mechanism of OAS in host immune defense has been extensively characterized in viral infections[160]. Upon the invasion of double-stranded RNA (dsRNA) virus into host cells, OAS can be activated and function as enzyme to catalyze the synthesis of 2′-5′-linked oligoadenylates (2-5A). 2-5A is a secondary messenger and activate the latent ribonuclease L (RNase L). Activated RNase L then cleaves viral RNA, resulting in the degradation of viral genetic material and the suppression of viral replication[161]. This arises great interest to investigate the origin of *P. falciparum*-derived dsRNA that activate OAS proteins in endothelial cells. One explanation is that EVs were secreted by IEs during coincubation and uptaken by endothelial cells. Double-stranded RNAs were released into cytosol and recognized by OAS proteins. In addition, it is also possible that IEs were internalized and lysed by HBMECs and free dsRNAs were captured by OAS proteins.

4.13 Conclusion:

In chapter I, we have identified EVs secreted by uninfected erythrocytes and *P. falciparum*-infected erythrocytes. The miRNA profiles of erythrocytes and the secreted EVs were analyzed by NGS. The expression level of a wide range of miRNAs were altered significantly in erythrocytes and their secreted EVs upon *P. falciparum* infection. The target genes of differentially expressed miRNAs were predicted by bioinformatic approaches and function enrichment analysis indicated that these miRNA candidates might play a role in immunoregulatory pathways during *P. falciparum* infection.

In chapter II, we have enriched a *P. falciparum* population which showed high binding affinity to TNF-α-activated HBMECs. Binding assay of enriched IEs demonstrated that their binding capacity to ICAM-1 and EPCR. Furthermore, the enriched IEs showed a significant impact on HBMECs, leading to the dysregulation of numerous differentially expressed genes.

4.14 Directions for future studies:

4.14.1 The interplay of iRBC-EVs and HBMEC:

In **Chapter I 2.1** section, we have extracted EVs derived from uninfected erythrocytes and *P. falciparum*-infected erythrocytes and deciphered their miRNA profiles. The results showed that the miRNA profile of erythrocyte-derived EVs changed dramatically upon *P. falciparum* infection. It is of interest to investigate the significance of EVs derived from *P. falciparum*-infected erythrocytes in the interaction between *P. falciparum* and host cells, particularly endothelial cells. At first, EVs labeled with specific dye can be incubated with HBMECs to explain if HBMECs can function as target cells and have the ability to internalize erythrocyte-derived EVs. Then, the transcriptomes of HBMECs can be analyzed after stimulated with EVs derived from uninfected erythrocytes and EVs derived from *P. falciparum*-infected erythrocytes. This might unravel the impact of EVs on HBMECs and further illustrate the potential role of EVs in the pathogenesis of malaria.

4.14.2 The function of differentially expressed miRNA candidates:

In **Chapter I 2.1** section, a wide range of differentially expressed miRNA candidates were identified in EVs derived from *P. falciparum*-infected erythrocytes. The certain function of these miRNAs on HBMECs remain unknown. At first, the target genes of miRNA of interest can be identified by bioinformatic approaches based on the sequence complementarity in the 3' UTR and 5' UTR region of target genes. Lentivirus is a mature and effective tool to study the distinct function of miRNA[162]. Lentivirus carrying the miRNA sequence of interest can be transduced into HBMECs. Then, the transcript expression levels and protein expression levels of predicted target genes as well as cellular phenotype can be detected. In the end, northern blot can be used to validate the direct interaction between the miRNA candidate and predicted target genes.

4.14.3   Investigate host-parasite interaction under flow condition:

Our study illustrated the binding properties of enriched IEs population on the receptors of HBMECs and further elucidate the effect of cytoadhesion on HBMECs. However, all the experiment were performed under static condition. In **Chapter I 2.2** section, we have built a laminar flow system which can be utilized for understanding the interaction between IEs and host endothelial cells under shear stress. This *in vivo*-like flow system has two crucial advantages for studying host-parasite interaction. At first, it provides a better way to investigate the binding affinity of different *Pf*EMP1s to endothelial receptors. A previous study in our lab has revealed that IEs exhibited rolling adhesion phenotype to CD36 under different shear stresses while IEs showed stationary adhesion behavior to ICAM-1, P-selectin, CD9 and CSA[163]. A dynamic flow system might better characterize the binding affinity between different *Pf*EMP1 proteins and host receptors. In addition, this system reflects the human blood circulation by simulating vascular mechanobiology under physiological condition. Endothelial cells exhibit different intracellular responses with altered expression levels of inflammation-related genes when exposed to various shear stresses[164]. Therefore, a flow system might better reflect the real pathophysiological progression in malaria patients.

4.14.4   Cytoadhesion-mediated endothelial response:

We have enriched a *P. falciparum* line which showed high binding capacity to HBMECs. This population of parasites were co-incubated with HBMECs to study the effect of cytoadhesion on endothelial cells. However, we cannot exclude the possibility that the confounding factors apart from cytoadhesion are also involved in inducing immune response on HBMECs. As indicated in **Chapter I 2.4** section, circulating plasmodial antigens and released substances from the plasma of malaria patients exert immune reactions on HBMECs[165]. *P. falciparum*-derived antigens such as HRP2 and hemozoins can be recognized by PRR on immune cells and activate downstream signal pathway. Our results in **Chapter I 2.2** section also suggested that EVs secreted by IEs might elicit immunomodulatory functions facilitated by the miRNA contents in EVs.

The fact that IEs keep releasing *P. falciparum*-derived components during co-incubation period might hinder the study of endothelial response exclusively mediated by cytoadhesion. Hence, HBMECs can be co-incubated with initial IT4, which showed low-binding affinity to HBMECs. Afterwards, the transcriptome can be compared with HBMECs co-incubated with enriched IT4 to elucidate the contribution of cytoadhesion in the detected endothelial response. Furthermore, cytochalasin D can chemically disrupt the actin cytoskeleton in cell membrane and dampen cellular process such as endocytosis[166]. HBMECs can be treated with cytochalasin D before the co-incubation period to impair the internalization of EVs and minimize EV-mediated effects. Over and above that, beads coupling with recombinant CIDRα1.1 or DBLβ5 domains can be the alternatives of adherent IEs as they are absent of plasmodial antigens and EVs.

4.14.5   Interpretation of enriched pathways:

We have detected 101 DEGs in the co-incubation experiment and pathway enrichment analysis suggested that these DEGs might be involved in interferon induced signaling and signaling by interleukins pathways. Further efforts are required to better interpret the results. At first, the pivotal genes in the pathways of interest can be validated on protein expression level to confirm the expression changes. In addition, the transcriptomic data can be integrated with other omics data such as proteomics and metabolomics. This might provide a comprehensive understanding of the dysregulated molecules in response to cytoadhesion.

5. References:

1. WHO. World Malaria Report 2022. 2022.
2. Cowman AF, Healer J, Marapana D, Marsh K. Malaria: Biology and Disease. Cell. 2016;167(3):610-24.
3. Phillips MA, Burrows JN, Manyando C, van Huijsduijnen RH, Van Voorhis WC, Wells TNC. Malaria. Nat Rev Dis Primers. 2017;3:17050.
4. Buffet PA, Safeukui I, Deplaine G, Brousse V, Prendki V, Thellier M, et al. The pathogenesis of Plasmodium falciparum malaria in humans: insights from splenic physiology. Blood. 2011;117(2):381-92.
5. Battle KE, Baird JK. The global burden of Plasmodium vivax malaria is obscure and insidious. PLOS Medicine. 2021;18(10):e1003799.
6. Chen I, Clarke SE, Gosling R, Hamainza B, Killeen G, Magill A, et al. "Asymptomatic" Malaria: A Chronic and Debilitating Infection That Should Be Treated. PLOS Medicine. 2016;13(1):e1001942.
7. White MT, Karl S, Battle KE, Hay SI, Mueller I, Ghani AC. Modelling the contribution of the hypnozoite reservoir to Plasmodium vivax transmission. eLife. 2014;3:e04692.
8. Ghanchi N, Khan AA, Raheem A, Beg MA. Plasmodium vivax Mimicking Morphologic Features of Plasmodium falciparum. Cureus. 2020;12(11):e11406.
9. Collins WE, Jeffery GM. Plasmodium ovale: parasite and disease. Clin Microbiol Rev. 2005;18(3):570-81.
10. Coatney GR, Collins WE, Warren M, Contacos PG. The primate malarias. U S Government Printing Office, Washington, DC. 1971.
11. ELLIS McKENZIE F, JEFFERY GM, COLLINS WE. Plasmodium malariae Blood-Stage Dynamics. Journal of Parasitology. 2001;87(3):626-37.
12. White NJ. Plasmodium knowlesi: The Fifth Human Malaria Parasite. Clinical Infectious Diseases. 2008;46(2):172-3.
13. Aly AS, Vaughan AM, Kappe SH. Malaria parasite development in the mosquito and infection of the mammalian host. Annu Rev Microbiol. 2009;63:195-221.
14. Cowman AF, Crabb BS. Invasion of red blood cells by malaria parasites. Cell. 2006;124(4):755-66.
15. Bennink S, Kiesow MJ, Pradel G. The development of malaria parasites in the mosquito midgut. Cell Microbiol. 2016;18(7):905-18.
16. Baker DA. Malaria gametocytogenesis. Mol Biochem Parasitol. 2010;172(2):57-65.
17. White NJ, Ashley EA. Malaria. In: Jameson JL, Fauci AS, Kasper DL, Hauser SL, Longo DL, Loscalzo J, editors. Harrison's Principles of Internal Medicine, 20e. New York, NY: McGraw-Hill Education; 2018.
18. Oakley MS, Gerald N, McCutchan TF, Aravind L, Kumar S. Clinical and molecular aspects of malaria fever. Trends Parasitol. 2011;27(10):442-9.
19. Crawley J, Chu C, Mtove G, Nosten F. Malaria in children. Lancet. 2010;375(9724):1468-81.
20. Phillips A, Bassett P, Zeki S, Newman S, Pasvol G. Risk factors for severe disease in adults with falciparum malaria. Clin Infect Dis. 2009;48(7):871-8.
21. WHO. WHO guidelines for malaria. 2022.
22. Sharma R, Dutta AK. Malaria and National Vector Borne Disease Control Programme. Indian J Pediatr. 2011;78(12):1527-35.
23. Kotlyar S, Nteziyaremye J, Olupot-Olupot P, Akech SO, Moore CL, Maitland K. Spleen volume and clinical disease manifestations of severe Plasmodium falciparum malaria in African children. Trans R Soc Trop Med Hyg. 2014;108(5):283-9.
24. White NJ. Anaemia and malaria. Malaria Journal. 2018;17(1):371.
25. Beare NA, Taylor TE, Harding SP, Lewallen S, Molyneux ME. Malarial retinopathy: a newly established diagnostic sign in severe malaria. Am J Trop Med Hyg. 2006;75(5):790-7.
26. Polimeni M, Prato M. Host matrix metalloproteinases in cerebral malaria: new kids on the block against blood-brain barrier integrity? Fluids Barriers CNS. 2014;11(1):1.

27.   Gillrie MR, Lee K, Gowda DC, Davis SP, Monestier M, Cui L, et al. Plasmodium falciparum histones induce endothelial proinflammatory response and barrier dysfunction. Am J Pathol. 2012;180(3):1028-39.

28.   Storm J, Craig AG. Pathogenesis of cerebral malaria--inflammation and cytoadherence. Front Cell Infect Microbiol. 2014;4:100.

29.   Dunst J, Kamena F, Matuschewski K. Cytokines and Chemokines in Cerebral Malaria Pathogenesis. Front Cell Infect Microbiol. 2017;7:324.

30.   Taylor WR, Cañon V, White NJ. Pulmonary manifestations of malaria : recognition and management. Treat Respir Med. 2006;5(6):419-28.

31.   Taylor WRJ, Hanson J, Turner GDH, White NJ, Dondorp AM. Respiratory manifestations of malaria. Chest. 2012;142(2):492-505.

32.   Van den Steen PE, Deroost K, Deckers J, Van Herck E, Struyf S, Opdenakker G. Pathogenesis of malaria-associated acute respiratory distress syndrome. Trends Parasitol. 2013;29(7):346-58.

33.   Gardner MJ, Hall N, Fung E, White O, Berriman M, Hyman RW, et al. Genome sequence of the human malaria parasite Plasmodium falciparum. Nature. 2002;419(6906):498-511.

34.   Larremore DB, Sundararaman SA, Liu W, Proto WR, Clauset A, Loy DE, et al. Ape parasite origins of human malaria virulence genes. Nature Communications. 2015;6(1):8368.

35.   Miles A, Iqbal Z, Vauterin P, Pearson R, Campino S, Theron M, et al. Indels, structural variation, and recombination drive genomic diversity in Plasmodium falciparum. Genome Res. 2016;26(9):1288-99.

36.   Mok BW, Ribacke U, Sherwood E, Wahlgren M. A highly conserved segmental duplication in the subtelomeres of Plasmodium falciparum chromosomes varies in copy number. Malar J. 2008;7:46.

37.   Ribacke U, Mok BW, Wirta V, Normark J, Lundeberg J, Kironde F, et al. Genome wide gene amplifications and deletions in Plasmodium falciparum. Mol Biochem Parasitol. 2007;155(1):33-44.

38.   Hamilton WL, Claessens A, Otto TD, Kekre M, Fairhurst RM, Rayner JC, et al. Extreme mutation bias and high AT content in Plasmodium falciparum. Nucleic Acids Res. 2017;45(4):1889-901.

39.   Claessens A, Hamilton WL, Kekre M, Otto TD, Faizullabhoy A, Rayner JC, et al. Generation of Antigenic Diversity in Plasmodium falciparum by Structured Rearrangement of Var Genes During Mitosis. PLOS Genetics. 2014;10(12):e1004812.

40.   Scherf A, Lopez-Rubio JJ, Riviere L. Antigenic variation in Plasmodium falciparum. Annu Rev Microbiol. 2008;62:445-70.

41.   Su XZ, Heatwole VM, Wertheimer SP, Guinet F, Herrfeldt JA, Peterson DS, et al. The large diverse gene family var encodes proteins involved in cytoadherence and antigenic variation of Plasmodium falciparum-infected erythrocytes. Cell. 1995;82(1):89-100.

42.   Fernandez V, Hommel M, Chen Q, Hagblom P, Wahlgren M. Small, clonally variant antigens expressed on the surface of the Plasmodium falciparum-infected erythrocyte are encoded by the rif gene family and are the target of human immune responses. J Exp Med. 1999;190(10):1393-404.

43.   Kyes SA, Rowe JA, Kriek N, Newbold CI. Rifins: a second family of clonally variant proteins expressed on the surface of red cells infected with Plasmodium falciparum. Proc Natl Acad Sci U S A. 1999;96(16):9333-8.

44.   Kaviratne M, Khan SM, Jarra W, Preiser PR. Small variant STEVOR antigen is uniquely located within Maurer's clefts in Plasmodium falciparum-infected red blood cells. Eukaryot Cell. 2002;1(6):926-35.

45.   Niang M, Bei AK, Madnani KG, Pelly S, Dankwa S, Kanjee U, et al. STEVOR is a Plasmodium falciparum erythrocyte binding protein that mediates merozoite invasion and rosetting. Cell Host Microbe. 2014;16(1):81-93.

46.   Spielmann T, Fergusen DJ, Beck HP. etramps, a new Plasmodium falciparum gene family coding for developmentally regulated and highly charged membrane proteins located at the parasite-host cell interface. Mol Biol Cell. 2003;14(4):1529-44.

47.   Winter G, Kawai S, Haeggström M, Kaneko O, von Euler A, Kawazu S, et al. SURFIN is a polymorphic antigen expressed on Plasmodium falciparum merozoites and infected erythrocytes. J Exp Med. 2005;201(11):1853-63.

48.   Oberli A, Slater LM, Cutts E, Brand F, Mundwiler-Pachlatko E, Rusch S, et al. A Plasmodium falciparum PHIST protein binds the virulence factor PfEMP1 and comigrates to knobs on the host cell surface. Faseb j. 2014;28(10):4420-33.

49.   Nguitragool W, Bokhari AA, Pillai AD, Rayavara K, Sharma P, Turpin B, et al. Malaria parasite clag3 genes determine channel-mediated nutrient uptake by infected red blood cells. Cell. 2011;145(5):665-77.

50.   Nunes MC, Okada M, Scheidig-Benatar C, Cooke BM, Scherf A. Plasmodium falciparum FIKK kinase members target distinct components of the erythrocyte membrane. PLoS One. 2010;5(7):e11747.

51.   Rask TS, Hansen DA, Theander TG, Gorm Pedersen A, Lavstsen T. Plasmodium falciparum erythrocyte membrane protein 1 diversity in seven genomes--divide and conquer. PLoS Comput Biol. 2010;6(9).

52.   Deitsch KW, Dzikowski R. Variant Gene Expression and Antigenic Variation by Malaria Parasites. Annu Rev Microbiol. 2017;71:625-41.

53.   Lavstsen T, Salanti A, Jensen AT, Arnot DE, Theander TG. Sub-grouping of Plasmodium falciparum 3D7 var genes based on sequence analysis of coding and non-coding regions. Malar J. 2003;2:27.

54.   Kraemer SM, Smith JD. Evidence for the importance of genetic structuring to the structural and functional specialization of the Plasmodium falciparum var gene family. Mol Microbiol. 2003;50(5):1527-38.

55.   Jensen AR, Adams Y, Hviid L. Cerebral Plasmodium falciparum malaria: The role of PfEMP1 in its pathogenesis and immunity, and PfEMP1-based vaccines to prevent it. Immunol Rev. 2020;293(1):230-52.

56.   Goel S, Palmkvist M, Moll K, Joannin N, Lara P, R Akhouri R, et al. RIFINs are adhesins implicated in severe Plasmodium falciparum malaria. Nature Medicine. 2015;21(4):314-7.

57.   Doumbo OK, Thera MA, Koné AK, Raza A, Tempest LJ, Lyke KE, et al. High levels of Plasmodium falciparum rosetting in all clinical forms of severe malaria in African children. Am J Trop Med Hyg. 2009;81(6):987-93.

58.   Rowe A, Obeiro J, Newbold CI, Marsh K. Plasmodium falciparum rosetting is associated with malaria severity in Kenya. Infect Immun. 1995;63(6):2323-6.

59.   Deans A-M, Rowe JA. Plasmodium falciparum: Rosettes do not protect merozoites from invasion-inhibitory antibodies. Experimental Parasitology. 2006;112(4):269-73.

60.   Wahlgren M, Carlson J, Udomsangpetch R, Perlmann P. Why do Plasmodium falciparumm-infected erythrocytes form spontaneous erythrocyte rosettes? Parasitology Today. 1989;5(6):183-5.

61.   Degarege A, Gebrezgi MT, Ibanez G, Wahlgren M, Madhivanan P. Effect of the ABO blood group on susceptibility to severe malaria: A systematic review and meta-analysis. Blood Reviews. 2019;33:53-62.

62.   Joannin N, Kallberg Y, Wahlgren M, Persson B. RSpred, a set of Hidden Markov Models to detect and classify the RIFIN and STEVOR proteins of Plasmodium falciparum. BMC Genomics. 2011;12:119.

63.   Sanyal S, Egée S, Bouyer G, Perrot S, Safeukui I, Bischoff E, et al. Plasmodium falciparum STEVOR proteins impact erythrocyte mechanical properties. Blood. 2012;119(2):e1-e8.

64.   Milner DA, Jr. Malaria Pathogenesis. Cold Spring Harb Perspect Med. 2018;8(1).

65.   Sierro F, Grau GER. The Ins and Outs of Cerebral Malaria Pathogenesis: Immunopathology, Extracellular Vesicles, Immunometabolism, and Trained Immunity. Front Immunol. 2019;10:830.

66.   Smith JD, Rowe JA, Higgins MK, Lavstsen T. Malaria's deadly grip: cytoadhesion of Plasmodium falciparum-infected erythrocytes. Cell Microbiol. 2013;15(12):1976-83.

67.   Fairhurst RM, Wellems TE. Modulation of malaria virulence by determinants of Plasmodium falciparum erythrocyte membrane protein-1 display. Curr Opin Hematol. 2006;13(3):124-30.

68.   Groom AC, Schmidt EE, MacDonald IC. Microcirculatory pathways and blood flow in spleen: new insights from washout kinetics, corrosion casts, and quantitative intravital videomicroscopy. Scanning Microsc. 1991;5(1):159-73; discussion 73-4.

69.   Wahlgren M, Goel S, Akhouri RR. Variant surface antigens of Plasmodium falciparum and their roles in severe malaria. Nat Rev Microbiol. 2017;15(8):479-91.

70.   Metwally NG, Tilly AK, Lubiana P, Roth LK, Dörpinghaus M, Lorenzen S, et al. Characterisation of Plasmodium falciparum populations selected on the human endothelial receptors P-selectin, E-selectin, CD9 and CD151. Sci Rep. 2017;7(1):4069.

71.   Boeuf P, Hasang W, Hanssen E, Glazier JD, Rogerson SJ. Relevant assay to study the adhesion of Plasmodium falciparum-infected erythrocytes to the placental epithelium. PLoS One. 2011;6(6):e21126.

72.   Janes JH, Wang CP, Levin-Edens E, Vigan-Womas I, Guillotte M, Melcher M, et al. Investigating the host binding signature on the Plasmodium falciparum PfEMP1 protein family. PLoS Pathog. 2011;7(5):e1002032.

73.   Turner L, Lavstsen T, Berger SS, Wang CW, Petersen JE, Avril M, et al. Severe malaria is associated with parasite binding to endothelial protein C receptor. Nature. 2013;498(7455):502-5.

74.   Lavstsen T, Turner L, Saguti F, Magistrado P, Rask TS, Jespersen JS, et al. Plasmodium falciparum erythrocyte membrane protein 1 domain cassettes 8 and 13 are associated with severe malaria in children. Proc Natl Acad Sci U S A. 2012;109(26):E1791-800.

75.   Silverstein RL, Febbraio M. CD36, a scavenger receptor involved in immunity, metabolism, angiogenesis, and behavior. Sci Signal. 2009;2(72):re3.

76.   Pepino MY, Kuda O, Samovski D, Abumrad NA. Structure-function of CD36 and importance of fatty acid signal transduction in fat metabolism. Annu Rev Nutr. 2014;34:281-303.

77.   Cabrera A, Neculai D, Kain KC. CD36 and malaria: friends or foes? A decade of data provides some answers. Trends Parasitol. 2014;30(9):436-44.

78.   Robinson BA, Welch TL, Smith JD. Widespread functional specialization of Plasmodium falciparum erythrocyte membrane protein 1 family members to bind CD36 analysed across a parasite genome. Mol Microbiol. 2003;47(5):1265-78.

79.   Hsieh F-L, Turner L, Bolla JR, Robinson CV, Lavstsen T, Higgins MK. The structural basis for CD36 binding by the malaria parasite. Nature Communications. 2016;7(1):12837.

80.   Newbold C, Warn P, Black G, Berendt A, Craig A, Snow B, et al. Receptor-specific adhesion and clinical disease in Plasmodium falciparum. Am J Trop Med Hyg. 1997;57(4):389-98.

81.   Hubbard AK, Rothlein R. Intercellular adhesion molecule-1 (ICAM-1) expression and cell signaling cascades. Free Radic Biol Med. 2000;28(9):1379-86.

82.   Oppenheimer-Marks N, Davis LS, Bogue DT, Ramberg J, Lipsky PE. Differential utilization of ICAM-1 and VCAM-1 during the adhesion and transendothelial migration of human T lymphocytes. J Immunol. 1991;147(9):2913-21.

83.   Frick C, Odermatt A, Zen K, Mandell KJ, Edens H, Portmann R, et al. Interaction of ICAM-1 with beta 2-integrin CD11c/CD18: characterization of a peptide ligand that mimics a putative binding site on domain D4 of ICAM-1. Eur J Immunol. 2005;35(12):3610-21.

84.   Storm J, Jespersen JS, Seydel KB, Szestak T, Mbewe M, Chisala NV, et al. Cerebral malaria is associated with differential cytoadherence to brain endothelial cells. EMBO Mol Med. 2019;11(2).

85.   Lennartz F, Smith C, Craig AG, Higgins MK. Structural insights into diverse modes of ICAM-1 binding by Plasmodium falciparum-infected erythrocytes. Proc Natl Acad Sci U S A. 2019;116(40):20124-34.

86.   Esmon CT. Structure and functions of the endothelial cell protein C receptor. Crit Care Med. 2004;32(5 Suppl):S298-301.

87.   Bouwens EA, Stavenuiter F, Mosnier LO. Mechanisms of anticoagulant and cytoprotective actions of the protein C pathway. J Thromb Haemost. 2013;11 Suppl 1(0 1):242-53.

88.   Aird WC, Mosnier LO, Fairhurst RM. Plasmodium falciparum picks (on) EPCR. Blood. 2014;123(2):163-7.

89.   Gillrie MR, Avril M, Brazier AJ, Davis SP, Stins MF, Smith JD, et al. Diverse functional outcomes of Plasmodium falciparum ligation of EPCR: potential implications for malarial pathogenesis. Cell Microbiol. 2015;17(12):1883-99.

90.   Kessler A, Dankwa S, Bernabeu M, Harawa V, Danziger SA, Duffy F, et al. Linking EPCR-Binding PfEMP1 to Brain Swelling in Pediatric Cerebral Malaria. Cell Host & Microbe. 2017;22(5):601-14.e5.

91.   Maubert B, Guilbert LJ, Deloron P. Cytoadherence of Plasmodium falciparum to intercellular adhesion molecule 1 and chondroitin-4-sulfate expressed by the syncytiotrophoblast in the human placenta. Infect Immun. 1997;65(4):1251-7.

92.   Viebig NK, Gamain B, Scheidig C, Lépolard C, Przyborski J, Lanzer M, et al. A single member of the Plasmodium falciparum var multigene family determines cytoadhesion to the placental receptor chondroitin sulphate A. EMBO Rep. 2005;6(8):775-81.

93.   Fried M, Duffy PE. Adherence of Plasmodium falciparum to chondroitin sulfate A in the human placenta. Science. 1996;272(5267):1502-4.

94.   Moore KA, Simpson JA, Scoullar MJL, McGready R, Fowkes FJI. Quantification of the association between malaria in pregnancy and stillbirth: a systematic review and meta-analysis. Lancet Glob Health. 2017;5(11):e1101-e12.

95.   Dimonte S, Bruske EI, Enderes C, Otto TD, Turner L, Kremsner P, et al. Identification of a conserved var gene in different Plasmodium falciparum strains. Malar J. 2020;19(1):194.

96.   Srivastava A, Gangnard S, Dechavanne S, Amirat F, Lewit Bentley A, Bentley GA, et al. Var2CSA minimal CSA binding region is located within the N-terminal region. PLoS One. 2011;6(5):e20270.

97.   Pais TF, Penha-Goncalves C. Brain Endothelium: The "Innate Immunity Response Hypothesis" in Cerebral Malaria Pathogenesis. Front Immunol. 2018;9:3100.

98.   Pal P, Daniels BP, Oskman A, Diamond MS, Klein RS, Goldberg DE. Plasmodium falciparum Histidine-Rich Protein II Compromises Brain Endothelial Barriers and May Promote Cerebral Malaria Pathogenesis. mBio. 2016;7(3).

99.   Shio MT, Eisenbarth SC, Savaria M, Vinet AF, Bellemare MJ, Harder KW, et al. Malarial hemozoin activates the NLRP3 inflammasome through Lyn and Syk kinases. PLoS Pathog. 2009;5(8):e1000559.

100.   Sharma S, DeOliveira RB, Kalantari P, Parroche P, Goutagny N, Jiang Z, et al. Innate immune recognition of an AT-rich stem-loop DNA motif in the Plasmodium falciparum genome. Immunity. 2011;35(2):194-207.

101.   Johnstone RM, Adam M, Hammond JR, Orr L, Turbide C. Vesicle formation during reticulocyte maturation. Association of plasma membrane activities with released vesicles (exosomes). J Biol Chem. 1987;262(19):9412-20.

102.   Harding C, Heuser J, Stahl P. Endocytosis and intracellular processing of transferrin and colloidal gold-transferrin in rat reticulocytes: demonstration of a pathway for receptor shedding. Eur J Cell Biol. 1984;35(2):256-63.

103.   Tricarico C, Clancy J, D'Souza-Schorey C. Biology and biogenesis of shed microvesicles. Small GTPases. 2017;8(4):220-32.

104.   Babatunde KA, Yesodha Subramanian B, Ahouidi AD, Martinez Murillo P, Walch M, Mantel PY. Role of Extracellular Vesicles in Cellular Cross Talk in Malaria. Front Immunol. 2020;11:22.

105.   Nantakomol D, Dondorp AM, Krudsood S, Udomsangpetch R, Pattanapanyasat K, Combes V, et al. Circulating red cell-derived microparticles in human malaria. J Infect Dis. 2011;203(5):700-6.

106.   Regev-Rudzki N, Wilson DW, Carvalho TG, Sisquella X, Coleman BM, Rug M, et al. Cell-cell communication between malaria-infected red blood cells via exosome-like vesicles. Cell. 2013;153(5):1120-33.

107.   Dieckmann-Schuppert A, Franklin RM. Compounds binding to cytoskeletal proteins are active against Plasmodium falciparum in vitro. Cell Biol Int Rep. 1989;13(2):207-14.

108.   Mantel PY, Hoang AN, Goldowitz I, Potashnikova D, Hamza B, Vorobjev I, et al. Malaria-infected erythrocyte-derived microvesicles mediate cellular communication within the parasite population and with the host immune system. Cell Host Microbe. 2013;13(5):521-34.

109.   Mantel PY, Hjelmqvist D, Walch M, Kharoubi-Hess S, Nilsson S, Ravel D, et al. Infected erythrocyte-derived extracellular vesicles alter vascular function via regulatory Ago2-miRNA complexes in malaria. Nat Commun. 2016;7:12727.

110.   Sisquella X, Ofir-Birin Y, Pimentel MA, Cheng L, Abou Karam P, Sampaio NG, et al. Malaria parasite DNA-harbouring vesicles activate cytosolic immune sensors. Nat Commun. 2017;8(1):1985.

111. Ye W, Chew M, Hou J, Lai F, Leopold SJ, Loo HL, et al. Microvesicles from malaria-infected red blood cells activate natural killer cells via MDA5 pathway. PLoS Pathog. 2018;14(10):e1007298.

112. Havelange V, Garzon R. MicroRNAs: emerging key regulators of hematopoiesis. Am J Hematol. 2010;85(12):935-42.

113. O'Brien J, Hayder H, Zayed Y, Peng C. Overview of MicroRNA Biogenesis, Mechanisms of Actions, and Circulation. Front Endocrinol (Lausanne). 2018;9:402.

114. Denli AM, Tops BB, Plasterk RH, Ketting RF, Hannon GJ. Processing of primary microRNAs by the Microprocessor complex. Nature. 2004;432(7014):231-5.

115. Okada C, Yamashita E, Lee SJ, Shibata S, Katahira J, Nakagawa A, et al. A high-resolution structure of the pre-microRNA nuclear export machinery. Science. 2009;326(5957):1275-9.

116. Zhang H, Kolb FA, Jaskiewicz L, Westhof E, Filipowicz W. Single processing center models for human Dicer and bacterial RNase III. Cell. 2004;118(1):57-68.

117. Kristensen LS, Andersen MS, Stagsted LVW, Ebbesen KK, Hansen TB, Kjems J. The biogenesis, biology and characterization of circular RNAs. Nat Rev Genet. 2019;20(11):675-91.

118. Xu W, San Lucas A, Wang Z, Liu Y. Identifying microRNA targets in different gene regions. BMC Bioinformatics. 2014;15 Suppl 7(Suppl 7):S4.

119. Jo MH, Shin S, Jung SR, Kim E, Song JJ, Hohng S. Human Argonaute 2 Has Diverse Reaction Pathways on Target RNAs. Mol Cell. 2015;59(1):117-24.

120. Ameres SL, Horwich MD, Hung JH, Xu J, Ghildiyal M, Weng Z, et al. Target RNA-directed trimming and tailing of small silencing RNAs. Science. 2010;328(5985):1534-9.

121. Ketprasit N, Cheng IS, Deutsch F, Tran N, Imwong M, Combes V, et al. The characterization of extracellular vesicles-derived microRNAs in Thai malaria patients. Malar J. 2020;19(1):285.

122. Omer FM, Kurtzhals JA, Riley EM. Maintaining the immunological balance in parasitic infections: a role for TGF-beta? Parasitol Today. 2000;16(1):18-23.

123. Dandewad V, Vindu A, Joseph J, Seshadri V. Import of human miRNA-RISC complex into Plasmodium falciparum and regulation of the parasite gene expression. J Biosci. 2019;44(2).

124. Baum J, Papenfuss AT, Mair GR, Janse CJ, Vlachou D, Waters AP, et al. Molecular genetics and comparative genomics reveal RNAi is not functional in malaria parasites. Nucleic Acids Res. 2009;37(11):3788-98.

125. Chakrabarti M, Garg S, Rajagopal A, Pati S, Singh S. Targeted repression of Plasmodium apicortin by host microRNA impairs malaria parasite growth and invasion. Dis Model Mech. 2020;13(6).

126. Rathjen T, Nicol C, McConkey G, Dalmay T. Analysis of short RNAs in the malaria parasite and its red blood cell host. FEBS Lett. 2006;580(22):5185-8.

127. Guan T, Dominguez CX, Amezquita RA, Laidlaw BJ, Cheng J, Henao-Mejia J, et al. ZEB1, ZEB2, and the miR-200 family form a counterregulatory network to regulate CD8(+) T cell fates. J Exp Med. 2018;215(4):1153-68.

128. Majer A, Caligiuri KA, Gale KK, Niu Y, Phillipson CS, Booth TF, et al. Induction of Multiple miR-200/182 Members in the Brains of Mice Are Associated with Acute Herpes Simplex Virus 1 Encephalitis. PLoS One. 2017;12(1):e0169081.

129. Schulte LN, Eulalio A, Mollenkopf HJ, Reinhardt R, Vogel J. Analysis of the host microRNA response to Salmonella uncovers the control of major cytokines by the let-7 family. Embo j. 2011;30(10):1977-89.

130. Wang W, Knovich MA, Coffman LG, Torti FM, Torti SV. Serum ferritin: Past, present and future. Biochim Biophys Acta. 2010;1800(8):760-9.

131. Zou JX, Revenko AS, Li LB, Gemo AT, Chen HW. ANCCA, an estrogen-regulated AAA+ ATPase coactivator for ERalpha, is required for coregulator occupancy and chromatin modification. Proc Natl Acad Sci U S A. 2007;104(46):18067-72.

132. Zuehlke AD, Beebe K, Neckers L, Prince T. Regulation and function of the human HSP90AA1 gene. Gene. 2015;570(1):8-16.

133. Goh SH, Lee YT, Bouffard GG, Miller JL. Hembase: browser and genome portal for hematology and erythroid biology. Nucleic Acids Res. 2004;32(Database issue):D572-4.

134. Chen SY, Wang Y, Telen MJ, Chi JT. The genomic analysis of erythrocyte microRNA expression in sickle cell diseases. PLoS One. 2008;3(6):e2360.

135.   LaMonte G, Philip N, Reardon J, Lacsina JR, Majoros W, Chapman L, et al. Translocation of sickle cell erythrocyte microRNAs into Plasmodium falciparum inhibits parasite translation and contributes to malaria resistance. Cell Host Microbe. 2012;12(2):187-99.

136.   Trager W, Gill GS. Plasmodium falciparum gametocyte formation in vitro: its stimulation by phorbol diesters and by 8-bromo cyclic adenosine monophosphate. J Protozool. 1989;36(5):451-4.

137.   Ono T, Cabrita-Santos L, Leitao R, Bettiol E, Purcell LA, Diaz-Pulido O, et al. Adenylyl cyclase alpha and cAMP signaling mediate Plasmodium sporozoite apical regulated exocytosis and hepatocyte infection. PLoS Pathog. 2008;4(2):e1000008.

138.   Li J, Cox LS. Isolation and characterisation of a cAMP-dependent protein kinase catalytic subunit gene from Plasmodium falciparum. Mol Biochem Parasitol. 2000;109(2):157-63.

139.   Avril M, Brazier AJ, Melcher M, Sampath S, Smith JD. DC8 and DC13 var genes associated with severe malaria bind avidly to diverse endothelial cells. PLoS Pathog. 2013;9(6):e1003430.

140.   Azasi Y, Lindergard G, Ghumra A, Mu J, Miller LH, Rowe JA. Infected erythrocytes expressing DC13 PfEMP1 differ from recombinant proteins in EPCR-binding function. Proc Natl Acad Sci U S A. 2018;115(5):1063-8.

141.   Magallon-Tejada A, Machevo S, Cistero P, Lavstsen T, Aide P, Rubio M, et al. Cytoadhesion to gC1qR through Plasmodium falciparum Erythrocyte Membrane Protein 1 in Severe Malaria. PLoS Pathog. 2016;12(11):e1006011.

142.   Tuikue Ndam N, Moussiliou A, Lavstsen T, Kamaliddin C, Jensen ATR, Mama A, et al. Parasites Causing Cerebral Falciparum Malaria Bind Multiple Endothelial Receptors and Express EPCR and ICAM-1-Binding PfEMP1. J Infect Dis. 2017;215(12):1918-25.

143.   Shabani E, Hanisch B, Opoka RO, Lavstsen T, John CC. Plasmodium falciparum EPCR-binding PfEMP1 expression increases with malaria disease severity and is elevated in retinopathy negative cerebral malaria. BMC Med. 2017;15(1):183.

144.   Kessler A, Dankwa S, Bernabeu M, Harawa V, Danziger SA, Duffy F, et al. Linking EPCR-Binding PfEMP1 to Brain Swelling in Pediatric Cerebral Malaria. Cell Host Microbe. 2017;22(5):601-14 e5.

145.   McGuire W, Hill AV, Greenwood BM, Kwiatkowski D. Circulating ICAM-1 levels in falciparum malaria are high but unrelated to disease severity. Trans R Soc Trop Med Hyg. 1996;90(3):274-6.

146.   Joste V, Guillochon E, Fraering J, Vianou B, Watier L, Jafari-Guemouri S, et al. PfEMP1 A-Type ICAM-1-Binding Domains Are Not Associated with Cerebral Malaria in Beninese Children. mBio. 2020;11(6).

147.   Suurbaar J, Moussiliou A, Tahar R, Olsen RW, Adams Y, Dalgaard N, et al. ICAM-1-binding Plasmodium falciparum erythrocyte membrane protein 1 variants elicits opsonic-phagocytosis IgG responses in Beninese children. Sci Rep. 2022;12(1):12994.

148.   Alencar Filho AC, Lacerda MV, Okoshi K, Okoshi MP. Malaria and vascular endothelium. Arq Bras Cardiol. 2014;103(2):165-9.

149.   Chakravorty SJ, Carret C, Nash GB, Ivens A, Szestak T, Craig AG. Altered phenotype and gene transcription in endothelial cells, induced by Plasmodium falciparum-infected red blood cells: pathogenic or protective? Int J Parasitol. 2007;37(8-9):975-87.

150.   Tripathi AK, Sullivan DJ, Stins MF. Plasmodium falciparum-infected erythrocytes increase intercellular adhesion molecule 1 expression on brain endothelium through NF-kappaB. Infect Immun. 2006;74(6):3262-70.

151.   Viebig NK, Wulbrand U, Förster R, Andrews KT, Lanzer M, Knolle PA. Direct activation of human endothelial cells by Plasmodium falciparum-infected erythrocytes. Infect Immun. 2005;73(6):3271-7.

152.   Sokol CL, Luster AD. The chemokine system in innate immunity. Cold Spring Harb Perspect Biol. 2015;7(5).

153.   Glass WG, Hickey MJ, Hardison JL, Liu MT, Manning JE, Lane TE. Antibody targeting of the CC chemokine ligand 5 results in diminished leukocyte infiltration into the central nervous system and reduced neurologic disease in a viral model of multiple sclerosis. J Immunol. 2004;172(7):4018-25.

154.   Were T, Hittner JB, Ouma C, Otieno RO, Orago AS, Ong'echa JM, et al. Suppression of RANTES in children with Plasmodium falciparum malaria. Haematologica. 2006;91(10):1396-9.

155.   Borden EC, Sen GC, Uze G, Silverman RH, Ransohoff RM, Foster GR, et al. Interferons at age 50: past, current and future impact on biomedicine. Nat Rev Drug Discov. 2007;6(12):975-90.

156.   He X, Xia L, Tumas KC, Wu J, Su XZ. Type I Interferons and Malaria: A Double-Edge Sword Against a Complex Parasitic Disease. Front Cell Infect Microbiol. 2020;10:594621.

157.   deWalick S, Amante FH, McSweeney KA, Randall LM, Stanley AC, Haque A, et al. Cutting edge: conventional dendritic cells are the critical APC required for the induction of experimental cerebral malaria. J Immunol. 2007;178(10):6033-7.

158.   Montes de Oca M, Kumar R, Rivera FL, Amante FH, Sheel M, Faleiro RJ, et al. Type I Interferons Regulate Immune Responses in Humans with Blood-Stage Plasmodium falciparum Infection. Cell Rep. 2016;17(2):399-412.

159.   Vigário AM, Belnoue E, Grüner AC, Mauduit M, Kayibanda M, Deschemin JC, et al. Recombinant human IFN-alpha inhibits cerebral malaria and reduces parasite burden in mice. J Immunol. 2007;178(10):6416-25.

160.   Chebath J, Benech P, Revel M, Vigneron M. Constitutive expression of (2'-5') oligo A synthetase confers resistance to picornavirus infection. Nature. 1987;330(6148):587-8.

161.   Hornung V, Hartmann R, Ablasser A, Hopfner KP. OAS proteins and cGAS: unifying concepts in sensing and responding to cytosolic nucleic acids. Nat Rev Immunol. 2014;14(8):521-8.

162.   Liu YP, Berkhout B. miRNA cassettes in viral vectors: problems and solutions. Biochim Biophys Acta. 2011;1809(11-12):732-45.

163.   Lubiana P, Bouws P, Roth LK, Dörpinghaus M, Rehn T, Brehmer J, et al. Adhesion between P. falciparum infected erythrocytes and human endothelial receptors follows alternative binding dynamics under flow and febrile conditions. Sci Rep. 2020;10(1):4548.

164.   Rashad S, Han X, Saqr K, Tupin S, Ohta M, Niizuma K, et al. Epigenetic response of endothelial cells to different wall shear stress magnitudes: A report of new mechano-miRNAs. J Cell Physiol. 2020;235(11):7827-39.

165.   Raacke M, Kerr A, Dörpinghaus M, Brehmer J, Wu Y, Lorenzen S, et al. Altered Cytokine Response of Human Brain Endothelial Cells after Stimulation with Malaria Patient Plasma. Cells. 2021;10(7).

166.   Stevenson BR, Begg DA. Concentration-dependent effects of cytochalasin D on tight junctions and actin filaments in MDCK epithelial cells. J Cell Sci. 1994;107 (Pt 3):367-75.

6. Supplements:

6.1 Additional materials:

6.1.1 Chemical and biological reagents:

Reagents	Manufacturer
Accutase Cell Detachment Solution	PAN Biotech
Biocoll separating solution	Biochrom
Bovine Serum Albumin	Biomol
Descosept Pur	Ecolab
Dimethylsulfoxid (DMSO)	ROTH
D-Sorbitol	Sigma
Ethanol	Merck
Gelatin powder	Sigma
Gelatin solution	Sigma
Gentamicin	Ratiopharm
Giemsa solution	Merck
Glutaraldehyde (25%)	Merck
Glycerol	Merck
Human Blood (O$^+$)	Universitätsklinikum Hamburg-Eppendorf
Human brain endothelial cell medium, Supplement Kit (H1168-Kit)	Cell Biologics
Human Serum (A$^+$)	Interstate Blood Bank, (Memphis, TN, USA)
Human TNF-α	PeprotTech
Immersion oil	Zeiss
Penicillin-Streptomycin	Merck
RNase AWAY Spary	ROTH
Trizol Reagent	Life Technology

6.1.2   Kits and standards

Kits	Manufacturer
Aglient RNA 6000 Pico Kit	Aglient Technologies
Aglient High Sensitivity DNA Kit	Aglient Technologies
NestSeq 500/550 Mid Output Kit v2.5	Illumina
PureLink RNA Mini Kit	Thermo Fisher Scientific
QIAseq FastSelect RNA Removal Kit	Qiagen
QIAseq Stranded (m)RNA Library Kit	Qiagen
ScriptSeqTM v2 RNA-Seq Library Kit	Illumina

6.1.3   Cell lines

Cell	Manufacturer
Human primary brain microvascular endothelial cells (HBMEC), (PB-CH-1104011)	PELOBiotech

6.1.4   Antibodies

Host	Reactivity	Antigen	Fluorophore	Supplier	Accession#
Mouse	Human	CD54/ICAM-1	APC	Biolegend	322712
Mouse	Human	CD201/EPCR	APC	Biolegend	351906

6.2   Additional methods:

6.2.1   Cultivation of HBMECs

HBMECs were cultured in a T25 tissue culture flask pre-coated with gelatin-based solution and incubated in 5 ml of Culture Complete Growth Medium at 37°C and 5% CO_2. Cell viability and morphology were monitored daily using the EVOS XL inverted microscope.

6.2.2   Procedure for passaging HBMECs

Once the cell confluence reached 90%, passaging should be performed to avoid the cell density exceeding the capacity of the medium. At first, spent culture media was removed and residual media was carefully washed off with 1 ml PBS. Secondly, adherent HBMECs were treated with 500 ul accutase and incubated at 37 °C until cells are fully detached from the flask. Thirdly, 10 ml of culture media was added to the flask to inhibit the digestion of accutase. Finally, dispersed cell suspension was divided evenly into two gelatin-precoated T25 flasks and incubated as usual.

6.2.3   Freezing of HBMECs

After cells were detached by accutase as mentioned above, cells were resuspended with 5 ml culture medium and spun down at 1200 g for 2 min. Then, supernatant was withdrawn and the pellet was dispersed in 1 ml HBMECs freezing media. Afterwards, the suspension was transferred into a cryovial and placed in a "Mr Frosty" freezing container containing 100% isopropyl alcohol at –80 °C for 24 h. In the end, vials were transferred to liquid N_2 for indefinite storage.

6.2.4   Thawing of HBMECs

Cryovial was thawed by promptly incubating in a 37 °C water bath for 1 min. Cryopreserved cells were dispersed in 5 ml prewarmed HBMECs culture medium and spun down at 1200 rpm for 2 min. The pellet was resuspended in 5 ml culture media and cultured following standard protocol.

6.2.5   Enrichment of IEs over HBMECs

Enrichment experiments were conducted when the parasitemia reached 5% and trophozoites were dominant in the culture. At first, knob enrichment was performed to separate trophozoite-stage parasites. A blood smear was made to ensure the culture contains at least 70% trophozoites. HBMECs were pre-incubated with RPMI serum-free media for 5 min. After that, trophozoites were resuspended in 5 ml RPMI serum-free media and co-incubated with HBMECs in a 37°C incubator for 1 hour. During co-incubation, the flask was shaken gently in different directions, in order to enable each iRBC to have the chance to communicate with HBMECs. After co-

incubation, HBMECs were carefully washed by RPMI serum-free media to remove unbound iRBCs whereas binding iRBCs were kept in the flask. Images of adherence status were taken under an EVOS XL microscope. Subsequently, 5 ml RPMI culture media and 300 ul erythrocytes were added to the flask and cultured in a 37°C incubator till the next day.

On the next day, trophozoites developed into rings and detached from HBMECs. Erythrocytes were transferred into a falcon and spun down at 2,000 rpm for 5 min. Afterwards, the pellet was resuspended in 7ml RPMI serum-free media and gently placed on top of 7 ml Biocoll solution in another falcon, enabling a clear boundary between the two layers. The flacon was centrifuged at 2,300 rpm for 5 min without brake. Finally, the pellet was supplied with 10 ml RPMI culture media and 300 ul of human blood and cultured as usual.

This procedure was repeated for several rounds until an intense cytoadherence was observed.

6.2.6 TNF-α treatment for HBMECs

10 ng/ml of TNF-α was added to the culture supernatant 24 h before analysis.

6.2.7 Co-incubation experiment

IT4 enriched over TNF-α-activated HBMECs was used in co-incubation experiments. The experiments were performed when trophozoites dominated the culture and the confluence of HBMECs reached at least 70% in T25 flasks. At first, parasites were synchronized by 1% gelatin solution and trophozoites were collected. HBMECs were washed with 5 ml RPMI serum-free media. Afterwards, 3×10^6 trophozoites were resuspended in 5 ml RPMI serum-free media and added to each HBMECs culture flask in a 37 °C incubator. During the first hour of coincubation, culture flasks were shaken gently in different directions. Afterwards, unbound iRBCs were washed off with RPMI serum-free media whereas remaining bound iRBCs were continued for a further 3 h or 7 h of coincubation. At the end of coincubation, culture supernatant was collected in flacons and HBMECs were detached and lysed in 4 ml TRIzol. Samples were stored at -80 °C until further use.

6.2.8   Flow cytometry

On the day of assay, HBMECs were washed twice in FACS buffer (1*PBS, 2%FBS). Afterward, cells were incubated with 2 μl of anti-human-APC-conjugated antibodies against ICAM-1 (100 μg/ml) or EPCR (100 μg/ml) for 15 mins over ice. All samples were resuspended in 500 μl of FACS buffer and analyzed on a Becton-Dickinson Accuri C6 flow cytometer by counting 20,000 events. The median fluorescence intensity (MFI) of samples was analyzed using FLOWJO 10.7 software. Normalized median fluorescence intensity (nMFI) was calculated by dividing the MFI of the stained sample by the MFI of the negative control.

6.3 Additional results:
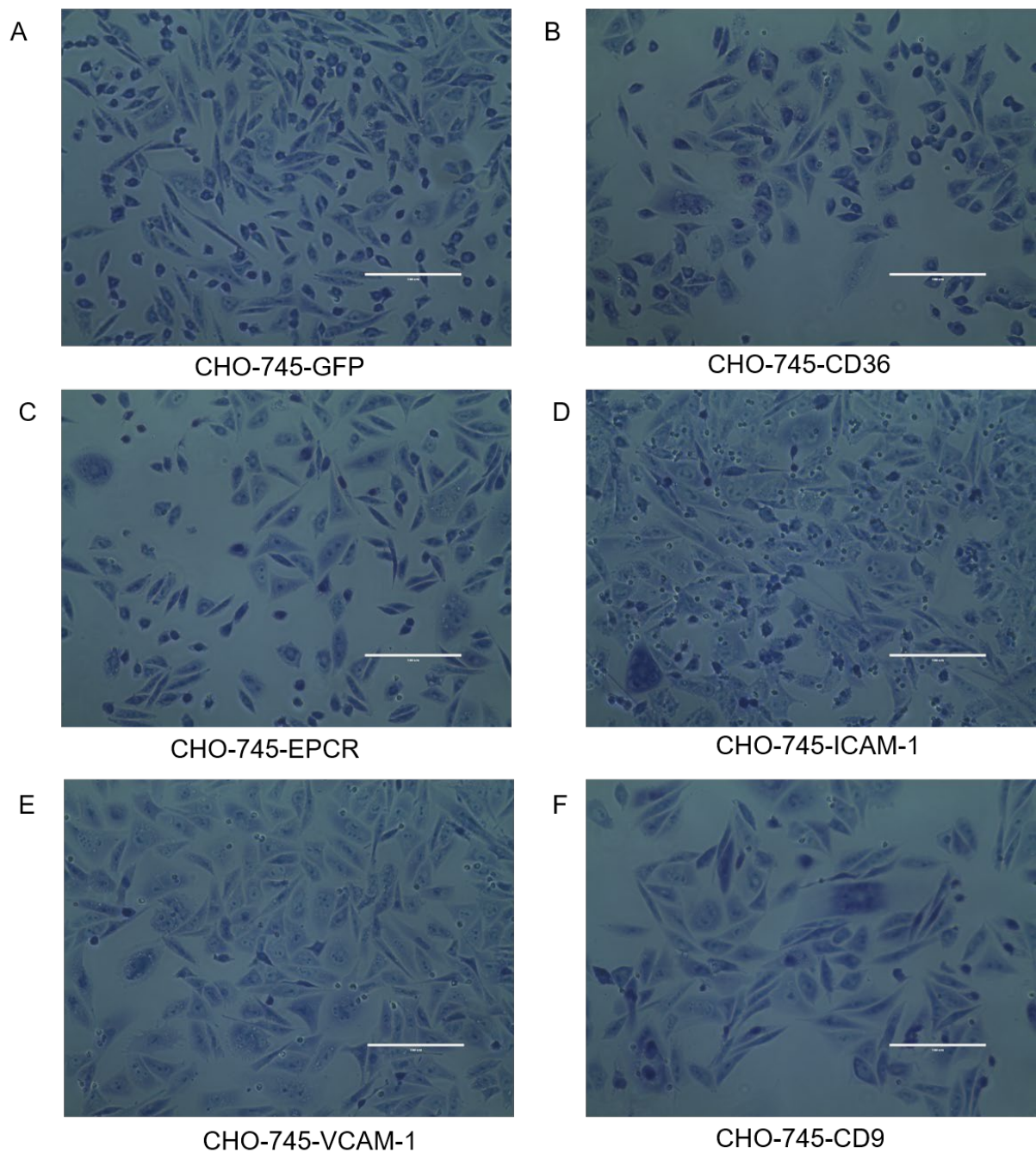
Supp. Figure 1: Binding properties of enriched IT4 to various endothelial receptors. CHO-745-GFP **(A)** and CHO-745 overexpressing CD36 **(B)**, -EPCR **(C)**, -ICAM-1 **(D)**, -VCAM-1 **(E)** and -CD9 **(F)** were seeded on cover slips in 24-well plate and co-incubated with IT4-HBMEC-TNF-α. The cover slips were fixed with 1% glutaraldehyde and finally stained with Giemsa solution. Pictures were taken after washing steps with EVOS XL inverted microscope at a 400 × magnification. Scale bars = 100 μm.
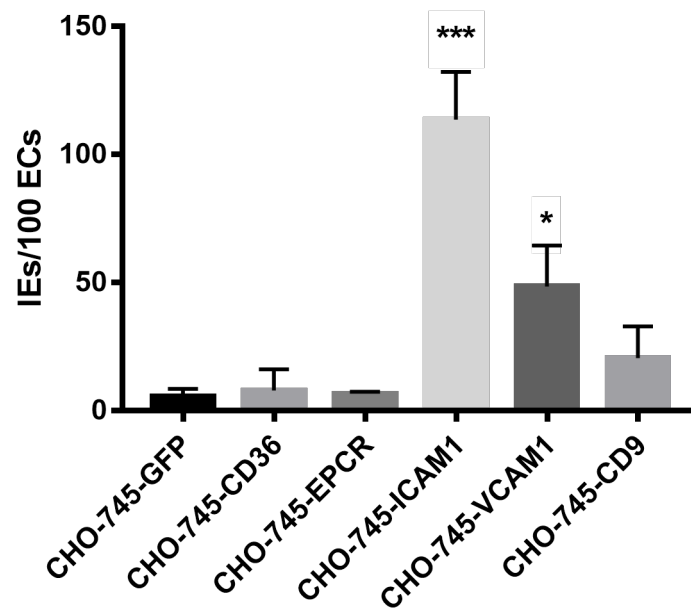
Supp. Figure 2: Quantification of enriched IT4 to various endothelial receptors. The number of IEs bound to 100 CHO cells were examined three times for each experimental replicate. Data are shown as Mean $\pm$ SD and analyzed by unpaired t-test. *, $p < 0.05$; ***, $p < 0.001$.

6.4　Additional table and text

Supp. Table 1. Part of the miRNA profile analysis of riRBCs and trRBCs compared to niRBCs.

Name	RBCs-1	RBCs-2	RBCs-3	RBCs-4	RBCs-5	RBCs-6	Rings-1	Rings-2	Rings-3	Rings-4	Rings-5	Rings-6	Rings-7	Rings-8	Rings-9	Tophs-1	Tophs-2	Tophs-3	Tophs-4	Tophs-5	Tophs-6	Tophs-7	Tophs-8	Tophs-9	Rings-FC	Log2FC	R-P-value	Rings-FDR	Trophs-FC	Trophs-Log2FC	T-P-value	Trphs-FDR
hsa-miR-427	36	41	72	36	5	11	50	111	182	267	170	520	297	171	16	548	539	556	366	876	361	137	343	284	8.697258	3.120561	7.12E-09	5.32E-06	24.82206	4.633551	2.73E-17	2.57E-14
hsa-miR-139	313	313	526	308	404	966	73	42	26	46	24	24	34	141	26	53	54	54	34	24	49	36	11	18	5.89671	-2.55991	5.97E-08	3.23E-05	-6.89575	-2.78571	1E-10	1.57E-08
hsa-miR-322341	61181	61181	26168	144851	40658	36578	5466	6790	4335	28869	30061	1960	4766	6977	2642	19465	1676	4726	3199	4542	3606	4726	3200	2754	5.29881	-2.40567	1.08E-07	2.7E-05	-7.39699	-2.88694	2.82E-13	6.62E-11
hsa-miR-7	707496	716146	826609	162401	320825	1827598	182877	255957	183220	123938	129876	97359	129720	285525	71116	160091	117971	125428	84990	53401	64104	116588	86980	61997	5.00648	-2.3238	3.12E-07	5.83E-05	-7.80697	-2.96476	1.64E-13	6.62E-11
hsa-let-7	3387	1867	1347	2897	14659	17167	251	1248	672	3408	529	218	196	357	124	762	801	254	108	407	524	234	131	78	-6.80927	-2.7675	8.78E-07	0.000131	-11.8549	-3.56741	2.39E-13	6.62E-11
hsa-miR-30	3	2	3	11	2	4	3	4	6	19	11	69	96	9	29	36	3	18	43	11	69	26	24	41	12.76183	3.673763	3.91E-06	0.000487	11.76386	3.55629	5.23E-05	0.001754
hsa-miR-14458	12400	12400	5423	3089	27047	27578	1546	919	945	2354	2429	1903	847	5560	771	2438	692	1476	829	2488	2067	958	854	610	-4.61968	-2.20779	4.69E-06	0.000501	-4.98229	-2.31681	1.04E-06	5.15E-05
hsa-miR-130	337	337	34	758	69	151	6	6	3	53	51	18	6	39	6	11	5	0	0	10	11	2	3	3	-7.94866	-2.99071	1.89E-05	0.001659	-17.7097	-4.14647	5.36E-11	1.01E-08
hsa-miR-49072	11407	11407	16087	109564	6275	16545	2805	1594	1384	15162	12409	3564	2403	8192	1550	9720	1876	2789	1976	4537	3458	1463	1040	847	-4.52217	-2.17701	1.2E-05	0.001682	-5.6954	-2.5098	2.9E-07	1.95E-05
hsa-miR-354	128	128	395	128	228	474	79	47	83	77	47	40	52	123	55	122	66	100	50	32	28	57	18	10	-3.31664	-1.72972	2.26E-05	0.001682	-4.07726	-2.0276	6.24E-05	0.00202
hsa-miR-550	26	38	17	26	2	19	37	13	20	541	568	128	79	193	13	34	6	2	68	32	2	26	15	4	6.522302	2.705381	2.47E-05	0.001682	1.200955	0.264182	0.729429	0.861356
hsa-miR-5374	5586	5586	11380	2294	14588	12187	2869	2068	1351	1914	1288	818	1345	2035	639	914	1460	1675	1256	806	1234	1147	590	368	3.47497	1.797	4.15E-05	0.002585	4.85645	-2.2799	1.25E-09	1.31E-07
hsa-miR-12490	2923	2923	3585	1289	4022	4719	752	675	551	791	643	505	572	1192	406	836	842	695	400	553	667	455	249	199	-3.23186	-1.69236	5.53E-05	0.003183	-3.54892	-1.82738	6.33E-07	3.72E-05
hsa-let-7	1470299	832607	1744143	556343	3001318	3156040	306562	502489	332580	714120	695160	388011	1336	779344	228665	401517	266159	305788	223964	122436	180476	343398	234127	188306	-2.60797	-1.38293	0.000102	0.005236	-4.05696	-2.0204	8.54E-09	8.03E-07
hsa-miR-48171	8065	8065	12972	6818	8331	10169	9211	12061	10441	27523	26316	18788	11935	32125	8314	30711	1357.1	9839	7925	1429	10361	10027	5440	4388	2.475123	1.3075	0.000105	0.005236	2.037193	1.027483	0.000544	0.019102
hsa-miR-390	189	189	179	167	189	269	44	37	14	50	24	38	23	46	4	51	20	6	8	40	6	14	7	6	-4.1337	-2.04743	0.00013	0.006096	-5.83354	-2.54437	2.84E-07	1.95E-05
hsa-miR-43	12	12	4	111	7	8	1	13	11	8	17	8	0	11	2	61	22	6	1	13	0	4	3	2	-9.09	-3.18428	0.000206	0.008564	-17.6447	-4.14116	7.12E-05	0.001557
hsa-let-7	1144	39	50	271	616	1025	184	110	153	673	570	578	319	215	174	839	391	419	403	647	420	260	312	281	4.98823	2.317253	0.000309	0.012156	8.659381	3.114264	1.27E-06	5.7E-05
hsa-miR-360	61	61	13	72	19	27	8	13	14	14	19	8	5	3	0	24	2	6	8	13	7	4	3	2	-4.86405	-2.77088	0.000126	0.011243	-6.82526	-2.77088	0.000126	0.003119
hsa-miR-530	68	68	106	64	32	70	32	104	70	384	241	135	112	242	61	321	89	91	70	5	48	11	86	30	3.065262	1.616011	0.000427	0.015223	2.286686	1.192583	0.012647	0.073839
hsa-miR-30	10	10	0	10	40	7	1	1	1	2	0	0	0	1	0	0	0	0	5	87	0	0	1	0	-57.2211	-5.83847	0.000515	0.017522	2.090738	1.064013	0.391573	0.616547
hsa-miR-56	14	14	14	10	4	8	1	0	1	1	0	1	2	0	0	4	0	0	0	13	0	0	3	2	-6.36076	-2.6692	0.000541	0.0176	-6.37234	-2.67182	0.004098	0.037898
hsa-let-7	183106	113368	226384	89393	544880	412009	48917	72333	43210	124878	132339	76234	59919	137591	29579	61946	38809	48473	29273	28474	35277	39951	30159	27523	2.44704	1.29104	0.000592	0.018238	4.0094	2.00339	9.54E-09	8.16E-07
hsa-miR-82	184	184	109	145	66	87	18	14	17	64	44	35	25	12	17	97	18	30	22	10	45	23	11	15	3.1028I	-1.63357	0.00061	0.018238	-3.82814	-1.93664	0.000476	0.008598
hsa-miR-4147	24263	116	250	1411	109	277	26	29	9	206	218	45	45	221	22	97	9	27	18	0	47	111	20	15	3.85638	-1.94725	0.000865	0.0295	-6.73658	-2.75202	1.19E-06	5.6E-05
hsa-miR-860	92	92	139	132	84	58	162	169	84	255	297	181	181	206	76	110	61	156	102	48	78	136	98	86	2.605085	1.381331	0.000853	0.0295	1.870589	0.903492	0.048413	0.173697
hsa-miR-415	14	14	18	354	11	43	2	3	5	50	33	5	4	10	4	3	3	2	2	11	0	2	45	40	5.22683	-2.38594	0.000979	0.026151	-30.8014	-4.94492	3.68E-08	2.89E-06
hsa-miR-3113	127	127	160	80	63	136	195	146	139	306	268	153	62	557	172	547	82	237	241	198	195	107	37	40	2.53499	1.34198	0.001022	0.026354	2.579104	1.3687	0.005149	0.042832
hsa-miR-139	29	29	73	49	37	76	88	44	56	177	134	96	78	324	119	200	85	136	114	144	88	83	37	45	3.302713	1.723652	0.00143	0.028138	3.474218	1.796688	9.19E-05	0.002618
hsa-miR-37	9	9	2	2	6	4	3	1	7	7	21	5	41	8	0	6	2	0	4	18	14	4	2	4	8.24316	3.043198	0.001173	0.028138	3.296951	1.721133	0.001204	0.192283
hsa-miR-380	380	309	304	156	330	633	68	70	59	150	172	87	73	210	27	93	49	63	2	27	55	73	38	34	2.73264	-1.4503	0.001271	0.028818	-2.9305	-1.57194	0.05872	0.194174
hsa-miR-24263	11942	11942	10161	6460	26520	18735	8696	2706	2971	2315	3483	2794	3177	7785	2875	4326	3734	5224	11491	5641	5409	3993	2134	951	-2.67608	1.42012	0.001417	0.03117	3.52638	1.81819	0.00271	0.005594
hsa-miR-103	92	92	68	196	130	146	26	20	49	88	103	3	16	20	9	49	33	35	5	15	18	16	24	12	3.22024	-1.68717	0.001697	0.036259	-4.16663	-2.05888	8.55E-05	0.002532
hsa-miR-46	7	7	34	38	110	7	35	50	39	19	17	5	32	13	24	26	32	46	16	24	4	38	6	12	3.593314	1.845315	0.002225	0.046232	3.158781	1.659368	0.004265	0.038548
hsa-miR-1239	144	144	2881	170	275	544	26	50	49	114	135	54	65	133	32	141	55	16	32	17	18	34	29	27	2.64503	1.40329	0.002667	0.054326	3.81791	1.93278	0.000401	0.00173
hsa-miR-442	2221	2221	638	638	650	1400	84	87	71	305	295	141	108	269	96	191	74	101	54	147	143	97	72	28	2.75657	-1.46288	0.002937	0.055436	3.3972	-1.76435	0.000112	0.002929
hsa-miR-64	10	10	0	49	12	1	4	3	0	5	5	0	2	4	0	17	5	0	0	0	7	2	0	0	13.59479	3.764982	0.00283	0.055436	14.64696	3.87253	0.010016	0.064934
hsa-miR-98	11	11	12	35	19	20	1	146	101	874	913	32	90	212	60	497	17	126	83	146	136	93	80	37	4.67156	2.2239	0.002965	0.055436	-3.64657	-1.86654	0.03385	0.112155
hsa-miR-100	71	71	94	35	93	93	7	22	23	14	11	0	20	51	10	32	16	20	0	27	34	26	8	12	2.95193	-1.56166	0.00313	0.057122	-2.38036	-1.25118	0.014453	0.08039
hsa-miR-3421	357	357	268	1160	268	439	83	67	34	466	443	22	49	100	23	193	12	70	29	31	46	50	46	50	3.1804	-1.66921	0.003735	0.063824	-5.10153	-2.35093	4.7E-07	2.95E-05
hsa-miR-30	1	1	2	1	8	2	3	0	0	0	101	0	2	3	1	3	1	3	0	15	3	65	64	1	-5.01332	-2.32577	0.003754	0.063824	41.66382	5.380723	2.8E-05	0.00013
hsa-miR-46	10	10	4	1	8	20	0	0	1	19	17	0	0	1	2	0	5	16	0	24	4	0	0	2	-7.72656	-2.94983	0.003877	0.06444	-9.36678	-3.22755	0.001591	0.019172
hsa-miR-13	13	13	4	170	12	33	26	50	49	114	135	54	108	133	32	141	55	101	54	77	18	34	28	27	-7.72656	-3.4987	0.00308	0.06444	11.3127	-3.4987	0.14725	0.031129
hsa-miR-5	6	6	13	4	19	12	1	5	1	0	3	0	2	3	0	3	3	7	3	7	7	0	2	7	-4.49208	-2.16738	0.004408	0.071676	3.3972	1.19041	0.14725	0.035877
hsa-miR-64	8	8	6	12	12	15	2	3	2	5	1	4	0	4	0	0	5	0	2	2	0	0	7	0	-4.27106	-2.09459	0.004546	0.072354	6.41712	-2.68193	0.003048	0.031129
hsa-miR-862	947	947	511	2412	861	935	140	146	101	874	913	32	90	212	60	497	17	126	83	146	136	93	80	37	-3.56742	-1.83488	0.00488	0.074117	-5.30226	-2.40661	9.6E-05	0.002655
hsa-miR-58	73	84	116	73	47	69	21	15	6	19	30	18	15	57	8	14	9	15	11	18	16	31	30	18	-2.73484	-1.45146	0.004826	0.074117	-4.24275	-2.085	0.0042	0.038334
hsa-miR-33244	32244	24639	33960	22555	1108	996	3604	2804	2534	5434	5941	3805	3759	4439	1558	5913	3231	3418	1985	1038	1270	3651	2263	2129	2.146001	1.101651	0.004954	0.074117	1.934211	0.951745	0.016706	0.098721

73

Supp. Table 2. Part of the miRNA profile analysis of riRBC-EVs and trRBC-EVs compared to niRBC-EVs.

Name	RBCs-1	RBCs-2	RBCs-3	RBCs-4	RBCs-5	Rings-1	Rings-2	Rings-3	Rings-4	Rings-5	Trophs-1	Trophs-2	Trophs-3	Trophs-4	Trophs-5	Rings-FC	Log2FC	R-P-value	Rings-FDR	Trophs-FC	Log2FC	T-P-value	Trophs-FDR
hsa-miR-200a-3p	11	1	0	2	286	755	21	74	6	233	759	54	0	0	284	42.9920075	5.4259967	2.4753E-06	0.00174954	18.3415169	4.19704105	0.0008421	0.09646236
hsa-miR-483-3p	5	0	1	212	43	43	6	778	1	59	8	873	3	19	21	49.3871182	5.62606288	5.1742E-06	0.00174954	30.6800558	4.9392292	2.8365E-05	0.0192052
hsa-miR-200b-3p	2	0	0	1	111	416	2	43	2	102	358	39	0	0	127	58.2128759	5.86326639	5.2539E-06	0.00174954	26.3923138	4.7220459	0.00034261	0.06845299
hsa-miR-31-5p	26	0	32	102	271	117	64	138	83	279	47	17	0	3	243	15.1329655	3.91962283	0.00013519	0.01321989	1.74673286	0.80465898	0.49359182	0.75393767
hsa-miR-18b-5p	39	16	0	912	924	2	0	0	0	0	12	5	0	0	17	-10.683675	-6.7392642	0.00013519	0.0250409	-11.547418	-3.5294984	0.00148729	0.14857997
hsa-miR-10a-5p	157	10	94	1564	260	2379	6	366	213	292	2425	439	0	20	293	11.3652991	3.50656375	0.0001504	0.0250409	5.59731908	2.48473599	0.00761379	0.25353926
hsa-miR-6826-3p	0	94	0	1	151	0	0	0	88	7	3	0	0	374	0	276.073632	8.10890929	0.0005575	0.07956349	-5.4116574	-2.4360705	0.60422191	0.77324222
hsa-miR-1255b-5p	20	12	28	1539	1930	0	0	0	7	0	3	0	0	0	0	-31.810055	-4.991411	0.0006641	0.0829299	-48.352524	-5.5955193	0.00014734	0.0367972
hsa-miR-100-5p	153	13	128	113	151	973	113	846	101	125	392	439	15	374	258	6.80212549	2.76598562	0.0009281	0.09450732	2.78504353	1.47769988	0.0754385	0.47843185
hsa-miR-455-3p	0	0	0	3	7	10	1	21	1	11	7	33	0	6	9	39.2146901	5.29332229	0.00109355	0.09450732	32.2586719	5.01161514	0.00055466	0.0875112
hsa-miR-1247-5p	0	0	0	0	0	4	0	5	1	2	8	3	0	0	1	103.03061	6.68692921	0.00124501	0.09450732	64.1168507	6.00263166	0.00615277	0.23246074
hsa-miR-122-3p	0	1	1	46	3	6	1	16	3	6	7	482	3	142	1	24.1693154	4.59510471	0.00125144	0.09450732	31.558956	4.97997758	5.7719E-05	0.00192052
hsa-miR-34a-5p	31	5	69	452	253	447	0	370	185	174	372	362	7	290	220	7.88153697	2.978477	0.00125501	0.09450732	7.12600015	2.83309251	0.00221181	0.01853911
hsa-miR-6726-3p	2	0	1	8	3	6	3	16	73	25	11	15	1	142	3	43.8838629	5.45561862	0.00132443	0.09450732	-24.040418	-4.5873901	0.33712927	0.7016029
hsa-miR-376a-3p	0	1	0	2	3	6	0	16	6	6	11	15	0	290	0	26.764175	4.74223132	0.00146212	0.09737706	18.068012	4.17536587	0.0028927	0.01947835
hsa-miR-675-3p	0	0	0	0	0	27	0	27	1	0	23	15	0	0	0	218.091356	7.7688787	0.00155981	0.09739048	106.616763	6.73629048	0.01040017	0.2660441
hsa-miR-10b-5p	84	1	8	979	103	579	1	150	27	130	630	214	3	9	250	9.1466318	3.1932707	0.00205569	0.1208017	5.1383339	2.3613005	0.023796	0.37466563
hsa-miR-196a-5p	19	12	12	8	14	197	0	100	5	1	197	142	6	0	1	13.8260856	3.78932086	0.00241071	0.1250475	7.52760908	2.91219171	0.02538691	0.37466563
hsa-miR-125b-2-	0	0	5	5	1	7	0	11	4	3	0	4	7	0	0	29.9889194	4.90635763	0.00244403	0.1285047	16.7992002	4.0703206	0.01538703	0.30743278
hsa-miR-10a-3p	0	0	0	2	0	12	0	7	0	0	12	4	0	0	0	84.1512759	6.39491324	0.00279245	0.1324019	34.6869118	5.1163195	0.00849471	0.2564743
hsa-miR-375-3p	8	2	21	21	364	59	16	147	15	277	34	178	9	7	328	11.627812	3.53950775	0.0028105	0.1324019	7.82648283	2.96836412	0.00606614	0.23246074
hsa-miR-137-3p	0	0	0	1	0	2	0	6	1	6	3	3	0	0	1	58.5349538	5.87122647	0.00291576	0.1324019	14.5101373	3.85899926	0.0298818	0.37466563
hsa-miR-615-3p	0	0	2	0	1	29	2	4	1	3	24	3	2	0	1	28.0065078	4.8076902	0.00316423	0.1374378	13.0757375	3.7088204	0.03167404	0.38123336
hsa-miR-3659	0	0	59	21	0	15	0	0	0	0	0	0	0	0	0	168.375469	7.39553816	0.004068	0.1454608	#N/A	#N/A	#N/A	#N/A
hsa-miR-204-5p	60	1	0	1103	57	102	4	38	733	260	105	78	5	272	351	7.01760139	2.810978	0.0041177	0.1454608	4.73390645	2.240312	0.02063043	0.34931859
hsa-miR-106a-5p	16	0	0	907	224	0	0	1	0	0	0	1	0	0	32	-33.776094	-5.079306	0.0042806	0.1454608	-3.87489	-1.954154	0.16212888	0.56006542
hsa-miR-199a-3p	393	4	195	1514	686	670	29	1477	338	277	829	1470	23	11	333	5.31287974	2.40949406	0.0045853	0.1454608	2.82554759	1.49853049	0.09410349	0.49213009
hsa-miR-202-5p	7	16	0	0	5	0	0	2	0	2	0	2	0	0	0	-102.99309	-6.6864038	0.0046695	0.1454608	-1469.2374	-10.520852	0.03571983	0.38732134
hsa-miR-376b-5p	0	0	0	0	0	7	0	2	0	0	0	0	0	0	0	96.7050508	6.59551934	0.0046748	0.1454608	10.6167727	3.40827338	0.08509078	0.47993602
hsa-miR-193a-3p	0	1	1	2	1	2	0	9	2	3	3	14	0	0	2	24.169376	4.59510832	0.0047325	0.1454608	20.8821434	4.3841979	0.01339538	0.30743278
hsa-miR-339-5p	9	4	25	464	24	2	0	2	1	1	4	5	1	0	20	-14.505557	-3.8585338	0.0047578	0.1454608	-4.7283478	-2.2413362	0.04825352	0.3920295
hsa-miR-629-5p	14	0	0	980	355	1	0	1	0	0	8	3	0	0	15	-29.735044	-4.8940923	0.0050182	0.1454608	-5.5974269	-2.4847638	0.06466724	0.45494768
hsa-miR-1271-3p	0	0	0	0	0	1	2	4	1	2	1	5	0	0	1	101.6646	6.6676736	0.0050184	0.1454608	#N/A	#N/A	#N/A	#N/A
hsa-miR-24-1-3p	0	0	5	0	16	102	4	26	5	37	15	19	0	24	6	53.3402229	5.73720063	0.0052906	0.1454608	36.7848796	5.20104096	0.00908685	0.25936464
hsa-miR-214-5p	0	35	158	15	16	11	7	50	5	242	56	29	0	194	163	11.6816933	3.54617751	0.0053556	0.1454608	3.99563891	1.99842621	0.17840339	0.56006542
hsa-miR-454-3p	374	0	2	11964	5381	1	0	20	0	5	16	16	0	0	0	-6.9691407	-2.8009808	0.0054419	0.1454608	-3.2441322	-1.6978326	0.09841087	0.49864998
hsa-miR-455-5p	0	0	0	2	8	6	0	1	0	0	4	4	0	0	1	23.997492	4.58481177	0.0056921	0.1454608	14.1209961	3.8197696	0.01346077	0.30743278
hsa-miR-493-3p	0	0	0	0	13	6	0	1	1	0	13	5	0	1	1	76.4637988	6.25670497	0.0057837	0.1454608	47.8021752	5.57900436	0.00796495	0.2564743
hsa-miR-130b-3p	0	0	21	570	117	495	26	20	0	74	424	17	3	1	70	-30.117984	-4.9125533	0.0058049	0.1454608	-3.876603	-1.954793	0.13268958	0.56006542
hsa-miR-429	8	11	0	9	79	9	0	3	3	0	12	7	0	0	0	11.0880284	3.47093095	0.0058276	0.1588455	4.22780337	2.07990828	0.11895109	0.05328956
hsa-miR-100-3p	0	0	0	0	0	9	0	10	0	5	12	7	0	3	1	54.2465564	5.76145965	0.0063976	0.1588455	15.8532487	3.9867066	0.04635437	0.3920295
hsa-let-7e-3p	1	0	0	4	2	9	2	4	1	2	1	5	0	0	1	26.3555766	4.72003635	0.0069594	0.1655346	18.1680811	4.18333415	0.0097631	0.2636404
hsa-miR-622	0	1	3	0	0	9	1	3	2	0	6	15	0	24	1	102.543495	6.68009216	0.0074051	0.1720426	#N/A	#N/A	#N/A	#N/A
hsa-miR-320c	62	1	3	538	353	0	0	3	0	3	6	15	0	24	71	-13.002732	-3.7007428	0.0079846	0.1812868	-1.0659312	-0.0921143	0.92274719	0.94935576
hsa-miR-6849-5p	0	0	0	0	0	9	0	2	0	19	0	0	0	0	0	71.2225193	6.15426156	0.0097799	0.21285514	#N/A	#N/A	#N/A	#N/A
hsa-miR-127-3p	259	7	17	139	85	852	11	199	23	178	802	216	10	244	20	6.65220737	2.73383314	0.0099662	0.21285514	4.81792839	2.26841295	0.02893667	0.37466563
hsa-miR-1228-3p	0	0	0	61	6	0	13	0	0	0	1	0	0	20	2	42.1458815	5.39731975	0.0100142	0.21285514	2.07587348	1.05371851	0.53883779	0.75923673
hsa-miR-335-3p	0	0	2	0	1	1	0	4	3	1	1	5	1	0	0	20.1944509	4.33586701	0.0102335	0.21229627	18.5184843	4.21089412	0.01785632	0.32879501
hsa-miR-5090	0	0	0	0	1	1	0	0	0	0	0	0	0	0	0	83.1196437	6.37711756	0.0106621	0.21737795	#N/A	#N/A	#N/A	#N/A
hsa-miR-200c-3p	4	0	2	0	307	133	0	19	4	238	107	21	0	1	296	10.9258342	3.4496715	0.0113368	0.22571525	7.12780838	2.83345855	0.0290864	0.37466563

Supp. Table 3. Part of the target genes prediction of differentially expressed miRNAs.

ID	Source	Confidence	Symbol
hsa-miR-122b-3p	TargetScan Human	High (predicted)	AGTR1
hsa-miR-122b-3p	TargetScan Human	High (predicted)	CASP7
hsa-miR-122b-3p	TargetScan Human	High (predicted)	FBP1
hsa-miR-122b-3p	TargetScan Human	High (predicted)	FGF14
hsa-miR-122b-3p	TargetScan Human	High (predicted)	FPR2
hsa-miR-122b-3p	TargetScan Human	High (predicted)	HLA-DQA2
hsa-miR-122b-3p	TargetScan Human	High (predicted)	IL22RA2
hsa-miR-122b-3p	TargetScan Human	High (predicted)	LAMP1
hsa-miR-122b-3p	TargetScan Human	High (predicted)	NEK7
hsa-miR-122b-3p	TargetScan Human	High (predicted)	PNPLA8
hsa-miR-122b-3p	TargetScan Human	High (predicted)	PPP1CC
hsa-miR-122b-3p	TargetScan Human	High (predicted)	RHOB
hsa-miR-122b-3p	TargetScan Human	High (predicted)	TFRC
hsa-miR-122b-3p	TargetScan Human	High (predicted)	TP53
hsa-miR-1245b-5p	TargetScan Human	High (predicted)	CATSPER
hsa-miR-1245b-5p	TargetScan Human	High (predicted)	CTSO
hsa-miR-1245b-5p	TargetScan Human	High (predicted)	GABRA1
hsa-miR-1245b-5p	TargetScan Human	High (predicted)	GNG12
hsa-miR-1245b-5p	TargetScan Human	High (predicted)	IL17B
hsa-miR-1245b-5p	TargetScan Human	High (predicted)	MAPK13
hsa-miR-1245b-5p	TargetScan Human	High (predicted)	MMP19
hsa-miR-1245b-5p	TargetScan Human	High (predicted)	PRDX2
hsa-miR-1245b-5p	TargetScan Human	High (predicted)	PRKCI
hsa-miR-1245b-5p	TargetScan Human	High (predicted)	RAP1B
hsa-miR-1245b-5p	TargetScan Human	High (predicted)	TCF7
hsa-miR-135a-3p	TargetScan Human	High (predicted)	APEX1
hsa-miR-135a-3p	TargetScan Human	High (predicted)	BRS3
hsa-miR-135a-3p	TargetScan Human	High (predicted)	CCR2
hsa-miR-135a-3p	TargetScan Human	High (predicted)	CD4
hsa-miR-135a-3p	TargetScan Human	High (predicted)	CLDN16
hsa-miR-135a-3p	TargetScan Human	High (predicted)	GNAL
hsa-miR-135a-3p	TargetScan Human	High (predicted)	HLA-A
hsa-miR-135a-3p	TargetScan Human	High (predicted)	IL1RAP
hsa-miR-135a-3p	TargetScan Human	High (predicted)	IL2RA
hsa-miR-135a-3p	TargetScan Human	High (predicted)	KCNMB2
hsa-miR-135a-3p	TargetScan Human	High (predicted)	PPP2R2B
hsa-miR-135a-3p	TargetScan Human	High (predicted)	PPP3R2
hsa-miR-135a-3p	TargetScan Human	High (predicted)	TFRC
hsa-miR-135a-3p	TargetScan Human	High (predicted)	TNFSF8
hsa-miR-148a-5p	TargetScan Human	High (predicted)	ATP6V1G3
hsa-miR-148a-5p	TargetScan Human	High (predicted)	FGF5
hsa-miR-148a-5p	TargetScan Human	High (predicted)	HSPA5
hsa-miR-148a-5p	TargetScan Human	High (predicted)	IFI6
hsa-miR-148a-5p	TargetScan Human	High (predicted)	IL22RA2
hsa-miR-148a-5p	TargetScan Human	High (predicted)	NMBR
hsa-miR-148a-5p	TargetScan Human	High (predicted)	OAS1
hsa-miR-148a-5p	TargetScan Human	High (predicted)	RAB5A
hsa-miR-148a-5p	TargetScan Human	High (predicted)	TFRC
hsa-miR-5587-5p	TargetScan Human	High (predicted)	AP1S2
hsa-miR-5587-5p	TargetScan Human	High (predicted)	AP2M1

Supp. Table 4. Part of the mRNA profile analysis of riRBCs and trRBCs compared to niRBCs.

Name	RBCs-ctrl-17.2#1	RBCs-ctrl-17.2#2	RBCs-ctrl-18.2#1	RBCs-ctrl-18.2#2	rings-18.2#1	rings-18.2#2	trophs-17.2#1	trophs-17.2#2	rings-18.2 vs ctrls 18.2 - Fold change	rings-18.2 vs ctrls 18.2 - Log fold change	rings-18.2 vs ctrls 18.2 - P-value	rings-18.2 vs ctrls 18.2 - FDR p-value	trophs-17.2 versus ctrls 17.2 - Fold change	trophs-17.2 versus ctrls 17.2 - Log fold change	trophs-17.2 versus ctrls 17.2 - P-value	trophs-17.2 versus ctrls 17.2 - FDR p-value
RPL5	21	17	10	16	43	54	19	27	65.5660624	6.03487735	1.66357E-98	2.08944E-95	137.8061457	7.106496418	1.025E-106	2.5267E-103
HSP90AA1	5	3	3	2	245	267	318	303	1574.33476	10.62052663	6.16915E-98	3.87423E-95	8424.864566	13.04043778	3.3331E-92	4.10808E-89
CALM2	1	4	20	15	243	306	632	785	2601.36152	11.34505119	7.20596E-74	3.0169E-71	30485.11428	14.89581733	1.6606E-85	1.36447E-82
HBA1	2456602	2360129	1997783	1941566	29440	39936	2154	2418	-2.6782063	-1.42126707	3.44363E-69	1.0813E-66	-8.97843274	-3.16646363	3.5332E-14	3.78668E-12
MARCH6	6	6	21	17	28	49	36	45	160.267193	7.324335325	3.19908E-60	8.03608E-58	753.0838298	9.556666658	9.8502E-63	4.85613E-60
NCL	2	1	3	1	218	264	77	119	3593.8395	11.81131026	6.5077E-52	1.36228E-49	6720.235027	12.71429597	1.3772E-45	3.08607E-43
P4HA2	1	2	1	0	159	167	71	65	2439.53262	11.25238906	3.96728E-47	7.11843E-45	4392.602922	12.10086037	1.4089E-44	2.89409E-42
ATAD2	0	1	0	2	3262	3645	2307	2776	121424.407	16.88969892	3.79631E-46	5.9602E-44	400357.551	18.61092949	1.998E-49	5.47233E-47
HBA2	3119537	3316127	2808471	2744632	47172	67817	3320	4083	-2.166805	-1.11556935	2.14544E-43	2.99408E-41	-7.34955133	-2.87765618	5.1592E-11	3.26086E-09
HMGB1	7	2	6	6	23	28	21	26	139.817484	7.12740097	2.45394E-43	3.08215E-41	571.4022272	9.158362849	8.681E-70	5.34964E-67
HBB	1033831	1139258	740342	698457	16608	24491	879	1080	-2.0501319	-1.03571676	1.85397E-37	2.11689E-35	-9.38753334	-3.23074613	4.3809E-14	4.15344E-12
RPS27A	61	58	78	78	23	21	33	34	9.58523701	3.260814106	2.52806E-34	2.4425E-32	63.27919484	5.983659338	1.6129E-54	5.67962E-52
HSPA8	3	0	4	5	53	54	95	99	797.903319	9.640070138	2.37953E-34	2.4425E-32	6410.564897	12.64623578	9.2362E-48	2.27673E-45
NPM1	3	0	1	3	39	56	17	24	707.705954	9.467006246	4.60621E-33	4.13243E-31	1370.655894	10.42065071	3.4348E-38	6.51293E-36
DONSON	63	39	203	253	29	16	87	83	11.7862673	3.55903498	1.65639E-30	1.38695E-28	55.26563111	5.788310663	6.8237E-51	2.10255E-48
UBA52	27371	26858	47982	46921	476	637	62	79	-1.874783	-0.9067236	5.39207E-23	4.23278E-21	-3.316677065	-1.72977925	4.8498E-05	0.001494356
PTP4A2	1	1	6	4	75	90	46	69	2879.30436	11.49150458	4.41753E-22	3.26377E-20	9151.407579	13.15977795	1.8403E-25	3.2403E-23
DDX5	1	4	0	0	9	13	2	0	104.25454	6.703966398	8.78704E-22	6.1314E-20	41.01653787	5.358133817	2.3182E-05	0.000723326
PHF14	7	10	12	7	10	8	14	13	26.7903993	4.74364418	2.19994E-21	1.45428E-19	174.0131429	7.443052464	2.0197E-61	8.29756E-59
ARID4B	0	1	0	0	48	62	15	20	1918.96333	10.90611143	5.77732E-20	3.62816E-18	2692.895496	11.39494253	4.2949E-21	6.22765E-19
PSMD1	0	3	1	3	13	10	7	10	171.502143	7.422082797	7.94985E-19	4.75476E-17	551.2580391	9.10658398	3.1192E-25	5.12591E-23
FTL	8709	8284	8205	8046	123	210	3	5	-1.9663556	-0.97552425	9.4125E-18	5.37368E-16	-18.8330513	-4.23519486	3.776E-12	2.73762E-10
HBG2	6057	6006	6902	6357	94	125	3	3	-2.1178915	-1.08262871	1.88054E-17	1.02694E-15	-21.3965905	-4.41930902	7.1299E-10	4.08726E-08
C14orf37	1	0	0	1	29	28	12	13	994.950048	9.958480286	1.02089E-16	5.34266E-15	1881.104827	10.87736453	3.6711E-19	5.02743E-17
NEXN-AS	0	1	0	0	21	29	8	6	872.268572	9.768628599	4.30821E-16	2.16444E-14	1053.004181	10.04029545	1.1302E-15	1.393E-13
KMT2D	0	0	0	0	295	360	49	29	34709.2981	15.08303457	2.49136E-13	1.20352E-11	17610.75428	14.10416908	1.0851E-11	7.22879E-10
BDH1	16	10	52	68	8	5	7	3	12.7779953	3.675589609	2.89426E-13	1.34637E-11	42.54105544	5.410783922	2.4447E-21	3.76635E-19
GYPC	4222	4420	3353	3292	79	88	5	3	-1.9880326	-0.99134142	8.85366E-13	3.9715E-11	-9.58190355	-3.26031229	4.6867E-08	2.26526E-06
FLT1	0	0	0	0	167	206	97	146	19758.8896	14.27021425	4.42276E-12	1.91551E-10	58362.51766	15.8327545	3.9945E-14	4.1027E-12
RPL41	7750	7781	14287	13403	153	199	10	19	-1.6963702	-0.76245189	1.06911E-11	4.47599E-10	-4.74459189	-2.246284	1.179E-06	4.54112E-05
RPS12	8771	8932	15826	15812	169	241	14	18	-1.6616772	-0.73264017	1.34686E-11	5.45695E-10	-4.90303465	-2.29367496	1.2421E-07	5.77709E-06
MTERFD2	1	0	0	0	9	8	3	9	296.761114	8.213158251	5.88238E-11	2.30883E-09	526.5276775	9.04036556	7.7138E-11	4.63767E-09
SLC25A37	5236	4959	5453	5709	99	121	8	13	-1.7808621	-0.83257578	6.11891E-11	2.3289E-09	-4.30281017	-2.10527919	4.3876E-06	0.000148158
HLA-F	0	0	1	0	76	105	94	145	9581.35432	13.22601388	1.43701E-10	5.3085E-09	57518.2221	15.81173146	4.3471E-14	4.15344E-12
YWHAE	0	0	0	2	61	74	116	134	7150.62578	12.80385379	5.49049E-10	1.9703E-08	58627.27754	15.83928444	3.2016E-14	3.58729E-12
DAPP1	0	0	0	0	60	72	41	45	6991.98948	12.7714873	6.07529E-10	2.1196E-08	19823.84966	14.27494953	6.7394E-12	4.74647E-10
RPS24	1264	1294	2603	2380	5	26	1	4	-3.1750243	-1.66676761	1.03268E-09	3.50552E-08	-4.53640474	-2.18154936	0.00080122	0.020573
PSMC6	0	0	0	2	49	65	100	123	6036.44239	12.55948282	1.17254E-09	3.87554E-08	52576.86111	15.68240319	5.5171E-14	4.68955E-12
PFDN5	1929	1948	3492	3296	16	49	6	8	-2.2962475	-1.19927814	1.35139E-09	4.35215E-08	-2.455552271	-1.29604779	0.00696191	0.109306474
CASQ2	0	0	0	0	48	56	24	28	5509.13972	12.42761114	1.75671E-09	5.51606E-08	11947.71835	13.54444751	6.7363E-11	4.51126E-09
RPS15	1519	1398	1727	1664	17	26	4	4	-2.6081271	-1.38301418	4.58189E-09	1.40362E-07	-4.31253332	-2.1085356	0.00099212	0.02395609
RPS11	2801	2690	3968	3798	48	63	3	4	-1.90175	-0.92732763	7.15647E-09	2.14012E-07	-6.95603904	-2.79826603	6.584E-06	0.000216394
RPL30	2065	1953	3454	3341	23	50	7	4	-2.1180372	-1.08272795	9.57729E-09	2.79746E-07	-3.24028301	-1.69611983	0.00090866	0.0239569
RP11-281	0	0	0	0	42	20	83	162	3450.17539	11.75245399	1.54791E-08	4.41857E-07	60094.54659	15.87494646	4.7428E-14	4.28515E-12
CSNK1A1	2	0	0	0	3	4	6	3	73.1854194	6.193484347	1.77177E-08	4.94521E-07	406.0091207	8.665368327	4.5159E-15	5.30085E-13
RPL21	6920	6956	9899	9470	133	211	17	22	-1.5535325	-0.63555243	1.8123E-08	4.94836E-07	-3.15274582	-1.65660880	7.967E-05	0.002424512
TPT1	3578	3488	3843	3722	80	76	4	3	-1.7388914	-0.79816787	1.89649E-08	5.06806E-07	-8.95268963	-3.16232117	3.7329E-07	1.53358E-05
MAT2A	0	0	0	0	29	29	84	97	3073.06181	11.58546107	2.1365E-08	5.47642E-07	42353.11399	15.37018043	1.6345E-13	1.34304E-11
SRGAP1	0	0	0	0	31	27	24	41	3075.38921	11.58655329	2.12979E-08	5.47642E-07	15637.39063	13.93271217	2.6527E-11	1.72074E-09
CYLC2	0	0	0	0	22	35	56	66	3017.72914	11.55924761	2.30406E-08	5.78779E-07	28502.0458	14.79877786	1.2462E-12	9.30846E-11
RPL12	2425	2409	3919	3891	45	53	3	9	-1.8957313	-0.92275452	3.92768E-08	9.67287E-07	-3.5706779	-1.83621988	0.00046509	0.012738207
CTA-363E	1330	1369	2381	2175	16	27	0	0	-2.4136411	-1.27121114	7.25402E-08	1.75212E-06	-4.78559081	-2.25869705	0.00068029	0.017651811
ZC3H6	0	5	1	1	5	2	1	3	34.3640684	5.102828944	9.00615E-08	2.11672E-06	86.42646346	6.433401223	2.4006E-07	1.00298E-05
ETF1P3	0	0	0	0	18	23	13	6	2171.55769	11.08451457	9.10054E-08	2.11672E-06	5180.981971	12.33900985	2.4785E-09	1.32817E-07
HSPA8P18	0	0	0	0	15	21	1	0	1906.6053	10.89679049	1.52909E-07	3.49188E-06	226.089947	7.820753035	0.00195209	0.037593012
RPLP2	1396	1373	1663	1625	22	25	1	0	-2.2643333	-1.17908633	2.07891E-07	4.66269E-06	-8.18473807	-3.03293625	0.00029134	0.008160786
FKBP8	2297	2426	888	899	49	51	1	0	-1.8145573	-0.85961793	2.51083E-07	5.53264E-06	-6.98009431	-2.80324653	1.8793E-05	0.0005939
UBB	2694	2511	2742	2629	44	70	10	1	-1.7563252	-0.81255996	3.1015E-07	6.71636E-06	-4.19954743	-2.07023386	0.00013356	0.00401501
TPR	0	0	0	0	13	16	94	139	1536.16454	10.58511704	3.47514E-07	7.39793E-06	55866.53711	15.76969678	4.8715E-14	4.28515E-12
RPS17	871	878	1705	1688	19	0	0	0	-3.1138506	-1.64793641	3.5392E-07	7.40873E-06	-16853.9088	-14.0407956	0.76775477	0.936585562
RP11-406	0	0	0	0	16	12	14	12	1483.82524	10.53510547	4.08131E-07	8.40348E-06	5874.827419	12.52033076	1.2933E-09	7.24563E-08
USP15	9	4	12	13	5	2	0	0	13.517554	3.756762219	8.43697E-07	1.70917E-05	-130.043341	-7.02284871	0.88258001	0.936585562
NPM1P31	0	0	0	0	14	9	0	8	1230.17623	10.26464929	8.72698E-07	1.73986E-05	2144.368237	11.06633696	3.3219E-06	8.17639E-05
YBX1	1294	1233	742	787	14	30	3	5	-2.2090826	-1.14344737	1.01287E-06	1.98775E-05	-2.80113412	-1.48601106	0.00642268	0.101883838
RPS15A	1157	1063	1789	1548	16	21	0	0	-2.306413	-1.20565509	1.78935E-06	3.45758E-05	-3.93626887	-1.97682877	0.03420697	0.042290697
MSR1	0	0	0	0	6	13	4	4	1006.29377	9.97483582	1.85056E-06	3.52168E-05	1807.610557	10.81986817	5.6261E-07	2.2735E-05
NCOR1	2	3	4	3	1	6	0	0	23.733342	4.568843362	1.97136E-06	3.69557E-05	119.986943	6.90673062	2.9101E-13	2.31404E-11
OAZ1	853	821	315	282	8	15	0	0	-2.7982596	-1.48452981	2.18553E-06	4.0368E-05	-16131.1577	-13.9775624	0.76877084	0.936585562
HSPA5	0	0	2	1	11	7	6	9	955.174183	9.899620033	2.5368E-06	4.61772E-05	3391.667435	11.727779	2.003E-08	1.00764E-06
TRIM13	0	0	0	0	7	10	2	1	900.621683	9.815242542	2.9803E-06	5.34752E-05	1355.954118	10.40509265	1.8793E-06	6.54886E-05
RP11-24J2	0	0	0	0	9	8	0	0	900.840279	9.815127525	3.02427E-06	5.34997E-05	#N/A	#N/A	#N/A	#N/A
ETF1	0	1	0	0	3	2	1	8	87.3824496	6.449271644	3.68603E-06	6.43007E-05	1128.522544	10.14021952	5.4867E-16	7.11822E-14
CHD1	2	1	0	2	1	1	0	0	37.3246915	5.222058432	4.22049E-06	7.26155E-05	161.1569412	7.332322518	2.0197E-11	1.49227E-08
RPS10	606	608	763	761	4	8	0	0	-3.8882781	-1.95913142	4.28298E-06	7.26948E-05	-11699.9309	-13.5142124	0.77622828	0.936585562
RPS17L	73	33	24	10	2	19	5	6	4.8065106	2.264989914	6.25619E-06	0.00010477	11.83665635	3.565189697	8.8579E-12	6.60519E-10
SEC62	1106	1122	2631	1182	65	72	21	12	1.60023922	0.678287587	6.61299E-06	0.000109288	1.669059576	0.739035452	0.05099718	0.690703547
ATP6V1A	0	0	0	0	9	5	8	6	746.001122	9.54303399	7.25297E-06	0.000116791	3615.444238	11.81995721	1.4018E-08	7.19864E-07
DRG1	0	0	0	0	9	5	3	3	746.001122	9.54303399	7.24318E-06	0.000116791	1355.719312	10.4048428	2.7646E-06	5.75513E-05
RPL35A	1497	1411	2445	2193	26	34	4	5	-1.8631727	-0.89776139	1.16573E-05	0.000185914	-6.44637174	-2.68848739	0.00042356	0.011731169
TTC39B	0	0	0	0	4	6	1	5	529.972517	9.049773738	1.97763E-05	0.000310487	1459.340976	10.51110129	1.7747E-06	6.43332E-05
CDKN2B-	0	0	0	0	2	9	7	2	570.548905	9.156206744	2.21804E-05	0.000343934	677.8743476	9.407410681	4.0001E-05	0.004154376
FBXO7	329	292	292	360	20	27	0	0	1.96755351	0.976402869	2.73051E-05	0.000418235	-5987.11667	-12.5476457	0.79185064	0.936585562
SPDYA	0	0	0	0	5	4	66	88	477.105144	8.89816343	3.08682E-05	0.00047613	36500.74172	15.15563816	3.9865E-13	3.07089E-11
GNAS	788	803	582	572	11	15	3	0	-2.3523507	-1.23410316	3.14374E-05	0.000470064	-4.705067	-2.23441527	0.00541527	0.128662064
RPL28	402	363	401	370	3	1	2	0	-7.3392403	-2.87563073	7.62294E-05	0.001126401	-3.39380308	-1.76290286	0.08530842	0.936585562
UBAP2	1	2	4	2	2	4	0	0	22.4204988	4.486746469	8.46983E-05	0.001236989	32.25314655	5.011368009	0.00845568	0.128662064
RARS	1	0	0	0	2	0	4	0	67.7012924	6.08111147	9.9785E-05	0.001440574	-14.4414145	-3.85214016	0.9354457	0.936585562
SRSF1	0	1	0	0	4	0	1	0	75.8348894	6.244789838	0.000103027	0.001470475	300.9147244	8.233210892	6.9767E-09	3.65908E-07
MYT1	0	0	0	0	5	2	5	7	371.224414	8.536147783	0.000122289	0.001725029	2343.198183	11.19426326	1.8784E-07	8.41886E-06
TUBA8	0	0	0	0	8	0	3	7	475.883921	8.894465899	0.000124222	0.001733587	2343.198183	11.19426326	1.8676E-07	8.41886E-06
CYB5R4	0	0	0	0	3	3	1	1	318.197884	8.313780432	0.000135137	0.001865193	452.0179499	8.820236254	0.00063512	0.016834178
SENP3	0	0	0	0	3	3	1	1	318.197884	8.313780432	0.000136866	0.001868523	1129.635954	10.14170605	2.7646E-06	5.59839E-05
CTLA4	0	0	0	0	2	4	2	4	318.159069	8.313604436	0.000138827	0.00187491	1355.954118	10.40509265	1.7015E-06	6.25996E-05
MLLT3	2	1	4	6	3	0	0	0	22.4232691	4.486924719	0.000170894	0.002283439	-33.7084605	-5.07503883	0.91500577	0.936585562
RPL31	1307	1252	2655	2454	32	25	4	5	-1.724396	-0.78609112	0.00017382	0.002298007	-2.52163851	-1.33436147	0.01269078	0.18845049
SLC25A39	1062	989	450	398	19	24	0	1	-1.8335326	-0.87462595	0.000221853	0.002850244	-18.1775293	-4.18408421	0.00377509	0.064622145
PSMC1	0	0	0	0	5	3	5	4	265.223809	8.051066806	0.000253486	0.003282225	2033.390478	10.98967157	1.9413E-07	8.54519E-06
POLR3B	0	0	0	0	0	6	0	0	293.766275	8.195324971	0.000296396	0.003798709	#N/A	#N/A	#N/A	#N/A
EIF5A2	0	0	0	0	4	1	0	0	269.226511	8.072676669	0.000333775	0.004234564	#N/A	#N/A	#N/A	#N/A

Supplement text 1:
R script for volcano plot generation

```
library("xlsx")
library ("ggplot2")
library ("purrr")
library ("tibble")
library ("dplyr")
library ("tidyr")
library ("stringr")
library ("readr")
library ("forcats")
D <- read.xlsx("00.xlsx", 1)
head(D)
# Make a basic volcano plot
with(D, plot(Rings.FC,-log2(R..P.value), pch=16, main="b", xlim=c(-30,30), ylim=c(0,25)))
with(subset(D, Rings.FC>5 ), points(Rings.FC, -log2(R..P.value), pch=16, col="tomato1"))
with(subset(D, Rings.FC< -5 ), points(Rings.FC, -log2(R..P.value), pch=16, col="olivedrab3"))
```

Supplement text 2:
R script for heatmap generation

```
library(pheatmap)
library(RColorBrewer)
library(ggplot2)
library("xlsx")
D <- read.xlsx("mirrbcs.xlsx", 1)
head(D)
row.names(D) <- D$Name
D1=subset(D,select=-Name)   #remove row names
D_matrix <- data.matrix(D1)
D_heatmap <- pheatmap(D_matrix, color = colorRampPalette
            ((brewer.pal(n = 1, name ="RdYlBu")))(1000),
            margin=c(8,6),
            cellwidth = 20, cellheight = 5, scale="row",
            main = "",
            notecol="black", breaks = NA,  cutree_cols = 1000,
            border_color = NA, fontsize_col = 5, fontsize_row = 5,
            kmeans_k = NA, cluster_rows=FALSE, cluster_cols=FALSE,
            angle_col = "45",
            treeheight_col = 1000, height = 10000, show_colnames =T,
            show_rownames = T)
```